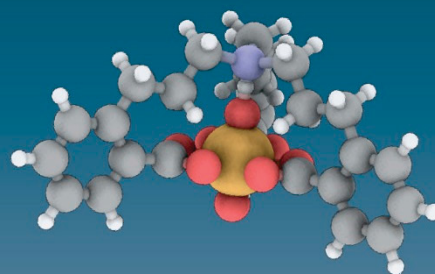
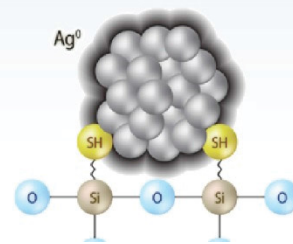


# Material Recovery and Waste Form Development 2016 Accomplishments

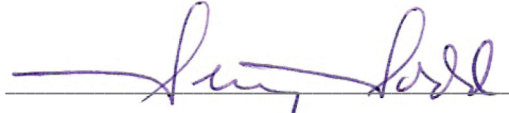


Material Recovery &  
Waste Form Development



## 2016 ACCOMPLISHMENTS

Approved by:



Terry Todd, MRWFD Director

Prepared for the  
U.S. Department of Energy  
Office of Nuclear Energy  
Under DOE Idaho Operations Office  
Contract DE-AC07-05ID14517

**DISCLAIMER**

This information was prepared as an account of work sponsored by an agency of the U.S. Government. Neither the U.S. Government nor any agency thereof, nor any of their employees, makes any warranty, expressed or implied, or assumes any legal liability or responsibility for the accuracy, completeness, or usefulness, of any information, apparatus, product, or process disclosed, or represents that its use would not infringe privately owned rights. References herein to any specific commercial product, process, or service by trade name, trade mark, manufacturer, or otherwise, does not necessarily constitute or imply its endorsement, recommendation, or favoring by the U.S. Government or any agency thereof. The views and opinions of authors expressed herein do not necessarily state or reflect those of the U.S. Government or any agency thereof.

## Table of Contents

Introduction _____	1
Collaborations _____	4
Nuclear Energy University Program (NEUP) Partnerships _____	10
Reference Technologies and Alternatives _____	14
Sigma Team – Advanced Actinide Recycle _____	38
Sigma Team – Off-Gas _____	53
Waste Form Development and Performance _____	68
CoDCon Demonstration _____	111
Fundamental Separation Data and Methods _____	117
Domestic Echem _____	127
Fuel Resources _____	132
Acronyms and Abbreviations _____	146
Publications (5-year cumulative) _____	150

# Introduction

The Material Recovery and Waste Form Development (MRWFD) Campaign under the U.S. Department of Energy (DOE) Fuel Cycle Technologies (FCT) Program is responsible for developing advanced separation and waste form technologies to support the various fuel cycle options defined in the *DOE Nuclear Energy Research and Development Roadmap, Report to Congress* (April 2010). This MRWFD accomplishments report summarizes the results of the research and development (R&D) efforts performed within MRWFD in Fiscal Year (FY) 2016. Each section of the report contains an overview of the activities, results, technical point of contact, applicable references, and documents produced during the FY.

This report briefly outlines campaign management and integration activities but primarily focuses on the many technical accomplishments of FY 2016. The campaign continued to use an engineering-driven, science-based approach to maintain relevance and focus.

MRWFD management and integration activities included international collaboration activities (with France, China, Japan, the European Union, and the International Atomic Energy Agency), integration activities with other campaigns (i.e., Advanced Fuels, Used Fuel Disposition, Fuel Cycle Options, and Material Protection, Accountancy and Control Technology), and integration with the DOE Office of Environmental Management (EM).

Technical accomplishments are reported under the following R&D categories:

- Reference Technologies and Alternatives
- Sigma Team for Advanced Actinide Recycle
- Sigma Team for Off-Gas Capture and Immobilization
- Fundamental Separation Data/Methods
- Waste Form Development and Performance
- Domestic Electrochemical Processing
- Co-Decontamination Process (CoDCon) Demonstration
- Fuel Resources.

### MRWFD Mission

**Develop advanced fuel cycle separation and waste management technologies that improve current fuel cycle performance and enable a sustainable fuel cycle, with reduced processing, waste generation, and potential for material diversion.**

### MISSION

The MRWFD Campaign applies expertise and technical capabilities to a wide array of applications. The mission of MRWFD is to:

*Develop advanced fuel cycle separation and waste management technologies that improve current fuel cycle performance and enable a sustainable fuel cycle, with minimal processing, waste generation, and potential for material diversion.*

Mission implementation is outlined in the *Material Recovery and Waste Form Development Campaign Implementation Plan* issued in November 2012. The plan will be revised following issuance of a new Nuclear Energy Roadmap, which is expected in FY 2017.

### OBJECTIVES

The objectives of the MRWFD Campaign are to:

- Develop technologies that support the current once-through fuel cycle and have near-term potential application
- Develop a fundamental and practical understanding of methods for the separation of uranium and transuranic elements from used nuclear fuel (UNF)
- Develop a fundamental and practical understanding of the factors affecting performance of advanced waste forms
- Develop and demonstrate enabling technologies to separate and immobilize gaseous fission products from UNF treatment
- Demonstrate predictable performance of advanced waste forms and processes with greatly improved cost and performance.

### CHALLENGES

Challenges facing the MRWFD Campaign include:

- Separating trivalent actinides from lanthanides
- Capturing and immobilizing off-gas constituents of UNF, including iodine, krypton, tritium, and potentially carbon in a cost-effective manner meeting current U.S. regulations
- Developing separation technologies and waste forms that are interrelated with the types of fuels being processed, the types of fuels being fabricated, and the reactors used to burn recycled fuels
- Measuring waste form lifetimes in a laboratory, which is impossible, considering that lifetimes are on the order of hundreds of thousands to millions of years
- Assessing proliferation risk of separation technologies that is very subjective and must be done in the context of the entire fuel cycle (mining to disposal).

### CAMPAIGN STRUCTURE

The campaign is organized in a flat structure to facilitate cross-campaign integration. Federal project directors are responsible for oversight and approval of all MRWFD work activities. The national technical director (NTD) and deputy NTD are responsible for work prioritization, integration, and management.

Campaign leadership consists of:

- NTD, Dr. Terry Todd, Idaho National Laboratory (INL)

## 2016 ACCOMPLISHMENTS

- Deputy NTD, Dr. John Vienna, Pacific Northwest National Laboratory (PNNL)
- Director, NE-51, Office of Systems Engineering and Integration, Dr. Patricia Paviet, DOE-NE
- Federal project director, Dr. James Bresee, DOE-NE
- Federal project director, Domestic Electrochemical Separations Technology and Fuels Resources, Dr. Stephen Kung, DOE-NE
- Federal project director, Waste Forms Development and Performance and Sigma Team for Off-Gas Capture and Immobilization, Ms. Kimberly Gray, DOE-NE.

## Collaborations

T. A. Todd (INL) and J. D. Vienna (PNNL)

### INTERNATIONAL ATOMIC ENERGY AGENCY

The United States (U.S.) has a long history of nuclear energy R&D collaboration with the international community through the International Atomic Energy Agency. Specific areas of MRWFD collaboration in FY 2016 include:

- Participation in the Technical Meeting on Advanced Fuel Cycles for Waste Burden Minimization
- Participation in the coordinated research project known as Processing Technologies for High-Level Waste, Formulation of Matrices, and Characterization of Waste Forms
- Participation in the preliminary study known as Waste from Innovative Types of Reactors and Fuel Cycles.

These collaborations share methods, technologies, and research among practitioners from the member states. As such, there is a distinct advantage to campaign participation in that researchers gain valuable insight into the results from a wide range of member states. This insight and these results can be leveraged in meeting campaign R&D objectives.

### EU-DOE

The European Union (EU) Framework Safety of Actinide Separation ProceSses (SACSESS) program is a 3-year effort that follows the successful EU Actinide reCycling by SEParaTion (ACSEPT) program that ran for the 4 previous years and developed and demonstrated a number of new minor actinide separation processes. This program includes most of the leading European separation experts from the Commissariat à l'Énergie Atomique (CEA) in France; the National Nuclear Laboratory in the United Kingdom (UK); Forschungszentrum Jülich (FZ-J), Karlsruhe Institute of Technology, and the Institute for Transuranium Elements in Germany; Chalmers University in Sweden; and the Czech Technical University and the Nuclear Research Institute in the Czech Republic, along with 15 other European universities.

Irradiation of process samples representative of the EU's innovative selective actinide extraction (SANEX) process were completed in the INL solvent degradation test loop. Previous static irradiations of the system performed at Centro de Investigaciones Energéticas, Medioambientales y Tecnológicas in Spain indicated that the aqueous soluble stripping reagent would completely decompose within 250 kGY of irradiation. Results from the testing in the solvent degradation test loop indicated that when the stripping agent is irradiated in contact with the organic solvent, very little degradation takes place. This finding was critical for the SACSESS program to move forward with the innovative SANEX process for flowsheet testing. A journal article summarizing this work was published in *Industrial and Engineering Chemistry Research*.

A successful lab-scale flowsheet test of the Advanced Trivalent Actinide Lanthanide Separation by Phosphorus-reagent Extraction from Aqueous Komplexes (TALSPEAK) system was performed at FZ-J in June 2016 as part of the SACSESS collaboration. This test used a simulated feed solution containing lanthanide

## 2016 ACCOMPLISHMENTS

elements and was spiked with  $^{241}\text{Am}$  and  $^{244}\text{Cm}$  to determine the degree of separation between the lanthanides and the minor actinides. Excellent hydrodynamic performance was observed in the 1-cm centrifugal contactors used in the test. High separation factors between the lanthanides and actinides were achieved in the test. A series of three journal articles is being prepared to describe the Advanced TALSPEAK system.

In the frame of the U.S.-Czech scientific collaboration program, Pavel Bartl, a Ph.D. student from the Czech Technical University in Prague, Faculty of Nuclear Sciences and Physical Engineering, spent more than 5 months studying the kinetics of actinide solvent extraction at Argonne National Laboratory (ANL) under supervision of Dr. Artem Gelis.

MRWFD personnel participated in the final SACSESS International Workshop held in Montpellier, France, in June 2016. This workshop was held directly following the 5th International ATALANTE Conference on Nuclear Chemistry for Sustainable Fuel Cycles held in Montpellier, France.

### CEA-DOE

The U.S. and France share a long history of nuclear energy R&D collaboration, particularly in the area of separations and waste management. These collaborations are primarily with the CEA. Five primary areas of collaboration between CEA and DOE were active in FY 2016: online monitoring, solvent degradation, radioiodine separation and immobilization, radionuclide release from glass, and glass waste form property modeling. The U.S.-CEA Bilateral Steering Group meeting was held May 2016 in Paris, France.

#### Online Monitoring

The first area of focus for FY 2016 was associated with advancement of technology for in situ analytical measurements of nitric acid, lanthanides, and actinides in solvent extraction media. FY 2016 collaboration focused on the application, measurement, and analysis of solutions in microfluidic cells. A micro-Raman probe was obtained by PNNL through a Small Business Innovation Research program collaboration for the purposes of integration with microfluidic cells. Initial testing of this micro-Raman probe and microfluidic cell was performed as described in "Reference Technologies and Alternatives" on page 16.

#### Solvent Degradation

The radiolytic stability of potential fuel cycle extractants of common interest is being investigated as a collaboration between INL and CEA. The study of one such extractant, diethylhexylisobutyramide (DEHiBA), has been completed. DEHiBA has been irradiated under various conditions of acidity and aeration, and the radiolysis rates and products were evaluated at both INL and CEA. Degradation rates and impact on extraction of uranium have been evaluated, and specific degradation products formed have been identified. Results indicate the DEHiBA is relatively radiation-stable. A collaborative journal manuscript that addresses these findings in detail has been prepared with co-authors at INL and CEA-Marcoule.

#### Radioiodine Separation and Immobilization

Progress was made in FY 2016 in collaborations associated with the capture and immobilization of radioiodine. Oak Ridge National Laboratory (ORNL) fabricated and tested an iodine capture cell compatible with the CEA ATelier Alpha et Laboratoires pour ANALyses, Transuraniens et Etudes de retraitement

(ATALANTE) dissolver off-gas stream. This capture cell is to be installed at the ATALANTE facility by CEA and used to test iodine capture materials developed by both the U.S. and France to generate data on prototypic dissolver off-gas streams and compare media. Approval was received to ship the unit to France by the ORNL export control office. The decision on shipping the unit remains with the DOE-NE program office and CEA.

### Radionuclide Release from Glass

Improved understanding of the mechanisms and rates of glass corrosion is another focus of the DOE-CEA collaboration. During FY 2016, a joint research paper (Gin, S., L. Neill, M. Fournier, P. Frugier, T. Ducasse, M. Tribet, A. Abdelouas, B. Parruzot, J. Neeway, and N. Wall, 2016, "The controversial role of inter-diffusion in glass alteration," *Chemical Geology*, Vol. 440, pp. 115–123) was published. This paper describes the results of tests aimed at understanding the conditions in which inter-diffusion and surface reaction occur. It was found that, far-from- and close-to-saturation conditions must be distinguished. Inter-diffusion takes place in acidic conditions and far from saturation. However, closer to saturation, when a sufficiently dense layer is formed, a new approach is proposed requiring a full description of chemical reactions taking place within the alteration layer and an accurate budget of hydrous species along the profile, because it is thought that the access of a sufficient amount of water to the pristine glass may be the rate-limiting process in these conditions.

### Glass Waste Form Property Modeling

For more than 30 years, DOE and CEA have invested heavily in the development of nuclear waste glass technology. Sharing of data, methods, and models benefits both nations in our efforts to improve the science and technology of waste vitrification.

In FY 2016, PNNL evaluated a combined U.S. and French database of long-term static corrosion test results to determine composition effects on acceleration of alteration. The results are being prepared for discussion with CEA-Marcoule colleagues in our planned exchange in FY 2017. Plans also include the modeling of physical properties of MoO<sub>3</sub>-rich melts, including viscosity, electrical conductivity, phase separation temperature, and density. Both organizations have developed such data on a limited number of compositions, and the combined data will allow for significantly improved understanding of composition effects.

### PEOPLE'S REPUBLIC OF CHINA–DOE

As the two largest energy consumers in the world, the U.S. and the People's Republic of China (PRC) share the view that nuclear energy is indispensable as an energy source for combating climate change as well as ensuring energy security. Further cooperation between both countries in the area of peaceful uses of nuclear energy will advance our shared objectives of nuclear nonproliferation, safety, and security. The PRC–U.S. Bilateral Civil Nuclear Energy Cooperation Action Plan signed in Vienna, Austria, on September 18, 2007, is a programmatic commitment for both countries to further facilitate joint long-term R&D collaborative activities in advanced civilian nuclear technologies. Six technical working groups have been established and organized under the U.S.-China nuclear energy action plan cooperation framework: (1) Advanced Separation Technologies, (2) Fast Reactor Technologies, (3) Advanced Fuels and Materials

## 2016 ACCOMPLISHMENTS

Development, (4) Nuclear Safety Enhancement, (5) Spent Fuel Storage and Repository Sciences, and (6) High-Temperature Reactor Technologies.

The Separations Technology Working Group's mission is the collaborative development of advanced reprocessing and waste-form production methods that enhance safeguards, provide economic benefits, and reduce environmental impacts. The working group's objective is achieving a mutually beneficial and equitable program of technological collaboration on the back end of the nuclear fuel cycle. Collaborative activities have been focused on:

- Tritium and iodine management for advanced reprocessing
- Development of advanced aqueous product conversion methods
- Pyrochemical recycling research facilities and technology development
- Advanced online process monitoring and control instrumentation developments.

Information-exchange meetings have taken place to discuss topics related to head-end tritium capture, including requirements and regulatory issues, iodine capture, iodine waste forms, and other off-gas management issues.

The Eighth Joint Technical Working Groups Meeting under the China–U.S. Bilateral Civil Nuclear Energy Cooperation Action Plan was held October 27–29, 2015, in Qingdao, China. Iodine capture and immobilization remained the primary focus for collaboration, because iodine is the most challenging volatile radionuclide to control and is an area of continued R&D interest worldwide. The near-term goal is to exchange primary iodine sorbent materials (to the extent possible), conduct comparative tests, and critically assess results. Following the meeting, the U.S. team had the opportunity to tour the AP1000 reactors under construction at Haiyang Nuclear Power Plant.

The Ninth Joint Technical Working Groups Meeting was held September 19–21, 2016, in Idaho Falls, Idaho. The following were identified as areas for future activities: iodine capture and management, tritium management, and co-extraction and co-decontamination studies. The next technical working group meeting should be held in China (possibly Beijing) and may include tours of the China Reprocessing and Radiochemical Laboratory.

### **Six-Nation Collaboration on Long-Term Performance of Glass**

DOE is co-leading a Six-Nation collaborative effort to develop the technical basis for an international consensus on nuclear waste glass corrosion rate model along with CEA (France) and the Japan Atomic Energy Agency (JAEA). Participating in the collaboration are Belgium (SCK-CEN), France (CEA, Subatech), Germany (University of Bonn), Japan (JAEA, Kyushu University, Tokyo University), the UK (National Nuclear Laboratory, Sheffield University, Amec), and the U.S. (ANL, PNNL, Pennsylvania State University, Savannah River National Laboratory [SRNL], University of North Texas, Washington State University).

Although the international community agrees on which phenomena occur during glass alteration, insufficient data are available on alteration rates to understand which control long-term performance under which disposal conditions. These processes include:

- Ion exchange between solid glass and solution
- Surface-controlled reaction
- Transport of ions to and from reacting glass surface
- Impact of alteration product formation.

Representatives from the six major partners shared data, techniques, and theories at two international workshops associated with a major conference in May in Madison, Wisconsin, and in September in Sheffield, UK. The status of the series of collaborative research tasks were discussed. This effort resulted in the production of four research articles between different international teams during the year.

### JAEA-DOE

Collaboration with Japan on separations technology is carried out by the Civil Nuclear Working Group chartered under the U.S.–Japan Bilateral Commission on Civil Nuclear Cooperation. Japanese technical participation in the activities of the working group is primarily from JAEA, with occasional involvement of the Central Research Institute of the Electric Power Industry (CRIEPI).

The fourth meeting of the Civil Nuclear Working Group, as well as a steering committee meeting, was held at Oarai, Japan, in January 2016 to review action plans and initiate discussions on detailed collaboration topics. Three areas relative to MRWFD are part of the collaboration: aqueous separation from oxide fuels, borosilicate glass corrosion, and uranium extraction from seawater.

In 2016, branched alkylamide extractants synthesized at JAEA were shipped to INL for testing with Am(VI) extraction. A researcher from JAEA, Masahito Nakase, visited INL for 2 months and participated in testing of Am(VI) extraction with the branched alkyl monoamide (BAMA) ligands.

The objective of the borosilicate glass dissolution study is to improve the understanding of the mechanisms governing glass dissolution in different geological environments, leading to a robust and defensible model for calculating long-term radionuclide releases under potential disposal conditions. Near-term cooperation will focus on (1) identification of alteration rate acceleration mechanism and conditions, (2) investigation of the protective nature of glass alteration layers in closed or open systems, and (3) development of fully coupled reactive transport models to consider the long-term impacts on disposal environments. Detailed plans for three tasks were previously finalized, and collaborations continued throughout the year. Progress in FY 2016 was promoted through three technical expert meetings and joint research experiments. In Task 1, PNNL developed a novel in situ monitoring technique to detect rate acceleration conditions, while JAEA ran dynamic (flow-through) tests in a micro-channel reactor to quickly determine how ions other than silicon impact dissolution. The results from these techniques will be combined to improve understanding of alteration acceleration. In Task 2, layers from micro-channel flow-through tests performed at Kyushu University were evaluated with ellipsometry, secondary ion mass spectrometry (SIMS), and laser scanning microscopy at PNNL, and micro-Raman at JAEA. The results suggest that layers formed in near-saturation flowing conditions with a range of different solutes. A joint research article was drafted and is ready for submission. Research in Task 3 between both nations has developed reactive transport corrosion models that will be compared and benchmarked in the future Six-Nation Collaboration on Long-Term Performance of Glass.

## 2016 ACCOMPLISHMENTS

### OFFICE OF NUCLEAR ENERGY-OFFICE OF ENVIRONMENTAL MANAGEMENT COLLABORATION

A long-standing interaction exists between DOE-NE and DOE-EM, particularly in the areas of separations, waste forms, and disposal research. Many laboratory researchers work jointly for DOE-NE and DOE-EM, and many of the program objectives are similar. This close collaboration was formalized in 2011 by a memorandum of understanding between DOE-EM and DOE-NE for UNF and radioactive waste management and processing R&D. The memorandum of understanding, signed by Assistant Secretaries P. Lyons and I. Triay in March 2011, describes a policy of collaborative research and highlights several collaborative research tasks.

A joint DOE-EM/DOE-NE/international glass corrosion study started in 2010 and continued through 2016. In FY 2016, a joint DOE-EM/DOE-NE Integrated Research Project was funded at Rutgers University to understand the fundamental science governing the development and performance of nuclear waste glasses. Over the next 3 years, results will be generated at the nexus of the DOE-EM and DOE-NE objectives in waste glass design and testing.

## Nuclear Energy University Program (NEUP) Partnerships

### ACTIVE PROJECTS AWARDED IN 2013

Lead University	Title	Principle Investigator
Texas A&M University	Mixed Metal Phosphonate-Phosphate Resins for Separation of Lanthanides from Actinides	Abraham Clearfield
Pennsylvania State University	Glass Composition and Solution Speciation Effects on Stage III Dissolution	Carlo Pantano
University of Illinois at Chicago	Performance of a Steel/Oxide Composite Waste Form for Combined Waste Streams from Advanced Electrochemical Processes over Geological Time Scales	J. Ernesto Indacochea
Oregon State University	Organic Speciation and Interactions in ALSEP - 1 Step Partitioning Process of Minor Actinides, Lanthanides, and Fission Products	Alena Paulenova
Washington State University	Managing Zirconium Chemistry and Phase Compatibility in Combined Process Separations for Minor Actinide Partitioning	Nathalie Wall
University of North Texas	Molecular Dynamics-Based Simulations of Bulk/Interfacial Structures and Diffusion Behaviors in Nuclear Waste Glasses	Jincheng Du
University of Idaho	Off-Gas Treatment: Evaluation of Nano-Structured Sorbents for Selective Removal of Contaminants	Vivek Utgikar
University of California, Davis	Thermally and Chemically Responsive Nanoporous Materials for Efficient Capture of Fission Product Gases	Pieter Stroeve

## 2016 ACCOMPLISHMENTS

### ACTIVE PROJECTS AWARDED IN 2014

Lead University	Title	Principle Investigator
Rutgers University	Apatite- and Sodalite-Based Glass-Bonded Waste Forms for Immobilization of $^{129}\text{I}$ and Mixed Halide Radioactive Wastes	Ashutosh Goel
Clemson University	A New Paradigm for Understanding Multi-Phase Ceramic Waste Form Performance	Kyle Brinkman
Syracuse University	Sorption Modeling and Verification for Off-Gas Treatment	Lawrence Tavlarides
Colorado School of Mines	Controlling Hexavalent Americium – A Centerpiece to a Compact Nuclear Fuel Cycle	Jenifer Braley
University of California, Irvine	Combining Experiments and Simulations of Extraction Kinetics and Thermodynamics in Advanced Separation Processes for UNF	Mikael Nilsson
Georgia Institute of Technology	Zeolite Membranes for Krypton/Xenon Separation from Spent Nuclear Fuel Reprocessing Off-Gas	Sankar Nair
Ohio State University	Rare Earth Electrochemical Property Measurements and Phase Diagram Development in a Complex Molten Salt Mixture for Molten Salt Recycle	Jinsuo Zhang
University of Nevada, Reno	Effect of Metallic Li on the Behavior of Metals in Molten Salts	Dev Chidambaram

ACTIVE PROJECTS AWARDED IN 2015

Lead University	Title	Principle Investigator
Washington State University	Understanding Influence of Thermal History and Glass Chemistry on Kinetics of Phase Separation and Crystallization in Borosilicate Glass-Ceramic Waste Forms for Aqueous Reprocessed High-Level Waste	John McCloy
University of Nevada, Las Vegas	Purification of Zirconium Cladding Using a Chloride Volatility Process	Frederic Poineau
Missouri University of Science & Tech	Phase Separation and Crystallization of Complex Borosilicate Melts for Glass-Ceramic Waste Forms	Richard Brow
Colorado School of Mines	Kr/Xe Separation over Metal Organic Framework Membranes	Moises Carreon
University of Tennessee at Knoxville	Purification of Zirconium Tetrachloride from UNF Cladding	Craig Barnes
California State University, Long Beach	Elucidation of the Kinetics of Advanced Separation Systems	Stephen Mezyk
California State University, Long Beach	Building Quantitative Relationships between Ligand Structure and Its Reactivity with Organic Radical Species	Stephen Mezyk
Pennsylvania State University	Fundamental Electrochemical Properties of Liquid Metals in LiCl-KCl for Separation of Alkali/Alkaline-Earths (Cs, Sr, and Ba)	Hojong Kim

## 2016 ACCOMPLISHMENTS

### ACTIVE PROJECTS AWARDED IN 2016

Lead University	Title	Principle Investigator
Colorado School of Mines	Overcoming Kinetic Barriers to Actinide Recovery in ALSEP	Mark Jensen
Florida International University	Americium Separation by Electrochemical Oxidation	Chris Dares
Syracuse University	Mechanistic Understanding of Silver Sorbent Aging Processes in Off-Gas Treatment	Larry Tavlarides
University of Idaho	Advanced Electrochemical Separations of Actinide/Fission Products via the Control of Nucleation and Growth of Electrodeposits	Batric Pesic
University of Nevada, Reno	In Situ Raman Spectroscopy for Determining Actinide Speciation and Concentration	Dev Chidambaram
University of Utah	Immobilization of High-Level Waste Salt in Dechlorinated Zeolite Waste Forms	Krista Carlson

## MATERIAL RECOVERY AND WASTE FORM DEVELOPMENT

### FUEL RESOURCES PROJECTS AWARDED IN 2013

Lead University	Title	Principle Investigator
University of Texas at Austin	Cost and System Analysis of Innovative Fuel Resources Concepts	Erich Schneider
City College of New York	Recovery of Uranium from Seawater: Polymer-Supported Aminophosphinates as Selective Extractants	Spiro D. Alexandratos
Woods Hole Oceanographic Institution	Advances in the recovery of uranium from seawater: studies under real ocean conditions	Ken O. Buesseler
University of Chicago	Development of Novel Porous Sorbents for Extraction of Uranium from Seawater	Wenbin Lin
University of Idaho	Innovative Elution Processes for Recovering Uranium and Transition Metals from Amidoxime-Based Sorbents	Chien M. Wai
University of Alabama	Using Ionic Liquids for the Development of Renewable Biopolymer-Based Adsorbents for the Extraction of Uranium from Seawater and Testing Under Marine Conditions	Robin D. Rogers

### FUEL RESOURCES PROJECTS AWARDED IN 2014

Lead University	Title	Principle Investigator
University of California Berkeley	Selective ligands for uranyl via combinatorial peptoid libraries: A synthetic, structural, thermodynamic and computational study	John Arnold
University of South Florida	Functionalized Porous Organic Polymers as Uranium Nano-Traps for Efficient Recovery of Uranium from Seawater	Shengqian Ma
Georgia Institute of Technology	Optimizing Polymer-Grafted Amidoxime-based Adsorbents for Uranium Uptake from Seawater	Sotira Yiacoumi
Massachusetts Institute of Technology	Extraction of Uranium from Seawater: Design and Testing of a Symbiotic System	Alexander H. Slocum

## 2016 ACCOMPLISHMENTS

### FUEL RESOURCES PROJECTS AWARDED IN 2015

Lead University	Title	Principle Investigator
University of California Riverside	Quantitative Prediction of Uranium Speciation and Amidoxime Binding in Seawater from Advanced Simulation Techniques	De-en Jiang
University of Maryland	Enhancement of the Extraction of Uranium from Seawater	Mohamad Al-Sheikhly

## Reference Technologies and Alternatives

### SOLVENT DEGRADATION MECHANISMS

*D. R. Peterman and J. D. Law (INL)*

Researchers at INL are studying the impacts of gamma radiolysis on the actinide lanthanide separation (ALSEP) extraction process. The ALSEP process was developed through a joint collaboration between ANL and PNNL (Gelis and Lumetta 2014, Lumetta et al. 2014). This process uses an organic solvent consisting of a neutral diglycolamide extractant, *N,N,N',N'*-tetraoctyldiglycolamide (TODGA) or *N,N,N',N'*-tetra(2-ethylhexyl)diglycolamide (T2EHDGA), and an acidic extractant 2-ethylhexylphosphonic acid mono-2-ethylhexyl ester (HEH[EHP]) dissolved in an aliphatic diluent. The actinides and lanthanides are co-extracted from relatively high nitric acid, and the actinides are selectively stripped using a carboxylic acid buffered aminopolycarboxylic acid solution. The structures of the compounds used in the ALSEP process organic phase are depicted in Figure 1.

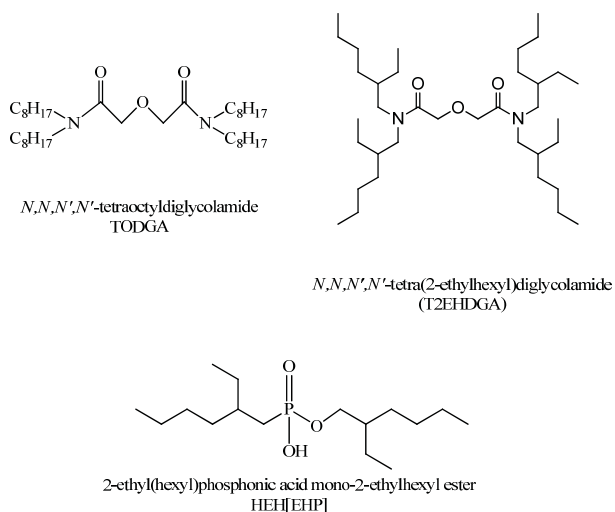


**Figure 1. Structures of compounds used in the ALSEP process.**

During FY 2015, the solvent degradation mechanisms experimental program at INL focused on examining two different ALSEP solvent compositions irradiated in contact with different aqueous-phase acidities. The ALSEP solvent compositions studied contained 0.040 M T2EHDGA + 0.60 M HEH[EHP] dissolved in n-dodecane or 0.050 M T2EHDGA + 0.75 M HEH[EHP] dissolved in n-dodecane; these are denoted as ALSEP A and ALSEP B, respectively. Static irradiation experiments were designed in order to irradiate the ALSEP A and B solvent while in contact with either 2 M or 4 M nitric acid (Peterman et al. 2015). During FY 2016, research efforts focused on the analysis of these ALSEP static irradiations. The results of these analyses were used to finalize the aqueous and organic phase compositions that were utilized for the ALSEP test loop irradiation experiments performed in FY 2016. The original plan was to conduct one test loop experiment (ALSEP B in contact with 4 M nitric acid); however, three additional tests were completed. The ALSEP test loop experiments performed were:

## 2016 ACCOMPLISHMENTS

- Irradiate ALSEP B in contact with 4 M nitric acid
- Irradiate ALSEP B in contact with 2 M nitric acid
- Irradiate ALSEP B in contact with a scrub diluted feed
- Conduct ALSEP B 4 M nitric acid hydrolysis.

For each of these test loop irradiations, the solvent systems were exposed to approximately 0.8 MGy total absorbed gamma dose, which corresponds to 180 hours of test loop operation per test.

The impact of gamma radiolysis was evaluated by determining americium, europium, and cerium distribution ratios ( $D_M = [\text{Metal}]_{\text{org}}/[\text{Metal}]_{\text{aq}}$ ) for each solvent system as a function of absorbed gamma dose. Plots of the variation of determined values of  $D_{\text{Am}}$ ,  $D_{\text{Eu}}$ , and  $D_{\text{Ce}}$  as a function of absorbed dose for the 4 M nitric acid, 2 M nitric acid, and scrub diluted feed test loop experiments are shown in Figure 2.

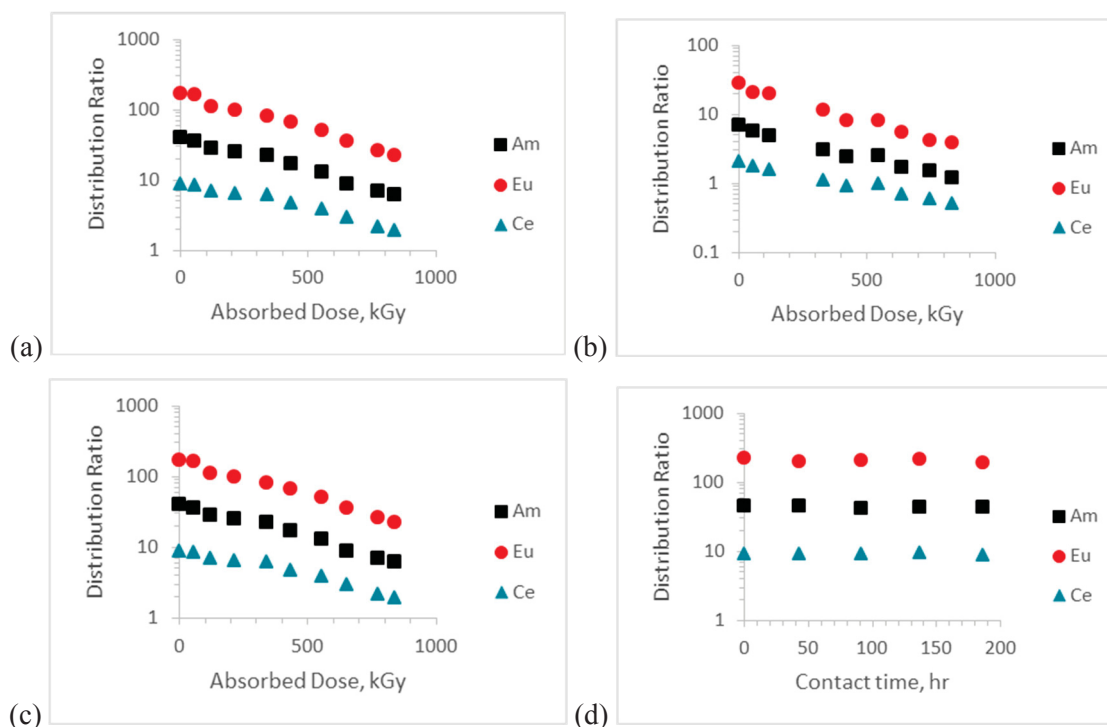


**Figure 2. Values of  $D_{\text{Am}}$ ,  $D_{\text{Eu}}$ , and  $D_{\text{Ce}}$  determined as a function of absorbed dose for the test loop irradiation of 0.050 M T2EHDGA/0.75 M HEH[EHP]/n-dodecane (ALSEP "B") in contact with (a) 4.0 M nitric acid, (b) 2.0 M nitric acid, (c) ALSEP scrub diluted feed, and (d) 4.0 M nitric acid without gamma irradiation.**

For each ALSEP “B” solvent system irradiated, gamma-irradiation does result in radiolytic degradation of the ALSEP solvent. However, it should be noted that the impacts of radiolytic degradation on the efficacy of the ALSEP process appear to be relatively minor. The possible impacts of hydrolytic degradation of the ALSEP solvent due to prolonged contact with nitric acid was evaluated by determining values of DAM, DEu, and DCe as a function of contact time with 4 M nitric acid. This experiment was performed in the INL test loop without gamma irradiation. The values of the distribution ratios determined for the ALSEP hydrolysis test are also presented in Figure 2. The highest contact time shown in Figure 2d (~185 hours) would correspond to an absorbed dose of ~ 560 kGy. The distribution data presented in Figure 2d clearly demonstrate that hydrolytic degradation processes will not adversely impact the efficacy of the ALSEP solvent extraction process.

### References

Gelis, A. V., and G. J. Lumetta, 2014, “Actinide Lanthanide Separation Process—ALSEP,” *Industrial and Engineering Chemistry Research*, Vol. 53, pp. 1624–1631.

Lumetta, G. J., A. V. Gelis, J. C. Carter, C. M. Niver, and M. R. Smoot, 2014, “The Actinide-Lanthanide Separation Concept,” *Solvent Extraction and Ion Exchange Journal*, Vol. 4, No. 32, pp. 333–347.

Peterman, D. R., L. G. Olson, and R. G. McDowell, 2015, *Gamma Irradiation of the ALSEP Process Solvent*, FCRD-MRWF-2015-000238, Idaho National Laboratory, September 30, 2015.

### TRITIUM PRETREATMENT (NON-AQUEOUS)

*G. D. DelCul, J. A. Johnson, and B. B. Spencer (ORNL)*

The FY 2016 accomplishments regarding the development of a tritium pretreatment process were (1) a preliminary design of instrumentation, data acquisition, and controls; (2) a design of the kilogram-scale reaction equipment; and (3) fabricated primary reaction equipment components. These accomplishments were steps toward performing kilogram-scale (DelCul et al. 2016) experiments that will be performed at ORNL in the coming years. These experiments will help resolve questions related to scaled performance and cost.

A dry pretreatment process based on the oxidation of used nuclear fuel is being studied for the removal and capture of tritium and iodine (DelCul et al. 2015) prior to the fuel dissolution step. The process converts oxide fuel into a fine powder at low temperature using oxygen and nitrogen dioxide (NO<sub>2</sub>) as a shuttling agent. The powder product can be selected to be triuranium octoxide (U<sub>3</sub>O<sub>8</sub>), uranium trioxide (UO<sub>3</sub>), or a nitrated form of uranium by adjusting the processing conditions. The UO<sub>3</sub> dissolves readily in HNO<sub>3</sub> without gas evolution, allowing for a rapid “fumeless” dissolution that can produce higher concentrations of uranyl nitrate at lower acidities than may be obtained from direct dissolution of uranium dioxide (UO<sub>2</sub>). Therefore, the dissolution time can be shortened from several hours to minutes while also reducing the volume and acid concentration of the dissolver solution and generating a dissolver product with higher actinide concentration. The latter advantage potentially translates into smaller tankage and less volume of residual raffinate waste, decreased facility footprint, and reduced facility cost. Both the UO<sub>3</sub> and the nitrated form can be readily dissolved by an organic solvent (e.g., tributyl phosphate [TBP]), leaving behind most of the fission products that remain insoluble, greatly reducing the volume of the high-acid raffinate waste stream.

## 2016 ACCOMPLISHMENTS

To date, all of the major tenets of the process to convert from pellets to oxide or nitrate have been tested and successfully corroborated at kilogram scale with surrogate materials. Inline trapping of iodine and water, and direct extraction by TBP of either the oxide or nitrate forms, has been tested at laboratory scale with surrogate materials.

### System and Equipment Design

The experimental system will utilize NO and O<sub>2</sub> to produce NO<sub>2</sub> reactant gas, which will oxidize de-clad UO<sub>2</sub> fuel (to minimize variability). The NO<sub>2</sub> reaction system with gas recirculation is depicted in Figure 3. This schematic shows three primary in-cell reaction components, the reaction vessel (Figure 4), an intermediate reaction vessel for NO<sub>2</sub> generation, and recirculation pump. The planned instrumentation for the flowsheet shown in Figure 3 designated by the numbered instruments. A data-acquisition unit will be employed to monitor the data associated with these measurements. Due to the value of hot cell floor space, the equipment has been designed to be compact, as illustrated in Figure 4. The primary reaction vessel that has been fabricated (Figure 5) runs perpendicular to the recirculation pump, which is located below the reactor vessel on a tongue-and-groove removable sheet of aluminum. The primary reaction vessel and mixer rest above the stand to allow for easy manipulation. The intermediate vessel is housed on the opposite side of the base. The vessel will be removable, and the stand has a cylindrical lip to secure the vessel in place. The spacing of the recirculation pump and the intermediate vessel allows for the rotation of the reactor to empty product powder after reaction. The entire stand will be fabricated of aluminum for reduced weight for easier remote manipulation.

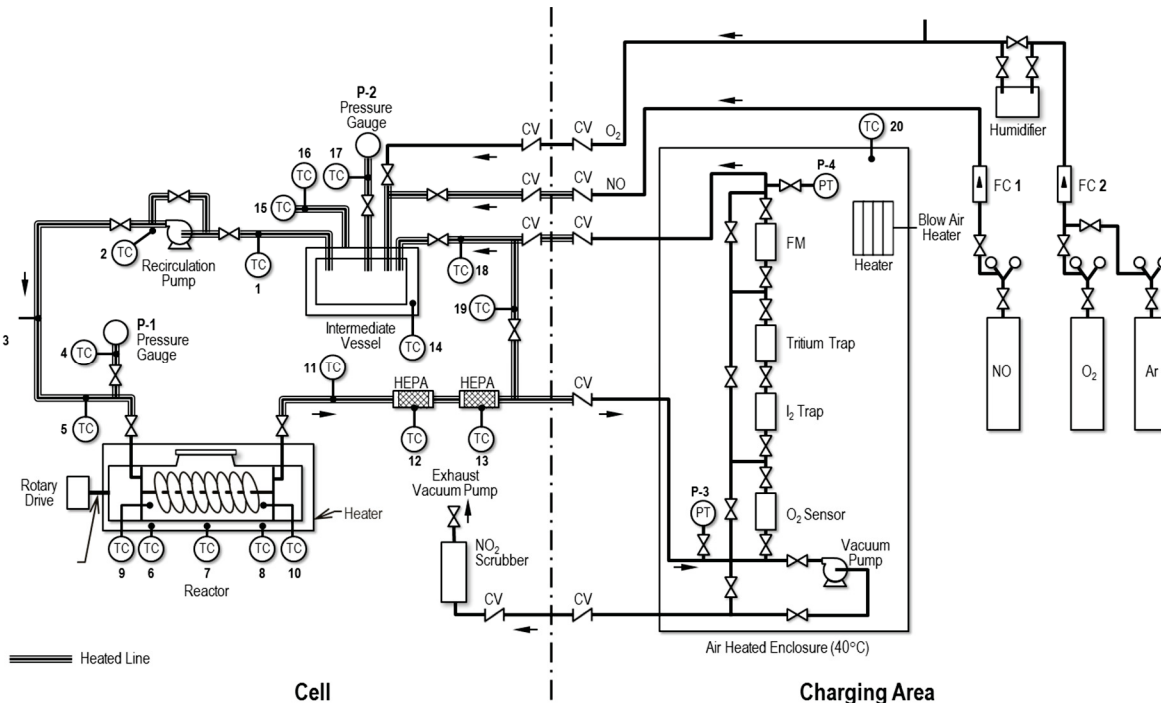


Figure 3. Flowsheet for NO<sub>2</sub> treatment at ORNL's Building 3525.



Figure 4. Stand design with primary components present.

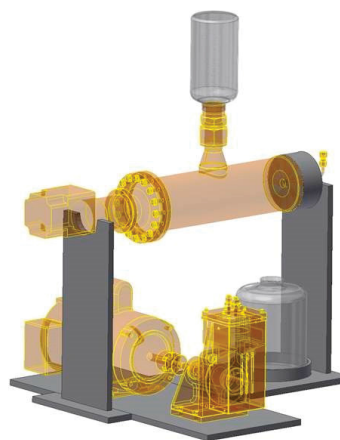


Figure 5. Primary reaction vessel and mixer.

The next steps likely to be performed in FY 2018 are to include fabrication of the frame; procurement of heating elements, instrumentation, and control equipment; and cold testing of the system before installation. As a result of the modularity, simplicity, and maneuverability of the system, it will serve as a versatile and durable reaction unit.

#### References

DelCul, G. D., B. B. Spencer, E. D. Collins, and R. T. Jubin, 2016, "A Flexible Advanced Dry Head-End for the Processing of Used Nuclear Fuel that Can Be Directly Interfaced to Solvent Extraction or Fluoride Volatility Separative Processes," *14th International Exchange Meeting on Actinide and Fission Product Partitioning and Transmutation*, San Diego, CA, October 17–20, 2016.

DelCul, G. D., R. D. Hunt, B. B. Spencer, J. A. Johnson, and R. T. Jubin, 2015, "Development of an Advanced Dry Head-end for the Processing of Used Nuclear Fuel," *39th Actinide Separations Conference*, Salt Lake City, Utah, May 18–21, 2015.

#### TRITIUM SEPARATION FROM AQUEOUS

*R. Bhave (ORNL)*

The release of tritium (as tritiated water [HTO]) from nuclear facilities poses a potential hazard to the environment. As a result, there is a need to control tritium release to the environment. The application of combined electrolysis and catalyst exchange (CECE) has been reported for tritium removal from water. CECE is generally recognized as the current state of the art for decontamination of tritium in light water and heavy water (HDO) nuclear power reactors where HDO is used both as a reactor moderator and coolant. For the CECE process, the processing cost for tritium recovery/concentration is directly proportional to the volume and also requires careful balance of concentration profiles in the column, which is packed with a hydrophobic catalyst and inert packing material to promote isotopic exchange between aqueous solution and gaseous hydrogen. Membrane-based tritium concentration, the subject of this effort, may offer several

## 2016 ACCOMPLISHMENTS

advantages over the current state of the art. The membrane system has low operating costs and is relatively easy to fabricate and directly scalable to handle large-volume, dilute streams. The low-cost operating features include separation and concentration at ambient temperature and low pressure compared to CECE or cryogenic distillation.

As discussed in the FY 2015 annual accomplishments report (INL 2015), the proof of principle research was performed for the separation and concentration of deuterated water using silica aluminophosphate (SAPO-34) molecular sieve zeolite membranes. Several SAPO-34 zeolite membranes were synthesized and evaluated for the separation and concentration of HDO. Ideal selectivity calculated from the measured deuterium concentrations (165 to 2,500 ppm) ranged from about 1.9 to 10.5, depending on membrane properties and operating conditions. The permeate was recovered under vacuum.

The separation factor of HTO over H<sub>2</sub>O is defined as:

$$\alpha_{HTO/H_2O} = \frac{C_{HTO}^P/C_{H_2O}^P}{C_{HTO}^F/C_{H_2O}^F} \quad (1)$$

where,  $C_{HTO}^P$  and  $C_{H_2O}^P$  are concentrations of HTO and H<sub>2</sub>O in the permeate, respectively, and  $C_{HTO}^F$  and  $C_{H_2O}^F$  are concentrations in the feed or retentate solution. Ideal selectivity is the ratio of vapor permeance (measured in GPU) of HTO over H<sub>2</sub>O. GPU (gas permeation unit); 1 GPU = 1 x10<sup>-6</sup> cm<sup>3</sup>/[cm<sup>2</sup>·sec·cm Hg].

The research focus in FY 2016 was on the evaluation of uncharged (neutral) SAPO-34 and cation exchanged (modified) SAPO-34 membranes to separate and concentrate HTO from dilute HTO-bearing aqueous streams. One of the approaches to increase the preferential diffusion of HTO is to vary the self-diffusion coefficient of water in zeolite pores by incorporating monovalent and divalent cations. It has been reported that the diffusion coefficient of water can be tuned by several orders of magnitude when the zeolite structure was exchanged with other cations such as Li<sup>+</sup>, Na<sup>+</sup>, K<sup>+</sup>, and Co<sup>2+</sup>. The objective of this effort is to reduce the pore size of the zeolite membrane by modifying the neutral SAPO-34 structure with selected monovalent and divalent cations. This is due to the fact that small-size polyvalent cations on zeolite framework sites interact strongly with water dipoles, allowing a more compact packing and ordering of water molecules in the pores. This is anticipated to substantially reduce the sorption and diffusion of H<sub>2</sub>O compared to HTO, leading to an increase in HTO selectivity over H<sub>2</sub>O. Reducing membrane thickness is another approach to reduce adsorption and increase permeance of HTO. These approaches would allow modification and optimization of the characteristics of cation-exchanged SAPO-34 membranes in terms of both adsorption and diffusion selectivity.

Hydrogen-exchanged H-SAPO-34 membranes were first prepared by secondary growth on disk-type  $\alpha$ -alumina supports (25.4-mm diameter and 1-mm thickness, CoorsTek). The substrates were seeded using the smaller-size (100 to 200 nm) SAPO-34 crystals via the steam-assisted conversion method. The seeded substrate was placed vertically in a Parr autoclave, and hydrothermal growth was carried out at 220°C followed by calcination at 600°C. The acetate salts of various cations (Li<sup>+</sup>, Na<sup>+</sup>, K<sup>+</sup>, and Co<sup>2+</sup>) dissolved in ethanol were used to introduce them in H-SAPO-34. Concentration of metal salts in ethanol was 0.05 M for monovalent cations and 0.01 M for divalent ions. The SAPO-34 membrane composition was estimated by energy dispersive spectroscopy (EDS) analysis and the amount of ion introduced in a single unit cell of

SAPO-34. For neutral SAPO-34, the composition was  $H_{1.5}Si_{3.9}Al_{16.8}P_{15.4}O_{72}$ , and for K-exchanged SAPO-34, it was estimated to be  $H_{0.1}K_{1.6}Si_{4.5}Al_{16.6}P_{14.9}O_{72}$ .

The SAPO-34 seed crystals and membrane were characterized by x-ray diffraction (XRD), and the synthesized membranes were tested for single-gas permeation in which the driving force is a pressure gradient. These data were used to calculate the membrane permeance and selectivity from a single gas-permeation unit. This was helpful to determine the desirable membrane properties in terms of selectivity and presence of defects. The XRD patterns were analyzed to confirm the previously known and established phase identification of the synthesized seed crystals. The krypton/xenon separation factor values for the monovalent and divalent cation-exchanged SAPO membranes were somewhat higher in the range of 15 to 25 compared to those reported for neutral SAPO-34 membranes where the separation ranged from 5 to 15. The higher ideal gas selectivity values may be indicative of the superior potential for achieving a preferential selectivity for HTO over  $H_2O$ .

Experiments were performed over a range of HTO concentration that corresponds to the range anticipated in a nuclear fuel processing system, including both acid and water recycle streams. The HTO concentration can be in the range of 200 to 1,000 Ci/m<sup>3</sup> or 0.2 to 1 mCi/mL. The HTO concentration at the upper end of the range was used in this study. On a comparative basis, these concentrations are at least 3 orders of magnitude lower than HDO concentration in HDO experiments. The tritium concentration of 1 mCi/mL corresponds to about 0.1 ppm HTO in the aqueous solution. The results are summarized in Table 1. The analysis of HTO concentration in the feed, retentate, and permeate from the pervaporation system was performed using liquid scintillation analyzer (LSA).

Experiments with HTO were performed using the neutral, monovalent K-exchanged, and divalent co-exchanged SAPO membrane. The feed HTO concentration was about 1 mCi/mL. In order to simulate the water recycle stream, pH was varied in the range of 4 to 7. Preliminary experiments show significantly higher (by a factor of 2 to 3) HTO and  $H_2O$  permeance values than those reported previously for the neutral SAPO-34 membrane. This is encouraging as high-vapor permeance combined with high selectivity and is critical to the development of a cost-effective tritium separation process. The HTO permeance was measured at 365 and 116 GPU for the co-SAPO-34 and the neutral SAPO-34, respectively. The calculated ideal separation factor (HTO/ $H_2O$ ) was 1.11. Optimization of membrane synthesis is ongoing, which may further improve selectivity and vapor permeance. Plans for experiments include comprehensive evaluations of modified (Na-, K-, Li-, and co-exchanged) SAPO membranes to increase vapor transport while maintaining preferential selectivity for HTO over  $H_2O$ . In FY 2017, efforts will also be directed to develop a better understanding of the mechanism for the separation of HDO along with the investigation of adsorption and transport of HTO and  $H_2O$  through the zeolite membrane layer. (Figure 6)

## 2016 ACCOMPLISHMENTS

TABLE 1. SEPARATION OF HTO WITH SAPO-34 AND K-SAPO-34 ZEOLITE MEMBRANES.

MEMBRANE	SAPO-34	SAPO-34	K-SAPO-34	CO-SAPO-34	CO-SAPO-34
pH	7	4	7	7	5
HTO in retentate (mCi/mL)	1.135	1.054	1.162	1.162	1.162
HTO in permeate (mCi/mL)	0.946	0.946	1.189	1.081	1.108
HTO permeance (GPU)	115.83	190.89	2087.12	365.15	371.39
H <sub>2</sub> O permeance (GPU)	116.01	177.50	1701.52	327.54	324.99
Separation factor	0.83	0.89	1.023	0.93	0.95
Ideal selectivity	0.998	1.08	1.23	1.11	1.14

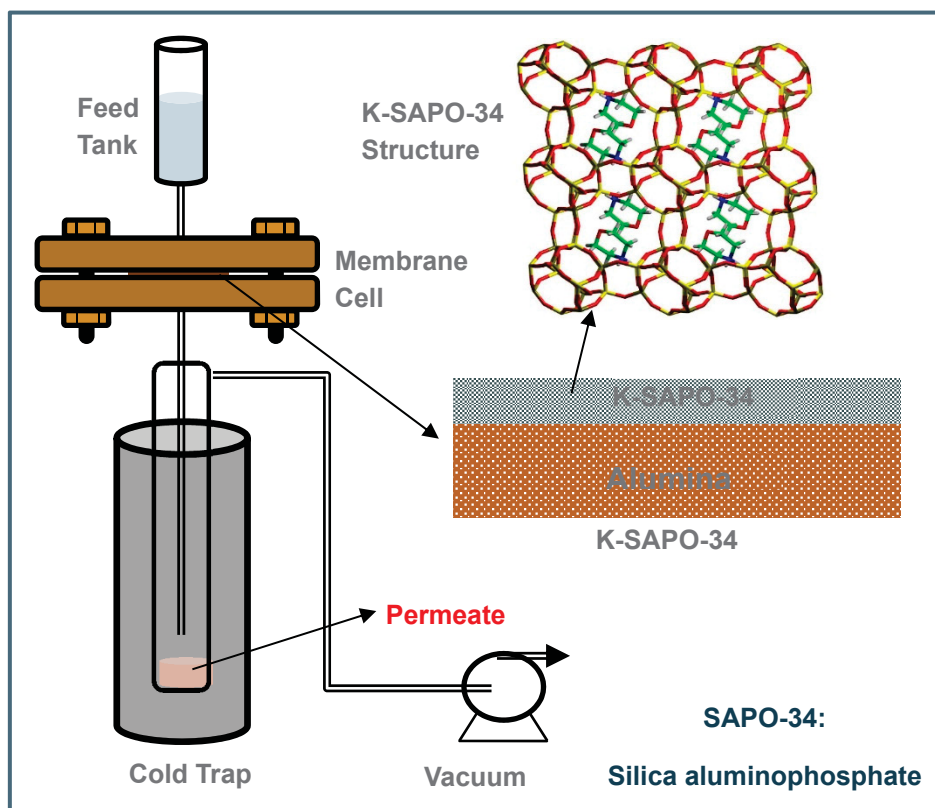


Figure 6. Schematic of the pervaporation system for the separation of HTO.

### Reference

INL, 2015, *Material Recovery and Waste Form Development 2015 Accomplishments*, INL/EXT-15-37053, November 2015.

## ONLINE SAMPLING AND MONITORING

*S. A. Bryan, A. J. Casella, and A. M. Lines (PNNL)*

PNNL, operated for DOE by Battelle Memorial Institute, has been investigating spectroscopic-based approaches for real-time, online monitoring of fuel cycle processes under the Fuel Cycle Research and Development program. The overall objective of this task is to obtain the fundamental information needed for the design of online, real-time, process spectroscopic instrumentation for use in monitoring and controlling fuel reprocessing flowsheets. The capability for continuous online monitoring provides the benefits of enhanced: accountability of fissile materials, control of the process flowsheet, information on flow parameters, solution composition and chemical speciation, performance and reduction of worker dose by eliminating the need for traditional analytical “grab samples.” Continuous online monitoring also improves operational and criticality safety and reduces opportunity for human error.

The first area of focus for FY 2016 was associated with the second-year continuation of the international collaboration between the Laboratory of Analysis and Material Metrology of the CEA in Marcoule France and PNNL for DOE. The purpose of the collaboration is to advance the technology for innovative in situ analytical measurements of lanthanides and actinides in solvent extraction media. FY 2016 focused on the application, measurement, and analysis of solutions in microfluidic cells. Figure 7 shows the schematic and photograph of the micro-Raman probe obtained by PNNL through a Small Business Innovation Research program collaboration for the purposes of integration with microfluidic cells as well as the resulting measurements within a microfluidic chip.

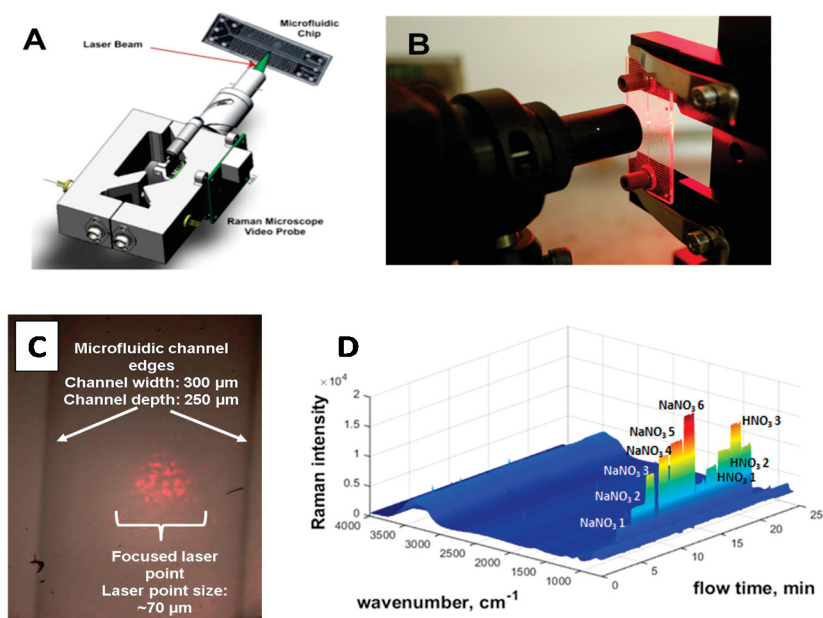


**Figure 7. (A) Schematic and (B) photograph of the micro-Raman probe focused on a microfluidic chip; (C) photograph taken through micro-Raman lens of the laser beam focused within the microfluidic device; and (D) Raman measurements of variable sodium nitrate/nitric acid solutions within the microfluidic chip.**

## 2016 ACCOMPLISHMENTS

Work using the micro-Raman probe involved the following: assessment of the detection limits of uranium and nitric acid solutions within a micro-flow cell and comparison of these limits with variable path-length cells; demonstration of calibration transfer to microfluidic-scale samples; integration of the micro-Raman technique with spectroscopic measurement within a microfluidic chip; and quantitative measurement of binary solutions containing sodium nitrate and nitric acid with a microfluidic chip using multivariate chemometric analysis of the micro-Raman measurements. The assembled micro-Raman probe with a micro-flow cell is shown in Figure 8A, with Raman spectra of various uranium and nitric acid solutions under flow conditions (Figure 8B) and model predictions for all solution species (Figure 8C).

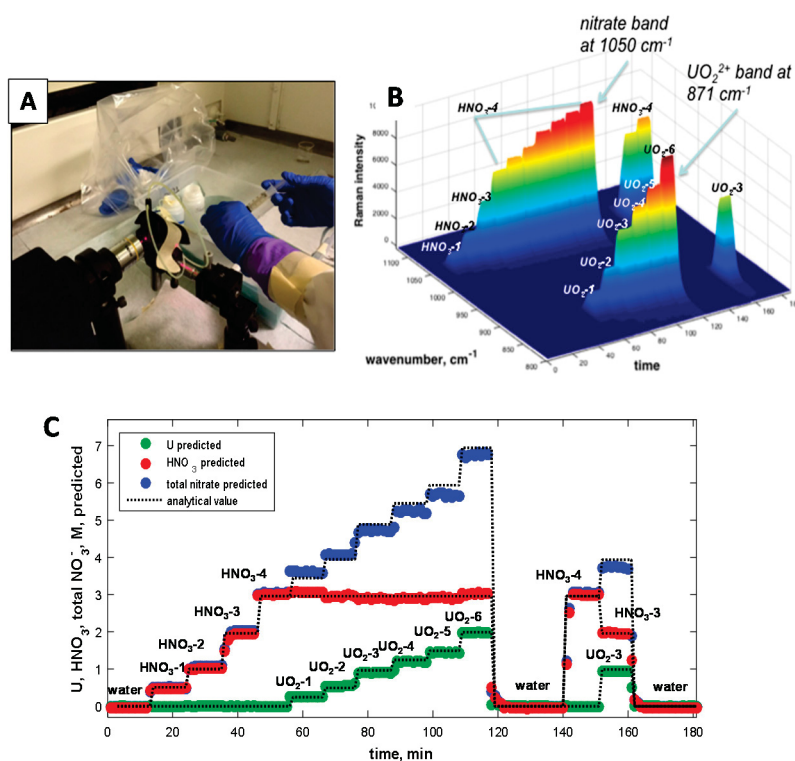


**Figure 8. (A) Photograph of the assembled micro-Raman probe with micro-flow cell during flow measurements; (B) Raman spectra from flow-cell experiment; and (C) model predictions of varying UO<sub>2</sub>(NO<sub>3</sub>)<sub>2</sub>, nitric acid, and total nitrate from solutions in 8- $\mu$ l micro-flow cells.**

The second focus area for FY 2016 involved the instrumentation and testing of online spectroscopic process monitoring equipment to measure metal extraction/separation processes. This instrumentation can be applied to mixer-settlers but was tested on a Lewis cell to determine kinetic parameters. A key result in FY 2016 was the discovery of an organic extraction phase lanthanide ion intermediate containing a higher number of coordinated waters of hydration compared to the bulk equilibrium phase metal species, as shown in Figure 9.

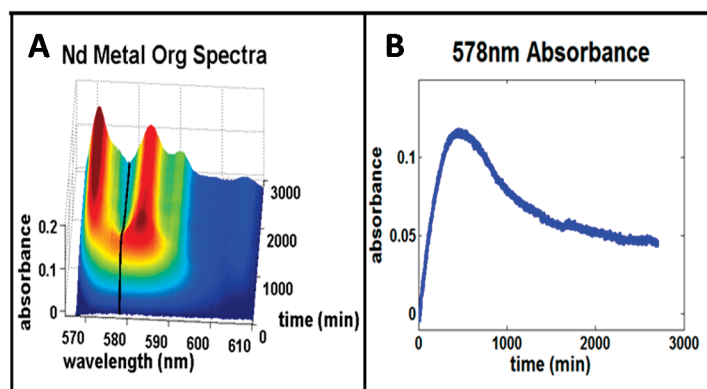


Figure 9. (A) Visible spectral variations of  $\text{Nd}^{3+}$  as a function of time for the organic phase and (B) changing maxima of the 578-nm peak from the organic spectra.

## LABORATORY-SCALE TESTING OF REFERENCE PROCESSES

*C. Pereira (ANL)*

The reference uranium/plutonium/neptunium recovery process, or co-decontamination, is centered on a co-extraction of uranium, plutonium, and neptunium from dissolved spent fuel, followed by selective stripping to recover product streams containing uranium/plutonium/neptunium and a second product stream containing the remaining uranium. The process requires predictable control of the behavior of the key species involved in the separations. In terms of flowsheet design, the major factors include controlling the uranium:transuranic (TRU) ratio in the uranium/plutonium/neptunium product, directing the majority of the neptunium to the uranium/plutonium/neptunium product, minimizing the extraction of fission products, and controlling technetium behavior. Laboratory-scale tests of the reference co-decontamination flowsheet conducted to date suggest that the fission products behave in a manner consistent with the behavior predicted using the Argonne Model for Universal Solvent Extraction (AMUSE) code.

In FY 2016, a new microfluidic solvent extraction system was developed and installed in a renovated radiological hood (Figure 10). A new system was required, because the older system is used extensively with alpha emitters that will significantly affect uranium and neptunium measurements, and that system is not capable of accurately measuring very fast kinetics, which is required for studying some TBP processes. The initial sets of tests on the new microfluidic system were run with a uranyl nitrate solution in order to eliminate the redox state as a variable in the extraction chemistry. Because of the convoluted neptunium extraction results attributed to a combination of redox chemistry, hydrodynamics, and interfacial phenomena, the focus this year was on characterizing the behavior of a systems for which the chemistry can be better controlled, specifically U(VI) in nitric acid in contact with TBP. The uranium tests would also shed light on any differences between observed behavior of individual species and those species in the presence of excess uranium. Unfortunately, the rapid kinetics of the higher acidity chemistries were found to be outside of the range that could be accurately measured by the microfluidic system (due to the limitations of membrane-based phase separation). The kinetics of the 3 M solutions were in a range that could be measured with the system; however, the effects of the unstable aqueous-organic interface (due to

## 2016 ACCOMPLISHMENTS

insufficient surfactant) could not be quantified. It was determined that other techniques may be more suitable for elucidating the complex extraction behavior of neptunium in the co-decontamination process.

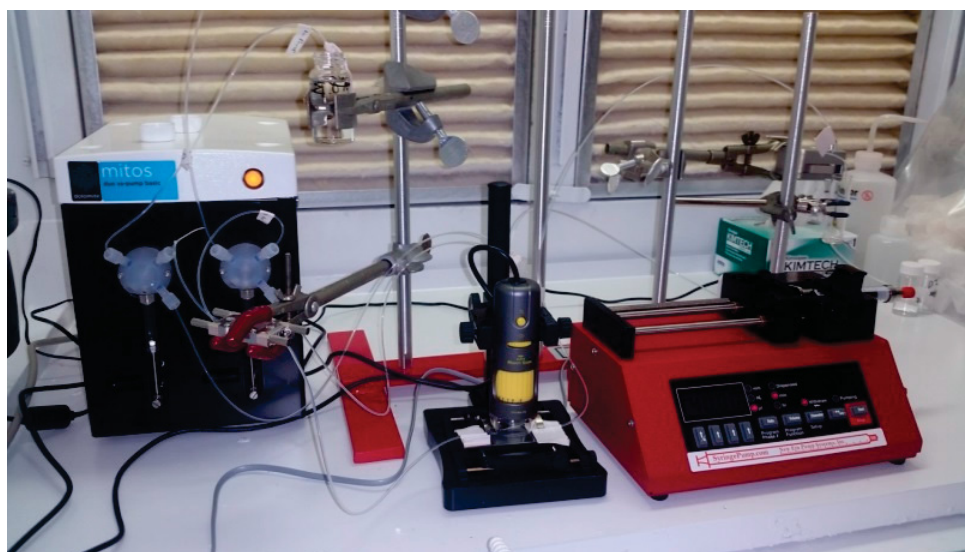


**Figure 10. Microsystem installed in refurbished radiological hood.**

An alternative approach is based on an electrode-based system to characterize redox chemistry. Once again, the behavior of uranium in contact with TBP was used to set a baseline prior to tests with plutonium, neptunium, and acetohydroxamic acid (AHA). The reduction of U(VI) to U(IV) was observed at approximately -0.95 V versus a platinum reference electrode. Because U(IV) prepared by electrolysis is used to reduce Pu(IV) to Pu(III), this is a simple method to quantify the uranium concentration in the feed or introduced as a reductant. The redox chemical interactions between Pu(IV) and U(IV) under an applied potential was studied and compared with the effect due to the presence of AHA. The separation factor ( $D_U/D_{Pu}$ ) was approximately 2.5 times higher when a potential was applied (124 versus 50) versus solely AHA (see Table 2).

**TABLE 2. COMPOSITIONS OF URANIUM AND PLUTONIUM, IN ELECTROCHEMICAL REDOX SYSTEM.**

Condition	Element	Organic Phase	Aqueous Phase	Distribution Ratio, D	Mass Balance
No Voltage	Pu	10%	89%	0.1	99%
Reduction @ -1 V	Pu	4%	95.5%	0.042	99.5%
Reduction @ -1 V	U	83.5%	16%	5.2	99.5%

To supplement the microfluidics tests, small-scale single-stage tests were run using a 1.25-cm long-residence time annular centrifugal contactor that was originally developed for americium-lanthanide separations (Figure 11) to better characterize the behavior of neptunium under the flowsheet conditions. The longer residence time was intended to overcome some of the limitations observed previously with the 2-cm standard design where changes in neptunium oxidation state were difficult to regulate. Under the conditions typical of co-decontamination processes, and absent oxidation or reduction, neptunium is present in nitric acid solution in multiple oxidation states and predominantly as inextractable Np(V). The reference flowsheet was based on maintaining conditions in the feed and the extraction section to promote conversion to extractable Np(VI). However, in process, the presence of nitrous acid induces the reduction of Np(VI) back to Np(V). In the experiment that was run, the effluents start with a relatively low D-value of 0.06, consistent with predominantly Np(V). Upon addition of oxidant, the D-value rises to 13.1 and then declines to  $D=7$  with nitrite reduction. The vanadium added to the feed is sufficient to oxidize essentially all of the neptunium to Np(VI), as evidenced by the increase in D-value.



**Figure 11. Photograph of a 1.25-cm, three-dimensional printed long-residence contactor used in testing.**

Because of the convoluted neptunium extraction results attributed to a combination of redox chemistry, hydrodynamics, and interfacial phenomena, the focus in FY 2016 was on characterizing the behavior of a system under which the chemistry can be better controlled, specifically U(VI) in nitric acid in contact with TBP. The very fast kinetics of uranium extraction by TBP proved problematic for the microfluidics approach used previously, so an alternative electrode-based microfluidics system was used to examine redox

## 2016 ACCOMPLISHMENTS

chemistry. The reduction of Pu(IV) to Pu(III) by U(IV) was easily measured, and the concentration of uranium in the solution was obtained by simply measuring the resulting current. Small-scale single-stage contactor tests were run to characterize the behavior of neptunium under the flowsheet conditions. The tests were run using a 1.25-cm long-residence time contactor neptunium behavior based on measured D-values consistent with the desired outcomes. The small-sized contactor did not appear to impact extraction and makes it much easier to carry out tests due to the reduced feed and waste requirements.

### LABORATORY-SCALE TESTING OF CANDIDATE PROCESSES

*J. D. Law (INL)*

Laboratory-scale testing research at INL is focused on evaluating the behavior of  $\text{TcO}_4^-$ , in the presence of other metals inherent to dissolved used fuel in the co-decontamination process for the separation of uranium and uranium/plutonium, as well as potentially neptunium and technetium. The extraction behavior of  $\text{TcO}_4^-$  in the co-decontamination process was assessed in the presence of metals that can strongly affect the  $\text{TcO}_4^-$  extraction. The presence of zirconium, ruthenium, and fluorine, as well as uranium, may affect the extraction product path for  $\text{TcO}_4^-$ . The concentration dependence of these metals and uranium has a direct impact as to whether the  $\text{TcO}_4^-$  follows the majority of the fission products or follows the uranium product stream. To this end, a series of solvent extraction batch contact flowsheet tests were designed to experimentally evaluate the behavior of the  $\text{TcO}_4^-$  within the co-decontamination process. Results from the previous year's experimental testing revealed that zirconium and technetium distributions differed from the projected AMUSE model results in the presence of a simulant containing many of the fission product metals. This year's research focused on controlling the concentrations of the key metals known to impact Tc extraction. Experiments were designed to pair technetium with individual metals, small groups of key fission products, and increased concentrations of key metals, such as zirconium, in order to evaluate the technetium distribution coefficients.

Experimental distribution coefficient data and computational values matched in many of the experiments performed, and it can be concluded that the AMUSE code predictions are within a reasonable margin of error calculated at  $\pm 3-20\%$  for technetium under most conditions, with the remaining fission product metals showing slightly lower than predicted extraction levels. Under specific conditions of the currently developed co-decontamination process flowsheet, AMUSE predicts technetium distribution coefficients considerably higher than experimental results indicate. An example of this is shown in Table 3 in which the distribution coefficients were measured for technetium at nitric acid concentration and zirconium concentration expected in the extraction section of the co-decontamination process. As can be seen from these results, the experimental technetium distribution coefficients were considerably lower than predicted by the AMUSE code. However, the experimental results still indicate the technetium will partition away from the raffinate as desired with this flowsheet. With future AMUSE modeling efforts for the co-decontamination flowsheet, one should be aware that AMUSE may overestimate the distribution ratios for technetium, and sensitivity studies should be performed to verify the overall behavior of technetium meets the desired results if the distributions were lower.

TABLE 3. ZIRCONIUM DEPENDENCE FOR TECHNETIUM SEPARATION. THE ORGANIC PHASE WAS PRE-EQUILIBRATED WITH 4.15 M HNO<sub>3</sub> ALONE AND WITH PRE-EQUILIBRATION USING 4.15 M HNO<sub>3</sub> CONTAINING 0.045 M ZIRCONIUM. THE O/A RATIO WAS VARIED BETWEEN 1.0 AND 1.9.

Sample Parameters	O/A	D <sub>Tc</sub>	AMUSE Model
Acid pre-equilibration in the presence of Zr	1.9	5.87	13.80
Acid pre-equilibration only	1.9	5.00	6.23
Acid pre-equilibration in the presence of Zr	1.0	5.80	14.10
Acid pre-equilibration only	1.0	5.41	8.57

### LABORATORY-SCALE TESTING OF CANDIDATE PROCESSES

*G. J. Lumetta, A. J. Casella, G. B. Hall, and T. G. Levitskaia (PNNL)*

Separating the lanthanide fission product elements from the minor actinide elements (americium and curium) at an industrial scale is one of the most daunting challenges to fully closing the nuclear fuel cycle (Hudson et al. 2013, Todd 2010). Because of the relatively large neutron cross sections of the light lanthanide elements, achieving this separation is necessary if the minor actinide elements are to be converted to short-lived or stable isotopes in fast reactors. Nearly all methods under investigation for separating the minor actinides from the lanthanides exploit the apparent slightly softer character of the trivalent actinide ions compared to the trivalent lanthanide ions. Thus, ligands containing nitrogen or sulfur donors have received considerable attention as agents to effect this separation (Hudson et al. 2013, Ekberg et al. 2008, Wang et al. 2001, Law et al. 2006). The ligands can be deployed in either the organic phase (as extractant) or in the aqueous phase (as an actinide-holdback reagent) in liquid-liquid extraction systems.

The Full Recycle Case Study that was performed in FY 2013 and then updated in FY 2014 and FY 2015 identified the TALSPEAK process (Weaver and Kappelman 1968, Nilsson and Nash 2007) as the primary candidate for separating the lanthanides from the minor actinides. The TALSPEAK process has previously been demonstrated at laboratory scale to separate the minor actinides from the lanthanides (Regalbutto 2011). However, the case study also identified a variation of the TALSPEAK process for potential near-term insertion into the fuel recycle flowsheet. In this variant of TALSPEAK, the traditionally used extractant, di-(2-ethylhexyl)phosphoric acid (HDEHP; Figure 12), is replaced with 2-ethylhexylphosphonic acid mono-2-ethylhexyl ester (HEH[EHP]; Figure 12) (Braley et al. 2012). This variant of the TALSPEAK process is now referred to as Advanced TALSPEAK. Experiments conducted at PNNL in FY 2013 to measure the equilibrium distribution ratios ( $D$  = concentration of the element in the organic phase divided by the concentration of the element in the aqueous phase) of americium and the lanthanide elements showed that Advanced TALSPEAK should be much more robust than conventional TALSPEAK with respect to variations in the aqueous phase pH. However, single-stage 2-cm contactor tests indicated the extraction of the lanthanide elements samarium, europium, and gadolinium was slow in the Advanced TALSPEAK system. The slow extraction of these elements led to ineffective separation from the trivalent actinide elements (Lumetta et al. 2015). For this reason, work in FY 2015 focused on exploring modifications to the Advanced TALSPEAK chemistry to increase the extraction rates for samarium, europium, and gadolinium. Work performed in FY 2016 built on the results of the batch extraction experiments performed in FY 2015, leading to single-stage flow-experiments and culminating in a successful Advanced TALSPEAK flowsheet experiment.

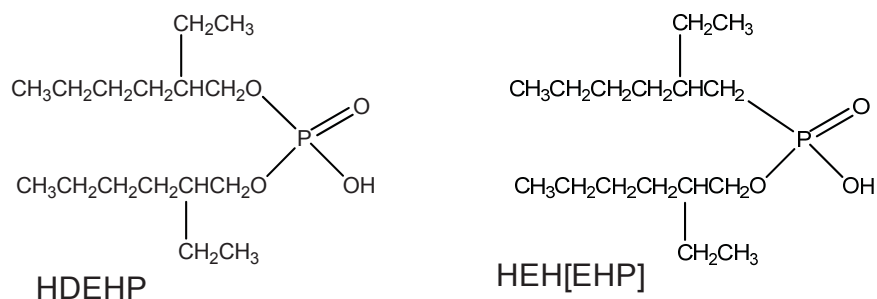


Figure 12. Chemical structures of the TALSPEAK (HDEHP) and Advanced TALSPEAK (HEH[EHP]) extractants.

### Process Concept

The Advanced TALSPEAK system operates by extracting the lanthanide ions into an aliphatic hydrocarbon phase containing HEH[EHP]. N-(2-hydroxyethyl)ethylenediamine-N,N',N'-triacetic acid (HEDTA; Figure 13) is added to the aqueous phase to suppress the extraction of americium and curium relative to the lanthanides. The soft amine donor groups in HEDTA preferentially bind the softer actinide ions, keeping them in the aqueous phase. Citric acid is also added to the aqueous phase to control the solution pH (Figure 13).

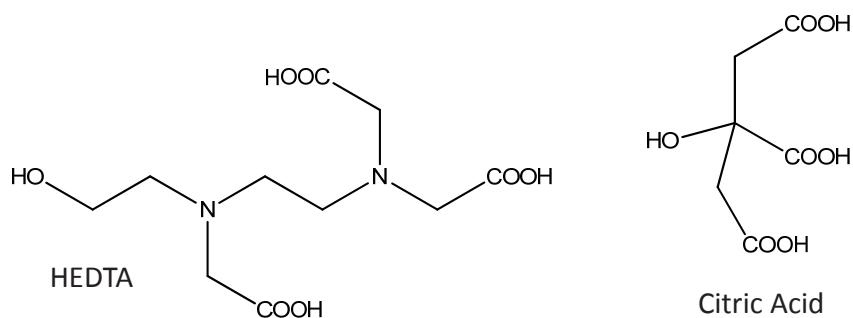


Figure 13. Chemical structures of the aqueous-phase complexant and buffers used in the Advanced TALSPEAK system.

### Objective

The objective of this work is to develop and demonstrate, at the bench scale, an Advanced TALSPEAK flowsheet for separating americium and curium from the lanthanide elements.

### Accomplishments

Two single-stage Advanced TALSPEAK experiments were conducted in FY 2016 to determine the stage efficiencies achieved in centrifugal contactors. In both of these experiments, aqueous solutions consisting of 0.125 mol/L HEDTA in a citrate buffer (pH 2.5 to 2.6) were used. The trivalent lanthanide elements added to the solution were lanthanum, cerium, praseodymium, neodymium, samarium, europium, and gadolinium. The solutions were also spiked with americium (<sup>241</sup>Am). The organic phase consisted of 1.0 mol/L HEH[EHP] dissolved in *n*-dodecane. The first experiment was performed at PNNL using a 2-cm centrifugal

contactor (Figure 14a). The extraction efficiency (defined as the distribution ratio measured in the contactor divided by the equilibrium distribution ratio obtained in batch contacts) in the 2-cm contactor was ~75% for most of the lanthanide elements examined. Europium and Gd displayed lower extraction efficiency, consistent with the previous reports of slow extraction rates for these elements (Lumetta et al. 2015). The americium distribution ratio measured in the 2-cm contactor was within 7% of the batch equilibrium value. Based on these results, an Advanced TALSPEAK flowsheet was designed, which was tested by Drs. Giuseppe Modolo and Andreas Wilden at FZ-J in Germany (see below).

The second single-stage Advanced TALSPEAK experiment was conducted at FZ-J using 1-cm centrifugal contactors (Figure 14b). Two different flow regimes were examined: a low flow of 10 mL/hour organic and 20 mL/hour of aqueous, and a high flow of 20 mL/hour organic and 40 mL/hour of aqueous. A substantial drop in performance for the 1-cm contactor occurred when the flow rates were doubled. The extraction efficiencies for samarium, europium, and gadolinium were particularly low at the higher flow rates. For this reason, the lower flowrate was chosen for the full countercurrent flowsheet test at FZ-J. Under the conditions of lower flow rate, the stage efficiencies for lanthanum, cerium, praseodymium, and neodymium were all higher in the 1-cm contactor than previously measured in the 2-cm contactor, and the stage efficiencies for samarium, europium, and gadolinium were comparable between the 1- and 2-cm contactors.

The Advanced TALSPEAK flowsheet was tested using the surrogate feed solution described above at FZ-J. In addition to <sup>241</sup>Am, the feed solution was also spiked with curium (<sup>244</sup>Cm) for the flowsheet experiment. The flowsheet test was very successful. Excellent separation of the lanthanide elements from americium and curium was achieved (Table 4). With the exception of Eu, the decontamination factors were on the order of 10<sup>4</sup> or greater. The concentration of europium in the raffinate was below the detection limit of the inductively coupled plasma mass spectrometry (ICP-MS) measurement. The values given in Table 4 are based on gamma spectroscopic analysis of a <sup>152</sup>Eu spike.

TABLE 4. DECONTAMINATION FACTORS ACHIEVED FOR THE SEPARATION OF THE LANTHANIDE ELEMENTS FROM THE MINOR ACTINIDE ELEMENTS (AMERICIUM AND CURIUM) DURING THE ADVANCED TALSPEAK FLOWSHEET TEST AT FZ-J.

LANTHANIDE	DECONTAMINATION FACTOR*	
	LANTHANIDE/AMERICIUM	LANTHANIDE/CURIUM
La	1.8 × 10 <sup>4</sup>	1.9 × 10 <sup>4</sup>
Ce	7.0 × 10 <sup>4</sup>	7.3 × 10 <sup>4</sup>
Pr	1.0 × 10 <sup>5</sup>	1.1 × 10 <sup>5</sup>
Nd	1.3 × 10 <sup>4</sup>	1.3 × 10 <sup>4</sup>
Sm	4.2 × 10 <sup>4</sup>	4.4 × 10 <sup>4</sup>
Eu	3.6 × 10 <sup>2</sup>	3.8 × 10 <sup>2</sup>
Gd	4.8 × 10 <sup>4</sup>	5.0 × 10 <sup>4</sup>

\*Decontamination factor for removal of the lanthanide element from the minor actinide product. Defined as (Ln/An)<sub>feed</sub> divided by (Ln/An)<sub>raffinate</sub> (An = Am or Cm).

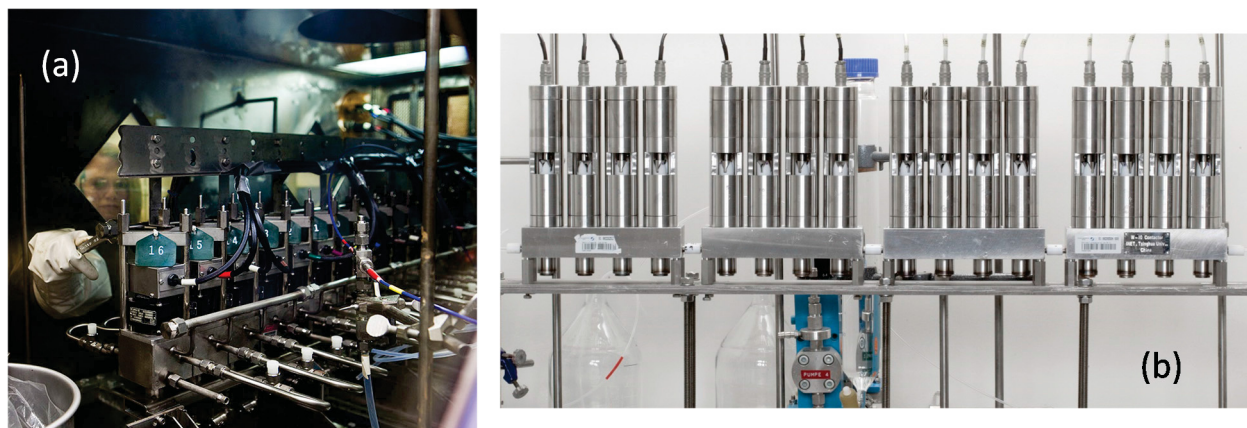


Figure 14. Centrifugal contactors used in the advanced TALSPEAK testing: (a) 2-cm centrifugal contactors at PNNL and (b) 1-cm centrifugal contactors used at FZ-J.

### Conclusions

An advanced TALSPEAK concept has been developed for separating americium and curium from the lanthanide fission products. Efficiently achieving this separation at an industrial scale will provide options to optimize geological disposal of the radioactive by-products from nuclear power production. The work conducted over the past several years in developing the advanced TALSPEAK concept has culminated in a successful countercurrent flow test of the concept. High efficiency was obtained in separating the trivalent actinides and lanthanides. Further development of this concept should include testing with actual irradiated fuel and developing protocols for solvent cleanup and recycle within the process.

### References

- Braley, J. C., Grimes, T. S., and Nash, K. L., 2012, "Alternatives to HDEHP and DTPA for Simplified TALSPEAK Separations," *Industrial and Engineering Chemistry Research*, Vol. 51, pp. 629–638.
- Ekberg, C., Fermvik, A., Retegan, T., Skarnemark, G., Foreman, M. R. S., Hudson, M. J., Englund, S., and Nilsson, M., 2008, "An overview and historical look back at the solvent extraction using nitrogen donor ligands to extract and separate An(III) from Ln(III)," *Radiochimica Acta*, Vol. 96, pp. 225–233.
- Hudson, M. J., Harwood, L. M., Laventine, D. M., and Lewis, F. W., 2013, "Use of Soft Heterocyclic N-Donor Ligands to Separate Actinides and Lanthanides," *Inorganic Chemistry*, Vol. 52, pp. 3414–3428.
- Law, J. D., Peterman, D. R., Todd, T. A., and Tillotson, R. D., 2006, "Separation of trivalent actinides from lanthanides in an acetate buffer solution using Cyanex 301," *Radiochimica Acta*, Vol. 94, pp. 261–266.
- Lumetta, G. J., Casella, A. J., Rapko, B. M., Levitskaia, T. G., Pence, N. K., Carter, J. C., Niver, C. M., and Smoot, M. R., 2015, "An Advanced TALSPEAK Concept using 2-Ethylhexylphosphonic Acid Mono-2-Ethylhexyl Ester as the Extractant," *Solvent Extraction Ion Exchange*, Vol. 33, pp. 211–223.

Nilsson, M., and Nash, K. L., 2007, "Review Article: A Review of the Development and Operational Characteristics of the TALSPEAK Process," *Solvent Extraction Ion Exchange*, Vol. 25, pp. 665–701.

Regalbuto, M. C., 2011, "Alternative separation and extraction: UREX+ processes for actinide and targeted fission product recovery," *Advanced Separation Techniques for Nuclear Fuel Reprocessing and Radioactive Waste Treatment*, Nash, K. L., Lumetta, G. J., Eds, Woodhead Publishing: Oxford, pp. 176–200.

Todd, T. A., 2010, "Separations Research for Advanced Nuclear Fuel Cycles," *Nuclear Energy and the Environment*; Wai, C. M. and Mincher, B. J., Eds; American Chemical Society: Washington, DC, pp. 13–18.

Wang, X., Zhu, Y., and Jiao, R., 2001, "Separation of Am from Macro Amount of Lanthanides by a Countercurrent Multistage Extraction with Purified Cyanex 301 and TBP," *Solvent Extraction Ion Exchange*, Vol. 19, pp. 1007–1015.

Weaver, B., and Kappelmann, F. A., 1968, "Preferential Extraction of Lanthanides Over Trivalent Actinides by Monoacidic Organophosphates from Carboxylic Acids and From Mixtures of Carboxylic Acids and Aminopolyacetic Acids," *Journal of Inorganic Nuclear Chemistry*, Vol. 30, pp. 263–272.

## TRITIUM CAPTURE STUDIES FOR ZIRCONIUM RECYCLE SYSTEM

*B. B. Spencer (ORNL) and S. H. Bruffey (ORNL)*

The zirconium recycle process releases radioactive tritium held in the metal matrix of used nuclear fuel. This tritium capture study was conducted to develop methods to capture the tritium to prevent its release to the environment. FY 2016 accomplishments were (1) completion of a literature review to discover the expected chemical compound containing the tritium; (2) narrowing of the identified chemical processes to those having the best chance of success; (3) designing, building, and testing prototype processes in the laboratory; and (4) recommending a process to support implementation of the experimental zirconium recycle system in a hot-cell environment.

Recovery of zirconium using a chlorination process is currently under development at ORNL. The approach is to treat the Zircaloy<sup>®</sup> cladding with chlorine gas to convert the zirconium in the alloy (~98 wt% of the alloy mass) to zirconium tetrachloride. The ZrCl<sub>4</sub> is volatile and readily separates from the nonvolatile alloy components and recoil embedded fuel fragments. Tritium trapped in the cladding matrix, presumably as zirconium hydride, is released as volatile <sup>3</sup>HCl. Based on predicted operating conditions, including chlorine feed rate, carrier gas flow rate (e.g., argon), estimated quantities of hydrides in the irradiated cladding, and total condensation of the volatile metal chloride products during zirconium recovery, an approximate off-gas composition was estimated as shown in Table 5. As shown, a tritium recovery process needs to recover tritium in the chemical form of <sup>3</sup>HCl at very low concentrations in the off-gas.

## 2016 ACCOMPLISHMENTS

TABLE 5. ESTIMATED COMPOSITION OF OFF-GAS STREAM FROM CLADDING CHLORINATION PROCESS.

Component	Concentration (v/v)
Ar	0.925
Cl <sub>2</sub>	0.0476
HCl	1.19E-06
<sup>2</sup> HCl	5.83E-10
<sup>3</sup> HCl	2.66E-06
TOTAL	1.000
<sup>all</sup> HCl	3.85E-06

### Accomplishments

Two methods to remove the tritium were identified for testing, a chemical conversion with trapping and aqueous scrubbing (Spencer et al. 2016a). Proof-of-principle experiments were designed to demonstrate HCl recovery with both potential processes using a nonradioactive simulant off-gas stream containing deuterium chloride (DCl). The chemical conversion process was designed such that the simulated off-gas stream would pass through two heated solid beds, with the first bed containing finely divided copper shot, or steel wool, to convert DCl to D<sub>2</sub> and the second bed containing CuO pellets to convert D<sub>2</sub> to D<sub>2</sub>O. Recovery of D<sub>2</sub>O was then accomplished by condensation. The liquid scrubbing process was designed to absorb the DCl from the gas stream using NaOH solution, which could be analyzed to determine the amount of deuterium that had transferred into the solution. Because of its lower solubility, most of the Cl<sub>2</sub> passes through the scrubber along with the inert carrier gas (argon).

Both methods were shown to recover deuterium from the simulant gas stream (Spencer et al. 2016b, 2016c). However, the recovery was not quantitative (~35% for both methods), indicating incomplete conversion, condensation, and/or scrubbing, or alternatively, losses of DCl to system components.

The liquid scrubbing system was selected for implementation in the planned hot-cell demonstration testing of the zirconium recycle process due to its simple design and lesser dependence on hot-cell utilities. The parts for the hot-cell scrubber were purchased from commercial sources, with materials of construction including glass and polymeric materials. An additional experimental test with DCl-containing simulant is planned prior to the hot-cell demonstration in an effort to quantify the recovery of DCl by a NaOH liquid scrubbing system.

### References

Spencer, B. B., D. G. DelCul, and S. H. Bruffey, 2016a, "Methods to Capture the Tritium Released by Recovery/Recycle of Zirconium from Used Fuel Cladding: A Review," *2016 ANS Annual Meeting*, New Orleans, Louisiana, June 12-16, 2016 (presented June 13, 2016).

Spencer, B. B., T. B. Walker, S. H. Bruffey, and G. D. DelCul, 2016b, *Capture of Tritium Released from Cladding in the Zirconium Recycle Process*, ORNL/TM-2016/444, also FCRD-MRWFD-2016-000297, UT-Battelle, Oak Ridge National Laboratory, August 2016.

Spencer, B. B., T. B. Walker, S. H. Bruffey, and G. D. DelCul, 2016c, *Capture of Tritium Released from Cladding in the Zirconium Recycle Process*, ORNL/TM-2016/531, also FCRD-MRWFD-2016-000016 and FCRD-MRWFD-2016-000297, Rev. 1, UT-Battelle, Oak Ridge National Laboratory, September 2016.

## PUBLICATIONS FOR REFERENCE TECHNOLOGIES AND ALTERNATIVES

Bryan S. A., A. J. Casella, A. M. Lines, G. L. Nelson, and J. M. Bello, 2015, "Advances in On-Line Monitoring for Measurement within Nuclear Fuel Reprocessing Streams," *Proceedings of GLOBAL 2015: 21st International Conference and Exhibition*, Paris, France, September 21–24, 2015, PNNL-SA-107043.

Bryan S. A., A. M. Lines, A. J. Casella, G. L. Nelson, F. Heller, and J. M. Bello, 2016, *FY 2016 Status Report: On-line Sampling and Monitoring*, PNNL-25656, Pacific Northwest National Laboratory.

Casella, A. J., A. M. Lines, G. L. Nelson, J. M. Bello, and S. A. Bryan, "MicroRaman Measurements for Nuclear Fuel Reprocessing Applications," *Procedia Chemistry*, PNNL-SA-117014, in press.

Casella, A. J., L. R. Hylden, E. L. Campbell, T. G. Levitskaia, J. M. Peterson, F. N. Smith, and S. A. Bryan, 2015, "Development of On-Line Spectroscopic pH Monitoring for Nuclear Fuel Reprocessing Plants: Weak Acid Schemes," *Analytical Chemical*, Vol. 87, No. 10, pp. 5139–5147.

DelCul, G. D., and J. A. Johnson, 2016, *Identify Instrumentation and Data Acquisition and Control Needs for the FY17 Hot Test*, (Official Use Only-Export Controlled Information-Applied Technology report), ORNL/LTR-2016/1, Oak Ridge National Laboratory, January 2016.

Johnson, J. A. and G. D. DelCul, 2016, *Reaction System Design for NO<sub>2</sub> Oxidation of Used Nuclear Fuel for the FY17 Hot Test* (Official Use Only-Export Controlled Information-Applied Technology report), ORNL/LTR-2016/355, Oak Ridge National Laboratory, August 2016.

Nee, K., S. Bryan, T. Levitskaia, J. W.-J. Kuo, and M. Nilsson, 2016, "Combinations of NIR and Raman Spectroscopy for Improved Monitoring of Material in Used Nuclear Fuel Separation Processes," submitted to *Chemical Engineering Science*.

Nelson, G., A. Lines, A. Casella, J. Bello, and S. Bryan, 2016, "Development and Testing of a Novel Micro-Raman Probe and Application of Calibration Transfer Method for the Quantitative Analysis of Microfluidic Nitric Acid Streams," submitted to *Analytical Chemistry*.

Peterman, D., and L. Olson, 2016, *Summary of ALSEP Test Loop Solvent Irradiation Testing*, INL/EXT-16-39626, Idaho National Laboratory, August 2016.

## 2016 ACCOMPLISHMENTS

Peterman, D. R., R. G. McDowell, C. A. Zarzana, K. M. Johnson, S. M. Rowe, and G. S. Groenewold, 2015, *Investigation of the hydrolytic and radiolytic degradation of HEH[EHP]*, FCRD-MRWFD-2016-000532, Idaho National Laboratory, February 26, 2015.

Peterman, D., A. Geist, B. Mincher, G. Modolo, M. H. Galan, Montano, L. Olson, and R. McDowell, 2016, "Performance of an i-SANEX System Based on a Water-Soluble BTP under Continuous Irradiation in a  $\gamma$ -Radiolysis Test Loop," *Industrial and Engineering Chemistry Research*, Vol. 5, No. 39, pp.10427–10435.

Riddle, C. L. and L. R. Martin, 2016, *Report on the Behavior of Fission Products in the Co-decontamination Process*, FCRD-MRWFD-2016-000570, Idaho National Laboratory, September 2016.

Schroll, C. A., A. M. Lines, W. R. Heineman, and S. A. Bryan, 2016, "Absorption Spectroscopy for Quantitative Prediction of Lanthanide Concentrations in 3 LiCl–2 CsCl Eutectic at 723 K," *Analytical Methods*, Vol. 8, pp. 7731–7738.

Schroll, C. A., S. Chatterjee, T. G. Levitskaia, W. R. Heineman, and S. A. Bryan, 2016, "Spectroelectrochemistry of  $\text{EuCl}_3$  in four molten salt eutectics; 3 LiCl – NaCl, 3 LiCl – 2 KCl, LiCl – RbCl, and 3 LiCl – 2 CsCl; at 873 K," *Electroanalysis*, Vol. 28, No. 9, pp. 2158–2165.

## Sigma Team – Advanced Actinide Recycle

The efficient separations technology ALSEP for minor-actinide separation has matured to demonstration-readiness; game-changing actinide separations concepts are emerging; and fundamental understanding provides key directions for improving americium separations. In FY 2016, the Sigma Team for Advanced Actinide Recycle (STAAR) has made important strides toward the overarching goal to develop more efficient separation methods for actinides in support of the DOE objective of sustainable fuel cycles. Research in STAAR has been emphasizing the separation of americium and other minor actinides (MAs) to enable closed nuclear fuel recycle options mainly within the paradigm of aqueous reprocessing of used oxide nuclear fuel dissolved in nitric acid. STARR's major scientific challenge involves achieving selective and efficient separation of trivalent actinides from lanthanides. Highlights of accomplishments in FY 2016 are as follows:

- A flowsheet has been designed for an upcoming demonstration of the ALSEP process for separating americium and curium from lanthanides and other fission products in a co-decontamination raffinate.
- Improved centrifugal contactor designs facilitated by three-dimensional (3-D) printing have led to faster ALSEP stripping, resulting in a 56% higher promethium/americium separation factor approaching equilibrium performance.
- Experiments have proven that the structure of the aqueous complexant used in ALSEP stripping can have a marked beneficial effect on kinetics, pointing to chemical alternatives for faster stripping.
- The first-ever oxidation of Am(III) to Am(VI) at an electrode in nitric acid was reported in the prestigious journal *Science*. Yields of up to 90% Am(VI) were achieved.
- The first-ever group co-crystallization of hexavalent actinides with  $\text{UO}_2(\text{NO}_3)_2 \cdot 6\text{H}_2\text{O}$  has been achieved, suggesting an alternative one-step separation method for homogeneous actinide recycle.
- A successful hot test of tandem Am(III) oxidation and extraction demonstrated the generation and immediate extraction of Am(VI) together with its recovery by reductive stripping.
- Powerful new mixed N,O-donor extractants have been synthesized for the extraction of Am(III) from lanthanides.
- Theoretical calculations have provided new understanding of actinide binding.

### ELECTROCHEMICAL OXIDATION OF AMERICIUM

*C. Dares, A. M. Lapides, T. J. Meyer (University of North Carolina at Chapel Hill [UNC-CH]), and B. J. Mincher (INL)*

The first-ever oxidation of Am(III) at an electrode in a noncomplexing acidic aqueous medium was reported in the prestigious journal *Science* (Dares 2015). This result provides a proof of principle for the first step of a desired process to separate americium from trivalent actinides and lanthanides by oxidation to Am(VI) followed by a suitable separation specific for hexavalent actinides. Given the difficulty in generating and stabilizing the highly oxidizing Am(VI) species in nitric acid, a variety of oxidation approaches are under investigation, including electrochemical techniques. Electrochemical methods would have the particular

## 2016 ACCOMPLISHMENTS

advantage of avoiding the addition of chemical oxidants and corresponding increase in high-level waste (HLW) mass.

The experiments utilized a commercial glass electrode coated in such a way as to bind Am(III) and facilitate its oxidation to Am(VI). The use of a phosphonic acid derivatized terpyridine ligand (Figure 15) proved to be effective in the electrolysis of Am(III), while underivatized control electrodes gave no oxidation of Am(III). A custom cell was designed to allow for the concurrent production and spectroscopic monitoring of electrochemically generated Am(VI) in that the light passes through the electrode itself. Using this configuration, up to 90% of a 1.5 mM solution of americium was successfully oxidized to Am(VI) with approximately 6% Am(V) and only 4% Am(III) (Figure 16).

The electrochemical approach to Am(III) oxidation has been taken up in a new Nuclear Energy University Program (NEUP) project at Florida International University (Dares 2015). The project will seek more efficient and more robust electrode materials and greater mechanistic understanding of the oxidation process toward potential application of the electrochemical concept in americium recovery from reprocessing streams.

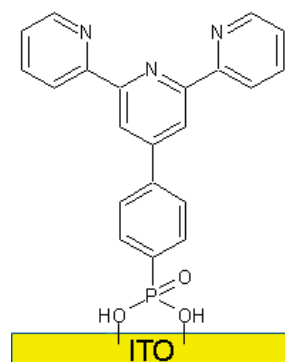


**Figure 15.** A terpyridine ligand bound to a tin-doped indium oxide particle on an electrode surface via a phosphonic acid linker.

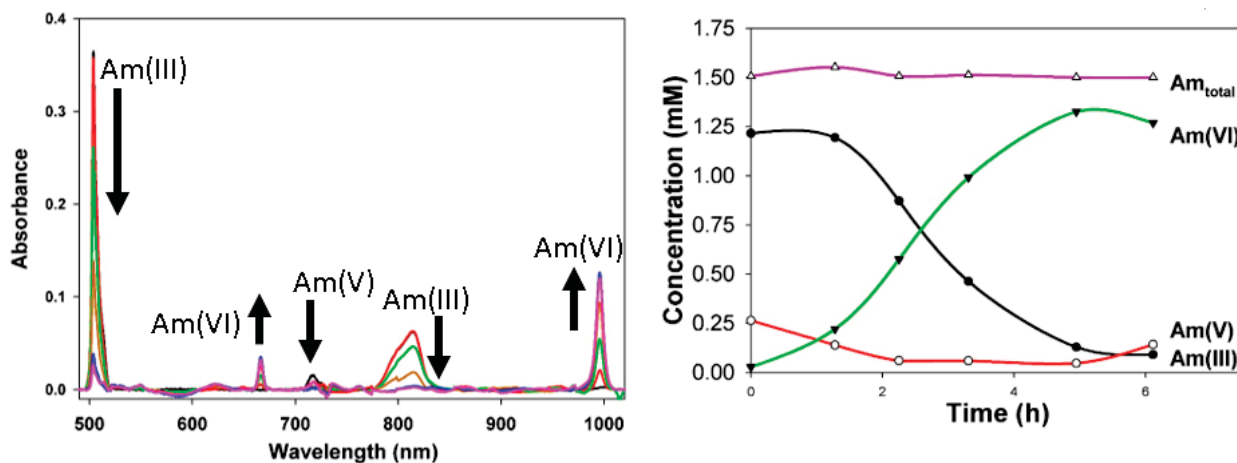


**Figure 16.** Electrochemical oxidation of Am(III) to Am(VI) with simultaneous spectroscopic monitoring occurring in the same compartment.

Conditions: 1.5 mM Am, 0.1 M HNO<sub>3</sub>, 1.0 M NaNO<sub>3</sub>, 2.5 V versus saturated calomel electrode.

## CONTACTOR DEMONSTRATION OF AM(VI) EXTRACTION AND STRIPPING

*B. J. Mincher, T. Grimes, R. Tillotson, and J. D. Law (INL)*

A hot test of tandem Am(III) oxidation to Am(VI) followed by solvent extraction was conducted, demonstrating that an immediate extraction of Am(VI) generated by an initial oxidation step can be accomplished together with a subsequent recovery of the extracted americium by reductive stripping. Following a previous test using the extractant diamylamyl phosphonate (DAAP) in a centrifugal contactor (Mincher 2016), the FY 2016 test pushed the envelope further by employing 3-D printed 2-cm contactors (Figure 17), adding an extra extraction and an extra strip stage, testing the alternative extractant *N,N*-di-2-ethylhexylbutyramide (DEHBA)/dodecane, and applying more aggressive stripping conditions. Sampling of the aqueous and organic effluents and the strip product stream of the test bed was performed at 2-minute intervals during the run, analyzing for americium and cerium by gamma spectrometry. At steady state, which was achieved within 3 minutes, 64% of the americium was extracted along with 98% of the cerium. Both metals were stripped quantitatively by the two stages of stripping with 0.1 M H<sub>2</sub>O<sub>2</sub>. The test enables the following conclusions: Am(III) can be oxidized by sodium bismuthate in a complex simulant, though some metals such as ruthenium may prove to be problematic. The oxidized feed solution can be filtered directly into centrifugal contactors. Extraction of Am(VI) may be successfully achieved using DEHBA as the extractant in dodecane, approximately as predicted by batch results. The co-oxidation Ce(III) and co-extraction of the product Ce(IV) occurs without apparent interference. The co-extracted Am(VI) and Ce(IV) are stripped efficiently together by 0.1 M H<sub>2</sub>O<sub>2</sub>.



**Figure 17. Contactor test bed for Am(VI) solvent extraction hot test featuring two countercurrent extraction and two countercurrent strip stages. The 2-cm contactors were 3-D printed, a new approach facilitating contactor testing.**

## GROUP CO-CRYSTALLIZATION OF HEXAVALENT ACTINIDE NITRATES

*J. D. Burns and B. A. Moyer (ORNL)*

The first-ever group co-crystallization of hexavalent actinides with  $\text{UO}_2(\text{NO}_3)_2 \cdot 6\text{H}_2\text{O}$  has been reported in *Inorganic Chemistry* (Burns 2016). Hexavalent neptunium, plutonium, and americium individually, and as a group, have all been co-crystallized with  $\text{UO}_2(\text{NO}_3)_2 \cdot 6\text{H}_2\text{O}$ , constituting the first demonstration of an An(VI) group co-crystallization. For homogeneous nuclear-fuel-recycle options, such a group separation makes possible a single uranium-TRU separation step using a single methodology, avoiding any use of solvents and potentially simplifying the very complex and costly combination of technologies otherwise needed to accomplish full actinide recycle. The crystallization principle follows in part from the development of the New Extraction System for TRU Recovery (NEXT) by JAEA in which the bulk of the uranium is removed from dissolver solution by crystallization prior to solvent extraction with tri-*n*-butylphosphate. The STAAR research shows that all of the hexavalent TRU actinides can be recovered as a group by co-crystallization with the uranyl nitrate.

Following the protocol shown in Figure 18, hexavalent dioxo cations of neptunium, plutonium, and americium were co-crystallized with  $\text{UO}_2(\text{NO}_3)_2 \cdot 6\text{H}_2\text{O}$  in near proportion by a simple reduction in temperature, while the lower valence states, An(III) and An(IV), were only slightly removed from solution, likely by simple entrainment. The separation was performed by cooling a solution initially containing 1.2 M [U(VI)], 0.74 mM [Np(VI)], 0.84 mM [Pu(VI)], and 0.99 mM [Am(VI)] at an acidity of 6.1 N to 2°C. Prior to preparing this mixture, sodium bismuthate had been used as the oxidant to bring the neptunium, plutonium, and americium to their hexavalent forms. After crystallization, centrifugation, and decantation,  $65 \pm 7\%$ ,  $62 \pm 6\%$ ,  $63 \pm 6\%$ , and  $62 \pm 6\%$  of U(VI), Np(VI), Pu(VI), and Am(VI) were found by ultraviolet-visible spectrophotometry to be removed from solution, respectively. In similar experiments, it was shown that Pu(IV) and Am(III) do not co-crystallize, indicating the specificity for hexavalent dioxo cations. On dissolution of the crystals in nitric acid in separate experiments, the Am(VI) was recovered nearly quantitatively. The highly oxidizing Am(VI) species is stable in the uranyl nitrate hexahydrate crystals for at least 2 weeks and persists in the uranyl hexahydrate solution matrix for days, easily long enough to permit multiple crystallizations. The selectivity of the co-crystallization concept was demonstrated in the presence of micro-curie levels of selected fission products, including potential troublemakers  $^{95}\text{Zr}$ ,  $^{95}\text{Nb}$ ,  $^{137}\text{Cs}$ , and  $^{144}\text{Ce}$ . While all of the hexavalent species were again removed from solution in near proportion, the fission products exhibited varying tendency to precipitate. Most notably,  $72 \pm 7\%$  of the  $^{95}\text{Nb}$  ( $t_{1/2} = 35$  d) crystallized from solution, presumably in the form of polymeric oxo Nb(V) species. Cerium is certainly present as  $\text{Ce}^{4+}$  and therefore could form the known double nitrate salt with  $\text{Cs}^+$ ,  $\text{Cs}_2\text{Ce}(\text{NO}_3)_6$ , and a similar mechanism for  $\text{Zr}^{4+}$  may be occurring. Dealing with fission product interferences will be a primary focus of work in FY 2017.

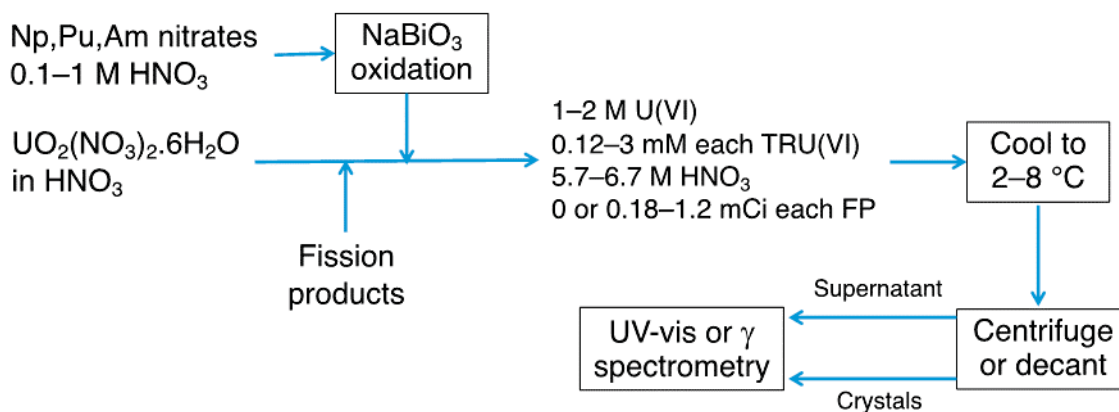


Figure 18. Experimental protocol used in the co-crystallization of hexavalent actinides separately or together, with and without fission products. Sodium bismuthate is used as the oxidant.

### STABILITY OF AMERICIUM(VI)

*C. Dares, A. M. Lapidés, and T. J. Meyer (UNC-CH)*

*B. J. Mincher, T. Grimes, R. Tillotson, and J. D. Law (INL)*

*J. D. Burns and B. A. Moyer (ORNL)*

*G. S. Goff (Los Alamos National Laboratory [LANL])*

Progress has been made in characterizing and understanding the stability of the higher oxidation states of americium in nitric acid solution. The stability of the highly oxidizing hexavalent state of americium in particular has become a key concern affecting the viability of separation approaches targeting the  $\text{AmO}_2^{2+}$  ion. The potentials needed to produce Am(VI) in solution are well in excess of that of water oxidation, and thus Am(VI) is inherently thermodynamically unstable. Coupon experiments have shown that many materials of equipment construction reduce Am(VI), and species such as  $\text{HNO}_2$  and  $\text{H}_2\text{O}_2$  expected to exist in strong nitric acid subjected to radiation (self-generated by americium as well as other radioactive species in solution) rapidly reduce Am(VI). In addition, chemicals and solvents introduced in carrying out separations of Am(VI) bring about its reduction. We are learning that Am(VI) stability to various conditions depends markedly on the method of oxidation. We are also learning that the reduction of Am(VI) is complicated, and a mechanistic understanding will require dedicated future effort. The ability of sodium bismuthate to act as its own holding oxidant confers unique benefits among the oxidants so far tested in stabilizing Am(VI). While the Bi(V) persists in solutions of Am(VI), co-crystallization with uranyl nitrate or even brief contact with certain extraction solvents can be carried out. The most successful extractant tested is DAAP, but DEHBA also appears promising. Crystallization with uranyl nitrate avoids use of organic compounds altogether. The following are some of the results from FY 2016 efforts on oxidation methods and stability of Am(V) and Am(VI):

- Subsequent to electrolysis of Am(III) to generate Am(VI) in 0.1 M  $\text{HNO}_3$ /0.9 M  $\text{NaNO}_3$ , autoreduction of the Am(VI) to Am(III) and Am(V) begins immediately, and though the behavior is not yet understood, the observed rate of disappearance of Am(VI) appears to be slow enough to allow separations

## 2016 ACCOMPLISHMENTS

(Figure 19). However, in contact with a solvent consisting of 1 M DAAP in dodecane, the Am(VI) is reduced in seconds.

- In acidic uranyl nitrate solutions (1–2 M U(VI), 5.7–6.7 M HNO<sub>3</sub>), Am(VI) prepared by sodium bismuthate oxidation appears to be reasonably stable over the timescale of crystallization experiments. A delay of 66 hours in the onset of autoreduction apparently corresponds to the depletion of residual Bi(V) in the system. In the co-crystallized form, Am(VI) hosted presumably as the americyl dioxo cation AmO<sub>2</sub><sup>2+</sup> in the uranyl nitrate hexahydrate crystals was found to be stable for at least 13 days.
- <sup>60</sup>Co radiolysis studies show that Am(VI) undergoes radiolytic reduction in nitric acid solution, providing our first understanding of the magnitude and mechanism of radiolytic processes affecting Am(VI) stability in simple solution. Experiments confirmed the radiolytic reduction of Am(VI), accompanied by a matching increase in Am(V) with only minor production of Am(III) prior to Am(VI) depletion. The apparent reduction is attributed to the products of aqueous HNO<sub>3</sub> radiolysis, though the mechanism is as yet unclear. It may be seen that Am(V) is the major product until Am(VI) is depleted, when Am(III) begins to grow in more rapidly.
- Promising alternative oxidation methods for conversion of Am(III) to Am(VI) were identified. Ozone catalyzed by the Co(II)/Co(III) and Ag(I)/Ag(II) couples proved to be functional, and a particularly interesting electrochemical oxidation of Am(III) to Am(VI) in nitric acid was observed using an ordinary commercial electrode.

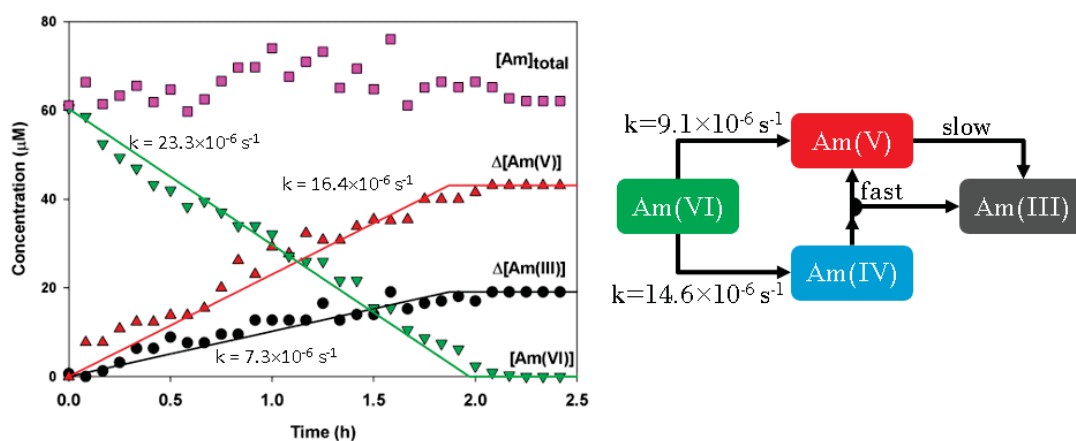


**Figure 19. Reduction kinetics for electrochemically generated Am(VI) and concurrent appearance of Am(V) and Am(III). Left: concentration profiles. Right: the modeled reduction path.**

### ALSEP PROCESS DEVELOPMENT FOR ACTINIDE/LANTHANIDE SEPARATION

*G. J. Lumetta, E. L. Campbell, A. J. Casella, G. B. Hall, V. E. Holfeltz, and T. G. Levitskaia (PNNL)  
M. A. Brown and A. V. Gelis (ANL)*

The ALSEP process concept (Lumetta et al. 2015) has been maturing within the STAAR program toward a bench-scale test in engineering equipment scheduled for FY 2017. ALSEP combines an acidic extractant with a neutral chelating extractant (Figure 20) to yield a single hybrid process for recovering the trivalent MA

elements americium and curium from acidic HLW raffinate generated by an initial co-decontamination step that removes the bulk of the uranium, plutonium, and neptunium. Interest in developing the ALSEP process stems from its potential to replace two separate processes previously required to achieve the MA separation, thus significantly simplifying a closed fuel cycle. The ALSEP concept involves (1) co-extracting the trivalent actinides and lanthanides, (2) selectively stripping the actinides from the loaded organic solvent, and (3) stripping the lanthanides and other fission products from the solvent. By design, the neutral extractant serves to co-extract the trivalent actinides and lanthanides from nitric acid solutions, while the acidic extractant serves to hold the trivalent lanthanides in the organic phase while americium and curium are selectively stripped into a carboxylate-buffered solution containing a polyaminocarboxylate complexant. Research results in ALSEP development have demonstrated the relative effectiveness of combinations of various candidate extractants, complexants, and buffers (Figure 20). Optimizing flowsheet design involving extraction, scrubbing, and stripping stages and controlling the behavior of the actinides, lanthanides, and fission products have been the object of efforts during the past 2 years, and single-stage tests in centrifugal contactors are in progress. In particular, improving the kinetics of stripping in the ALSEP process has risen to be the major focus with the goal to maximize the performance of ALSEP in upcoming demonstrations through chemical approaches and new contactor design. While the process in its current state with standard contactors is capable of carrying out the separation of the MAs from lanthanides, a major improvement could be achieved if stripping efficiency could be brought closer to that expected at equilibrium.

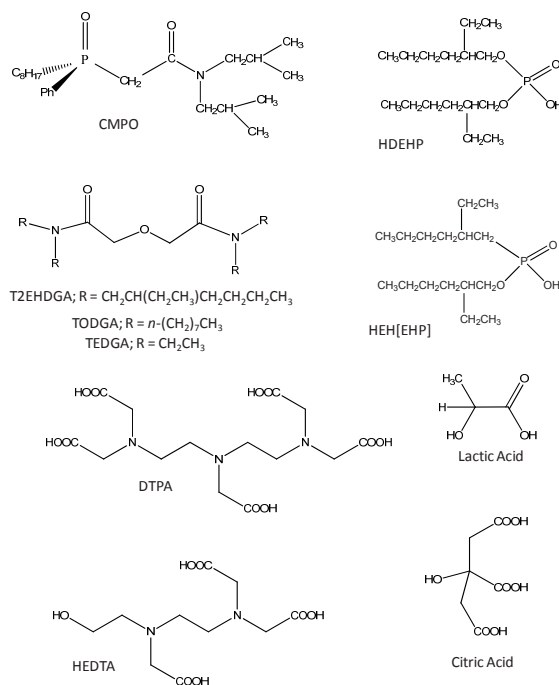


**Figure 20. Extractants and aqueous components used in the development of the ALSEP process. Neutral extractant carbamoylmethylphosphine oxide (CMPO) and cation-exchange extractant HDEHP together with aqueous complexant diethylenetriaminepentaacetic acid and lactic acid buffer were used in the initial TRUSPEAK concept. This formulation has given way to the more effective combination of T2EHDGA and HEH[EHP] with HEDTA complexant and citric acid buffer used in ALSEP. Research in FY 2017 may yet allow the identification of even more powerful ALSEP components.**

## IMPROVING THE STRIPPING EFFICIENCY OF ALSEP IN CENTRIFUGAL CONTACTORS

A. V. Gelis and M. A. Brown (ANL)

A successful approach to improving ALSEP stripping efficiency has been to modify the design of the centrifugal contactors used in stripping to increase the residence time in the mixing zone (Brown et al. 2016). Two designs of 2-cm contactors were tested in FY 2016, and it may be seen in Figure 21 that the effective distribution ratio achieved for americium stripping in the second design modification approaches that of the batch equilibrium value. By comparison, increasing the residence time by slowing down the flow rate at constant O:A = 3:4 has a much less dramatic effect. In the tests, the solvent was loaded using the PUREX (Plutonium Uranium Reduction Extraction) raffinate simulant prepared at PNNL. After loading, the solvent was scrubbed with nitric acid and then 0.75 M acetohydroxamic acid/0.2 M citrate buffer at pH 3 to remove molybdenum. The maximum promethium/americium separation factor achieved was 18 versus an equilibrium value of 23 in this system. By comparison, the best promethium/americium separation factor that was achieved in FY 2016 with the more selective but slower stripping complexant diethylenetriaminepentaacetic acid (DTPA) in a standard 2-cm ANL contactor was 11.5. Thus, a sizable increase of 56% in separation factor was enabled with the new contactor design. This result shows that the flowsheet performance of existing ALSEP process formulation can be greatly enhanced with redesign of the contacting equipment, thus compensating for the inherently slow stripping kinetics, but a drawback is the limited availability of the contactors having the new design. Particularly when fabricating industrial-scale equipment.

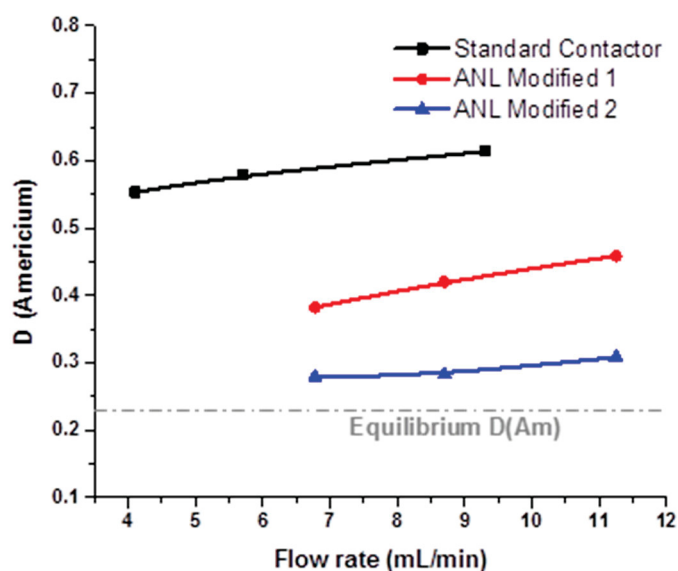


Figure 21. Stripping of Am(III) from loaded ALSEP solvent, 0.05 M T2EHDGA/0.75 M HEH[EHP] in dodecane, using 2-cm centrifugal contactors with standard and modified housings. Stripping conditions: 0.125 M HEDTA/0.2 M citrate solution at pH 2.8,  $T = 21^{\circ}\text{C}$ , O:A = 3:4.

A modified contactor with a smaller rotor diameter was also successfully demonstrated for ALSEP stripping. The 2-cm rotor diameter has been in widespread use in the DOE national laboratories since the 1980s, but even at this small size, typical solvent volumes required can be on the order of 1 L for multi-stage tests, and aqueous solution volumes consumed can be an order of magnitude greater. Figure 22 is a photograph of a new 3-D printed contactor with a rotor diameter of 1.25 cm. This new contactor requires significantly smaller volumes of the solutions for operation, thus minimizing waste volumes and the radionuclide inventory needed for a test. Using the unit shown, ALSEP stripping was successfully demonstrated for americium and the lanthanide promethium, feeding the organic and aqueous solutions to the contactor with a syringe pump. At an O:A ratio of 1:1, 0.6 mL/minute flow rate, and  $20.0 \pm 0.5^\circ\text{C}$ , the americium distribution ratio obtained was 0.23 compared with the batch equilibrium value of 0.22. The corresponding separation factor  $SF_{\text{Pm/Am}}$  was 20.3 in the contactor versus 23 on batch equilibration.



Figure 22. Photograph of a 3-D printed contactor with 1.25-cm rotor and extended mixing zone.

### IMPROVING THE STRIPPING CHEMISTRY OF ALSEP

*P. Zalupski, T. Grimes, C. Heathman (INL), and S. Jansone-Popova (ORNL)*

Results obtained in FY 2016 have proven the hypothesis that modifying the structure of the aqueous complexant used in ALSEP stripping can have a beneficial effect on kinetics. Research efforts in FY 2016 focused on the thermodynamic and kinetic assessment of two classes of aminopolycarboxylate (APC) reagents, as shown in Figure 23, where the nature of -R substitution has been varied. Multiple new APC candidates were synthesized at ORNL. For the amide-substituted class, where one acetate pendant arm was substituted by the *N*-dialkyl amide group, thermodynamic characterization of two reagents ( $R = -\text{CH}_2\text{CH}_3$ ,  $-\text{CH}_2\text{CH}_2\text{CH}_3$ ) indicated efficient aqueous complexation, but no phase-transfer kinetic benefits were observed. On the other hand, kinetic enhancement was observed within the amine-substituted APC reagents, where  $R = -\text{CH}_2\text{CH}_2\text{OH}$ ,  $-\text{CH}_2\text{CH}_2\text{CH}_2\text{OH}$ , and  $-\text{CH}_2\text{CH}_2\text{CH}_3$ , relative to the reference DTPA ( $R = -\text{CH}_2\text{COOH}$ , shown in Figure 23), though complexation was weaker than that of DTPA. The variant with  $R = -\text{CH}_2\text{CH}_2\text{OH}$ , referred to as *N*-hydroxyethyl-diethylenetriaminetetraacetic acid (HEDTTA), was examined in more detail in direct

## 2016 ACCOMPLISHMENTS

comparison to HEDTA (Figure 24) used in ALSEP. Due to the weaker complexation power of HEDTTA versus HEDTA, the HEH[EHP] concentration in the ALSEP solvent had to be lowered from 0.75 to 0.5 M to decrease  $D_{Am}$  for better stripping. As shown in Figure 24,  $Am^{3+}$  stripping equilibrium is attained approximately twice as fast for HEDTTA relative to that for HEDTA. Stripping selectivity for HEDTTA was found to be good:  $SF_{Am/Ce} = 35$  and  $SF_{Am/Eu} = 85$ .

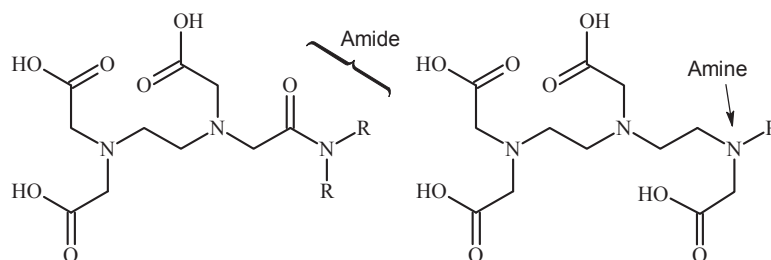


Figure 23. Structures of alternative aminopolycarboxylate reagents proposed to study phase-transfer kinetics.

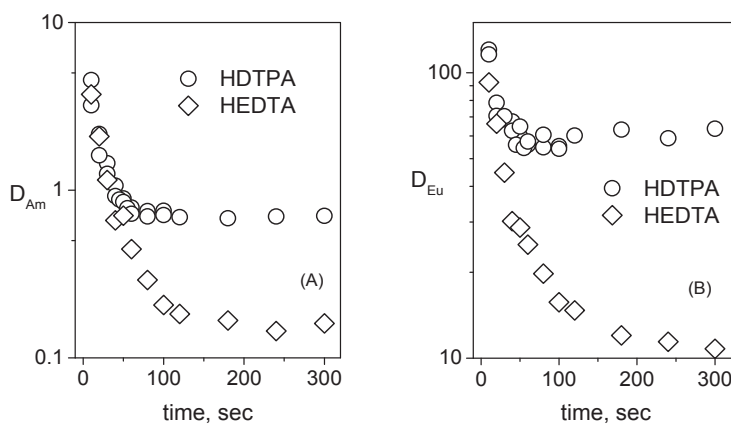


Figure 24. Americium (left) and europium (right) back-extraction kinetic trends collected for HEDTA and HEDTTA stripping systems. Organic phase: 0.05 M TEHDGA and 0.50 M HEH[EHP] in *n*-dodecane. Aqueous phase: 0.125 M complexant and 0.2 M citrate at pH = 3.0.

## MIXED-DONOR EXTRACTANTS

*S. Jansone-Popova, V. Bryantsev, F. V. Sloop, Jr., R. Custelcean, and B. A. Moyer (ORNL)*

New rigidified mixed *N,O*-donor extractants have been synthesized and shown to extract Am(III) with unusual avidity and selectivity versus trivalent lanthanides. Compared to ligands bearing all *N*-donor atoms, such as the bis(triazinyl)pyridine (BTP) family of extractants, mixed *N,O*-donor ligands are expected to offer stronger actinide binding, better stability to degradation, and less affinity for soft fission products (e.g., palladium and ruthenium). The question addressed by the research at this stage concerns the most promising design for the mixed-donor ligands, anticipating that the rigidity of the coordinating groups in mixed-donor ligands will lead to markedly enhanced strength in Am(III) extraction. To test this hypothesis, two novel preorganized bislactam 1,10-phenanthroline ligands **B** and **C** were synthesized and tested (Figure 25) for their extraction efficiency and selectivity in Am(III)/Eu(III) separation. Here are the conclusions based on the data obtained so far:

- Rigidification of two amide donor groups appended to 1,10-phenanthroline (**B** and **C** versus **A**) leads to strong Am(III) extraction at low-to-high nitric acid concentrations.
- The selectivity of **C** for trivalent actinide versus lanthanide is very high, with  $SF_{Am/Eu} > 1,000$  under some conditions, which is attributed to the presence of the double bond in the lactam rings and appended electron-withdrawing phenyl substituents.
- Five single-crystal x-ray structures of  $Pr^{3+}$ ,  $Nd^{3+}$ ,  $Eu^{3+}$ ,  $Gd^{3+}$ , and  $Tb^{3+}$  nitrates with a hexyl-substituted (versus octyl) analog of **B** showed formation of 1:1 monometallic complexes in which the metal is 10-coordinate and the coordination sphere is composed of the tetradentate 1,10-phenanthroline bislactam ligand and three bidentate nitrate ions.
- All ligands have good solubility in chlorinated solvents, 1-octanol, and nitrobenzene; however, good solubility in industrially preferred aliphatic diluents, such as Isopar and *n*-dodecane, has yet to be achieved.
- Both novel preorganized ligands **B** and **C** exhibit good stability in chloroform in the presence of 3 M nitric acid.

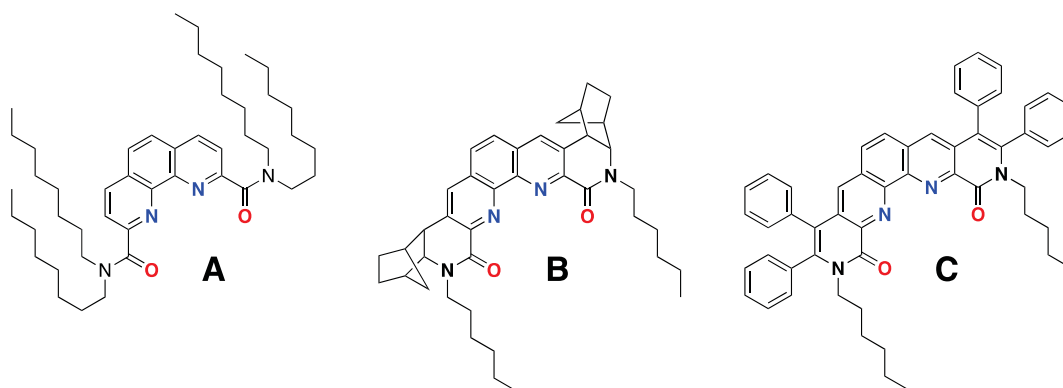


**Figure 25. Chemical structures of tetraoctyl-1,10-phenanthroline-2,9-dicarbonyl di-N-octylamide **A** and novel preorganized ligands **B** and **C**.**

## THEORETICAL PREDICTION OF AM(III) AND LN(III) BINDING

V. S. Bryantsev and A. A. Ivanov (ORNL)

Computational efforts have provided valuable insight into the effect of ligand structure on the binding affinity and selectivity of mixed *N,O*-donor ligands toward Am(III) and Ln(III) in terms of the energy cost of ligand reorganization upon binding (preorganization), internal electron-withdrawing effects in the ligand, and metal cation size (Ivanov and Bryantsev 2016). To simplify calculations using density functional theory (DFT), long chains were replaced by methyl groups. The most striking effect seen is due to preorganization, namely the effect of prepositioning of the binding groups in the rigid ligands **1b** and **2b** as compared with the flexible ligand **3b** in Figure 26. The oxygen atoms in **3b** are rotated in the opposite direction away from the binding cavity, and the energy cost of rotating them into the binding position is very large (19.1 kcal/mol). This effect may readily be understood visually from the structures shown in Figure 26. Each structure shown is an overlay of two separately calculated ligand structures corresponding to its unbound state and as complexed with Eu(III). It may be seen that the rigid **1b** and **2b** ligands overlay very precisely. The free and bound forms have nearly identical structure, so the energy cost to strain the ligands to bind the metal is very small (4.4 and 4.3 kcal/mol, respectively). However, ligand **3b** adopts the rotated structure in its free state and is predicted to strongly resist reorganizing to its binding geometry. The corresponding long-chain analog **C** indeed extracts Am(III) and Eu(III) very weakly as compared with **B** (Figure 25). DFT calculations also predict the observed stronger binding of **1b** versus **1a** according to the electron-withdrawing effect of the phenyl groups in **1a**. In addition, the calculations indicate that there should be a significant size effect in binding trivalent actinides and actinides, which will be more closely examined in the future both computationally and experimentally.

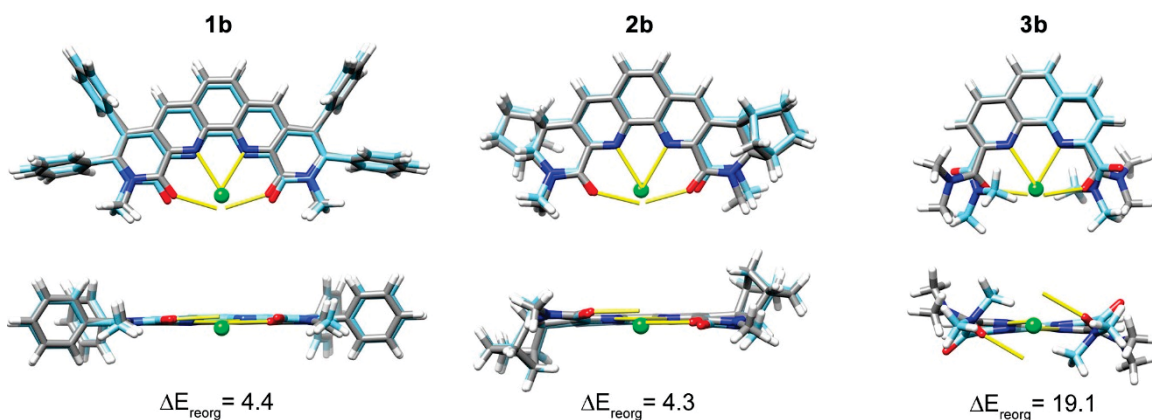


**Figure 26.** Overlays of calculated ligand geometries in their free (turquoise carbon backbone) and Eu<sup>3+</sup>-bound (grey carbon backbone) form and the corresponding reorganization energies,  $\Delta E_{\text{reorg}}$  (kcal/mol), associated with metal ion complexation. Vectors (yellow) emanating from the donor atoms illustrate the optimal placement of the metal ion relative to each donor group. The structures were optimized and energies calculated using DFT methods at the B3LYP/LC/6-311+G\*\* level. Note that **1a**, **2a**, and **3a**, respectively, correspond to the long-chain analogs **C**, **B**, and **A** in Figure 25.

## PUBLICATIONS FOR SIGMA TEAM – ADVANCED ACTINIDE RECYCLE

- Brown, M. A., K. E. Wardle, G. J. Lumetta, and A. V. Gelis, 2016, "Accomplishing Equilibrium in ALSEP: Demonstrations of Modified Process Chemistry on 3-D Printed Enhanced Annular Centrifugal Contactors," *Procedia Chemistry*, Vol. 21, pp. 167–173.
- Bryantsev, V. S., A. A. Ivanov, S. Jansone-Popova, and B. A. Moyer, 2016, *Using First-Principles Calculations to Facilitate the Design of Ligands for Actinide Separation*, FCRD-MRWFD-2016-000310, Oak Ridge National Laboratory, August 2016.
- Burns, J. D. and B. A. Moyer, 2016, "Group Hexavalent Actinide Separations: A New Approach to Used Nuclear Fuel Recycling," *Inorganic Chemistry*, Vol. 55, No. 17, pp. 8913–8919, DOI: 10.1021/acs.inorgchem.6b01430.
- Burns, J. D. and B. A. Moyer, 2016, *FY16 Progress Report on Co-crystallization*, FCRD-MRWFD-2016-000311, Oak Ridge National Laboratory, August 31, 2016.
- Dares, C. J., A. M. Lapides, B. J. Mincher, and T. J. Meyer, 2015, "Electrochemical Oxidation of  $^{243}\text{Am}(\text{III})$  in Nitric Acid by a Terpyridyl-Derivatized Electrode," *Science*, Vol. 350, pp. 652–655.
- Gelis, A. V., and M. A. Brown, 2016, *ALSEP Year-End Report*, FCRD-MRWFD-2015-000316, Argonne National Laboratory, September 2016.
- Gullekson, B. J., A. Breshears, M. A. Brown, J. B. Essner, G. A. Baker, J. R. Walensky, A. Paulenova, and A. V. Gelis, 2016, "Extraction of Water and Speciation of Trivalent Lanthanides and Americium in Organophosphorous Extractants," *Inorganic Chemistry*, Vol. 55, No. 24, pp. 12675–12685.
- Heathman, C., P. Zalupski, T. Grimes, and S. Jansone-Popova, 2016, *Structure-Function Relationships for the Modified Aminopolycarboxylate Aqueous Holdback Complexants*, FCRD-MRWFD-2016-000360, Idaho National Laboratory, September 30, 2016.
- Ivanov, A. S. and V. S. Bryantsev, 2016, "A Computational Approach to Predicting Ligand Selectivity for the Size-Based Separation of Trivalent Lanthanides," *European Journal of Inorganic Chemistry*, pp. 3474–3479.
- Jansone-Popova, S., V. S. Bryantsev, F. V. Sloop, Jr., R. Custelcean, and B. A. Moyer, 2016, *Design, Synthesis, and Testing of Trivalent Actinide Sequestering Agents*, FCRD-MRWFD-2016-000309, Oak Ridge National Laboratory, August 2016.
- Launiere, C. A. and A. V. Gelis, 2016, "High Precision Droplet-Based Microfluidic Determination of Americium(III) and Lanthanide(III) Solvent Extraction Separation Kinetics," *Industrial and Engineering Chemistry Research*, Vol. 55, No. 7, pp. 2272–2276.
- Lumetta, G. J., A. J. Casella, and A. V. Gelis, 2015, "Kinetics Challenges Associated with Minor Actinide Separations using 2-Ethylhexylphosphonic Acid Mono-2-ethylhexyl Ester," *Proceedings of Global 2015*, Paris, France, September 21–24, 2015, Société Française d'Énergie Nucléaire.

## 2016 ACCOMPLISHMENTS

Lumetta, G. J., and A. V. Gelis, 2016, *Recommended Conditions for the ALSEP Concept*, 2016, FCRD-MRWFD-2016-000040 (PNNL-25417), Pacific Northwest National Laboratory, May 2016.

Lumetta, G. J., E. L. Campbell, A. J. Casella, G. B. Hall, V. E. Holveltz, and T. G. Levitskaia, 2016, *Sigma Team for Advanced Actinide Recovery: PNNL FY 2016 Summary Report*, FCRD-MRWFD-2016-000324 (PNNL-25691), Pacific Northwest National Laboratory, August 2016.

Lumetta, G. J., S. I. Sinkov, J. A. Krause, and L. E. Sweet, 2016, "Neodymium(III) Complexes of Dialkylphosphoric and Dialkylphosphonic Acids Relevant to Liquid-Liquid Extraction Systems," *Inorganic Chemistry*, Vol. 55, pp. 1633–1641.

Mincher, B. J., J. D. Law, G. S. Goff, B. A. Moyer, J. D. Burns, G. J. Lumetta, S. I. Sinkov, T. C. Shehee, and D. T. Hobbs, 2015, *Higher Americium Oxidation State Research Roadmap*, FCRD-MRWFD-2016-000251, Idaho National Laboratory, December 18, 2015.

Mincher, B. J., R. D. Tillotson, J. D. Law, T. Garn, V. Rutledge, and N. C. Schmitt, 2016, "The Solvent Extraction of Am(VI) Using Centrifugal Contactors," *Journal of Radioanalytical and Nuclear Chemistry*, Vol. 307, pp. 1833–1836.

Mincher, B. J., T. Grimes, R. Tillotson, and J. Law, 2016, *Am(VI) Extraction Final Report: FY16*, FCRD-MRWFD-2016-000327, Idaho National Laboratory, August 11, 2016.

Moyer, B. A., 2016, *Sigma Team for Advanced Actinide Recycle FY2015 Accomplishments and Directions*, FCRD-MRWFD-2016-000355, Oak Ridge National Laboratory, September 30, 2016.

Shehee, T. C. and D. T. Hobbs, 2016, *Experimental Findings on Actinide Recovery Utilizing Oxidation by Peroxydisulfate as an Eluent for Inorganic Ion Exchange Material*, FCRD-MRWFD-2016-000306, Savannah River National Laboratory, September 2016.

Zalupski, P., T. Grimes, C. Heathman, and S. Jansone-Popova, 2015, *Evaluation of Phase Transfer Kinetics for the ALSEP Process Using Modified Aminopolycarboxylate Reagents. Part I. Amide-Substituted Ethylenediamine Backbone*, FCRD-MRWFD-2016-0002521, Idaho National Laboratory, December 10, 2015.

Zalupski, P., T. Grimes, C. Heathman, and S. Jansone-Popova, 2016, *Evaluation of Phase Transfer Kinetics for the Liquid-Liquid Systems Containing Modified Aminopolycarboxylate Reagents. Part II. Amine-Substituted Diethylenetriamine Backbone*, FCRD-MRWFD-2016-000270, Idaho National Laboratory, March 31, 2016.

Zalupski, P., T. Grimes, C. Heathman, and S. Jansone-Popova, 2016, *Initial Assessment of Back and Forward Extraction Kinetics of ALSEP Using Candidate Complexant*, FCRD-MRWFD-2016-000338, Idaho National Laboratory, August 29, 2016.

### PATENTS AND PATENT APPLICATIONS FOR SIGMA TEAM – ADVANCED ACTINIDE RECYCLE

Dares, C. J., A. M. Lapidus, B. J. Mincher, and T. J. Meyer, "Electrochemical Treatment of Nuclear Waste Streams," patent pending.

Gelis, A. V., and M. A. Brown, "Transition metal recovery from nitric acid," patent application submitted.

Gelis, A. V., "Actinide and Lanthanide Separation Process (ALSEP)," U.S. Patent 8354085, January 15, 2013.

Goff, G. S., L. S. Seaman, W. Runde, and G. D. Jarvinen, "Oxidation of Americium in Acidic Solution," patent pending.

## Sigma Team – Off-Gas

The Off-Gas Sigma Team was formed in FY 2010 to bring together multidisciplinary teams from across the DOE complex and academia that would work collaboratively to solve the technical challenges and to develop the scientific basis for the capture and immobilization of volatile radionuclides contained in the airborne effluents from used fuel treatment processes. This work has been performed with an ultimate goal of ensuring regulatory compliance for gaseous discharges by potential used fuel treatment facilities. The team is focused on development of effective methods to capture  $^{129}\text{I}$ ,  $^{14}\text{C}$ ,  $^{85}\text{Kr}$ , and tritium released from fuel treatment processes, thereby enabling a range of advanced fuel cycle options in the U.S.

The long-term scope of the Off-Gas Sigma Team includes the development, demonstration, and technical maturation of integrated off-gas treatment and immobilization systems for prototypical dissolver off-gas (DOG), vessel off-gas (VOG), tritium pretreatment off-gas (TOG), cell off-gas (COG), melter off-gas (MOG), electrorefiner off-gas, and lanthanide/actinide drawdown off-gas arising from aqueous and electrochemical fuel treatment processes. Five major thrust areas were included in the activities for FY 2016: (1) iodine capture, (2) iodine immobilization, (3) tritium separations, (4) krypton separations and storage, and (5) integrated off-gas treatment system development for aqueous reprocessing. Highlights from these activities are summarized below and described in detail in the associated technical reports generated for each task at each contributing laboratory. Participating laboratories in FY 2016 included INL, ORNL, and PNNL.

### CHARACTERIZATION OF IODINE REMOVAL FROM VOG STREAMS BY SILVER-BASED SORBENTS

*S. H. Bruffey, J. A. Jordan, and R. T. Jubin (ORNL)*

Estimations of required plant decontamination factors (DFs) are based on U.S. regulations requiring the removal of  $^{129}\text{I}$  from the off-gas streams of any used fuel treatment facility and will vary based on fuel burnup, cooling time, and other factors.<sup>1</sup> These DFs are likely to be  $>1,000$  and could be as high as 8,000. Multiple off-gas streams within a fuel-processing facility combine prior to environmental release, and each of these streams contains some amount of iodine. To achieve the DFs that are likely to be required by regulations, iodine removal from the VOG will be necessary.

VOG streams will contain iodine at low concentrations ( $\sim 10^{-8}$  levels) and in a multitude of chemical forms, which are likely to include elemental iodine, alkyl iodides of varying carbon chain lengths, and inorganic iodine species. Silver-based solid sorbents are currently being evaluated by DOE for use in iodine removal from off-gas streams, and VOG streams present a distinctive technical challenge as the behavior of silver-based solid sorbents has never been characterized in this concentration regime. Iodine removal from VOG streams was investigated by ORNL in FY 2016 for both candidate silver-sorbents, i.e., reduced silver-exchanged mordenite (AgZ) and silver-functionalized silica aerogel (AgAerogel). AgAerogel utilized in this testing was provided by PNNL. Three tests were completed: (1) adsorption of elemental iodine ( $\text{I}_2$ ) by AgAerogel, (2), adsorption of  $\text{I}_2$  by AgZ, and (3) adsorption of methyl iodide ( $\text{CH}_3\text{I}$ ) by AgZ.

---

<sup>1</sup> Decontamination factors are defined as the ratio of iodine concentration in the inlet to iodine concentration in the effluent.

Each sorbent was exposed to a prototypical VOG stream for 4 months with iodine present at concentrations of 40 ppb (for CH<sub>3</sub>I) or 7 ppb (for I<sub>2</sub>). The test system was designed with three beds in series. The first bed was very thin and was periodically removed during testing to provide iodine adsorption rate. The second bed was >10 cm in depth and provided information as to the penetration of iodine into a sorbent deep bed. A third thin bed was placed after the deep bed in an effort to determine time to breakthrough and system DF.

An experiment conducted with AgAerogel showed that CH<sub>3</sub>I penetrated into a AgAerogel sorbent bed to a depth of 3.9 cm under prototypical VOG conditions. Direct calculation of the DF was not possible, because no iodine was observed to break through the sorbent beds. The amount of iodine found on the sorbent upon analysis was not equal to the amount of iodine delivered to the system, and several short-term tests have been designed to assess the cause of this mass balance discrepancy.

The experiments performed with AgZ demonstrated that under prototypical off-gas conditions, I<sub>2</sub> penetrated an AgZ sorbent bed to a depth of 2.2 cm and CH<sub>3</sub>I penetrated a sorbent bed to 2.4 cm. As sorbent time online increased, the rate of I<sub>2</sub> adsorption decreased, but this same effect was not observed with CH<sub>3</sub>I adsorption by AgZ. A decreased rate of adsorption may indicate the sorbent is aging during exposure to these gas streams, and while the effects of aging on I<sub>2</sub> adsorption by AgZ are well-documented, no studies have been performed to examine the effects of aging on CH<sub>3</sub>I adsorption by AgZ. Because this result is an initial indication that CH<sub>3</sub>I and I<sub>2</sub> may behave differently with aged sorbents, additional testing on this topic is merited. The DFs for the AgZ test systems were not able to be determined, because no measureable iodine was observed in the bed effluent.

Continued studies on the adsorption of iodine from prototypical VOG streams by silver-based sorbents will attempt to resolve some of the questions raised here, both regarding mass balance and the effect of aging on iodine adsorption from a dilute gas stream. Other variables that merit examination are the dependence of the observed results on the inlet iodine concentration and upon the gas velocity of the test. Finally, alternative test designs will be considered in an effort to determine the mass transfer zone and system DF associated with iodine adsorption by silver-based sorbents under prototypical VOG conditions. The estimation of mass transfer zone is required for any future industrial implementation.

## REMOVAL OF METHYL IODIDE FROM NO<sub>x</sub>-CONTAINING DOG STREAMS BY AGAEROGEL DEEP BEDS

*N. Soelberg (INL)*

The intent of FY 2016 deep-bed CH<sub>3</sub>I adsorption testing was to further research and advance the technical maturity of silver-based solid sorbents under consideration for use in capturing <sup>129</sup>I present in off-gas streams. A major thrust was to characterize the effects of NO and NO<sub>2</sub> gases (present in the DOG stream) on AgAerogel material provided by PNNL. Adsorption testing for CH<sub>3</sub>I with higher levels of NO and NO<sub>2</sub> (approximately 3,300 and 10,000 ppm, respectively) in simulated DOG indicate that high-efficiency iodine capture by AgAerogel is possible under these conditions. In Figure 27, the initially dark-colored AgAero is shown to change to a light tan color as it adsorbs CH<sub>3</sub>I. Figure 28 shows that maximum CH<sub>3</sub>I DFs for the solid-sorbent based deep bed test system exceeded 3,000 until breakthrough. The gas composition during

## 2016 ACCOMPLISHMENTS

this test was 65 ppm CH<sub>3</sub>I, 0.59% water (with a dewpoint of ~0°C), 3,300 ppm NO, 9,600 ppm NO<sub>2</sub>, and balance air at 150°C.



Figure 27. AgAerogel before and after a 314-hour CH<sub>3</sub>I adsorption test.

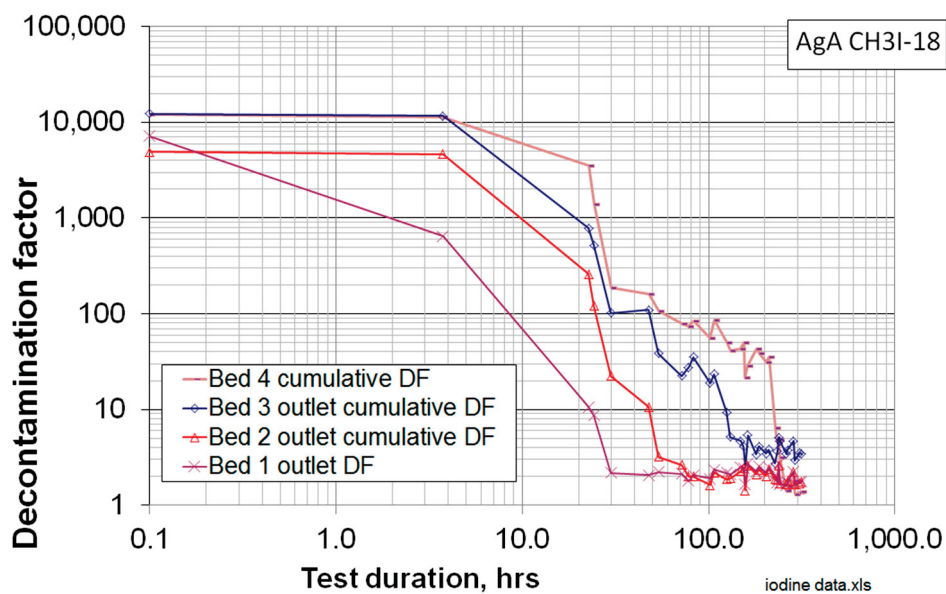


Figure 28. CH<sub>3</sub>I DFs in AgAerogel decreased most rapidly for shallower bed depths ranging from 1.3, 5, 10, and 20 cm (0.5, 2, 4, and 8 in.).

The CH<sub>3</sub>I molecules are cleaved in the sorbent bed, even after iodine adsorption was no longer efficient, so that uncaptured iodine was in the form of iodine species soluble in caustic scrubber solutions and detected and reported as diatomic I<sub>2</sub>. The mass transfer zone depths for CH<sub>3</sub>I adsorption by AgAerogel were estimated at 8 in., deeper than the 2 to 5-in. range estimated for both AgAerogel and AgZ in prior deep-bed tests with lower NO<sub>x</sub> levels. The maximum iodine adsorption capacity and silver utilization for these higher NO<sub>x</sub> tests, at about 5 to 15% of the original sorbent mass and about 12 to 35% of the total silver, respectively, were lower than for trends from prior AgAerogel and AgZ tests with lower NO<sub>x</sub> levels. Additional deep-bed testing and analyses are recommended to expand the database for organic iodide adsorption and increase the technical maturity of iodine adsorption processes.

### DIRECT CONSOLIDATION OF IODINE-LOADED AGAEROGEL TO A DENSIFIED WASTE FORM

*J. Matyáš, E. Ilton, N. Canfield, G. Kroll, and S. E. Sannoh (PNNL)*

Silver-functionalized silica aerogel has been shown to have high selectivity and sorption capacity for iodine, and FY 2016 efforts were focused on scale-up of the conversion processes that are used to manufacture an iodine-containing SiO<sub>2</sub>-based waste form.

The scaled-up consolidation of iodine-loaded AgAerogel with hot isostatic pressing (HIP) and spark plasma sintering (SPS) proved to be successful. HIP processing of a ~115-g pellet at 1,200°C with a 30-minute hold and under 207 MPa pressure produced a puck ~4.8 cm in diameter and ~2.2 cm thick. The sample contained ~43.8 mass% iodine in the form of uniformly dispersed nano- and micro-particles and micrometer-sized “veins” of AgI surrounding individual grains. The sample had a bulk density of 2.896 ± 0.0124 g/cm<sup>3</sup>; it contained a small amount of open porosity (~7%), but this porosity is expected to diminish with a better container design. Even better results were obtained for SPS. SPS processing of ~115-g powder at 1,200°C with a 30-minute hold and under 32 MPa pressure produced a puck ~6 cm in diameter and ~7 mm thick (Figure 29). The sample contained 41 mass% iodine, had a bulk density of 2.9370 ± 0.0212 g/cm<sup>3</sup>, and exhibited a small amount of open porosity, ~2.8%. The presence of some porosity was related to problems with a die during SPS processing that did not allow increasing the pressure above 32 MPa. Based on relative success of these preliminary first tests, it is highly likely that full density with appropriate microstructure will be achieved with minor design changes. Additional tests are planned in FY 2017 to investigate impacts of iodine loading, additives, and temperature/pressure schedule on the microstructure of densified Ag<sup>0</sup>-aerogel.



**Figure 29. Pucks of iodine-loaded Ag<sup>0</sup>-aerogel produced with HIP (left) and SPS (right).**

### MANUFACTURE OF AN IODINE-CONTAINING WASTE FORM BY HOT ISOSTATIC PRESSING OF AgZ

*S. H. Bruffey, R. T. Jubin, and J. A. Jordan (ORNL)*

Direct consolidation of iodine-loaded AgZ by HIP was advanced through additional studies at ORNL in FY 2016. Previous studies have shown that engineered forms of iodine-loaded AgZ can be successfully consolidated by HIP. The major aims of FY 2016 studies were to decrease the capsule failure rate occurring during HIP and to evaluate whether pure zeolite minerals could be converted to a distinctive mineral phase, such as iododosalite. While conversion of zeolites to a particular mineral phase is not required in order to produce a durable waste form, conversion to a well-studied mineral phase could decrease the amount of future R&D required to assess waste form stability.

Substantial improvements in capsule manufacture and sealing were achieved in FY 2016. The capsule lid was redesigned twice, with the final modifications including a recessed trepan lid and a vacuum port in the center of the lid. These improvements substantially decreased the amount of time and cost required to seal the capsules. The lid redesign also resulted in an improvement in weld quality and ultimately in the number of capsules that were able to be successfully compressed. The capsule modifications are shown in Figure 30. These redesigned capsules increased the success rate of the HIP process from 68 to 94%.



**Figure 30. Capsule lid modifications (left to right: original, inset cap, inset vacuum port lid).**

Each compressed sample was analyzed to determine its density and then cross-sectioned, with one half mounted and polished in epoxy to facilitate further examination by XRD and the second half used for determination of the waste form hardness. Cross sections of selected samples are shown in Figure 31. It was found that the density of the compressed samples increased from 220 to 490% of the original material densities. Planned efforts will transition this work from pure minerals to engineered zeolite minerals that contain clay binders and will assess scale-up of the HIP process.



Figure 31. Cross section of iodine-occluded sodium mordenite that underwent HIP (left) and iodine-loaded silver zeolite A (right).

## CHARACTERIZATION OF KRYPTON REMOVAL FROM OFF-GAS STREAMS BY AN IMPROVED METAL ORGANIC FRAMEWORK MATERIAL

*P. Thallapally (PNNL)*

FY 2016 efforts at PNNL on the removal and separation of krypton and xenon from off-gas streams were focused on the development of a newly identified calcium based metal organic framework (MOF) (calcium-based nanoporous MOF, SBMOF-1, also known as CaSDB). PNNL demonstrated experimentally that CaSDB was found to be the best for xenon/krypton adsorption at room temperature (RT) among 5,000 experimental MOFs screened *in silico* (Figure 32). Single column breakthrough experiments on CaSDB using a gas mixture containing 400 ppm xenon and 40 ppm krypton in air at RT suggest a very high xenon adsorption capacity (14 mmol/kg). This capacity is up to 50% higher than benchmark materials such as NiMOF-74 (7 mmol/kg) and CC3 (11 mmol/kg) under similar experimental conditions. xenon/krypton selectivity under breakthrough measurements was found to be 14, which is twice that of NiMOF-74. Remarkably, CaSDB retains its xenon uptake capacity even in the presence of 40% relative humidity, whereas water competes for the same adsorption sites as xenon/krypton in NiMOF-74 and CC3 under similar conditions.

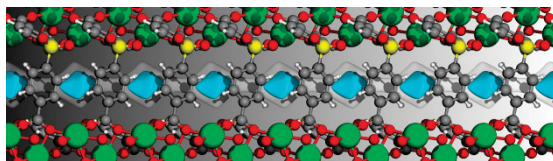


Figure 32. Pores within the CaSDB MOF (blue).

Two-column breakthrough experiments (Figure 33) and cycle studies were performed at RT using CaSDB. Passing a mixture of 400 ppm xenon and 40 ppm krypton in dry air through a CaSDB sorbent bed results in the selective capture of xenon with 15-mmol/kg capacity; the outlet gas mixture from the first sorbent bed, then containing 40 ppm krypton in air, was passed through a second CaSDB sorbent bed for krypton removal (0.25 mmol/kg capacity). The capacity of CaSDB for krypton has been observed to be as high as 3.36 mmol/kg at RT when concentrations of krypton in the gas mixture approach 1,000 ppm and no xenon

is present. Twenty adsorption and desorption cycles were performed at RT using CaSDB without any loss in xenon or krypton capacities or any other signs of degradation (Figure 34). These results show MOFs continue to be promising as materials for the removal and separation of xenon and krypton from air at RT. Based on these initial results, a sufficient quantity of CaSDB MOF (50 g) was fabricated, pelletized, and sieved to obtain engineered particles of the CaSDB MOF to test at INL. The increased xenon capacity of CaSDB under simulated conditions with and without water vapor makes this new MOF a leading candidate for separating the xenon/krypton from off-gas streams generated from used fuel processing.

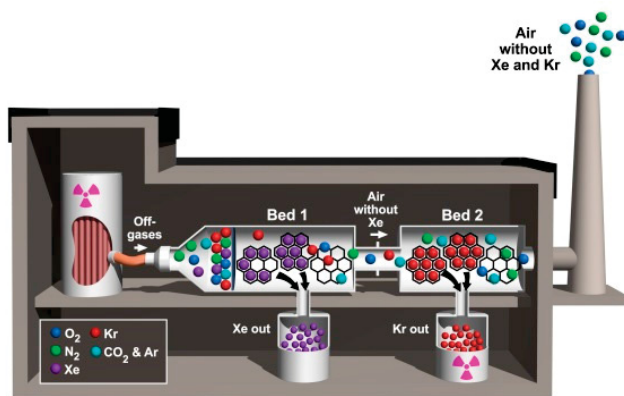


Figure 33. Schematic diagram of two-column breakthrough experiment.

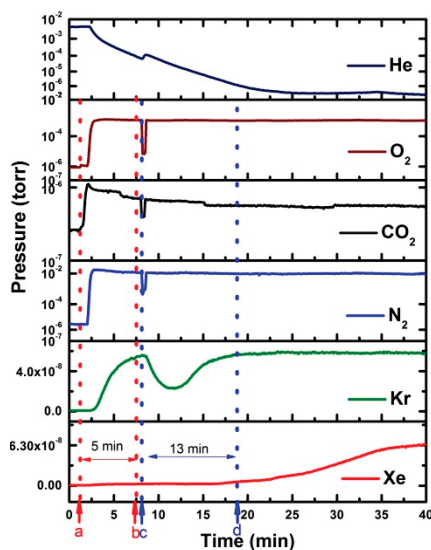


Figure 34. Curves for partial pressures of gas mixture components using two bed-adsorption modules at RT. Adsorbents in Beds 1 and 2 are CaSDB. Gas mixture consisting of xenon (400 ppm) and krypton (40 ppm) balanced with dry air flowed into Bed 1 at Time “a”; gas (krypton) breakthrough from Bed 1 is indicated as “b”; gas mixture from Bed 1 (xenon removed) was introduced to Bed 2 at Point “c”; breakthrough of krypton from Bed 2 at Point “d.”

**DEMONSTRATED SEPARATION OF KRYPTON AND XENON BY A MULTI-COLUMN AgZ-PAN/HZ-PAN SOLID SORBENT SYSTEM**

*T. G. Garn, M. Greenhalgh, A. K. Welty, and T. L. Watson (INL)*

Recent studies conducted at INL have demonstrated the separation of xenon from krypton in a mixed gas feed stream using mordenite-polyacrylonitrile (PAN) solid sorbents. The results of initial testing of a multi-column system with AgZ-PAN and HZ-PAN indicated that an excellent separation of xenon from krypton could be attained with these sorbents. FY 2016 efforts were focused on extending these results by demonstration of scaled-up sorbent beds, by testing of varied feed gas compositions, and by improved analysis of the individual capture columns' compositions.

The original multi-column system was modified by installing two Stirling coolers (SC#1 and SC#2) in series to accommodate this testing. The use of the coolers instead of the cryostat provided two desired improvements: (1) the removal of the large dilution due to the internal volume of the cryostat adsorption chamber and (2) the ability to increase the sorbent bed size for scale-up. Loaded into the first column was 44.8 g of AgZ-PAN sorbent (2.4 times more than previously tested) to capture the xenon while allowing the krypton to flow through and be routed to a second column containing 29.8 g of HZ-PAN sorbent (6.7 times more than previously tested) for krypton capture and analysis. Figure 35 is a schematic of the experimental system.

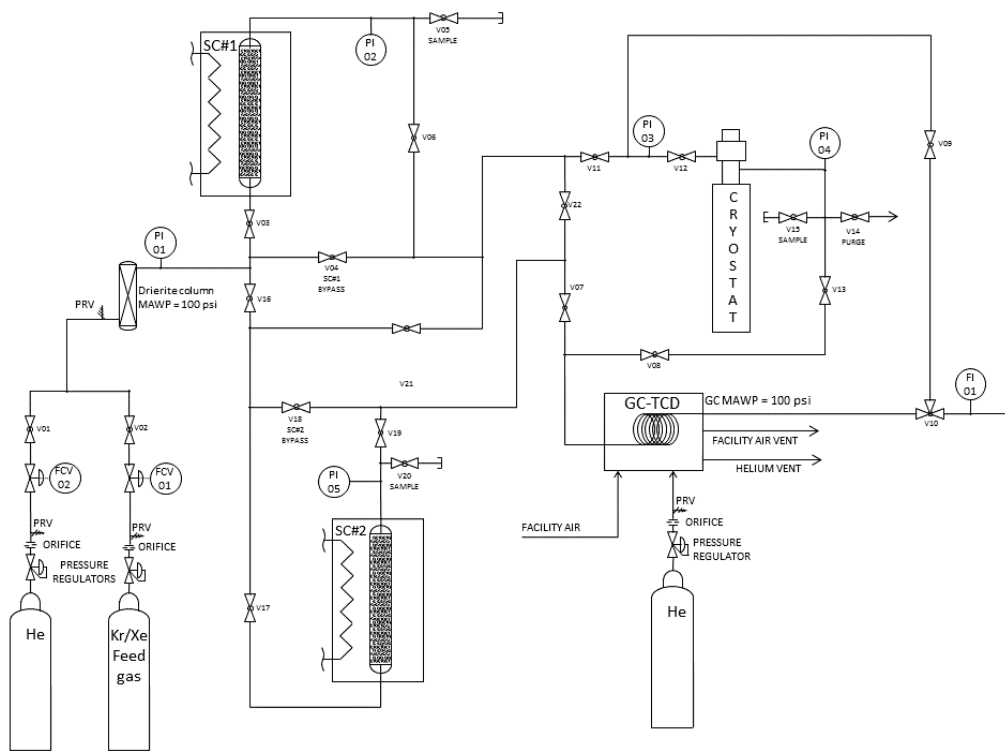


**Figure 35. Multi-column experimental test bed schematic for separation of krypton/xenon.**

## 2016 ACCOMPLISHMENTS

Two separation tests were performed with the AgZ-PAN (xenon column) temperature held at either 295 or 253 K, and the HZ-PAN (krypton column) was held at 191 K. The tests were performed with a feed gas of 400 ppmv xenon, 40 ppmv krypton in air balance with a superficial velocity of 23 cm/minute. The adsorption phases of the tests were operated for ~300 minutes, and the effluent from the columns was monitored via gas chromatography-thermal conductivity detector with neither xenon nor krypton being detected in the column effluent. The gases captured on both columns were sampled with evacuated sample bombs and subsequently analyzed via gas chromatography-mass spectrometry for both xenon and krypton. The results of the gas chromatography-mass spectrometry analysis are presented in Table 6.

TABLE 6. XENON/KRYPTON CONCENTRATIONS FROM SAMPLE BOMBS.

Temperature (K)	Column Sample	Average Xe (ppmv)	Average Kr (ppmv)
295	Xe Column	41.3	81.2
191	Kr Column	BDL	367
253	Xe Column	25.6	179
191	Kr Column	BDL	586

These results indicate that an excellent separation of xenon from krypton was achieved, because there was no detectable xenon found in the krypton column samples. The low xenon concentration for the xenon column samples along with the desorption data revealed that removal of xenon from the AgZ-PAN was ineffective. The sample bomb gas-collection procedure provided inconsistent results, even though a combination of high temperature and purge gas flow were utilized during the sampling of the columns.

The results of these tests can be used to develop the scope of future testing and analysis using this test bed for demonstrating the capture and separation of xenon and krypton using sorbents, for demonstrating desorption and regeneration of the sorbents, and for determining compositions of the desorbed gases. Future testing of sorbents should include desorption studies to determine parameters at which the cleanest separation between krypton and co-adsorbed species occurs, as well as the maximum purity of the final krypton product stream.

### ANALYSIS OF LEGACY KRYPTON WASTE FORM SAMPLES

*R. T. Jubin and S. H. Bruffey (ORNL)*

Legacy samples composed of <sup>85</sup>Kr encapsulated in solid zeolite 5A material and five small metal tubes containing a mixture of the zeolite combined with a glass matrix resulting from hot isostatic pressing have been preserved. The samples were a result of krypton R&D encapsulation efforts in the late 1970s performed at the Idaho Chemical Processing Plant. These samples were shipped to ORNL in mid-FY 2014 and repackaged into individual glass sample bottles for further analysis. Visual examination and x-ray imaging conducted in 2015 revealed that two of the five capsules had been breached. Capsule 2 was observed to have saw marks on the capsule and a quantity of loose pellet or bead-like material remaining in the capsule. Capsule 5 had been opened at an undetermined time in the past. The end of this capsule

appears to have been cut off, and there are additional saw marks on the side of the capsule. X-ray images confirmed the presence of residual material within this capsule. The material appears to be compacted but still retains some of the bead-like morphology.

Based on these initial images and the fact that there are at least two breached samples, it was proposed that FY 2016 efforts be directed at analysis of the breached specimens before opening the three intact capsules. Portions of material removed from Capsules 2 and 5 (Figure 36) were to be analyzed to determine the fraction of krypton/xenon remaining in the matrix and the amount of rubidium remaining in the matrix. The presence of rubidium, the sole decay product of  $^{85}\text{Kr}$ , was of especial interest, because its corrosive nature could have significant impacts on the integrity of container structures for any proposed krypton storage form. The inner surface of the breached capsules would be examined for corrosion. Due to the high radiation levels of these samples, all analyses beyond the initial imaging were facilitated by ORNL hot-cell facilities.

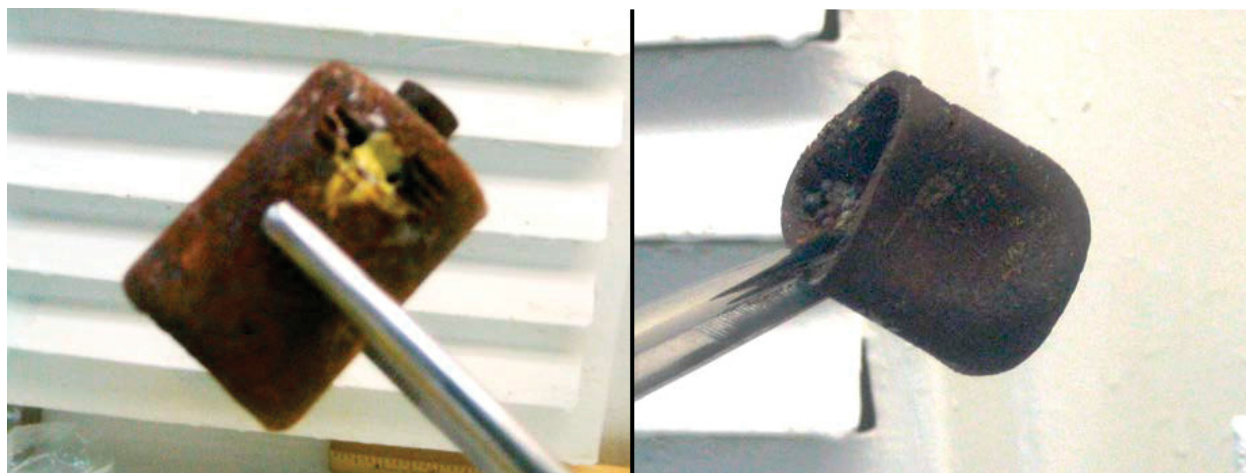


**Figure 36.  $^{85}\text{Kr}$  legacy waste from Capsule 2 (left) and Capsule 5 (right).**

The materials contained in Capsules 2 and 5 have been examined by scanning electron microscopy (SEM), EDS, and XRD. There appears to be a relatively uniform distribution of krypton and rubidium throughout the pellets examined (Figure 37). The EDS-derived chemical analysis indicates a chemical composition of the recovered materials consistent with zeolite 5A. The elemental mapping indicates that krypton and xenon are coincident with the silicon, aluminum, calcium, and sodium, implying that the noble gases have remained within the collapsed zeolite structure (Figure 37). The material contained within Capsule 5 showed ~1 at. % lead. The origin of the lead is currently indeterminate. XRD analysis shows a significant shift from the 5A structure, most likely due to the krypton encapsulation/sintering process that occurred when the samples were made.

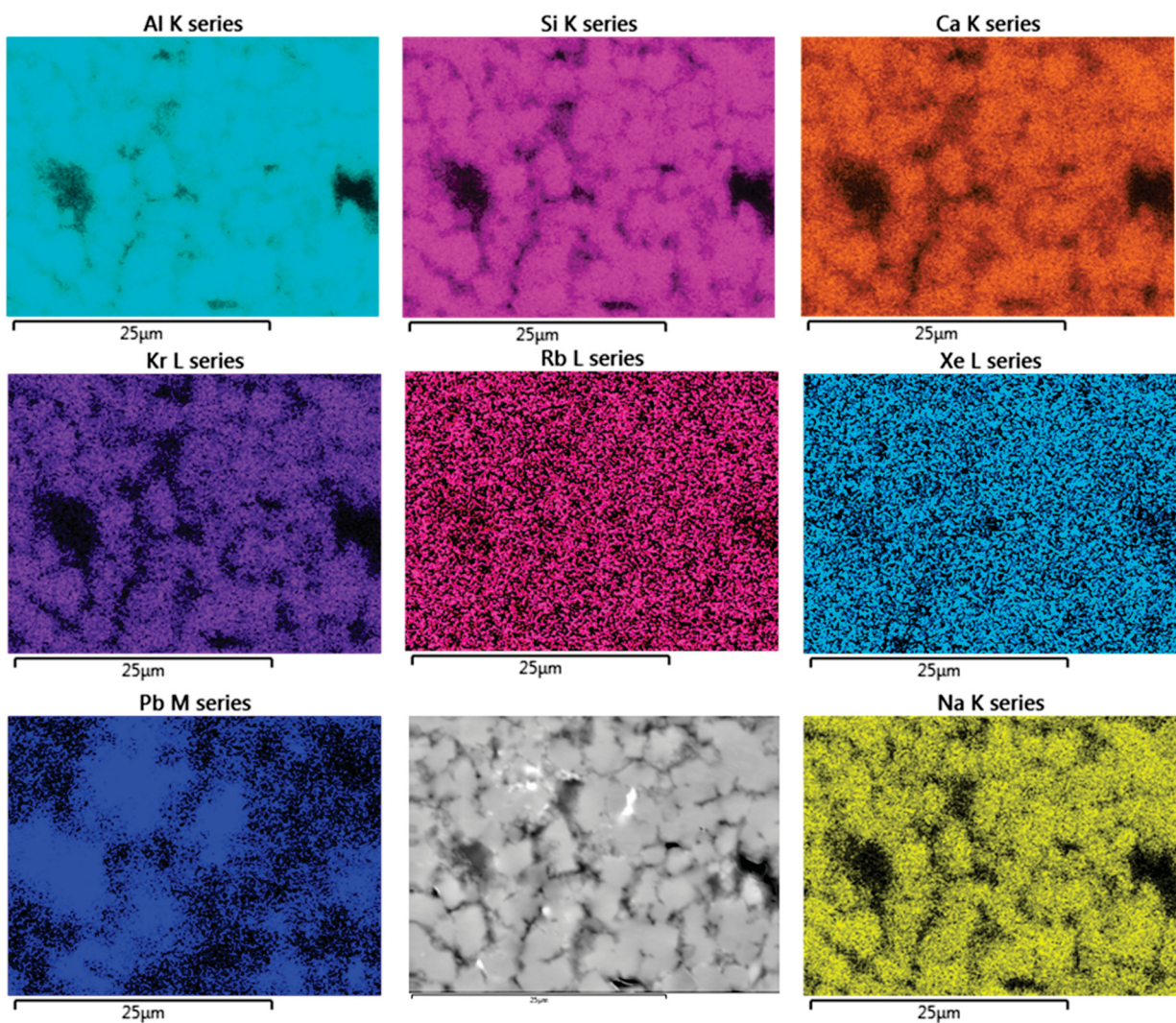


Figure 37. Elemental maps of an area near the center of a pellet recovered from Capsule 5 (Sample K5).

The walls of each capsule were also examined and showed extensive corrosion throughout (Figure 38). Elemental mapping of the capsule material appeared consistent with carbon steel, while the weld material appeared consistent with a stainless steel. The interior surface of the capsule appeared to have a layer of material containing aluminum, silicon, and calcium similar to the 5A molecular sieve. Analysis for rubidium within the corrosion sites was inconclusive.

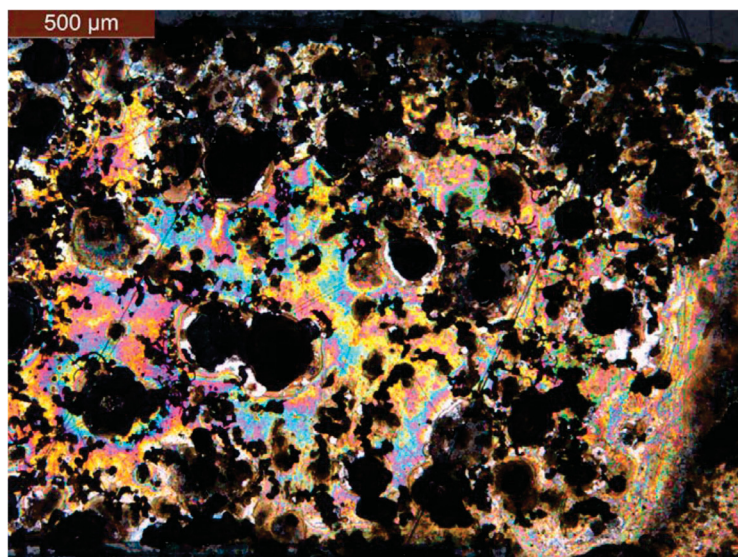


Figure 38. Optical microscope image at 50× magnification of Section “A” of Capsule 2.

## ENGINEERING EVALUATION OF AN INTEGRATED OFF-GAS TREATMENT SYSTEM FOR USED NUCLEAR FUEL REPROCESSING FACILITIES

*R. T. Jubin, J. A. Jordan, and B. B. Spencer (ORNL)*

*N. R. Soelberg, A. K. Welty, and M. Greenhalgh (INL)*

*D. M. Strachan (Strata-G, LLC)*

*P. K. Thallapally (PNNL)*

The capture and subsequent immobilization of four regulated volatile radionuclides ( $^3\text{H}$ ,  $^{14}\text{C}$ ,  $^{85}\text{Kr}$ , and  $^{129}\text{I}$ ) and relevant semivolatile species from the off-gas streams of a UNF reprocessing facility have been topics of significant research interest on the part of the DOE and other international organizations. Significant R&D has been conducted over the past decade. This study is an initial engineering evaluation and design of the off-gas abatement systems required to ensure that air emissions from a reprocessing facility can meet or exceed emission requirements set forth by the U.S. Environmental Protection Agency and the U.S. Nuclear Regulatory Commission. This study builds on a series of case studies that addressed various reprocessing options for the processing of UNF. This engineering design, while somewhat notional because this effort is not tied to a specific UNF processing facility, is intended to help all those involved with UNF reprocessing grasp the complexity and sizes of the required systems. This study covers only engineering options for the off-gas streams arising from head-end, fuel-dissolution, and process vessels for aqueous reprocessing. It is not intended to be an exhaustive, detailed design effort but, rather, a first attempt to evaluate (1) the relative sizes, (2) the material balances, (3) energy requirements, (4) key instrumentation requirements, (5) support system requirements, (6) extended operating cycles and associated requirements, and (7) the extent to which key design data are or are not available for the off-gas systems. This initial engineering evaluation addresses the designs of the head-end off-gas, which typically includes the shear off-gas and the DOG and VOG systems. Subsequent reports will add similar assessments for the COG, TOG, and MOG systems.

## 2016 ACCOMPLISHMENTS

The following summarizes the results of this study (not ordered by importance):

1. Common processes used in industry and existing nuclear facilities are perceived as being relatively easy to implement in a UNF reprocessing facility. These unit operations are those involving condensers, heat exchangers, scrubbers, valves, particulate filters, etc. These systems are well understood because of their widespread use in the nuclear industry. However, some uncertainties remain, including the actual performance of the NO<sub>x</sub> scrubber and the CO<sub>2</sub> scrubber under the actual operating conditions.
2. There is a surprising lack of clarity in the understanding of the speciation of volatile ruthenium under various facility conditions. The amount of ruthenium volatilized during fuel processing, either directly from the dissolved fuel or after the treatment to remove tritium separately, does not appear to be well understood. Once ruthenium is volatilized, its chemical form under the various conditions that exist in the facility and the behavior of the species in the off-gas stream are sufficiently ambiguous to result in large uncertainties in this study with respect to pathway and DFs. Silica gel is suggested as the best ruthenium sorbent. However, the capacity and the efficiency of this material under facility conditions do not appear to be well understood or at least not well articulated in the literature. This is important because of the very high ruthenium removal efficiency ( $3 \times 10^7$ ) that may be required to meet regulated releases even for UNF that has been cooled for 5 years.
3. There is a lack of pertinent engineering data, such as the length of the mass transfer zone, sorption kinetics, desorption kinetics, etc., on solid sorbents for the removal of xenon and krypton. This uncertainty means that the systems designed here require large and multiple columns to achieve the desired decontamination of the off-gas stream and purity of the krypton gas for storage. These data are needed to ensure the continued viability of these solid sorbent materials for xenon and krypton compared to the cryogenic process for the removal of these gases.
4. While the xenon and krypton capacities on the solid sorbent materials studied to date are quite high, they also have high capacities for air components, such as nitrogen, oxygen, argon, etc. These components are desorbed when the xenon and krypton are desorbed. In the case of the krypton desorption, these air components have a significant impact on the quality of the krypton-rich gas such that it is insufficiently pure to be sent directly to storage. Hence, a krypton-purification unit is installed to increase the krypton purity to acceptable levels for storage.
5. Iodine recovery based on silver-loaded mordenite requires multiple columns of material. This is a result of the rate at which the sorbent is consumed in removing iodine and bromine released to the off-gas during UNF dissolution and chlorine contained in the acid used to dissolve the fuel. Limits on the height of the columns because of practical hot cell dimensions also required the use of multiple columns. However, the airflow dynamics through the column and engineering norms imposed dimensional limitations that also resulted in the need for multiple columns.
6. The alternative iodine sorbent, silver-aerogel, is less dense than the mordenite material, but the silver-aerogel contains four to five times more silver (the active ingredient for removal of iodine). The combination means that the number of columns could be reduced or the time between column changeout could be lengthened by roughly a factor of 2.

7. Important to the sizing and use of the iodine sorbent is the amount of physisorbed (that which is not chemically bound to the sorbent) iodine. The quantities of physisorbed iodine are uncertain for all the materials proposed as iodine sorbents.
8. There is also lack of pertinent engineering data, such as the length of the mass transfer zone, sorption kinetics, and sorption capacity, for the capture of iodine at the much lower concentration found in the VOG systems.

#### PUBLICATIONS FOR SIGMA TEAM – OFF-GAS

Banerjee, D., et al., 2016, “Metal-organic framework with optimally selective xenon adsorption and separation,” *Nature Communications*, Article 7.

Bruffey, S. H., J. A. Jordan, and R. T. Jubin, 2016, *Iodine Adsorption by Ag-Aerogel under Prototypical Vessel Off-Gas Conditions*, FCRD-MRWFD-2016-000312, ORNL/TM-2016-417, August 2016.

Bruffey, S. H., R. T. Jubin, and J. A. Jordan, 2016 “Capture of Elemental and Organic Iodine from Dilute Gas Streams by Silver-exchanged Mordenite,” *Procedia Chemistry*, Vol. 21, pp. 293–299.

Bruffey, S. H., R. T. Jubin, and J. A. Jordan, 2016, *Organic Iodine Adsorption by AgZ under Prototypical Vessel Off-Gas Conditions*, FCRD-MRWFD-2016-000357, ORNL/TM-2016/568, September 2016.

Elsaidi, S. K., T. Pham, K. A. Forrest, H. T. Schaefer, A. Hogan, L. Wojtas, W. Xu, B. Space, M. J. Zaworotko, and P. K. Thallapally, 2016, “Hybrid Ultra-Microporous Materials for Selective Xenon Adsorption and Separation,” *Angewandte Chemie International Edition*, Vol. 55, No. 29, pp. 8285–8289.

Feng, X. H., Z. W. Zong, S. K. Elsaidi, J. B. Jasinski, R. Krishna, P. K. Thallapally, and M. A. Carreon, 2016, “Kr/Xe Separation over a Chabazite Zeolite Membrane,” *Journal of the American Chemical Society*, Vol. 138, pp. 9791–9794.

Garn, T. G., M. R. Greenhalgh, and J. D. Law, 2016, “Development and evaluation of a silver mordenite composite sorbent for the partitioning of xenon from krypton in gas compositions,” *Journal of Nuclear Science and Technology*, Vol. 53, No. 10, pp. 1484–1488.

Greenhalgh, M., T. G. Garn, A. K. Welty, and T. Watson, 2016, *Multi-Column Xe/Kr Separation with AgZ-PAN and HZ-PAN*, FCRD-MRWFD-2016-000046, August 19, 2016.

Greenhalgh, M., T. G. Garn, A. K. Welty, K. Lyon and T. Watson, 2015, *Multi-Column Experimental Test Bed for Xe/Kr Separation*, FCRD-MRWFD-2015-000047, August 31, 2015.

Jubin, R. T., and S. H. Bruffey, 2016, *Analysis of Selected <sup>85</sup>Kr Legacy Samples*, FCRD-MRWFD-2016-000047, ORNL/TM-2016-350, September 2016.

## 2016 ACCOMPLISHMENTS

Jubin, R. T., J. A. Jordan, B. B. Spencer, N. R. Soelberg, A. K. Welty, M. Greenhalgh, D. M. Strachan, and P. K. Thallapally, 2016, *Engineering Evaluation of an Integrated Off-Gas Treatment System for Used Nuclear Fuel Reprocessing Facilities*, FCRD-MRWFD-2016-000313, ORNL/TM/2016-447, INL/LTD-16-39698, September 2016. (NOTE: This report is official use only-exeptionally controlled information.)

Matyáš, J., 2015, *Silver-functionalized silica aerogel for FY16 testing at INL*, FCRD-MRWD-2016-000528, Pacific Northwest National Laboratory.

Matyáš, J., 2016, *Silver-functionalized silica aerogel for FY16 testing at ORNL*, FCRD-MRWD-2016-000517, Pacific Northwest National Laboratory.

Matyáš, J., N. Canfield, S. Sulaiman, and M. Zumhoff, 2016, "Silica-based waste form for immobilization of iodine from reprocessing plant off-gas streams," *Journal of Nuclear Materials*, Vol. 476, pp. 255–261.

Matyáš, J., S. E. Sannoh, G. R. Kroll, and N. Canfield, 2016, *Scaled-up consolidation processing of iodine-loaded Ag<sup>0</sup>-functionalized silica aerogel*, FCRD-MRWFD-2016-000042, Pacific Northwest National Laboratory.

Patil, R. S., D. Banerjee, J. L. Atwood, and P. K. Thallapally, 2016, "Gas Sorption and Storage Properties of Calixarenes," in *Calixarene Functionalization and Applications*, Professor Placido Neri, Jonathan L. Sessler, and Mei-Xiang Wang (eds.), Springer.

Patil, R. S., D. Banerjee, S. Cory, J. L. Atwood, P. K. Thallapally, and A. Noria, 2016, "A highly Xe-Selective Nanoporous Organic Solid," *Chemistry – A European Journal*, Vol. 22, pp. 1–7.

Soelberg, N. and T. Watson, 2016, *FY-2016 Methyl Iodide Higher NO<sub>x</sub> Adsorption Test Report*, FCRD-MRWFD-2016-000352, INL/EXT-16-40087, Idaho National Laboratory, September 29, 2016.

Thallapally, P. K., 2015, *Produce Sorption Materials at Sufficient Quantity for INL Two Column Testing*, FCRD-MRWFD-2016-000253, December 2015.

Thallapally, P. K., 2016, *A New Calcium Based MOF Material for Room Temperature Removal of Xenon and Krypton: Two Column Approach*, FCRD-MRWFD-2016-000276, May 2016.

Thallapally, P. K., 2016, *Perform Cycle Testing to Measure the Stability and Performance of Sorption Material*, FCRD-MRWFD-2016-000302, September 2016.

Welty, A. K., T. G. Garn, and M. Greenhalgh, 2016, *Multi-Column Experimental Test Bed Using CaSDB MOF for Xe/Kr Separation*, FCRD-MRWD-2016-000260, March 1, 2016.

Welty, A. K., T. G. Garn, and M. Greenhalgh, 2016, *Superficial Velocity Effects on HZ-PAN and AgZ-PAN for Kr/Xe Capture*, FCRD-MRWD-2016-000024, April 1, 2016.

## Waste Form Development and Performance

The Waste Form Development and Performance activities are performed to meet two primary objectives:

- 1) Make a U.S. fuel cycle more effective by developing the next generation of waste management technologies. Fuel cycles in which any UNF treatment are performed will generate wastes from the separations processes and the fabrication of advanced fuels or targets containing materials to be transmuted. Three associated objectives are used to guide the selection of waste management concepts and waste forms and the development of those technologies:
  - Technologies to enable the reuse of UNF components that would otherwise require treatment, storage, transportation, and disposal as waste. Examples of such materials include cladding, noble metal fission products, uranium, and noble gases.
  - Long-lived radionuclide waste forms which have improved durability and provide more reliable performance in a range of potential disposal environments (compared to HLW glass) to reduce the reliance on engineered and natural barrier systems to meet regulatory requirements and thereby open new disposal options and reduce disposal costs.
  - Waste forms and processes that will facilitate lower cost management due to less expensive and less complex processing, lower storage and disposal costs, and greater flexibility for use in a wide range of disposal environments and fuel cycles.

The activities associated with this objective provide proof-of-principle and data necessary to compare advanced waste forms and processes being evaluated with the reference waste forms and processes described in recent waste form flowsheet studies. Four tasks were performed during FY2016, with accomplishments described in the following subsections:

- Ceramic waste form for HLW raffinate and potentially TRU waste
  - Glass ceramic for HLW raffinate
  - More efficient waste forms and processes for HLW from the electrochemical (echem) processing of fast reactor fuels
  - Zirconium purification.
- 2) Improve the understanding of degradation behavior of waste forms in various disposal environments to improve the scientific basis of radionuclide source-term estimates, reduce the conservatism in waste form performance estimates (and thereby reduce costs of engineering systems), and guide the development of optimized waste forms. The study of waste form degradation is initially focused on borosilicate glass, as this is the primary current HLW waste form in the U.S. and internationally and is the subject of significant international collaboration at present. The methods and approaches developed to understand glass waste performance will be used to understand the performance of other promising waste forms in the near future. Two general tasks are to be performed in support of this objective:

## 2016 ACCOMPLISHMENTS

- Glass waste form degradation testing and modeling
- Iodine waste form degradation scoping tests.

The activities associated with this objective advance the development of quantitative models with strong scientific bases for the degradation and radionuclide releases from glass and iodine-bearing waste forms for a range of waste form compositions in various disposal environments.

### EVALUATION OF CERAMIC WASTE FORMS – COMPARISON OF HOT ISOSTATIC PRESSED AND MELT PROCESSED FABRICATION METHODS

J. Amoroso (SRNL) and M. Tang (LANL)

SRNL is developing melt-processed reference ceramic waste forms for treatment of waste streams generated by reprocessing commercial UNF. The waste form is designed to crystallize into an engineered multiphase ceramic upon cooling from a melt (i.e., melt processing). Compositions are designed based on combinations of the waste and additives to target various phases. Elements with a +3 or +2 valence form perovskite ( $(A^{+2})TiO_3$ ) and pyrochlore ( $(A^{+3})_2Ti_2O_7$ ) type phases (Gunn et al. 2012; Ubic et al. 1999). Zirconium (+4 valence) partitions to a zirconolite ( $CaZrTi_2O_7$ ) phase (Xu and Wang 2000). Cesium and rubidium partition to a hollandite structure based on the general formula  $Ba_xCs_yM_zTi^{+4}_{8-z}O_{16}$  where  $z = 2x+y$  for trivalent cations and  $z = x+y/2$  for divalent cations for charge compensation (Aubin-Chevaldonnet et al. 2007; Carter et al. 2004; Carter et al. 2003). The targeted phase assemblage utilized at SRNL is based on the synthetic rock (SYNROC) family of titanate ceramics, the design of which is built on the concept of simulating naturally occurring minerals that have immobilized radionuclides over geologic timescales (Donald 2010). While the majority of SYNROC compositions are produced via HIP, earlier work conducted at SRNL has demonstrated that these materials can be successfully fabricated by melt processing under appropriate conditions (Amoroso et al. 2014a, 2014b; Amoroso 2015; Brinkman 2013).

FY 2016 efforts were focused on direct comparison of multiphase ceramic waste forms produced via melt processing and HIP methods. Based on promising waste form compositions previously developed at SRNL (Amoroso and Marra 2015), simulant material was prepared at SRNL, and a portion was sent to the Australian Nuclear Science and Technology Organization (ANSTO) for HIP treatments, while the remainder of the material was melt processed at SRNL. The microstructure, phase formation, elemental speciation, and leach behavior, and radiation stability of the fabricated ceramics was performed. In addition, melt-processed ceramics designed with different fractions of hollandite, zirconolite, perovskite, and pyrochlore phases were investigated for performance and properties. Table 7 lists the samples studied.

Figure 39 and Figure 40 show representative SEM and EDS analysis of the as-fabricated hot isostatic pressed and melt-processed samples. Significant differences in the grain microstructure, phase assemblage, and elemental speciation were evident.

TABLE 7. MULTI-PHASE WASTE FORM BASELINE COMPOSITIONS FABRICATED VIA MELT PROCESSING AND HIP.

Designation	Hollandite (wt. %)	Zirconolite (wt. %)	Pyrochlore (wt. %)	Perovskite (wt. %)	Metal (wt. %)	Fabrication Method
HIP-1250 <sup>a</sup>	65.40	14.61	16.84	2.54	0.61	HIP: 1,250°C
HIP-1300 <sup>a</sup>	65.40	14.61	16.84	2.54	0.61	HIP: 1,300°C
CAF-11113 <sup>a</sup>	65.40	14.61	16.84	2.54	0.61	Melt processing
CAF-21113	48.59	21.71	25.02	3.78	0.90	Melt processing
CAF-41113	32.09	28.68	33.05	4.99	1.19	Melt processing
CAF-21223	57.06	25.50	14.69	2.22	0.53	Melt processing
CAF-22123	55.67	12.51	28.83	2.18	0.52	Melt processing

a. Baseline composition.

The melt-processed samples exhibited characteristic large hollandite grains (darker gray areas) surrounded by zirconolite, pyrochlore, and perovskite phases (lighter gray areas). Very small regions with an almost black hue were found to consist primarily of TiO<sub>2</sub>. The barium, titanium, chromium, iron, and aluminum (not shown) elemental maps clearly indicate the formation of large hollandite grains. However, higher concentrations of chromium were observed at the interior of many hollandite grains, while aluminum (not shown) and iron were found in higher concentrations near the grain boundaries. Upon cooling from a melt, it is possible that chromium-rich regions crystallize into the hollandite phase first due to the higher melting point of the Cr<sub>2</sub>O<sub>3</sub> rich phase. Ideally, a significant portion of the cesium remaining in the system will be immobilized at this point. The remaining liquid in the system is then deficient in chromium and, upon cooling to a suitably low temperature, the crystallization of hollandite rich in aluminum and iron occurs.

Another notable feature of the melt-processed samples is the close correspondence among calcium, zirconium, and neodymium in the elemental maps. In the zirconolite structure, Ca<sup>2+</sup> or Zr<sup>4+</sup> can be substituted by Nd<sup>3+</sup>, and extensive neodymium substitution into the zirconolite structure leads to partitioning into pyrochlore and/or perovskite phases (Amoroso et al. 2014a, 2014b). While more precise determinations of compound stoichiometries in the calcium-neodymium-zirconium areas of the melt-processed samples are ongoing, it is likely that nominal compositions of Ca<sub>1-x</sub>Zr<sub>1-x</sub>Nd<sub>2x</sub>Ti<sub>2</sub>O<sub>7</sub> are forming and partitioning into various perovskite and pyrochlore phases.

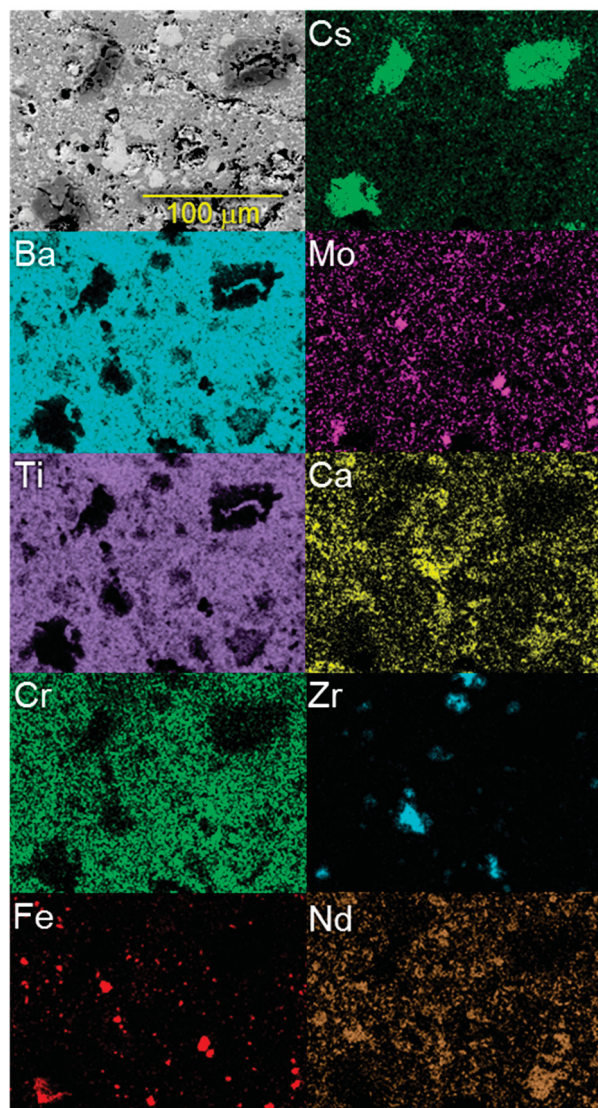


**Figure 39. SEM image and corresponding elemental maps of a sample hot isostatically pressed at 1,300°C.**

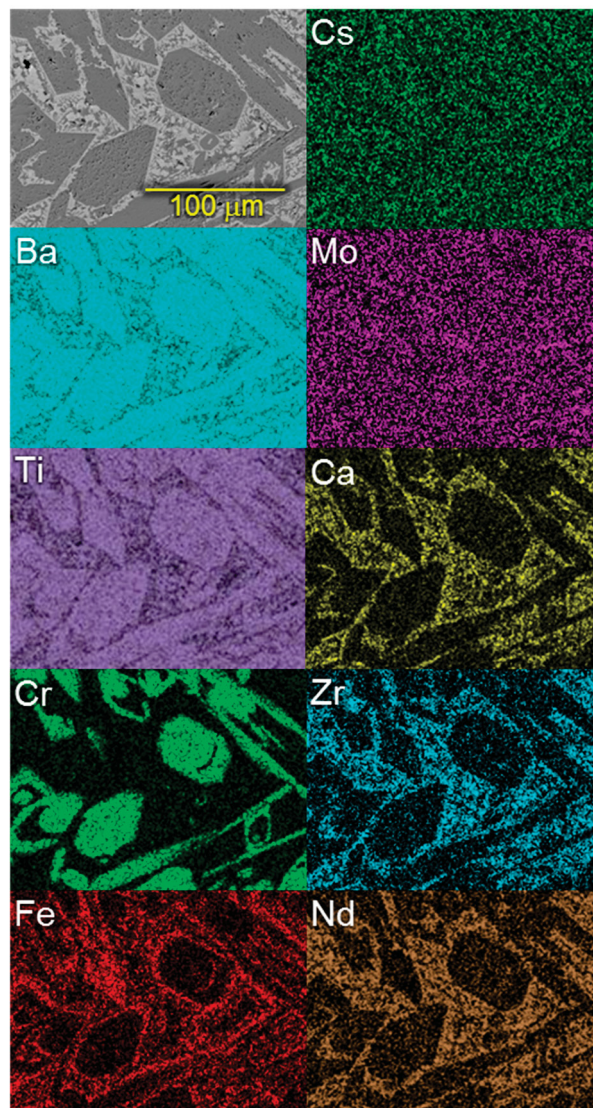


**Figure 40. SEM image and corresponding elemental maps of a CAF-11113 sample melt processed at 1,625°C.**

The samples that underwent HIP exhibited a more fine-grained microstructure characteristic of a solid-state densification process and displayed significant microstructural differences compared to the melt-processed samples. The samples that underwent HIP exhibited raised “islands” rich in cesium (dark in color in the SEM image) and appeared to be a cesium-titanate phase. This phase is consistent with the results of earlier work, where it was suggested that partial melting at HIP temperatures of 1,300 to 1,350°C results in cesium partitioning between the hollandite phase and an intergranular melt phase (Kesson 1983). There was a correspondence between the iron and molybdenum maps at several locations across the sample, suggesting

the formation of an iron-molybdenum compound. Also of significance is the speciation of calcium, neodymium, and zirconium compared to the melt-processed samples. In the melt-processed specimens, many regions were found to contain calcium, neodymium, and zirconium in comparable concentrations. In the samples that underwent HIP, higher concentrations of zirconium were found in localized regions, suggesting that the regions of high zirconium content could be  $ZrO_2$  or  $ZrTiO_4$  along with a perovskite phase.

Transmission electron microscopy (TEM) with energy-dispersive x-ray spectroscopy (EDX) was used to further identify crystalline phases and chemical composition in the multiphase ceramic waste form samples. Based on selected-area electron diffraction (SAED) patterns and EDX spectra, a hollandite phase (barium, aluminum, chromium, iron, titanium, oxygen), zirconolite/pyrochlore phases (calcium, zirconium, neodymium, titanium, oxygen), and a perovskite phase (strontium, calcium, titanium, oxygen) were identified in the melt-processed baseline sample. In the sample that underwent HIP, major crystalline phases, including hollandite and zirconolite, were found in addition to a phase not observed in the melt-processed sample and with chemical species including titanium, chromium, iron, molybdenum, and oxygen. Additionally, a perovskite phase was not observed in the sample subjected to HIP. Figure 41 shows a high-resolution TEM observation of an interface between hollandite and zirconolite phases in the baseline melt-processed sample.

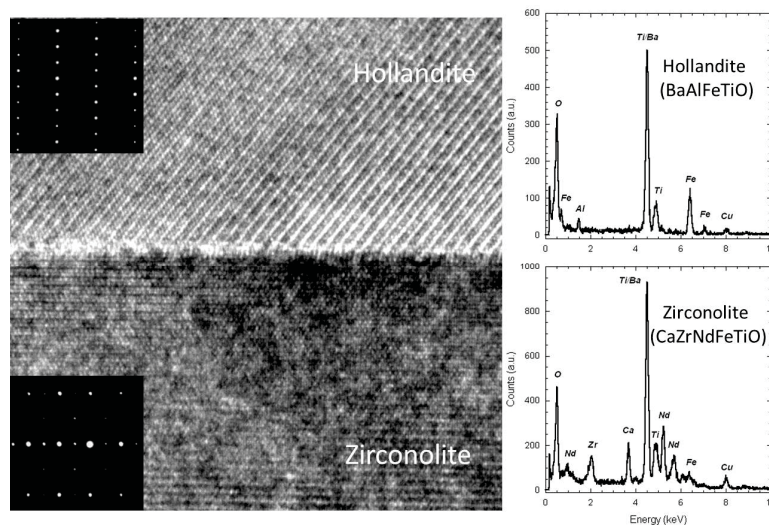


**Figure 41. High-resolution TEM observation of interface between hollandite and zirconolite phases in CAF-11113, including corresponding SAED patterns and EDX spectrums.**

Monolith leach tests were performed over 28 days to assess the chemical durability of melt-processed samples and samples subjected to HIP. Shown in Figure 42 is the cesium fractional release for the melt-processed and HIPed baseline composition as well as several other melt-processed compositions with varying targeted phase assemblages. It is evident that the cesium retention characteristics of the melt-processed baseline sample were superior to those of the other compositions. Although the sample that underwent HIP at 1,250°C exhibited less cesium release compared to the sample that underwent HIP at 1,300°C, both exhibited greater cesium release compared to melt-processed sample of the same

composition. Although the initial leach data provided are encouraging, it should be noted that the leach test data for other waste elements, including molybdenum and strontium, are still being analyzed.

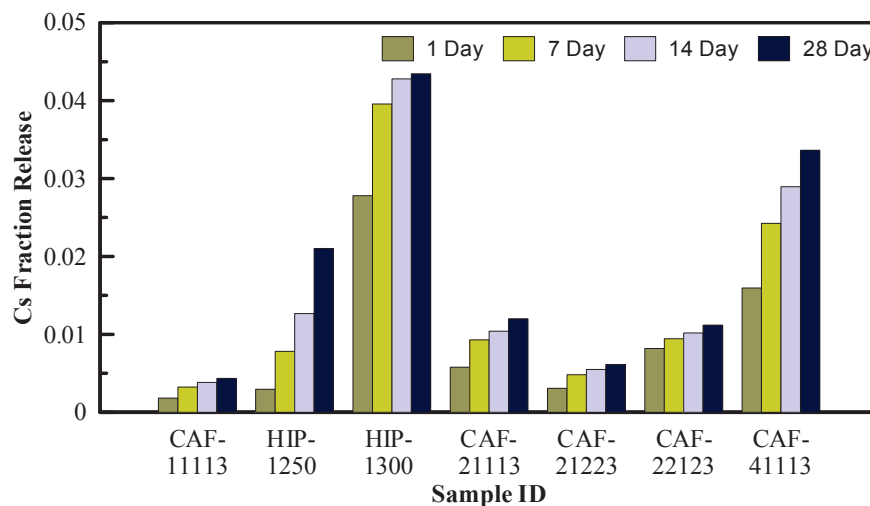


Figure 42. Fractional release of cesium from waste forms subjected to melt processing and HIP.

Samples that were subjected to melt processing and HIP were also irradiated with 400-keV krypton ions at a fluence of  $5 \times 10^{14}$  ions/cm<sup>2</sup>, corresponding to a dose level  $\sim 1$  displacement per atom (dpa). Radiation-induced microstructural evolution was investigated by cross-sectional TEM observation. The current study was focused on the hollandite and zirconolite phases. The TEM results, shown in Figure 43, indicate that the samples subjected to melt processing and HIP experience a nearly identical (even thickness of damage layer) amorphous transformation from crystalline under ion irradiation, suggesting that fabrication method does not affect radiation stability of the crystalline phases. Although, differential phase swelling may potentially be more impactful in melt processed samples due to large grain size.

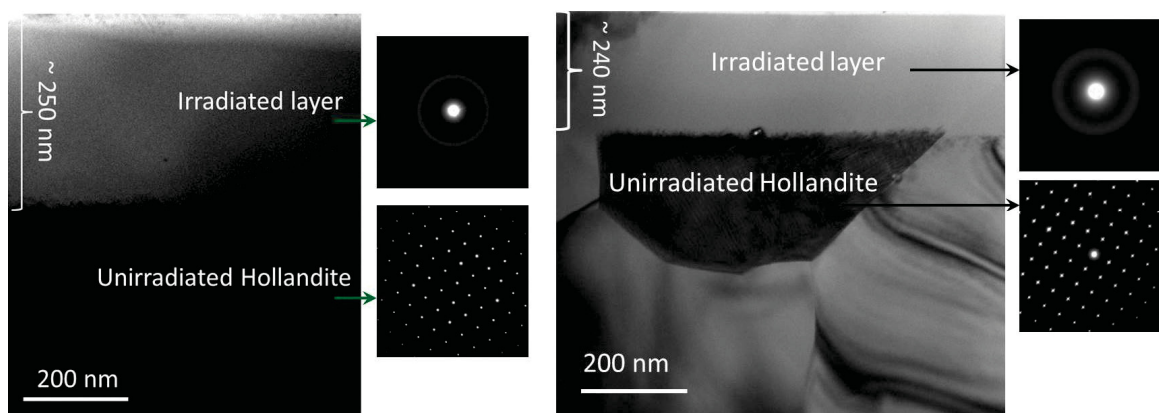


Figure 43. TEM observation of hollandite phase in irradiated CAF-11113 (left) and SW-1732 (right) samples.

### Synergistic Activities

A cooperative research and development agreement (CRADA) with ANSTO has also been in place to support the project. As part of the CRADA, the compositions developed at SRNL were prepared (subjected to HIP) at ANSTO and subsequently characterized by ANSTO, SRNL, and LANL. In addition, this work package is augmented by DOE-NEUP projects that are being conducted collaboratively with Alfred University and Clemson University. SRNL performed chemical-leach testing and analysis on various “designer” ceramic waste form materials being explored as a strategy to optimize the ceramic waste form through tailoring the amount and composition of the crystalline phases in the final waste form. Additionally, a student from Clemson University worked at SRNL during the summer to prepare, test, and analyze gallium-doped ceramic waste forms. Preliminary results indicate the retention of certain mobile species in aqueous environments can be significantly affected by the stoichiometry of the primary phases.

### References

Amoroso, J. W. and J. C. Marra, 2015, *Melt Processed Crystalline Ceramic Waste Forms for Advanced Nuclear Fuel Cycles - Final CRP Report for Research Agreement No. 17208*, U.S. Department of Energy Report SRNL-STI-2015-00437, Savannah River National Laboratory.

Amoroso, J. W., 2015, *Material Recovery and Waste Form Development – Ceramics Formulation optimization activities in FY15 – Preliminary Results (M4FT-15SR0307025)*, U.S. Department of Energy Report SRNL-L3100-2015-00185, Internal Memorandum, Savannah River National Laboratory.

Amoroso, J., J. C. Marra, M. Tang, Y. Lin, F. Chen, D. Su, and K. S. Brinkman, 2014, “Melt processed multiphase ceramic waste forms for nuclear waste immobilization,” *Journal of Nuclear Materials*, Vol. 454, No. 1–3, pp. 12–21.

Amoroso, J., J. Marra, S. D. Conradson, M. Tang, and K. Brinkman, 2014, “Melt Processed Single Phase Hollandite Waste Forms for Nuclear Waste Immobilization:  $Ba_{1.0}Cs_{0.3}A_{2.3}Ti_{5.7}O_{16}$ ; A = Cr, Fe, Al,” *Journal of Alloys and Compounds*, Vol. 584, pp. 590–599.

Aubin-Chevaldonnet, V., D. Caurant, A. Dannoux, D. Gourier, T. Charpentier, L. Mazerolles and T. Advocat, 2007, “Preparation and Characterization of  $(Ba,Cs)(M,Ti)_8O_{16}$  (M =  $Al^{3+}$ ,  $Fe^{3+}$ ,  $Ga^{3+}$ ,  $Cr^{3+}$ ,  $Sc^{3+}$ ,  $Mg^{2+}$ ) Hollandite Ceramics Developed for Radioactive Cesium Immobilization,” *Journal of Nuclear Materials*, Vol. 366, No. 1–2, pp. 137–160.

Brinkman, K., J. Amoroso, J. Marra, and M. Tang, 2013, *Crystalline Ceramic Waste Forms: Comparison of Reference Process for Ceramic Waste Form Fabrication*, U.S. Department of Energy Report SRNL-STI-2013-00442 (FCRD-SWF-2013-000229), Savannah River National Laboratory.

Carter, M. L., E. R. Vance, and H. Li, 2003, “Hollandite-rich Ceramic Melts for Immobilization of Cs,” *Materials Research Society Symposium Proceedings*, Vol. 807, pp. 249–254.

Carter, M. L., E. R. Vance, D. R. G. Mitchell, and Z. Zhang, 2004, “Mn Oxidation States in  $Ba_xCs_yMn_zTi_{8-z}O_{16}$ ,” *Materials Research Society Symposium Proceedings*, Vol. 824, pp. CC4.6.1–6.

## 2016 ACCOMPLISHMENTS

Donald, I. W., 2010, "Immobilization of Radioactive Materials as a Ceramic Wasteform," in *Waste Immobilization in Glass and Ceramic Based Hosts: Radioactive, Toxic and Hazardous Wastes*, Great Britain: John Wiley and Sons, pp. 185–203

Gunn, D. S. D., N. L. Allan, H. Foxhall, J. H. Harding, J. A. Purton, W. Smith, M. J. Stein, I. T. Todorov, and K. P. Travis, 2012, "Novel Potentials for Modelling Defect Formation and Oxygen Vacancy Migration in  $Gd_2Ti_2O_7$  and  $Gd_2Zr_2O_7$  Pyrochlores," *Journal of Materials Chemistry*, Vol. 22, No. 11, pp. 4675–4680.

Kesson, S. E., 1983, "The Immobilization of Cesium in SYNROC Hollandite," *Radioactive Waste Management and Environmental Restoration*, Vol. 4, No. 1, pp. 53–72.

Ringwood, A. E., S. E. Kesson, N. G. Ware, W. Hibberson, and A. Major, 1979, "Immobilization of High-level Nuclear-Reactor Wastes in SYNROC," *Nature*, Vol. 278, No. 5701, pp. 219–223.

Ubic, R., I. M. Reaney, and W. E. Lee, 1999, "Perovskite  $NdTiO_3$  in Sr- and Ca-doped  $BaO-Nd_2O_3-TiO_2$  Microwave Dielectric Ceramics," *Journal of Materials Research*, Vol. 14, No. 04, pp. 1576–1580.

Xu, H. F., and Y. F. Wang, 2000, "Crystallization Sequence and Microstructure Evolution of Synroc Samples Crystallized from  $CaZrTi_2O_7$  Melts," *Journal of Nuclear Materials*, Vol. 279, No. 1, pp. 100–106.

### GLASS CERAMIC WASTE FORM DEVELOPMENT FOR FISSION PRODUCTS FROM USED NUCLEAR FUEL (CLIENT NE)

*J. V. Crum (PNNL), M. Tang (LANL), and C. Crawford (SRNL)*

The borosilicate glass ceramic system is being developed to significantly increase waste loading of HLW generated during aqueous reprocessing of UNF relative to borosilicate glass (Crum et al. 2010, 2011). Glass ceramics are designed to be a single-phase melt at melting temperature and transform into a glass ceramic upon cooling inside the canister. This is achieved by tailoring the melt chemistry to favor crystallization of a large fraction of the insoluble  $MoO_3$  and lanthanides, which typically limit waste loading in borosilicate glass, into chemically durable and irradiation tolerant crystalline phases (oxyapatite, powellite, and lanthanide-borosilicate). Development work to date has demonstrated the potential of the glass ceramic waste form by achieving the following:

- Targeted crystalline phases upon slow cooling (FY 2012)
- 45 to 50 mass% waste loading (more than double that of borosilicate glass) (FY 2012)
- Targeted crystalline phases shown to be tolerant to gamma and ion irradiation (FY 2012–2014)
- Chemical durability of the waste form shown to be similar to that of borosilicate glass (FY 2014–2016)
- Melt viscosity and electrical conductivity shown to be within the operating envelope of a cold crucible melter (FY 2012–2015).

However, glass ceramics are still immature relative to borosilicate glass mainly due to the added complexity of a multiphase waste form. The transformation process from a single-phase melt to a glass ceramic is known qualitatively, but the exact sequence and temperatures when phase separation and crystallization occur is currently the subject of two ongoing NEUP projects. Understanding the transformation process is

important with regard to its impact on the melt rheology in the melter pour spout and canister as well as phase assemblage and microstructure upon canister cooling, considering that the microstructure and phase assemblage can impact the waste form durability. For these reasons, FY 2016 efforts focused on studying melt rheology and the chemical durability of the glass ceramic waste form.

**Glass Ceramic Melt Rheology (PNNL)**

During FY 2016, a rheology study was performed on a set of glass ceramics to determine the impact of crystallization on the melt rheology (yield stress and viscosity) in the melter pour spout and canister. Unlike borosilicate glass where the melter pour spout is cooled to stop flow between pouring events, the glass melt crystallizes significantly leading to high yield stress when pouring is restarted. The rheology of the glass ceramic must be understood as a function of chemistry, time, and temperature to properly design a robust pour spout. Additionally, as the melt flows into the canister it must flow sufficiently to spread and fill the canister.

Rheology measurements were made according to ASTM C 965-94 procedure (rotating spindle) on nine compositions as a function of temperature and time at temperature. Additionally, glass fibers were extracted at temperature to examine microstructures for comparison to the melt rheology. Newtonian behavior was observed at temperatures where melts were single-phase. Depending on the morphology of the melts, liquid phase separation and crystallization caused Bingham and more complex shear thinning rheologies. Figure 44 shows the effect of temperature on yield stress, viscosity, and morphology for the centroid glass ceramic composition (C42). The C42 composition showed fine- and large-scale phase separation and crystallization during rheology testing that impacted viscosity and yield stress. The yield stress of C42 increased due to liquid phase separation and fine-scale crystallization at ~1,275°C and further increased at temperatures <1,200°C due to further crystallization and crystal growth based on the observed fiber morphologies.

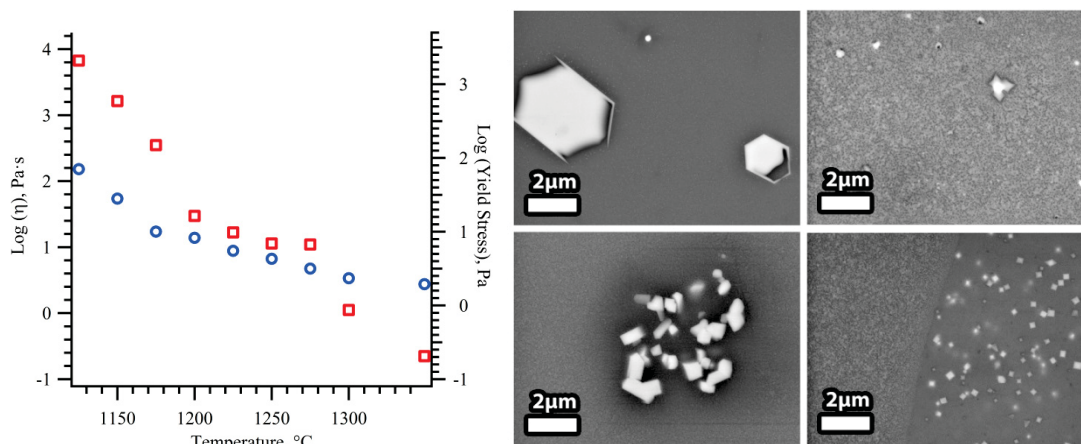


**Figure 44. Left: Viscosity (blue circles), yield stress (red squares), and morphology as a function of temperature with fixed 30-minute hold times for C42 (centroid composition). Right: SEM images—upper left, 1,174°C; lower left, 1,195°C; upper right, 1,249°C; and lower right, 1,298°C.**

## 2016 ACCOMPLISHMENTS

Table 8 summarizes the rheological behavior of the non-Newtonian melts, measured yield stress, and SEM observations of morphology as well as the resulting temperature required to remelt the crystallized glass inside the pour spout to a pourable rheology. Based on these results, the pour spout should be capable of operating consistently at 1,350°C to accommodate the full glass ceramic compositional space.

**TABLE 8. RHEOLOGY BEHAVIOR, OBSERVED PHASE, YIELD STRESS, AND PROJECTED POUR SPOUT TEMPERATURE OF MELTS.**

ID	Rheology Behavior	Fiber Observations	Yield Stress (Pa) at 1,125°C	Pour Spout (°C)
O23	Shear thinning	Crystals	1,177	>1,300
O24	Bingham	Undetermined	1,174	1,250
O25	Shear thinning	Droplets	3,235	1,350
O26	Bingham	Crystals	53	1,200
O27	Bingham	Crystals	34	1200
O28	Shear thinning	Crystals and droplets	1,904	1,250
O38	Bingham	Undetermined	315	1,200
O39	Bingham	Droplets	1073	1,175
C42	Bingham	Crystals	2,093	1,200

### Long-Term Static Corrosion Testing (SRNL)

Long-term static corrosion tests are ongoing with glass ceramics fabricated at crucible scale (Phase I at PNNL, Phase II at both PNNL and SRNL). Product consistency tests through 448 days using the ASTM C1285 (ASTM 2014) method have been completed on Phase II glass ceramics. Figure 45 shows the normalized concentration for boron versus time from these tests. Elemental analysis by NanoSIMS (Crum et al. 2016; Wang et al. 2016) shows that boron is detected in the glass phase and thus is a good indicator of glass corrosion rate. Two of the glass ceramics (Outer 22 and Inner 29) show significantly higher release than the other samples, which are all below 3 g/L. The overall trend in these longer-term corrosion data is similar to durable HLW glass waste forms that show relatively high initial release (Stage I) followed by a longer-term, lower-residual release (Stage II). These Phase II sample data are similar to the Phase I data that are also plotted in Figure 45. Non-leached powders as well as leached powders from the Phase II long-term 448 day tests that show highest release (O22 and I29) are currently being examined by SEM.

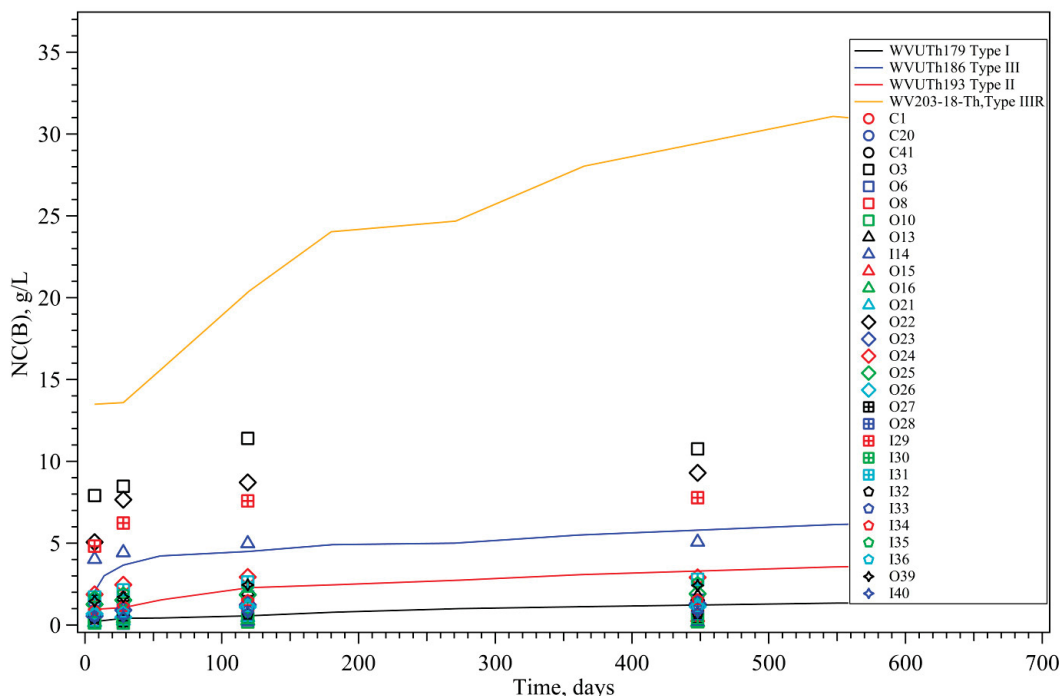


Figure 45. Phase II normalized concentration based on boron through 448 days. WF glasses from ALTGlass Database (Jantzen 2013). Concentrations normalized to full wasteform composition.

**Corrosion Testing in Dilute Conditions (PNNL)**

Single-pass flow-through testing was performed to gather release rate data in dilute conditions (near forward rate) for the C20 (centroid) glass ceramic produced at three different cooling rates (0.25X, 1X, and 4X, where X is the canister centerline cooling rate), at pH = 7 and 9, for a range of solution-flow-rate-to-glass-surface-area ratios (q/S) at 90°C. The measured steady-state release rates for boron, molybdenum, and neodymium at the highest tested q/S are given in Table 9 as a function of canister cooling rate and pH. Figure 46 shows the B release rate as a function of pH and q/S with the highest q/S being at or near the forward rate. Elemental analysis by NanoSIMS and SEM/EDS found B is essentially confined to the glass phase, molybdenum is mainly confined to the powellite phase, and neodymium is mainly confined to the oxyapatite phase. Thus, these elements can be used as indicators of the relative chemical durability of the individual phases. In this initial stage of corrosion, the oxyapatite shows the lowest dissolution, while the powellite and glass phase show similar dissolution rates at both test pHs. However, it should be noted that the glass phase is the continuous phase and can limit the exposure of powellite and oxyapatite over time, thus convoluting the results. All other major components in the glass ceramics are found in multiple phases.

In the future, each phase (residual glass, powellite, and oxyapatite) will be synthesized and tested separately to gain a better understanding of release rates for each phase and how they relate to the behavior of the overall waste form.

## 2016 ACCOMPLISHMENTS

TABLE 9. MEASURED STEADY-STATE RELEASE RATES OF BORON, MOLYBENUM, AND NEODYMIUM (NORMALIZED TO FULL WASTE FORM COMPOSITION) AS A FUNCTION OF CANISTER COOLING RATE AND PH FOR THE HIGHEST Q/S TESTED.

Cooling Rate	pH at RT	q/S m/s	SON68 Literature g/m <sup>2</sup> /d	B (glass) g/m <sup>2</sup> /d	Mo (powellite) g/m <sup>2</sup> /d	Nd-144 (oxyapatite) g/m <sup>2</sup> /d
1/4x	7	1.1E-05	3.0E-01 <sup>a</sup>	2.2E+01	3.6E+01	6.0E-01
1/4x	9	5.1E-06	4.5E+00 to 5.5E+00 <sup>b</sup>	4.0E+00	3.6E+00	<2.1E-03
1x	7	1.1E-05	3.0E-01 <sup>a</sup>	2.2E+01	8.4E+01	1.3E+00
1x	9	4.8E-06	4.5E+00 to 5.5E+00 <sup>b</sup>	4.2E+00	4.1E+00	<3.8E-04
4x	7	1.2E-05	3.0E-01 <sup>a</sup>	1.3E+01	4.4E+01	7.3E-01
4x	9	5.7E-06	4.5E+00 to 5.5E+00 <sup>b</sup>	2.7E+00	3.4E+00	<1.6E-03

a. Icenhower and Steefel 2015.

b. Jégou and Gin et al. 2000, Frugier and Gin et al. 2008.

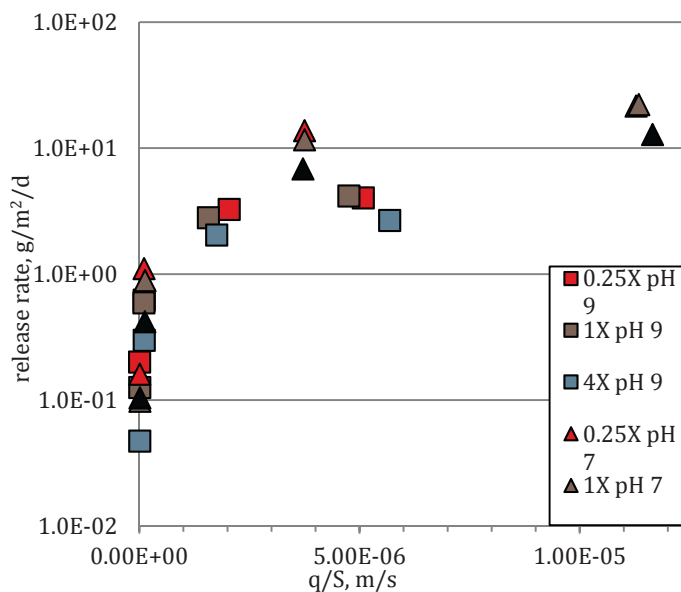
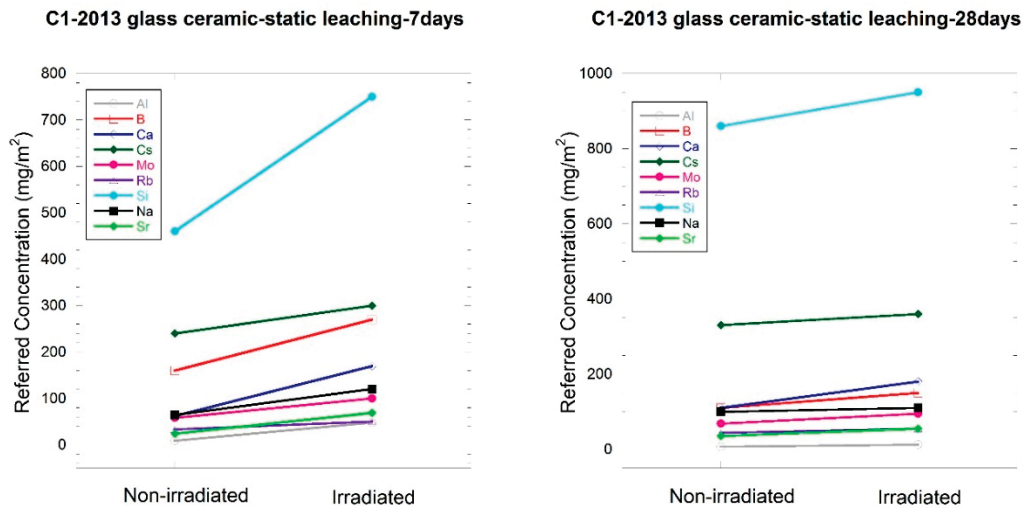


Figure 46. Boron release rate (normalized to full waste form composition) versus q/S ratio at 90°C and pH = 7 and 9.

**Chemical Durability and Radiation Stability (LANL)**

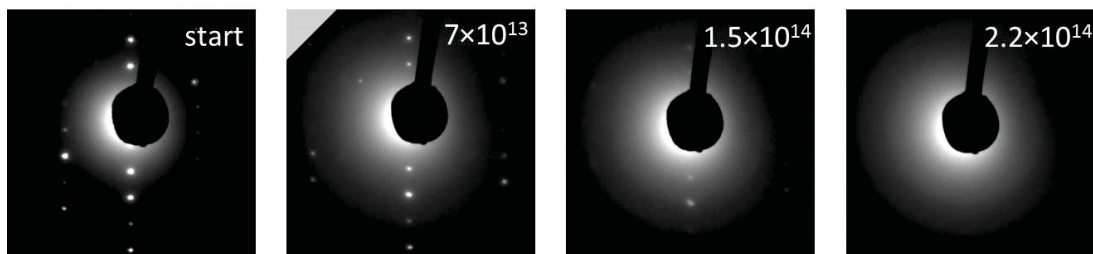
Static leach testing on nonirradiated and irradiated glass ceramic samples was performed using the ASTM C1220 method. Here, 200 keV He (alpha) irradiation with a fluence of  $1 \times 10^{17}$  ions/cm<sup>2</sup> (corresponding to a dose of  $\sim 2$  dpa) at RT was used to simulate self-radiation during nuclear waste form storage. The objective is to investigate radiation damage effects on chemical durability of glass ceramic waste form samples. Two glass ceramic samples labeled as “C1-2013” and “I2-2013,” which represent different locations in the canister, were tested in this study. ICP-MS and augur electron spectroscopy were used to analyze leachates. Figure 47 shows the concentration of elements of nonirradiated and irradiated C1-2013 samples after duration times of 7 and 28 days. Data from I2-2013 are not shown here, because they exhibited results similar to C1-2013 data. All measured elements in irradiated samples exhibit higher concentration in the leaching solution than those in nonirradiated samples, and long-term (28 days) leaching data also show the same trend as short-term (7 days) data. The data suggest that alpha radiation damage is detrimental to chemical durability of glass ceramic samples.



**Figure 47. Leaching results (7 and 28 days) of nonirradiated and irradiated glass ceramic C1-2013 samples.**

Oxyapatite has been proposed as a potential nuclear waste form prior to this work and is found in our multiphase glass-ceramic samples. Radiation stability of single-phase oxyapatite and oxyapatite phase in multiphase glass ceramic samples has been studied in past FYs. Here, in situ 1 MeV krypton ion irradiations were performed on single-phase oxyapatite with a chemical composition of Ca<sub>2</sub>Nd<sub>8</sub>Si<sub>6</sub>O<sub>26</sub> at various temperatures. The ion beam is produced by a tandem ion accelerator that is attached to a HITACHI H-9000NAR microscope. The microscope was operated at 200 kV, and the radiation-induced microstructural evolution was monitored intermittently by SAED patterns. The objective of these experiments was to study the temperature effect on radiation tolerance and determine the critical amorphization dose of oxyapatite. Figure 48 shows two sequences of SAED patterns of oxyapatite phase irradiated with 1 MeV krypton at RT and 250°C, respectively. The oxyapatite phase was readily amorphized at a fluence of  $2.2 \times 10^{14}$  krypton/cm<sup>2</sup> (corresponding to a dose of 0.3 dpa) at RT, while at elevated temperature 250°C, no amorphization was observed at very high fluences ( $2 \times 10^{15}$  Kr/cm<sup>2</sup>, corresponding to 3 dpa). The data suggest the radiation tolerance of the oxyapatite phase is improved at elevated temperature similar to waste storage temperature.

## Oxyapatite: in-situ 1 MeV Kr irradiation at room temperature



## Oxyapatite: in-situ 1 MeV Kr irradiation at 250 °C

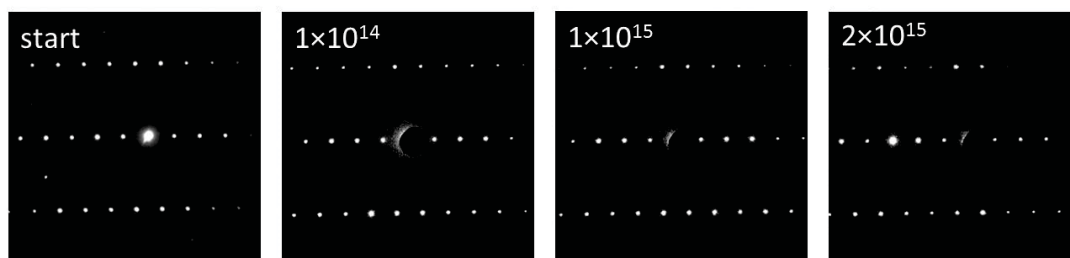


Figure 48. Sequences of SAED patterns for oxyapatites irradiated by 1 MeV krypton ions at RT and 250°C.

## References

ASTM C1285, 2002, "Standard Test Methods for Determining Chemical Durability of Nuclear, Hazardous, and Mixed Waste Glasses and Multiphase Glass Ceramics: The Product Consistency Test (PCT)," ASTM International.

Crum, J. V., L. R. Turo, B. J. Riley, M. Tang, A. Kossoy, and K. E. Sickafus, 2010, *Glass Ceramic Waste Forms for Combined CS+LN+TM Fission Products Waste Streams*, PNNL-19780, Pacific Northwest National Laboratory, September 24, 2010.

Crum, J., J. Neeway, B. Riley, Z. Zhu, M. Olszta, and M. Tang, 2016, "Dilute Condition Corrosion Behavior of Glass-Ceramic Waste Form," *Journal of Nuclear Materials*, Vol. 482, pp.1-11.

Crum, J. V., B. J. Riley, L. R. Turo, M. Tang, and A. Kossoy, 2011, *Summary Report: Glass-Ceramic Waste Forms for Combined Fission Products*, PNNL-20749, Pacific Northwest National Laboratory, September 23, 2011.

Frugier, P., S. Gin, Y. Minet, T. Chave, B. Bonin, N. Godon, J.E. Lartigue, P. Jollivet, A. Ayrat, L. De Windt, and G. Santarini, 2008, "SON68 Nuclear Glass Dissolution Kinetics: Current State of Knowledge and Basis of the New Graal Model," *Journal of Nuclear Materials*, Vol. 380, No. 1-3 pp. 8-21.

Icenhower, J. P. and C. I. Steefel, 2015, "Dissolution Rate of Borosilicate Glass SON68: A Method of Quantification Based Upon Interferometry and Implications for Experimental and Natural Weathering Rates of Glass," *Geochimica Et Cosmochimica Acta*, Vol. 157, pp. 147–163.

Jegou, C., S. Gin, and F. Larche. 2000. "Alteration Kinetics of a Simplified Nuclear Glass in an Aqueous Medium: Effects of Solution Chemistry and of Protective Gel Properties on Diminishing the Alteration Rate," *Journal of Nuclear Materials*, Vol. 280, No. 2, pp. 216–229.

Wang, Z., J. Liu, Y. Zhou, J. J. Neeway, D. K. Schreiber, J. V. Crum, J. V. Ryan, X.-L. Wang, F. Wang, and Z. Zhu, 2016, "Nanoscale imaging of Li and B in nuclear waste glass, a comparison of ToF-SIMS, NanoSIMS, and APT," *Surface and Interface Analysis*, Vol. 48, No. 13, pp. 1392–1401.

## ELECTROCHEMICAL (ECHEM) WASTE FORMS

Advanced waste forms and degradation models are being developed for metallic and salt waste streams generated during electrochemical processing of used fuel that optimize waste loading and simplify waste form production. Key aspects addressed regarding metal waste forms were (1) formulating durable compositions using HT9 clad fuel metal wastes, which has less chromium, molybdenum, and Ni than Type 316 steel and is less resistant to corrosion, (2) deriving environmental dependencies, and (3) measuring model parameter values for HT9-based waste forms. Tests with advanced ceramic waste forms (ACWF) addressed formulation of new binder glasses to increase salt waste loading, facilitate processing, and generate durable waste forms. Several ACWF compositions were examined in detail and subjected to corrosion tests to confirm our mechanistic understandings of waste form production and corrosion behavior.

### Echem Metal Waste Forms

*W. Ebert and V. Gattu (ANL) and L. Olson (SRNL)*

A degradation model is being developed for metallic waste forms used in advanced fuel cycles utilizing metallic fuels in steel cladding. A testing protocol using standard electrochemical methods has been developed to (1) establish the technical basis of the degradation model; (2) identify key variables affecting the corrosion rate and parameterize analytical models quantifying those effects, including waste form composition and environmental conditions; (3) relate the electrochemical corrosion behavior to the release rates of radionuclides immobilized in the waste form; and (4) provide confidence in the long-term release rates calculated with the degradation model (Ebert 2014). The degradation model uses separate terms to represent the effects of the alloy and solution compositions, the stabilizing effects of passivation, and the effect of solubility limits on radionuclide release into solution.

An electrochemically based testing protocol was developed to support model development and measure model parameter values (Ebert and Kolman 2013). Tests have been conducted to assess the chemical and redox effects of solutions on the corrosion behaviors of several representative alloy waste form (RAW) materials made with Type 316 or HT9 steel cladding and to understand corrosion processes for modeling long-term behavior. Because HT9 steel has less chromium, molybdenum, and nickel than Type 316 steel and is less resistant to corrosion, the benefits of adding trim metals to improve the long-term durability of HT9-based waste forms are being evaluated. Four variations of RAW-6 were formulated to evaluate the benefits

## 2016 ACCOMPLISHMENTS

of adding different amounts of chromium and nickel on the corrosion resistance of waste forms made with HT9 cladding (see Table 10). The fuel waste provides molybdenum, which benefits waste form durability, and the amounts of molybdenum in the RAW6 materials are included in the table.

TABLE 10. MASS FRACTIONS OF PASSIVATING ELEMENTS IN TYPE 316 AND RAW-6 MATERIALS.

Element	Type 316	RAW-6(Re)	RAW-6(Ni1)	RAW-6(Ni3)	RAW-6(Ni5)
Cr	0.184	0.1674	0.1822	0.1534	0.1257
Mo	0.023	0.0268	0.0308	0.0300	0.0293
Ni	0.124	0.1214	0.0304	0.0789	0.1255

Ingots of each material were prepared by melting HT9 and reagent metals, and specimens cut from each material were fashioned into electrodes for use in electrochemical corrosion tests. The testing approach includes four major steps to provide data used for modeling long-term durability: (1) perform potentiodynamic (PD) polarization scans to measure the bare surface corrosion behaviors in different solutions, (2) conduct potentiostatic (PS) tests to monitor the evolution of the corrosion current and electrical properties of the surface as it stabilizes at different imposed voltages in different solutions, (3) measure solution concentrations of RAW constituents during PS tests, and (4) characterize corroded electrodes to identify actively corroded phases. The tests discussed herein were conducted in 10 mM NaCl solutions adjusted to pH values from 2 to 12 using H<sub>2</sub>SO<sub>4</sub> or NaOH.

Figure 49 a shows the PD scans for these four materials in pH 3 solutions are very similar except for the following: the E<sub>corr</sub> value for RAW-6(Ni3) is lower (about -300 mV), transpassive corrosion of RAW6(Re) occurs at a higher potential (about 400 mV), and RAW6(Re) has higher corrosion currents in the passive region. Tests with RAW6(Re) were conducted at ANL using a microelectrode and microcell, whereas tests with the other materials were conducted at SRNL using a standard electrode and reaction cell. Figure 49b is a SEM image of the corroded surface of RAW6(Re) after the PD scan at pH 3. The bright phase (Phase 1) is a 45Fe-33Zr-8Ni-5Cr-2Mo solid solution; the black regions (X) are voids where some regions of Phase 1 have dissolved away; and the grey phase (Phase 2) is a 70Fe-20Cr-3Ni-3Mo intermetallic phase that is not visibly corroded. The small light spots are molybdenum-bearing corrosion products. The same phases were formed in the other RAW6 materials (with slightly different compositions) and corroded in similar fashion.

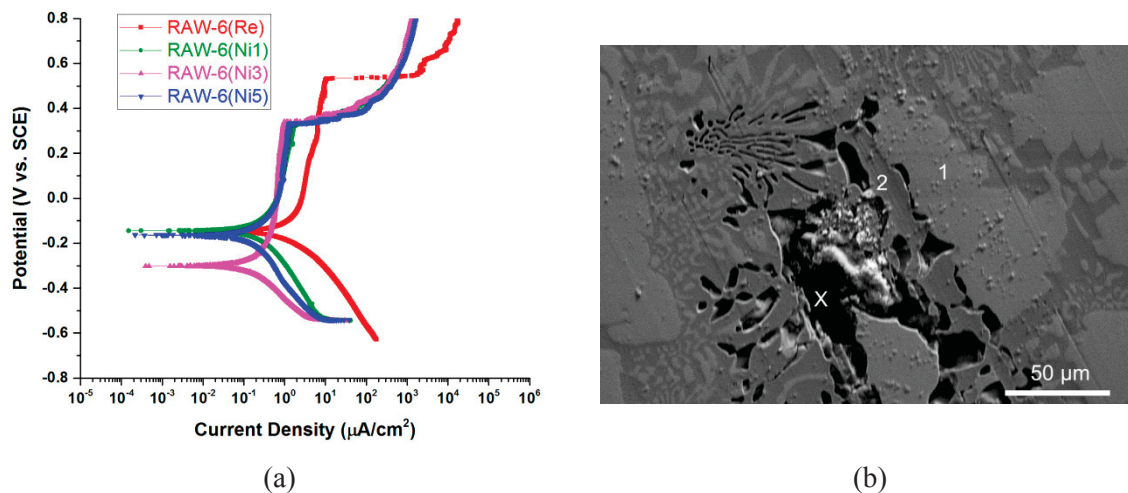
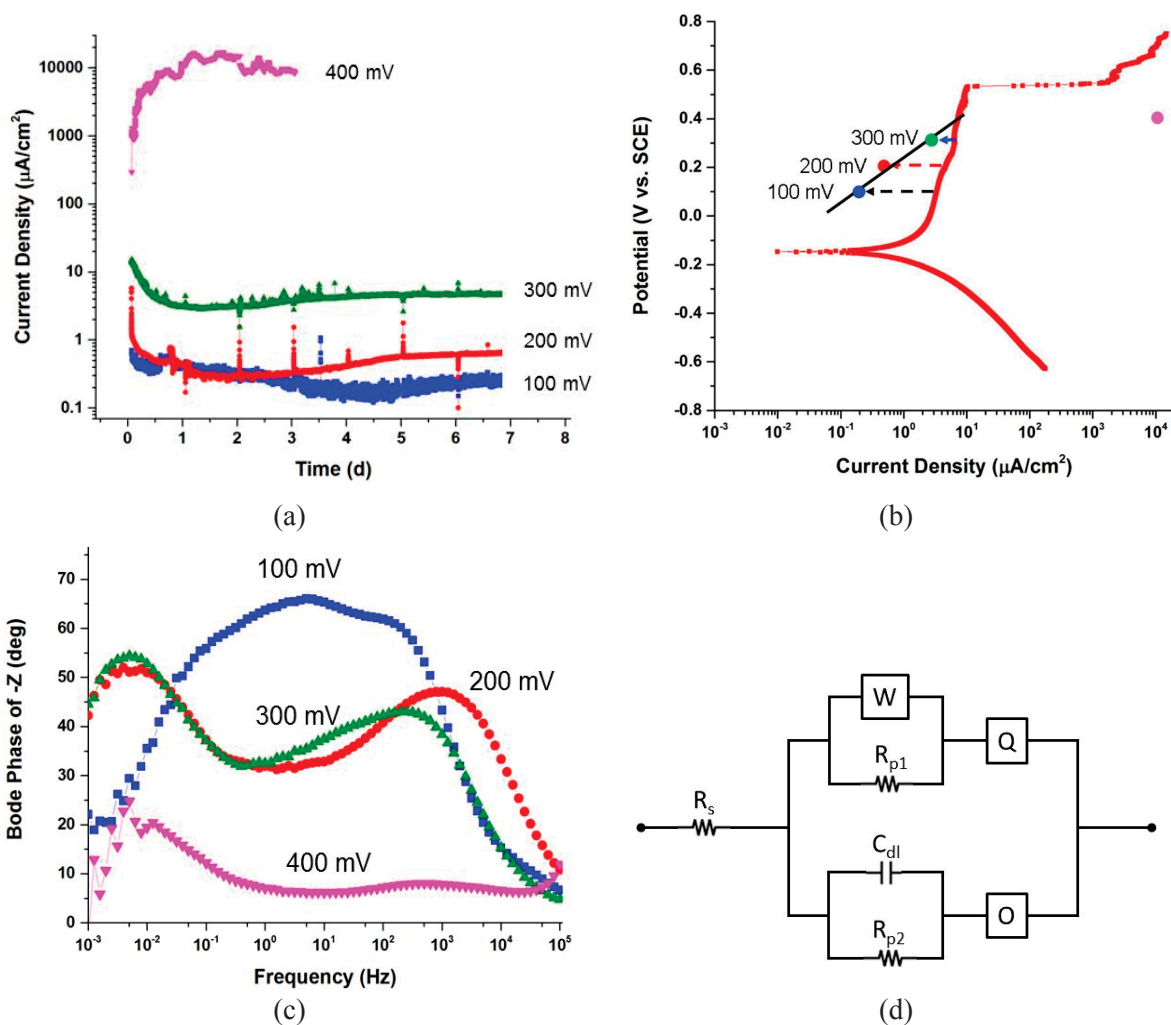


Figure 49. (a) PD scans of RAW6 materials in pH 3 solution and (b) corroded surface of RAW6(Re) after PD scan.

Figure 50a shows the evolution of corrosion current density in PS tests at each voltage. The surface stabilized in tests at 100, 200, and 300 mV but corroded actively in the test at 400 mV. The stabilized corrosion currents are shown as circles in Figure 50b for comparison with the currents measured for the bare surface in the PD scan. This shows moderate stabilization occurs due to passivation at moderate potentials, but the passivation indicated by the PD scan is not sustained in the PS tests. The line drawn through the results shows the dependences of the long-term rate on the redox potential of a solution that can be used in the degradation model below 400 mV for dissolution in a pH 3 solution. The corrosion current density measured in the PS test is used to represent the oxidation rate of the waste form, and the electrochemical impedance spectroscopy (EIS) results provide confidence in the long-term stability of that rate. The Bode phase angle plots of the EIS results shown in Figure 50c indicate that the RAW6(Re) surface does not passivate in the test at 400 mV, the same two similar passivating layers form in tests at 200 and 300 mV, and a different passivating layer forms at 100 mV. The EIS results can be represented using equivalent circuits to quantify changes in the electrical properties of surfaces stabilized at different potentials and calculate the current-voltage dependence of each passivated surface. Equivalent circuit modeling provides confidence in the long-term relevance of the behaviors measured in short-term PS tests. Figure 50d is a circuit diagram fitting the EIS results for PS tests at 200 and 300 mV. The upper branch represents the 45Fe-33Zr-8Ni-5Cr-2Mo solid (Phase 1), the lower branch represents the 70Fe-20Cr-3Ni-3Mo intermetallic phase (Phase 2), and  $R_s$  represents the solution resistance. Phase 2 is passivated by formation of a robust  $\text{Cr}_2\text{O}_3$  layer, which is represented by the capacitor  $C_{dl}$ . The circuit element “O” represents the oxidizing influence of autocatalytic  $\text{H}_2$  formation on the noble metals (Stern and Wissenburg 1959), which enhances formation of the  $\text{Cr}_2\text{O}_3$  layer. Phase 1 is weakly passivated by formation of both  $\text{ZrO}_2$  and  $\text{Cr}_2\text{O}_3$  layers: “W” is a Warburg element that represents the effect of  $\text{ZrO}_2$  dissolution (i.e., charge carried by  $\text{Zr}^{4+}$ ), and “Q” is a constant phase element that represents the weak influence of a  $\text{Cr}_2\text{O}_3$  film, which is not an efficient passivating film due to the low chromium content of Phase 1.



**Figure 50. Results for electrochemical tests with RAW6(Re) showing (a) corrosion current densities measured in PS tests, (b) comparison of currents measured in PD scan and PS tests, (c) Bode phase angle plots of EIS results, and (d) equivalent circuit fitting EIS results at 200 and 300 mV.**

As shown in Figure 51a, similar results were obtained for tests with RAW6(Ni3) at pH 3, except breakdown of passivation occurred at 300 mV, which is consistent with the differences seen in the PD scans, and cathodic reactions were dominant at -100 mV. The latter observation indicates  $E_{\text{corr}}$  increased from about -300 mV in the PD scan to above -100 mV due to surface stabilization. Figure 51b shows the normalized mass losses of chromium and molybdenum in PS tests at different voltages calculated from solution compositions measured after different test durations. Small amounts of chromium and molybdenum are released initially, but releases slow as  $\text{MoO}_2$ ,  $\text{Cr}_2\text{O}_3$ , and  $\text{ZrO}_2$  passive layers form in tests at 0, 100, and 200 mV; the initially released chromium is removed from solution as layers form in tests at 100 and 200 mV. Active release of chromium and molybdenum occurs in the PS test at 300 mV as the 45Fe-33Zr-8Ni-5Cr-2Mo phase corrodes. The release behavior of rhenium is represented by that of molybdenum. The current densities measured in the PS tests are included in Figure 51a to show how the Eh-dependence of the oxidation rate can be

modeled. The rates in the passive region are extrapolated to lower voltages to provide bounding values for conditions in which anodic currents are masked by cathodic currents. A discontinuity represents breakdown of passivation at the high potential limit, and the transpassive corrosion rate measured in the PD scan is used. This approach provides simple analytical functions for the Eh dependence at each pH, temperature, and Cl<sup>-</sup> concentration that can then be used to derive functions for the dependencies on those variables. The testing and modeling activities provide confidence in the approach taken for waste forms developed for metallic waste streams.

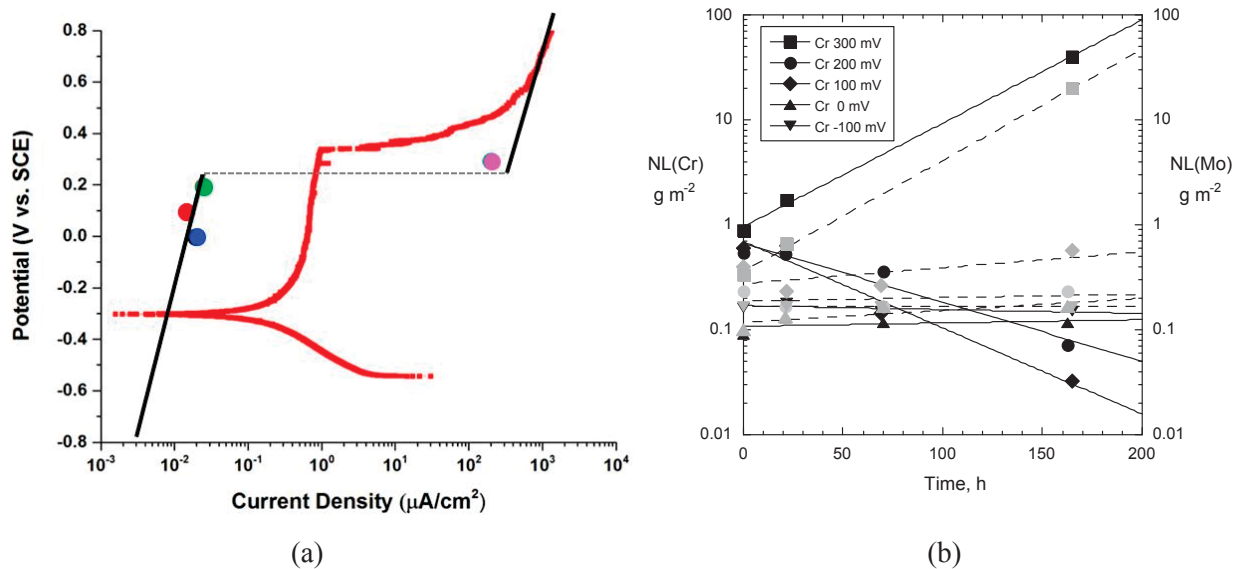


Figure 51. Results for electrochemical tests with RAW6(Ni3) showing (a) currents for stabilized surfaces in PS tests compared to PD scan and (b) releases of chromium (dark symbols) and molybdenum (light symbols) into solution during PS tests.

### References

Ebert, W. L., 2014, *Radionuclide Source Term Model for Metallic Waste Forms*, FCRD-SWF-2014-000244, Argonne National Laboratory.

Ebert, W. L. and D. Kolman, 2013, *Alloy Waste Form Testing Strategy Roadmap*, FCRD-SWF-2013-000226, Argonne National Laboratory.

Stern, M. and H. Wissenburg, 1959, "The influence of noble metal alloy additions on the electrochemical and corrosion behavior of titanium," *Journal of the Electrochemical Society*, Vol. 106, pp. 759–764.

## 2016 ACCOMPLISHMENTS

### Echem Salt Waste Forms

*W. Ebert (ANL), S. Frank (INL), and B. Riley (PNNL)*

ACWF materials are being developed to utilize Na<sub>2</sub>O from the binder glass to convert all of the Cl<sup>-</sup> in the waste salt to sodalite and optimize waste loading. The ACWF materials were formulated based on understanding the production and corrosion behavior of glass-bonded sodalite ceramic waste form (CWF) materials developed over the past 20 years (Ebert et al. 2016; Ebert 2005). The reaction used to generate sodalite (at about 850°C) is:



zeolite 4A          sodalite

Reactions of other alkali metal cations with zeolite 4A form aluminosilicates rather than equivalent chlorine-bearing phases. However, the addition of a sodium borosilicate glass to the system results in ion exchange between the M<sup>+</sup> from other alkali metal chlorides (MCl) and Na<sup>+</sup> from the glass to generate NaCl and incorporate M<sup>+</sup> into the glass phase at the processing temperature as:



and M<sup>2+</sup> as



The first terms on the left hand sides of Reactions 3 and 4 represent Na<sup>+</sup> associated with a non-bridging oxygen in the glass by a mostly ionic bond. These Na<sup>+</sup> exchange with M<sup>+</sup> and M<sup>2+</sup> from the salt to generate NaCl, which can then react with zeolite 4A to form sodalite, and M bonds with the non-bridging oxygen in the glass (i.e., M is dissolved in the glass). The stoichiometries of Reactions 2, 3, and 4 control the salt waste loadings in CWF materials. So-called ACWF materials are made using new binder glasses formulated to provide sufficient sodium to convert all of the Cl<sup>-</sup> to sodalite to optimize salt waste loading, processing operations, and waste-form performance. New binder glasses were also formulated with physical properties to enhance the efficiency of reactions to form sodalite and produce a densified waste form by thermal processing at ambient pressures. Characterizations performed on the as-made glasses included density, dilatometric measurements (for glass transition and softening temperatures), and thermal expansion measurements from RT to just above the softening temperature.

Prototype ACWF products were made using five new binder glasses having high Na<sub>2</sub>O contents and various amounts of a representative LiCl/KCl-based salt waste to generate ACWF materials with 11 to 14 mass% salt loadings. Table 11 summarizes the materials that have been evaluated and some physical characteristics. The baseline materials were made using P57 glass with 8 or 11 mass% salt. The “Phase 1” ACWF materials were all made with 11 mass% waste salt to compare the effectiveness of five new binder glass formulations. The “Phase 2” ACWF materials were made using binder glass N4 with different salt loadings and amounts of glass. The microstructures and corrosion behaviors were evaluated and compared with results of similar tests run with CWF products that were made using the original binder glass P57 with 8 mass% of the same salt (referred to as baseline CWF).

Analyses included optical microscopy and SEM to characterize morphology and porosity (open and closed); EDS, time-of-flight SIMS, and atom probe tomography for composition analyses; XRD (RT and hot-stage) for phase distribution; and pycnometry and Archimedes' technique for bulk density and closed porosity.

TABLE 11. MEASURED PHASE COMPOSITION, DENSITY, VOLUMETRIC POROSITY, AND SURFACE POROSITY OF CWF AND ACWF PRODUCTS.

Product ID	Salt Waste Loading, %	Phase Composition, mass%			Density, g cm <sup>-3</sup>	Porosity, vol %	Porosity, area %
		Sodalite	Halite	Glass			
Baseline CWF Materials							
CWF-P1-8	8	8.5	5.5	86	2.13	0.7	3.5
CWF-P6-11	11	39	4.2	57	1.50	33	43
Phase 1 ACWF Materials							
ACWF-N2-11	11	57	2.9	40	1.35	42	43
ACWF-N3-11	11	62	2.9	35	1.30	44	44
ACWF-N4-11	11	63	3.1	34	1.28	45	54
ACWF-N5-11	11	62	2.6	35	1.44	38	35
ACWF-N6-11	11	68	2.4	30	1.44	37	38
Phase 2 ACWF Materials							
ACWF-N4F-11	11	70	3.7	26	1.45	38	40
ACWF-N4-12	12	67	3.6	29	1.37	42	33
ACWF-N4-14	14	61	7.5	31	1.40	40	26
ACWF-N4G-10	10	50	3.4	47	1.90	8.0	5.1

Compositional analysis confirmed that alkali exchange occurred during processing: essentially all of the lithium and potassium in the salt-occluded zeolite were exchanged with sodium from the glass. Representative results are shown in Figure 52 for an ACWF made with new binder glass N3 and 11 mass% salt loading. The relative amounts of aluminum and silicon in the sodalite and glass phases reflect the sodalite stoichiometry, and all boron remained in the glass phase.

A series of corrosion tests were conducted with the ACWF materials to verify the degradation behaviors were the same as those measured for CWF materials. Most tests followed a modified ASTM C1308 procedure to focus on the initial dissolution behavior in dilute solutions. These test conditions highlighted the effect of element distributions between sodalite, glass, and unreacted salt (with the primary focus on cesium) and confirmed dissolution kinetics of the sodalite and binder glass phases were controlled by surface dissolution. For example, Figure 53a and Figure 53b show the cumulative releases of key elements from ACWF-N4-11 and ACWF-N4-14. The linear results indicate the releases of all are controlled by surface dissolution with no diffusion component, and the similar slopes for element releases from the different materials indicate the same phases are dissolving. The similar slopes for boron and cesium indicate they are being released from the glass phase, but the high y-intercepts for sodium from ACWF-N4-11 and both sodium and cesium from ACWF-N4-14 indicate that significant fractions are released from unincorporated

## 2016 ACCOMPLISHMENTS

salt. This indicates the waste salt is effectively incorporated at waste loadings of 10, 11, and 12 mass% but not at a waste loading of 14 mass%.

This work shows almost twice the amount of sodalite can be generated in ACWF materials using the new binder glasses as that in the baseline CWF to achieve higher waste salt loadings while generating less halite. Additionally, the thermal expansion coefficients of the ACWF materials better matched that of the sodalite than CWF materials, which should result in less cracking and fewer voids in the waste forms. The phase compositions in the ACWF materials confirmed our understanding of the reactions occurring during waste form production. However, the porosities of the resulting ACWF materials are higher than is desired; this is probably due to the lower glass-to-sodalite volume ratios in the ACWF materials. As shown by ACWF-N4G-10, the porosity can be decreased by adding more glass. This lowers the waste loading to about 10 mass% but does not significantly impact the waste loading on a volume basis and will not increase disposal costs. In addition, waste form heat output will probably limit the amount of waste salt that can be accommodated in a waste canister (Vienna et al. 2015), so ACWF materials near 10 mass% may be optimal for disposing of salt wastes.

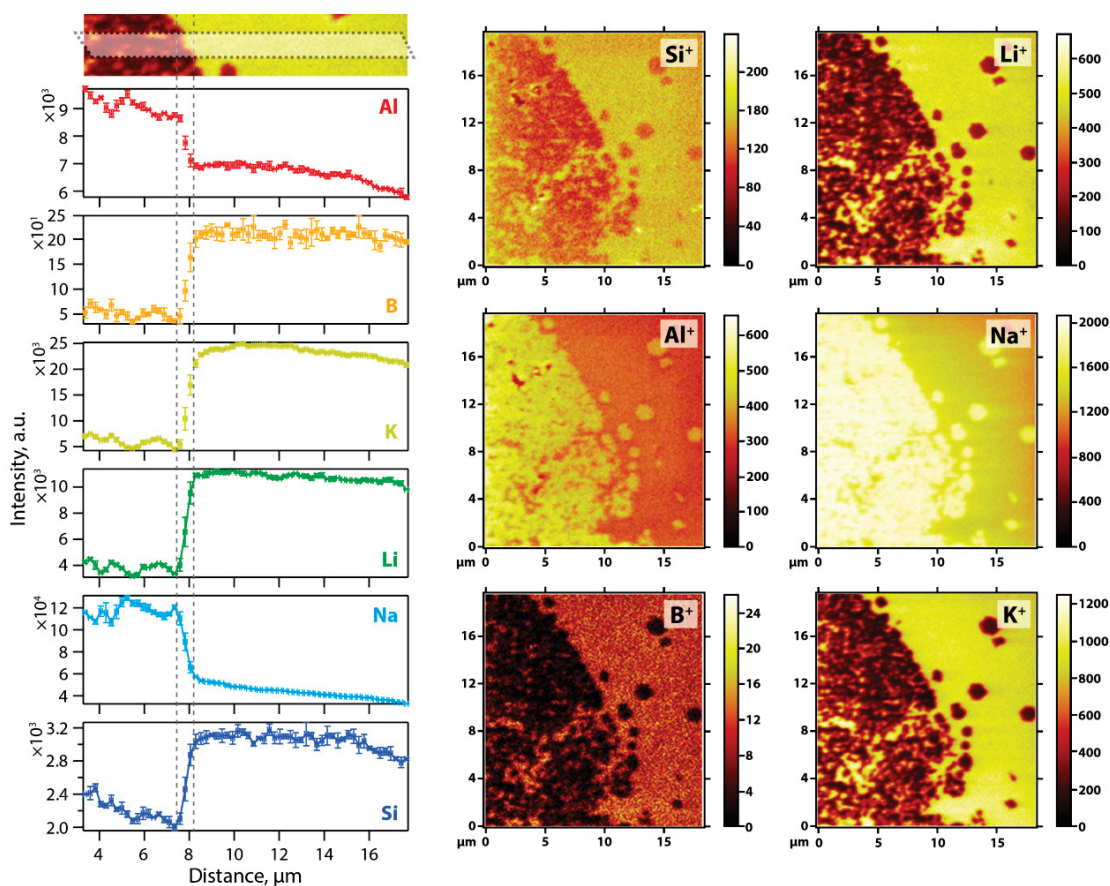


Figure 52. Time-of-flight SIMS data for ACWF-N3-11 shown as (left) lines cans showing elemental distributions and (right) distribution maps of Si<sup>+</sup>, Al<sup>+</sup>, B<sup>+</sup>, Na<sup>+</sup>, Li<sup>+</sup>, and K<sup>+</sup> near a sodalite-glass interface.

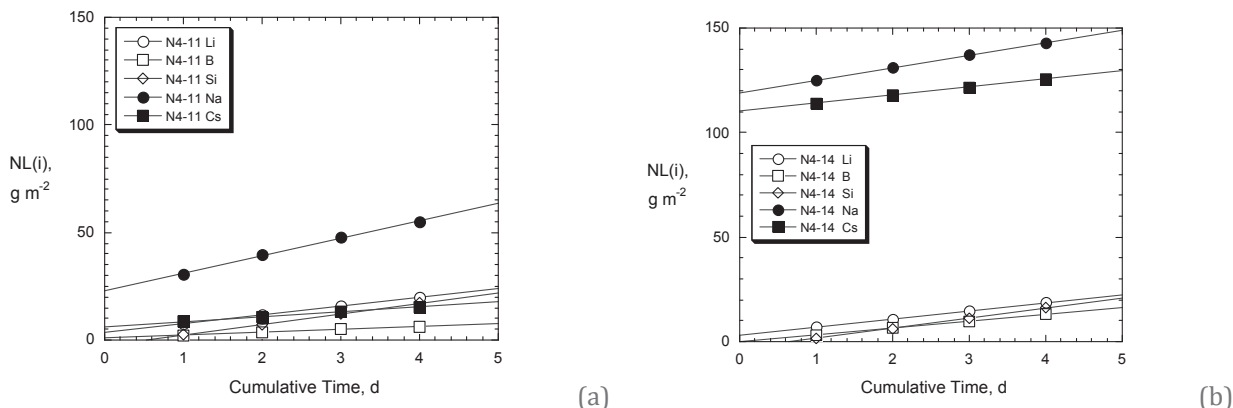


Figure 53. Results of ASTM C1308 tests with (a) ACWF-N4-11, and (b) ACWF-N4-14.

### References

ASTM C1308, 2008, "Standard Test Method for Accelerated Leach Test for Diffusive Releases from Solidified Waste and a Computer Program to Model Diffusive, Fractional Leaching from Cylindrical Waste Forms," American Society for Testing and Materials.

Ebert, W. L., 2005, *Testing to Evaluate the Suitability of Waste Forms Developed for Electrometallurgically Treated Spent Sodium-Bonded Nuclear Fuel for Disposal in the Yucca Mountain Repository*, ANL-05/43, Argonne National Laboratory.

Ebert, W. L., S. M. Frank, and B. J. Riley, 2016, *Designing Advanced Ceramic Waste Forms for Electrochemical Processing Salt Waste*, FCRD-MRWFD-2016-000038, Argonne National Laboratory.

Vienna, J. D., N. R. Soelberg, W. L. Ebert, J., Willit, M. A. Williamson, S. M. Frank, G. Frederickson, and B. J. Riley, 2015, *Initial Salt Waste Management Trade Study*, FCRD-MRWFD-2015-000469 (AT), Pacific Northwest National Laboratory.

### WASTE FORM DEGRADATION

Advanced waste forms and degradation models are being developed to immobilize wastes from aqueous processing in borosilicate glass and radioiodine recovered from off-gas as AgI in an inert matrix material. Experimental and modeling activities were conducted to develop a mechanistic understanding of waste form degradation processes to reliably calculate radionuclide releases over long disposal times and ensure that durable waste forms are produced. Waste form performance is also being simulated to provide confidence that the degradation models are consistent with experimental observations and radionuclide releases will be within regulatory limits.

## 2016 ACCOMPLISHMENTS

### **In-Situ Monitoring of Glass Corrosion Using Raman Spectroscopy**

*J. Ryan, B. Parruzot, S. Bryan, S. Devranathan, A. Lines, and A. Casella (PNNL)*

Four glass corrosion experiments monitored in real-time were started in early June 2016, reaching 120 days of alteration on 9/30/2016 and are continuing over FY 2017. In parallel, development of the in-situ monitoring technique for static corrosion experiments has continued over FY 2016.

The Raman in-situ monitoring system consists of a 671 nm red laser, a 10-channel laser beam splitter, and a 10-channel spectrometer. Each stainless steel vial containing a glass corrosion experiment is equipped with a probe (Figure 54) connected to the splitter and to the spectrometer through optical fibers. The acquisition of supplementary vials and probes enabled the full monitoring capacity of 10 simultaneous experiments.



**Figure 54. Stainless steel vessel for in-situ Raman spectroscopy of solutions contacting corroding glass.**

This capacity extension allowed the startup of six glass corrosion experiments: two glasses (LAWA76 and Advance Fuel Cycle Initiative) were altered at three different temperatures (20°C, 90°C, and 120°C). Experimental constraints did not allow successful monitoring of the glass alteration at 120°C, but further development of the experiment vial design should open the possibility of restarting these experiments. The room temperature and 90°C experiments are still ongoing as of 9/30/2016 (120 days). LAWA76 at 90°C shows a transition from Stage II to Stage III: Figure 55 shows the comparison of the BO4<sup>-</sup> Raman intensity measured by the in-situ instrument (blue dots, BO4<sup>-</sup> signal predominates) in parallel with the total boron concentration measured by ICP-OES (red squares). Additionally, shortly after the period shown here, the signal decreased abruptly. After investigation, it was found that a massive precipitation of zeolites had fouled the window of the probe, confirming our suspicions that the sample had entered into the accelerated Stage III behavior. Following cleaning of the window, concentration monitoring has continued and the rate of Stage III dissolution will be evaluated for this glass. The Advance Fuel Cycle Initiative composition is expected to enter Stage III soon.

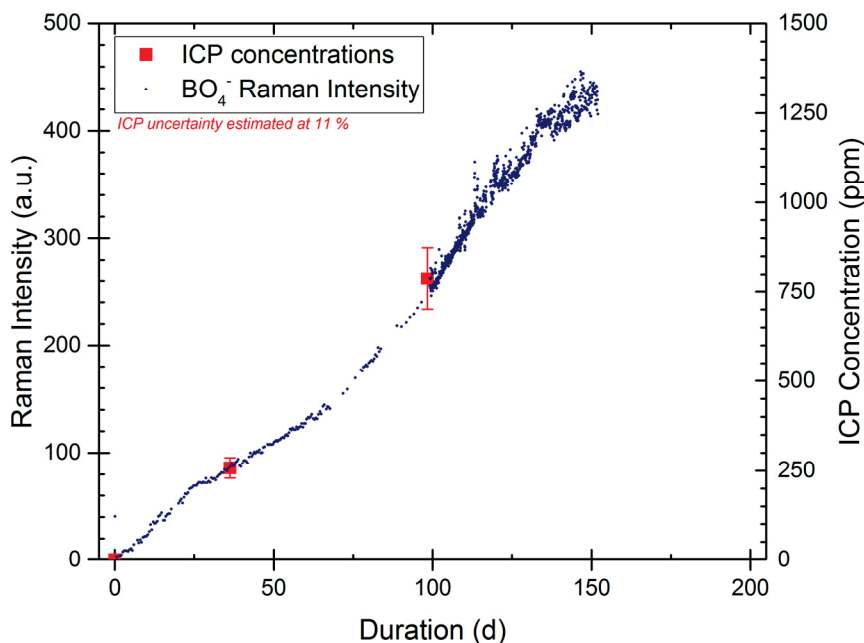


**Figure 55. Experiment LAWA76 at 90°C: comparison of the in-situ Raman signal from the BO<sub>4</sub><sup>-</sup> peak (blue dots and left axis, BO<sub>4</sub><sup>-</sup>-signal predominates) with the total Boron concentrations measured by ICP-OES (red squares and right axis).**

In parallel, method development continued both on the front end, through the acquisition of more data aiming to determine the detection and quantification limit and to calibrate both the B(OH)<sub>3</sub> and the BO<sub>4</sub><sup>-</sup>-signals from the in-situ measurements; and on the back end, through the structuration and the coding of Matlab routines aiming at importing and treating the large quantity of data acquired over the duration of the experiments.

Work performed during FY 2016 further demonstrated the ability of the in-situ Raman instrument to continuously monitor glass corrosion. Through the continuation of these experiments, further developments of the method, and the initiation of new targeted experiments, we aim to probe the triggering and sustaining mechanisms for Stage III in FY 2017.

#### Physics-based Model of Glass Corrosion

*J. Ryan, P. Rieke, S. Hu, and Y. Li (PNNL)*

The impetus behind the recent efforts to better understand and more accurately model glass corrosion stems from international agreement that none of the models, as present in 2009, fully represented all the observations during corrosion. The shortcomings of the many models have been pointed out in various journal articles through the years. In short, reaction affinity models (generally based on the transition state theory of mineral dissolution and the assumption that the decreasing rate of dissolution from Stage I to Stage II is due to the increase in silica concentration at the glass surface) often do not account for continued

## 2016 ACCOMPLISHMENTS

dissolution at high silica concentrations or explain the slowing of corrosion in systems where the solubility of silicon is extremely high. Models that evoke the limited transport of reactants and/or products due to a barrier layer within the alteration products cannot agree on either the species that is diffusion limited or the medium that is limiting diffusion. The discrepancies of these models suggest the need for an explanation that accounts for the formation and evolution of all the observed structures as well as the observed behaviors. Only through a thorough understanding of these mechanisms can a model with a strong technical basis be produced.

In FY 2015, we proposed a new model of glass dissolution based on the theory of morphological evolution. In this model, mobile elements such as sodium, lithium, and boron are rapidly dissolved from the surface of the glass during the initial contact of the glass material with water, leaving a silicate network with ion scale pores which rapidly consolidates into a dense hydrated silicate material. The material has a relatively low saturation point with respect to silica, and therefore is chemically stable in most high-silica conditions. The model also assumed that the transport of dissolved glass ions through this layer is also slow enough so as to be irrelevant when compared to the rates of other mechanisms. The model proposed that this film is driven by interfacial energy minimization to change its morphology, exposing new areas of glass that are then subject to further corrosion by the contacting solution. Therefore, the long-term dissolution rate is dictated by the movement of the altered glass at this interfacial region.

Although the model can theoretically account for many of the observations regarding glass corrosion, it is a dramatic departure from prior models. Rather than a chemistry-based approach to glass alteration, this new idea is based on physical processes: forces and flow. For this reason, the theory must be tested and demonstrated to be possible before it can be utilized. To this end we used phase-field modeling techniques to evaluate the physics behind the model. Navier-Stokes equations were used to govern fluid flow while terms for viscosity and surface tension were modified. Plateau-Rayleigh physics was used to generate the initial instabilities in perfectly flat films to cause uneven surface energetics. As seen in XX, microstructure changes at glass/fluid interface can be observed and we managed to produce a moving front that transitions to a different morphology. The physics used were deliberately simple and the parameters were not matched to any particular system, but the result was promising to at least show that the idea has scientific merit. Modeling the effects of thermodynamic and kinetic properties on the system is underway.

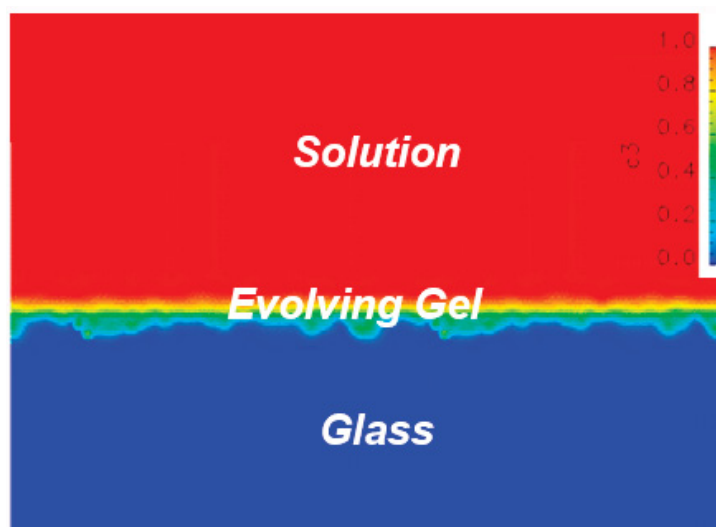


**Figure 56. Model representation of the glass/fluid interface in 2-dimensions with colors representing materials properties. Note the transition from a material with water as the solvent (red) to water as a solute.**

#### Gel Structure Characterization and Proxy Synthesis

*J. Reiser, B. Parruzot, and J. Ryan (PNNL)*

Beginning as an add-on from a NEUP project, we began a task to characterize and compare corrosion-induced glass alteration layers with compositionally identical silicate gels. Corrosion-induced glass alteration layers appear to have physical and chemical properties similar to those of synthetic silicate gels. The properties of the corrosion product gels, however, remain poorly understood despite being an important input in long-term performance models. This is because the alteration layers are relatively thin and are always attached to a much more massive portion of remaining glass. Also, glass alteration studies require long-term experiments (months to years) and the alteration layer is often too small for adequate characterization even after these long periods. Conversely, silicate gels are relatively easily synthesized and can be produced in large amounts. Isolating a structurally and chemically similar material will allow the use of relatively straightforward characterization techniques to parameterize the structural and geochemical properties of the material. In turn, this more complete dataset will dramatically improve the accuracy of waste form performance models.

Most U.S. performance assessments for vitrified nuclear currently utilize some version or simplification of an affinity-based rate law, with the dissolution dependent on the concentration of silicon in solution. While this type of model reproduces the release of boron well, and while boron is seen to be a proxy for network dissolution, the model cannot accurately reproduce concentrations of the rest of the species in solution without including the formation of another phase. In 2012, Pierce et al. (2013) produced a report that was notable for producing some of the best model fits for multiple elements to date. Their method was to use estimated geochemical parameters for a complex amorphous silicate material that precipitates during the

## 2016 ACCOMPLISHMENTS

entire corrosion period. They argued that this complex amorphous silicate was the porous gel that is always observed, which is a reasonable explanation. Experimentally determined parameters such as those produced by this effort would reduce the uncertainty for this method and advance it from theory to practice. Additionally, the work will add to the efforts to generate a mechanistic understanding behind the glass corrosion behavior.

To determine whether the proxy sol-gel materials are suitable analogues for alteration gel layers, both gel materials must share similar physical and chemical properties. Surface area, pore size and shape, density, and chemical bonding structure are all being evaluated. In FY 2016, PNNL pioneered the use of positron annihilation spectroscopy on corroded glasses, leading to a publication. PNNL also won beam time at the Advanced Photon Source at ANL, performing a series of x-ray scattering experiments on a matrix of corroded glasses and some sol-gel synthesized materials.

### **Reference**

Pierce, E. M., S. N. Kerisit, E. J. Krogstad, S. D. Burton, B. N. Bjornstad, V. L. Freedman, K. J. Cantrell, M. M. Valenta, J. V. Crum, and J. H. Westsik, 2013, *Integrated Disposal Facility FY 2012 Glass Testing Summary Report*, PNNL-21812, Rev. 1, Pacific Northwest National Laboratory, Richland, WA.

### **Glass Corrosion**

*W. Ebert (ANL)*

Methods were devised for implementing a glass degradation model in the transport model being developed for performance assessment (PA) simulations to provide reliable radionuclide source terms. The ANL Stage 3 glass dissolution model was used to represent the HLW glass degradation model that is being developed within the MRWFD campaign. The GeoChemist's Workbench® software was used to implement the Stage 3 model for the purpose of developing and refining computational methods that can be incorporated and executed in the PFLOTRAN code that will be used in PA simulations. Simulations were conducted to develop methods for dissolving glass and evolving the solution composition during the PA calculations, modifying the dissolution rate as conditions evolve, exchanging data between the glass degradation and transport models, and optimizing the time step used in the glass degradation model. These provided insights into the relative sensitivity of the modeled behavior of parameter values for describing glass corrosion and the modeled disposal system. The general glass dissolution behavior observed in laboratory tests is shown by the black curves in Figure 57, and representation of that behavior in the ANL Stage 3 model is illustrated in Figure 57. The curves represent the kinetics of glass converting to thermodynamically stable phases by a dissolution-precipitation mechanism. The most important aspect for modeling the long-term performance of glass waste forms is when (and if) the glass dissolution rate increases from the low Stage 2 rate to a high Stage 3 rate.

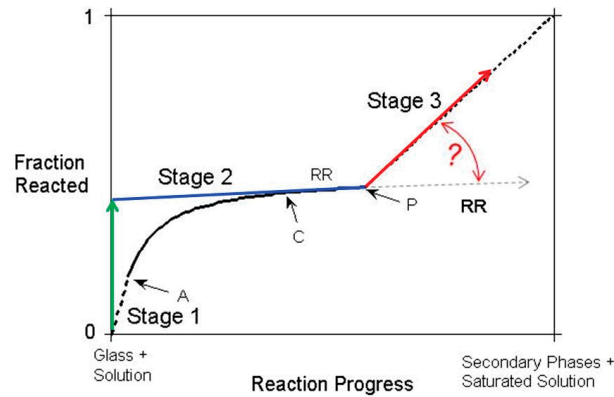


**Figure 57. Illustrations of observed glass dissolution behavior and representation in the ANL Stage 3 model.**

In PA calculations, various masses of glass will be dissolved into the volume of seepage water in a breached waste package during each time step based on the glass dissolution rate, which itself will depend on the composition of the seepage water (primarily the pH and dissolved silica concentration). Radionuclides will be released at the same relative rate that the glass dissolves. Parameter values for implementing the Stage 3 model were derived from the results for long-term dissolution tests conducted at 90°C with about 140 different borosilicate glasses formulated to immobilize high-level and low-activity waste streams. Tests were conducted following a modified ASTM C1285 procedure ( $S/V = 2000 \text{ m}^{-1}$ ) wherein small aliquants of the test solution were removed occasionally for analysis and replaced with equal amounts of fresh water. The derived parameter values included Stages 1, 2, and 3 dissolution rates, elemental partitioning values between solution and solids during glass dissolution in Stages 2 and 3, and solution conditions triggering Stage 3 dissolution behavior. Relationships between the parameter values, with the glass compositions, and with the measured glass corrosion behaviors were evaluated to gain insights into the interdependencies and sensitivities to ensure behavior predicted by the glass degradation model is consistent with observed behavior. Figure 58a shows the ranges of Stage 2 and Stage 3 rates derived from those test results, and Figure 58b shows the lack of a relationship between the Stage 2 rate and Stage 2 pH. The low activity waste glasses are represented by open symbols and dashed lines, and HLW glasses are represented by filled symbols and solid lines. The rates represent the mass fractions of B released from the glass and are normalized to the glass compositions and test conditions. The pH values were measured at room temperature and are about 1 unit higher than the pH at the test temperature of 90°C.

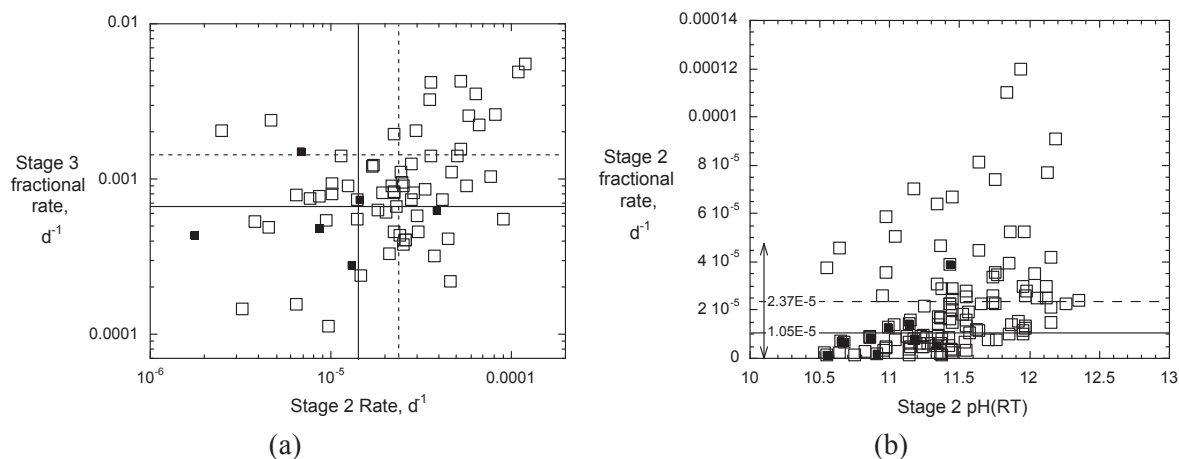


**Figure 58. Correlations between (a) Stage 3 rate and Stage 2 rate and (b) Stage 2 rate and Stage 2 pH.**

The test results were analyzed to relate the solution composition to when (if) Stage 3 was triggered. Although many tests have shown Stage 3 is coincident with zeolites precipitation, no correlation could be found with the concentrations of individual or combined species. For example, Figure 59 shows correlation between tests in which Stage 3 was triggered (blue symbols) or was not triggered (yellow symbols) with combinations of the pH or maximum concentrations of  $\text{Al}(\text{OH})_4^-$  or  $\text{HSiO}_3^-$ . With  $\text{Na}^+$ , these species are nutrients for secondary phases triggering Stage 3. The lack of direct correlation may possibly be attributed to an incubation time corresponding to the nucleation of zeolites in a super saturated solution, which is not taken into account in the correlation shown in Figure 56. The model was modified to include an incubation period that is initiated when the solution becomes saturated with respect to an unidentified secondary phase. For example, the lines drawn in Figure 59 indicate possible threshold concentrations that must be exceeded before the incubation period is initiated and Stage 3 is triggered. (Actual threshold concentrations remain to be determined for disposal systems and the values in Figure 56 are only used to demonstrate the approach.) These threshold concentrations are empirical parameters used to represent conditions necessary to nucleate secondary phases that lead to triggering Stage 3, including the solution chemistry and glass surface, but are not associated with any identified secondary phase. The phases that trigger Stage 3 are probably precursors to those secondary phases that maintain Stage 3 and are identified experimentally. The nearly constant Stage 3 rate observed experimentally is consistent with coupling the precipitation kinetics with glass dissolution kinetics, not nucleation. Tests are planned for FY 2017 to measure incubation times in modified ASTM C1285 tests conducted with several reference glasses in simulated threshold solutions, and the ALTGLASS database will be further evaluated to identify and assess incubation periods in those tests. These activities will be used to develop a method to include the effects of nucleation kinetics on triggering Stage 3 in the glass degradation model.

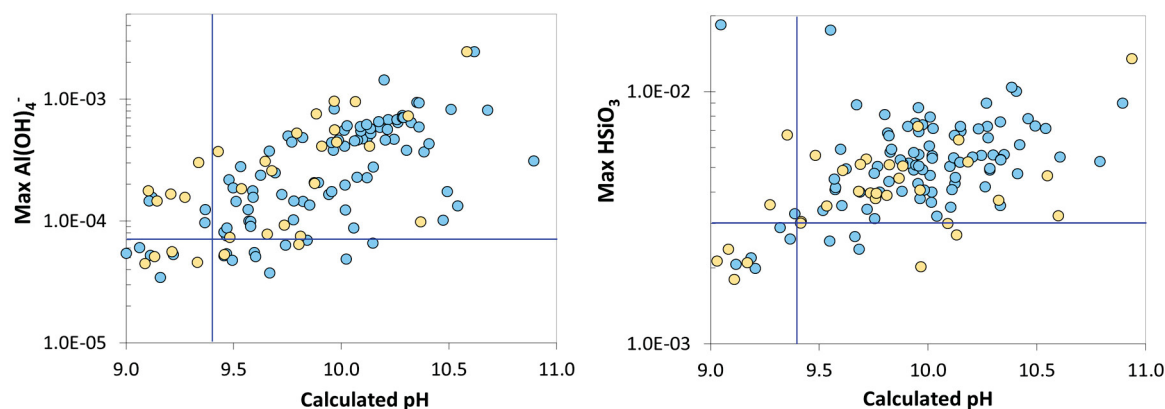


Figure 59. Scatter diagrams correlating whether Stage 3 was triggered (blue symbols) or not triggered (yellow symbols) with pH and the maximum molar concentrations of  $\text{Al}(\text{OH})_4^-$  or  $\text{HSiO}_3^-$ .

### Modeling and Simulation

*S. Kerisit (PNNL)*

The overall scope of this work is to integrate and further develop existing computational capabilities into a single geochemical reactive transport modeling tool that can provide a sound basis for understanding and predicting nuclear waste glass performance. It aims to provide an environment for developing, parameterizing, and assessing mechanistic models of glass corrosion and to ultimately inform the PA models of nuclear waste disposal systems. The work is divided into two main thrust areas: (1) The development of modeling tools to enable increasingly realistic glass corrosion simulations with a single multi-scale framework and (2) the evaluation of mechanistic models to quantitatively assess existing as well as newly proposed mechanistic models for a wide range of glass compositions and test conditions.

#### Development of Modeling Tools

The computational capabilities developed in this work consist of the Glass Corrosion Modeling Tool (GCMT), the Glass Waste Form (GWF) degradation function in PFLOTRAN, and a Monte Carlo (MC) code of glass corrosion.

GCMT runs in MatLab and is coupled to a geochemical code and a parameter-optimization program. These functions enable GCMT to run several glass corrosion models (e.g., Residual Rate model, Grambow-Müller model, and Glass Reactivity with Allowance for the Alteration Layer [GRAAL] model) and optimize model parameters for best fits to experimental data sets. In FY 2016, a new MatLab subroutine for solving nonlinear sets of differential equations was implemented, which resulted in a 100× speed up compare to the multi-physics software used up to now.

In FY 2016, the GWF degradation function was developed and implemented in PFLOTRAN, building on previous work at ANL and Sandia National Laboratories to integrate the Fuel Matrix Degradation Model into PFLOTRAN. This required extensive revisions of the waste form module in PFLOTRAN. The degradation function is based on the Aagaard-Helgeson model with an additional stochastically dependent Stage III

dissolution process whose onset time and rate may vary. Several demonstration simulations were performed that called the GWF degradation function and applied it to a subsurface process incorporating flow and transport (see examples shown in Figure 60). This computational capability was tested on both a Linux desktop and one of PNNL's supercomputers. Now that the interface with PFLOTRAN is operational, more sophisticated models of glass corrosion can be implemented with relative ease.

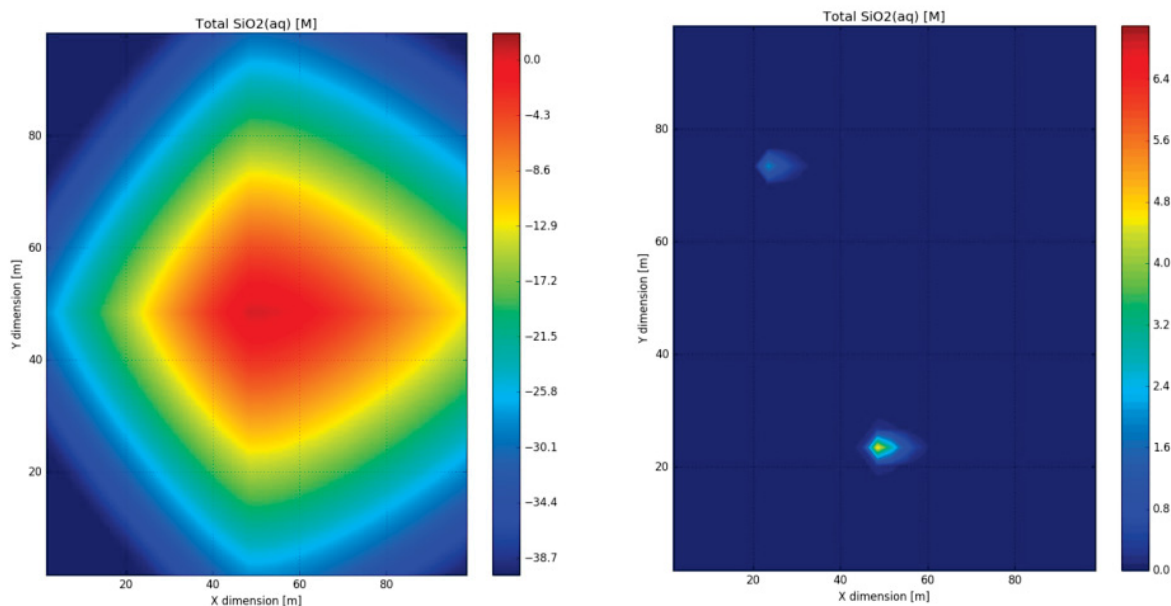


**Figure 60. Snapshots from PFLOTRAN simulations showing the total  $\text{SiO}_2(\text{aq})$  concentration after 40 years from the corrosion of (top) one waste form dissolving at a constant rate under left-to-right flow (log plot) and (bottom) two waste forms dissolving at a constant rate under left-to-right flow with the lower waste form transitioning to Stage III dissolution after 20 years (linear plot).**

Progress was also made toward enhancement of the atomistic capabilities, namely the MC code of glass corrosion developed over the past several years. Indeed, the MC code was coupled to PHREEQC, a geochemical code used to compute solution speciation and growth kinetics of secondary mineral phases. This coupling allows for leveraging the ability of the MC code to capture the dynamics of bond breaking and bond making in the gel layer, and thus the evolution of the gel structure, while also providing a realistic estimation of how dissolved glass components partition between specific solution species and how this can affect glass corrosion. Examples can be found in (Rieke and Kerisit 2016).

#### ***Evaluation of Mechanistic Models***

In FY 2015, an evaluation of four models (Aagaard-Helgeson, Residual Rate, Grambow-Müller, and GRAAL) was performed using GCMT against SON68 data for test conditions in which the flow rate and the surface-area-to-volume ratio were varied and data on the CJn family of glasses (Gin et al. 2012), in which composition was varied by adding calcium, aluminum, zirconium, cerium, and lithium to a sodium borosilicate base glass. Based on this evaluation, we suggested that improvements would likely be achieved through a more accurate treatment of the interactions between glass components within the alteration layer.

In FY 2016, we therefore developed and implemented in GCMT an application of end-member solid-solution theory to describe the gel layer, which we refer to as the Gel End Member (GEM) model. This work expands on recent work reported in the literature by French scientists from the CEA. This model retains the form used in the GRAAL model developed by CEA to describe hydrolysis of the pristine glass but describes the gel layer as a physical mixture of simple oxyhydroxide phases and a solid solution, whereby the relative mass of these phases may vary with time and their dissolution rate governs the concentration of each element found in the aqueous solution. The GEM model is based on the gel layer mass balance equation:

$$\frac{dG_i}{dt} = -\sum_m f_{i,m} G_m k_m \Gamma_m - \sum_n f_{i,n} G_n k_{SS} \Gamma_{SS} + f_i^{gls} C_{gls} k_{gls} \left[ \frac{mol}{m^2 s} \right] \quad (6)$$

where the first two terms on the right represent the flux out of the gel layer due to dissolution of  $m$  simple oxyhydroxides and that due to the dissolution of a solid solution with  $n$  end members, respectively. The third term represents the flux of elements into the gel by hydrolysis of the pristine glass. The terms  $f$ ,  $G$ ,  $k$ , and  $\Gamma$  are the stoichiometric factors, concentrations, dissolution rates, and degrees of supersaturation, respectively.

Overall, GEM aims to provide a rational way to select end members and determine the corresponding solubility constant and ion activity product, which is currently one of the limitations of GRAAL. A detailed derivation of the model can be found in Milestone M3FT-16PN030105146 (Rieke and Kerisit 2016).

### References

Gin, S., X. Beaudoux, F. Angeli, C. Jegou, and N. Godon, 2012, "Effect of Composition of the Short-Term and Long-Term Dissolution Rates of Ten Borosilicate Glasses of Increasing Complexity from 3 to 30 Oxides," *Journal of Non-Crystalline Solids*, Vol. 358, pp. 2559–2570.

Rieke, P. C., Kerisit, S.N., 2016, *Modeling Tool Enhancement Report*, Pacific Northwest National Laboratory.

### Iodine Waste Form Corrosion

*W. Ebert, T. Cruse, J. Jerden (ANL), and J. Ryan (PNNL)*

The strategy for developing a degradation model for AgI-based waste forms was derived from the Eh-pH diagram (as an example, see the diagram for  $[Ag^+]$  and  $[I^-]$  activities of  $1E-7$  molal in Figure 61a [Ebert et al. 2016]). The red lines separating the stability fields indicate the Eh values corresponding to the  $Ag/Ag^+$ ,  $I^-/I_2$ ,  $I_2/IO_3^-$ , and  $I^-/IO_3^-$  redox equilibria. The yellow area represents the thermodynamic stability field for AgI, the blue area represents the stability range of Ag(0), and the pink areas represent the stability ranges of I(I) and I(IV). The stability fields vary with the dissolved concentrations according to the Nernst equation. Under environmental conditions within the yellow area, AgI dissolution will occur primarily by chemical dissolution. In the blue and pink areas, AgI dissolution will also occur by the reduction of  $Ag^+$  to Ag(0) and by the oxidation of  $I^-$  to  $I_2$  or  $IO_3^-$ , respectively. In a disposal system, these reduction and oxidation reactions will be coupled to other redox reactions, such as the oxidation of ferrous to ferric as steel corrodes as



The stability fields of  $\text{Fe}^{2+}$  and  $\text{Fe}^{3+}$  are included in Figure 61a and show that Reaction 5 will be predominant in acidic solutions under reducing conditions. The rate of that reaction will depend on the Eh and pH of the solution, as well as the AgI surface area, and the Eh will depend on the  $\text{Fe}^{2+}$  concentration. The objective of the electrochemical tests is to determine the dependence of the AgI dissolution rate on the Eh-pH conditions. That rate dependence will then be used to model the degradation rates of AgI-bearing waste forms.

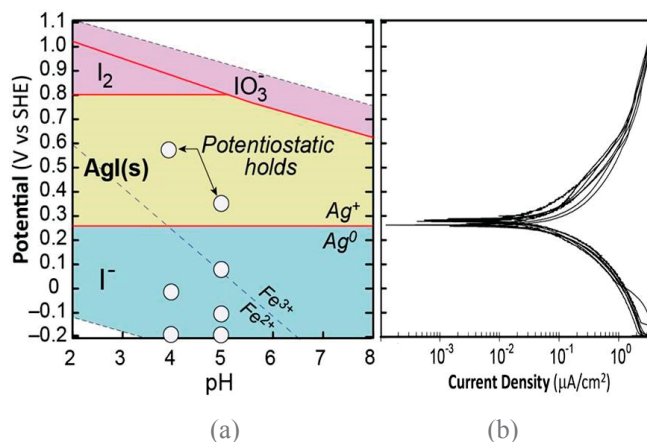


**Figure 61. (a) Stability diagram for  $1\text{E}-7$  molal  $\text{Ag}^+$  and  $\text{I}^-$  and (b) PD scans in pH 2, 3, 5, 8, 10, and 10 solutions.**

The stability diagrams provide the thermodynamically favored speciation but not the redox kinetics required for modeling waste form degradation. Electrochemical experiments are being used to measure the dissolution kinetics of AgI following the reductive-dissolution mechanism pertinent to conditions in the blue area, the oxidative-dissolution mechanism pertinent to the pink area, and the chemical dissolution mechanism pertinent to the yellow area. Proof-of-principle experiments were conducted in FY 2016 using electrodes made from pressed AgI powder fixed in epoxy and a potentiostat to represent the redox reactions supporting reductive and oxidative AgI dissolution. Key results are summarized below. Future experiments are planned in which  $\text{FeCl}_2$  (and other) solutions will be used to establish the solution Eh and measure the dissolution rates of AgI electrodes and loose AgI powder. The electrochemically measured kinetics will be used to interpret those experiments and to parameterize a degradation model.

Figure 61b shows a compilation of PD scans made at several pHs. As indicated in the Eh-pH diagram,  $\text{Ag}/\text{Ag}^+$  equilibrium is independent of the pH. The values of  $E_{\text{corr}}$  in the PD scans are likewise pH-independent and correspond with the  $\text{Ag}/\text{Ag}^+$  equilibrium potential. The corrosion currents, which reflect the reduction rate, are also pH-independent. This shows that the reduction of  $\text{Ag}^+$  and oxidation of  $\text{Ag}(0)$  are the dominant cathodic and anodic reactions in the system (i.e., the contribution of  $\text{H}^+$  reduction is negligible).

The symbols on the Eh-pH diagram in Figure 61a show conditions used in cyclic potentiostatic tests in which the electrode was initially immersed in a pH 4 or 5 solution at open circuit, and then a constant potential was applied to the electrode for 1 day and then removed for a day. This drove reductive dissolution for 1 day and then relaxed to  $E_{\text{corr}}$  under open circuit conditions for 1 day. Figure 62 shows the result of tests at -200 mV in the pH 4 solution. The upper panel shows the open circuit potentials measured between applications of -200 mV. The value of  $E_{\text{corr}}$  decreases slightly upon initial immersion, decreases significantly

after the first application of -200 mV, and decreases slowly thereafter. The decrease is attributed to the generation of Ag(0) and increased solution concentrations of I<sup>-</sup>. The lower panel shows the accumulation of charge during each half-cycle. The positive slopes represent the positive currents for all anodic reactions occurring in the system under open circuit conditions, and the negative slopes indicate negative currents for cathodic reaction occurring at -200 mV. The negative currents are due to reduction of Ag<sup>+</sup> to Ag(0), and the positive currents are due, in part, to reoxidation of Ag(0). The currents are proportional to the reaction rates, and the reductive dissolution rates are about four times higher than the oxidation rates in each cycle. Figure 63 shows the measured Ag<sup>+</sup> reduction rates as a function of the hold potential. (Note that E<sub>corr</sub> values decrease to about 80 mV during the tests, so the hold at 90 mV becomes anodic.) The equation of the regression line is  $rate = 0.72 \exp(-6.9 Eh)$ , where *rate* is in units of g(AgI) m<sup>-2</sup> d<sup>-1</sup> and *Eh* is in volts versus standard hydrogen electrodes.

These scoping tests indicate the electrochemical approach is appropriate for measuring the environmental dependencies of AgI dissolution rates for use in degradation models of waste forms made by encapsulating AgI.

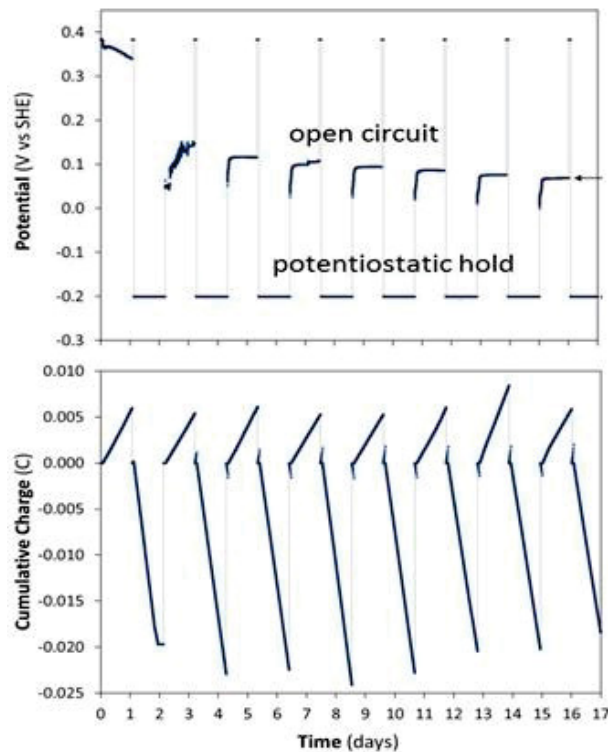


Figure 62. (a) Potentials measured in tests cycling between applied potential of -200 mV and open circuit and (b) charge response.

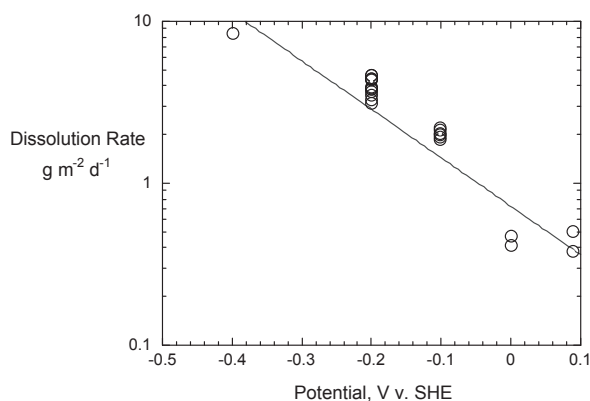


Figure 63. Cathodic dissolution rates measured in pH 4 and pH 6 solutions.

#### Reference

Ebert, W. L., T. A. Cruse, and J. L. Jerden, 2016, *Testing Roadmap for Iodine Waste Forms*, FCRD-MRWFD-2016-000256, Argonne National Laboratory.

## ZIRCONIUM RECYCLE

*E. Collins (ORNL)*

The FY 2016 accomplishments for the Zirconium Recycle Project included: (1) completed nonradiation operability test chlorination of scrap cladding with 100, 250, and 500 g of cladding in metal reactor/condenser test equipment to be used for a subsequent hot test; (2) modified equipment and the operating procedure to enable remote operation with hot cell manipulators; (3) prepared formal operating procedures and safety documentation and received ORNL management approval for installation and operation; (4) designed, fabricated, and installed accessory equipment (chlorine cylinder storage cabinet, piping and valves, flow control valves, and shielded plugs for conduction of piping and electrical/instrument wires into hot cell); (5) installed equipment in the hot cell; and (6) demonstrated the initial large-scale chlorination test of irradiated UNF cladding.

The metal equipment was prepared for use in future hot-cell tests to develop the chlorination process for recovery, purification, and possible recycle of zirconium from UNF cladding. The primary components of the equipment are shown in Figure 64 and include: (1) a horizontally oriented chlorination and sublimation reactor, designed to chlorinate 100- to 500-g batches of UNF cladding, (2) a vertically oriented condenser to de-sublimate, or condense, the zirconium tetrachloride ( $ZrCl_4$ ) salt product, (3) a replaceable bottle for collecting the salt product, and (4) an off-gas line and trapping system for collection of tritium gas released from the cladding during the chlorination and a neutralization trap for excess chlorine ( $Cl_2$ ). The reactor is constructed from stainless steel, with a nickel-plated internal surface to provide maximum resistance to corrosion, and is equipped with a perforated stainless-steel gas inlet and distribution tube and a stainless-steel thermocouple well to enable measurement of temperatures inside the reactor. The condenser vessel is also constructed from stainless steel and was initially equipped with a removable Teflon top plug and rotatable wall scraper (no longer used), plus a conical bottom and O-ring-sealed connection for the

replaceable salt product collection bottles and an off-gas exhaust tube. The reactor and condenser vessels are connected with a ~4-in.-long, 2-in.-diameter stainless-steel “neck” tube that initially contained a large Swagelok® connector but was later removed. Top and bottom heating mantles are provided for heating the reactor and neck tube to the reaction temperature (350 to 400°C), and the condenser is jacketed for air cooling to <200°C.

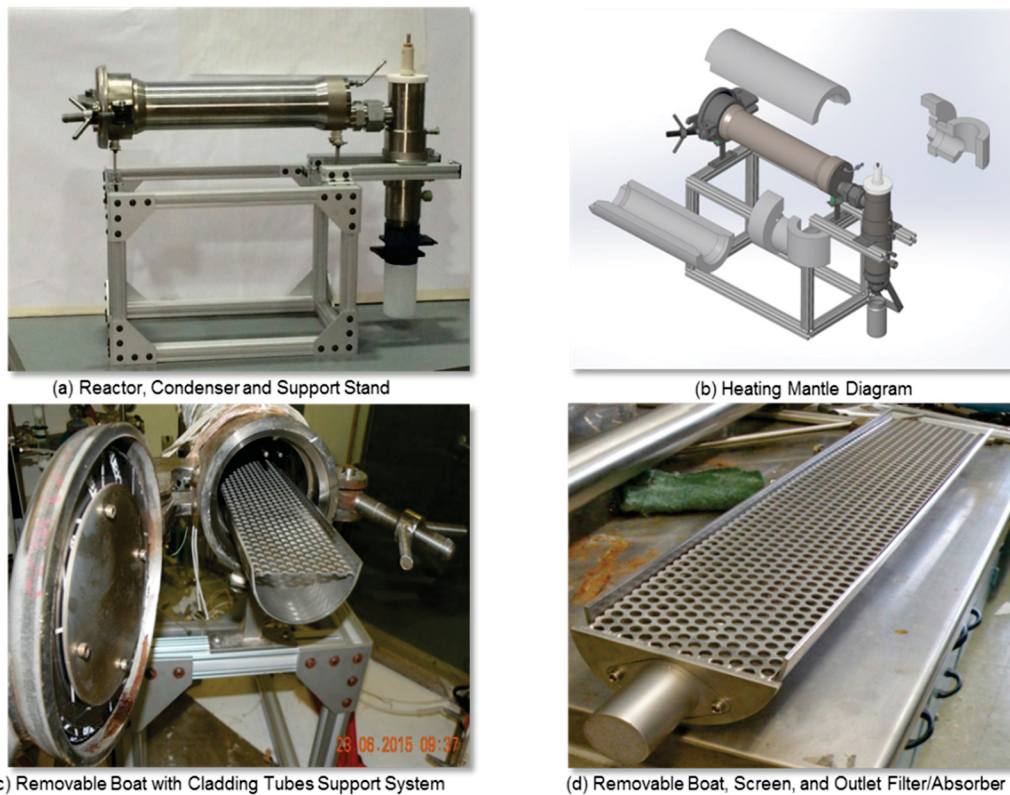


Figure 64. New metal test equipment for hot-cell tests with 100 to 500 g of UNF cladding per test.

**Nonradioactive Operability Tests**

The purpose of the nonradioactive operability tests in FY 2016 was to test the unit with batch chlorination of nonradioactive cladding samples and to identify components that needed further modification to enable satisfactory remote operation after installation in the hot cell. Three batch chlorination tests were conducted— sequentially using 100, 250, and 500 g of cladding—to test the operability of the metal equipment and identify needed modifications. In each batch test, the cladding consisted of 90% Zircaloy-2 and 10% Zirlo (high niobium) cladding. During the third test, which was conducted with 500 g of cladding, a procedure for stopping Cl<sub>2</sub> flow, changing the product collector bottle, and then restarting Cl<sub>2</sub> flow was tested, and three product salt fractions were collected; the fractions contained 346, 403, and 424 g of salt, respectively, for a total of 1.173 kg. Samples of each were analyzed by ICP-MS. Results are shown in Table 12.

## 2016 ACCOMPLISHMENTS

TABLE 12. RESULTS FROM 500-G CLADDING TEST.

Component	Feed Cladding	Product Salt			Condenser Inlet Deposit ppm Zr
	Calc. ppmp Zr	1 <sup>st</sup> (29%) ppmp Zr	2 <sup>nd</sup> (34%) ppmp Zr	3 <sup>rd</sup> (35%) ppmp Zr	
Fe	1,650	2,663	4,607	7,852	1,600
Cr	920	<8	13	28	89
Ni	620	<8	<7	<8	16
Nb	1,000	789	1,277	1,977	150
Sn	13,800	357	1,019	197	554

The extra iron, chromium, and nickel were likely due to corrosion of the stainless-steel components of the reactor. The chromium salt was only slightly volatile and appeared only in low concentration in the second and third product samples, while the nickel salt was nonvolatile. As indicated in previous tests, iron becomes more volatile, apparently changing from nonvolatile  $\text{FeCl}_2$  to volatile  $\text{FeCl}_3$ , during the course of the batch chlorination. Excess niobium is apparently an analytical variance but indicates that essentially all niobium is volatile, as previous tests have shown.

The color of the salt product from the first test was dark orange, which also indicated the presence of stainless-steel corrosion products. Subsequent mass analysis (ICP-MS) confirmed the presence of excess iron in the salt product. However, upon disassembly of the test apparatus, very little physical evidence of corrosion was observed, as shown in Figure 65 and Figure 66.

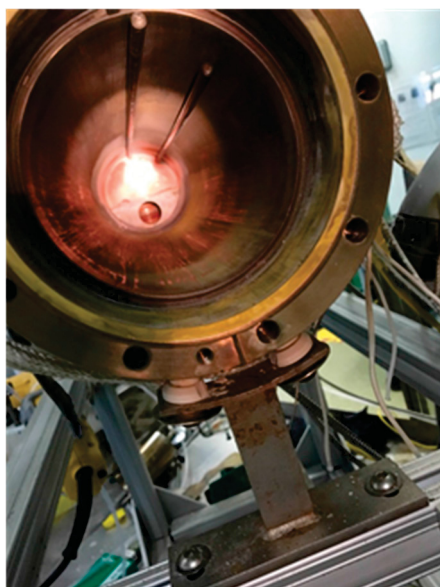


Figure 65. Bore of reactor.



Figure 66. Bore of condenser.

In summary of the operability testing, two additional heating tapes, in combination with the existing heating mantles, were found to provide the desired reactor temperature profile. Elimination of the rotating wall scraper within the condenser and replacement with an external vibrator was found to be the best practice for ensuring collection of the  $ZrCl_4$  salt product within the product collector bottles and minimizing maintenance operations. Methods for mitigating pressurization of the gas inlet line were developed. Accessory equipment was identified and designed for removal of residual ash powder from the reactor boat and for enabling hot-cell manipulator access to both the cladding feed inlet and the opposite end-product collection bottles.

### Out-of-Cell Accessory Facilities

Design, fabrication, and installation of the out-of-cell accessory equipment for the Zirconium Recycle Project tests with actual UNF cladding was completed on September 9, 2016, shortly before installation of the hot cell equipment. As indicated in Figure 67, the out-of-cell equipment includes (1) a gas cabinet for a chlorine cylinder, (2) piping and valves, (3) flow control valves, and (4) two shielded plugs in the hot cell walls, one for gas flow piping from the charging area and one for electric power and thermocouple instrumentation from the operating area.

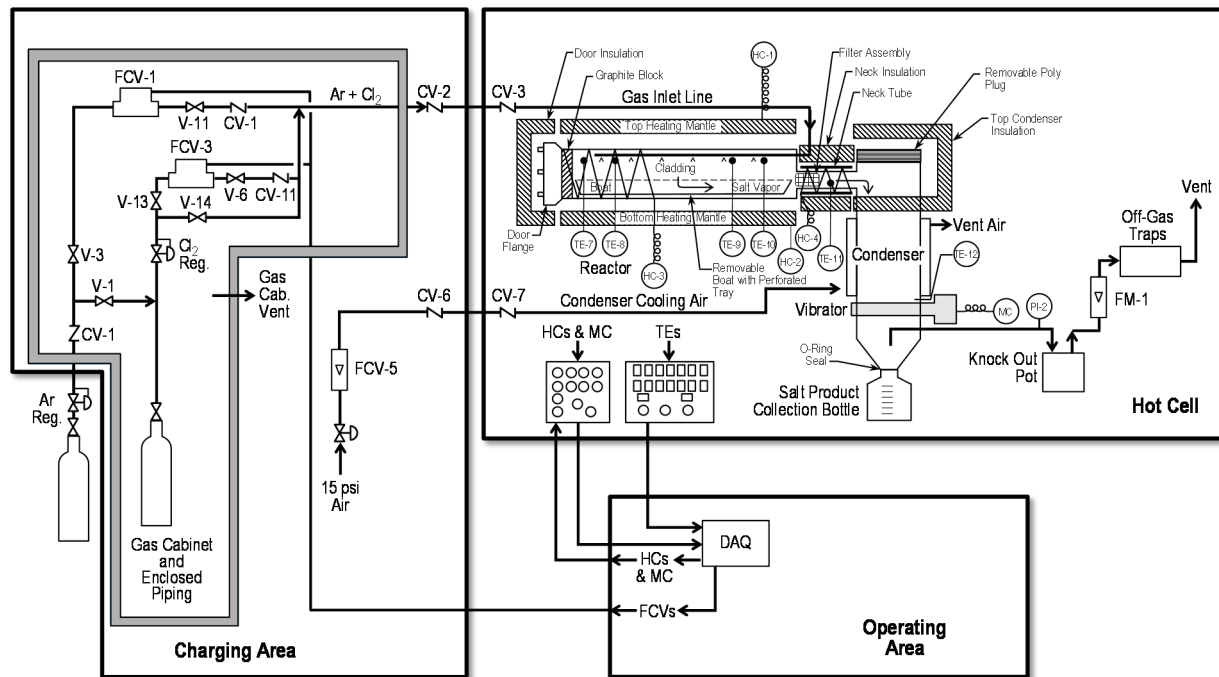


Figure 67. Zirconium recycle hot cell and out-of-cell equipment diagram.

### Initial Large-Scale Chlorination of Zirconium Alloy Cladding from Irradiated $UO_2$ Fuel

The initial large-scale chlorination of zirconium alloy cladding from irradiated  $UO_2$  fuel was completed. This test was conducted using 100 g of Zircaloy-4 and M-5 cladding from Advanced Test Reactor fuel tests and from a mixed oxide lead test assembly fuel rod. The irradiated fuel had burnup ranging from 9 to 50

## 2016 ACCOMPLISHMENTS

GWd/MT and was discharged in 2003 and 2008. Previous feasibility hot tests were made with ~15 g of Zircaloy-2 cladding from the Dresden-1 boiling water reactor, which had been irradiated to ~24 GWd/MT and discharged in 1975 (cooled for 38 years when the feasibility tests were conducted). The purpose of the initial large-scale test was to determine the effects of chlorinating larger amounts of irradiated fuel, processing higher-burnup and shorter-cooled UNF cladding, and using a chabazite absorber filter in the reactor off-gas line for chemical and radioactive purity of the  $ZrCl_4$  product salt. The chlorination test unit inside the hot cell is shown in Figure 68. A summary of the test parameters is given in Table 13.

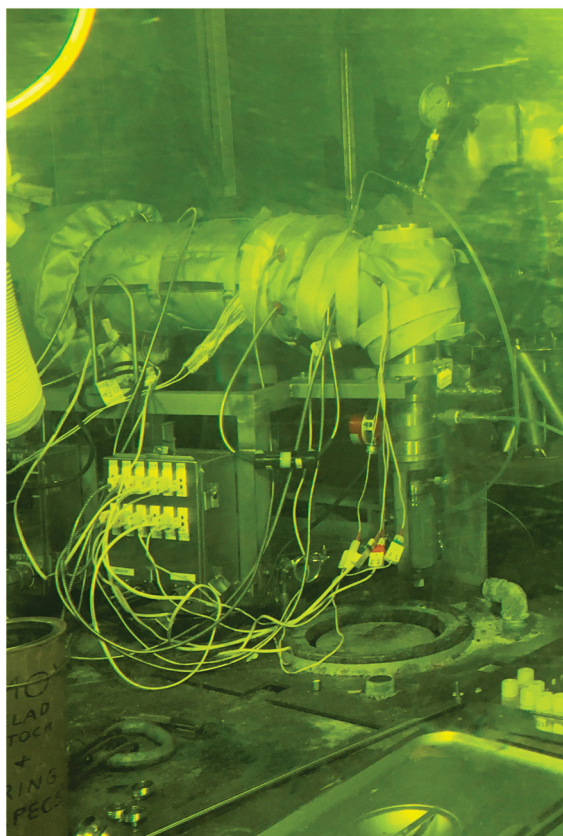


**Figure 68. Zirconium recycle test equipment in hot cell.**

Weighing, sampling, and analyses of the product salt and residual ash from the initial large-scale chlorination(s) will be done in FY 2017, and a mass balance will be determined. A similar large-scale chlorination with added equipment for tritium capture from the chlorination off-gas stream is planned in conjunction with the Reference Technologies and Alternatives Control Account, which is developing the tritium trapping process. The routing of the off-gas stream from the hot cell to the trapping system located in the charging area will require further safety approvals.

TABLE 13. TEST PARAMETERS FOR INITIAL LARGE-SCALE CHLORINATION TEST.

Type of Cladding	Zircaloy-4 ~ 5% M-5
Reactor Irradiation	Advanced Test Reactor, Catawba-1
Fuel Burnup	9-40 Gwd/MT
Fuel Discharge Date	2003, 2008
Weight of Cladding Tested	100.1g
Gas Flow Rates	
Ar	200–320 mL/min
Cl <sub>2</sub>	100–334 mL/min
Reactor Temperature Range	360–382°C
Condenser Temperature	40°C
Volume of ZrCl <sub>4</sub> Salt Collected	150–200 mL
Duration of Chlorination	5 hours

Additional large-scale chlorination tests on UNF claddings from other types of zirconium alloy cladding are planned for FY 2017, as well further scale-up tests to 500 g of cladding (which produces >1 kg of ZrCl<sub>4</sub> product salt). New accessory equipment to enable mechanical stripping of cladding from UNF fuel rods will be required to provide the larger amounts of UNF cladding.

Collaboration was initiated in FY 2016 on secondary purification of the ZrCl<sub>4</sub> chlorination product with the NEUP teams at the University of Nevada at Las Vegas and the University of Tennessee. This collaboration will continue in FY 2017.

#### PUBLICATIONS FOR WASTE FORM DEVELOPMENT AND PERFORMANCE

Amoroso, J. W., J. Marra, C. S. Dandeneau, K. Brinkman, Y. Xu, M. Tang, V. Maio, S. Webb and W. K. S. Chiu, 2016, “Cold Crucible Induction Melter Test for Crystalline Ceramic Waste Form Fabrication: A Feasibility Assessment,” submitted to *Journal of Nuclear Materials*.

Asmussen, R. M., J. J. Neeway, T. Kaspar, and J. V. Crum, 2016, “Corrosion Behavior and Impact of Microstructure of Glass-Ceramic Waste Forms,” submitted to *Journal of the American Chemical Society*.

Clark, B. M., P. Tumurugoti, S. K. Sundaram, J. Amoroso, J. Marra, V. Shutthanandan, and M. Tang, “Radiation Damage of Hollandite in Multiphase Ceramic Waste Forms,” submitted to *Nuclear Instruments and Methods in Physics Research, Section B*.

Cocco, A. P., M. B. DeGostin, J. A. Wrubel, P. J. Damian, T. Hong, Y. Xu, Y. Lin, P. Pianetta, J. Amoroso, K. S. Brinkman, and W. K. S. Chiu, “Three-Dimensional Mapping of Crystalline Ceramic Waste Form Materials,” submitted to *Journal of the American Ceramic Society*.

Crum, J. V., J. J. Neeway, B. J. Riley, Z. Zhu, M. J. Olszta, and M. Tang, 2016, “Dilute condition corrosion behavior of glass-ceramic waste form,” *Journal of Nuclear Materials*, Vol. 482, pp. 1–11.

## 2016 ACCOMPLISHMENTS

Lu, X., J. J. Neeway, J. V. Ryan, J. Du., 2016, "Influence of low concentration V and Co oxide doping on the dissolution behaviors of simplified nuclear waste glasses," *Journal of Non-Crystalline Solids*, in revision.

Mitroshkov A. V., J. V. Ryan, L. M. P. Thomas, and J. J. Neeway, 2016, "Comprehensive Isotopic and Elemental Analysis of a Multi-Oxide Glass by Multicollector ICP-MS in Isotope Substitution Studies," *Journal of Chromatography and Separation Techniques*, Vol. 7, No. 2.

Neeway, J. J., S. N., Kerisit, J. Liu, J. Zhang, Z. Zhu, B. J. Riley, and J. V. Ryan, 2016, "Ion-Exchange Interdiffusion Model with Potential Application to Long-Term Nuclear Waste Glass Performance," *Journal of Physical Chemistry C*, Vol. 120, No. 17, pp. 9374–9384.

Rabbi, F., K. Brinkman, J. Amoroso, and K. Reifsnider, 2016, "Finite Element Analysis of Ion Transport in Solid State Nuclear Waste Form Materials," submitted to *Computational Materials Science*.

Reiser, J. T. G., J. S. McCloy, M. Weber, B. P. G. Parruzot, J. V. Ryan, and N. A. O. Wall, 2016, "The Use of Positrons to Survey Alteration Layers on Synthetic Nuclear Waste Glasses," *Nuclear Materials*, in revision.

Ryan, J. V. et al., "Final Report: IAEA CRP on Processing Technologies for High Level Waste, Formulation of Matrices, and Characterization of Waste Forms," Member of Drafting Team, 8/30-9/2, Sheffield, England.

Ryan, J. V., E. C. Buck, A. Silvestri, J. L. Weaver, J. Bonetto, 2016, "Periodic Alteration Pattern on Ancient Glass from a Roman Era Shipwreck," submitted to *Nature Degradation of Materials*.

Tang, M., A. T. Nelson, E. S. Wood, S. A. Maloy, and Y.-Bi. Jiang, 2016, "Grazing incidence X-ray diffraction and transmission electron microscopy studies on the oxide formation of molybdenum in a water vapor environment," *Scripta Materialia*, Vol. 120, pp. 49–53.

Tang, M., J. A. Valdez, Y. Wang, J. Zhang, B. P. Uberuaga, and K. E. Sickafus, 2016, "Ion irradiation-induced crystal structure changes in inverse spinel MgIn<sub>2</sub>O<sub>4</sub>," *Scripta Materialia*, Vol. 125, pp. 10–14.

Tang, M., James A. Valdez, Yongqiang Wang, Jian Zhang, Blas P. Uberuaga, and Kurt E. Sickafus, 2016 "Ion irradiation-induced crystal structure changes in inverse spinel MgIn<sub>2</sub>O<sub>4</sub>," *Scripta Materialia*, Vol. 125, pp. 10–14.

Tang, M., P. Tumurugoti, B. M. Clark, S. K. Sundaram, J. Amoroso, J. Marra, C. Sun, P. Lu, Y. Wang, and Y.-B. Jiang, 2016, "Heavy ion irradiations on synthetic hollandite-type materials: Ba<sub>1.0</sub>Cs<sub>0.3</sub>A<sub>2.3</sub>Ti<sub>5.7</sub>O<sub>16</sub> (A = Cr, Fe, Al)," *Journal of Solid State Chemistry*, Vol. 239, pp. 58–63.

Tang, M., P. Tumurugoti, B. M. Clark, S. K. Sundaram, J. Amoroso, J. Marra, C. Sun, P. Lu, Y. Wang, and Y.-B. Jiang, 2016, "Heavy ion irradiations on synthetic hollandite-type materials: Ba<sub>1.0</sub>Cs<sub>0.3</sub>A<sub>2.3</sub>Ti<sub>5.7</sub>O<sub>16</sub> (A = Cr, Fe, Al)," *Journal of Solid State Chemistry*, Vol. 239, pp. 58–63, 2016.

Tang, Ming, Andrew T. Nelson, Elizabeth S. Wood, Stuart A. Maloy, and Ying-Bing Jiang, 2016, "Grazing incidence X-ray diffraction and transmission electron microscopy studies on the oxide formation of molybdenum in a water vapor environment," *Scripta Materialia*, Vol. 120, pp. 49–53.

Tumurugoti, P., S. K. Sundaram, S. T. Mixture, J. C. Marra, and J. W. Amoroso, 2016, "Crystallization behavior during melt-processing of ceramic waste forms," *Journal of Nuclear Materials*, Vol. 473, pp. 178–188.

Uberuaga, B. P., M. Tang, C. Jiang, J. A. Valdez, R. Smith, Y. Wang, and K. E. Sickafus, 2015, "Opposite correlations between cation disordering and amorphization resistance in spinels versus pyrochlores," *Nature Communications*, pp. 9750.

Uberuaga, Blas Pedro, Ming Tang, Chao Jiang, James A. Valdez, Roger Smith, Yongqiang Wang, and Kurt E. Sickafus, 2015, "Opposite correlations between cation disordering and amorphization resistance in spinels versus pyrochlores," *Nature Communications*, Article 8750.

Wang Z., J. Liu, Y. Zhou, J. J. Neeway, D. K. Schreiber, J. V. Crum, J. V. Ryan, X. Wang, F. Wang, and Z. Zhu, 2016, "Nanoscale Imaging of Li and B in Nuclear Waste Glass, a Comparison of ToF-SIMS, NanoSIMS and APT," *Surface and Interface Analysis*, Vol. 48, pp. 1392–1401.

Wang, Z., J. Liu, Y. Zhou, J. J. Neeway, D. K. Schreiber, J. V. Crum, J. V., Ryan, X.-L. Wang, F. F. Wang, and Z. Zhu, 2016, "Nanoscale imaging of Li and B in nuclear waste glass, a comparison of ToF-SIMS, NanoSIMS, and APT," *Surface and Interface Analysis*, Vol. 48, No. 13, pp. 1392–1401.

Weaver J. L., J. S. McCloy, and A. A. Kruger, 2016, "Ensuring Longevity: Ancient Glasses Help Predict Durability of Vitrified Nuclear Waste," *American Ceramics Society Bulletin*, Vol. 95, No. 4, pp. 18–23.

Wen, J., C. Sun, P. P. Dholabhai, Y. Xia, M. Tang, D. Chen, D. Y. Yang, Y. H. Li, B. P. Uberuaga, and Y. Q. Wang, 2016, "Temperature dependence of the radiation tolerance of nanocrystalline pyrochlores A<sub>2</sub>Ti<sub>2</sub>O<sub>7</sub> (A: Gd, Ho and Lu)," *Acta Materialia*, Vol. 110, pp. 175–184.

Wen, J., C. Sun, P. P. Dholabhai, Y. Xia, M. Tang, D. Chen, D. Y. Yang, Y. H. Li, B. P. Uberuaga, and Y. Q. Wang, 2016, "Temperature dependence of the radiation tolerance of nanocrystalline pyrochlores A<sub>2</sub>Ti<sub>2</sub>O<sub>7</sub> (A: Gd, Ho and Lu)," *Acta Materialia*, Vol. 110, pp. 175–184.

Xu, Y., Y. Wen, R. Grote, J. Amoroso, L. Shuller Nickles, and K. S. Brinkman, 2016, "A-site compositional effects in Ga-doped hollandite materials of the form Ba<sub>x</sub>Cs<sub>y</sub>Ga<sub>2x+y</sub>Ti<sub>8-2x-y</sub>O<sub>16</sub>: implications for Cs immobilization in crystalline ceramic waste forms," *Scientific Reports*, Vol. 6, pp. 27412.

Zhang, J., J. J. Neeway, Y. Zhang, J. V. Ryan, W. Yuan, T. Wang, Z. Zhu, 2016, "Nanoscale Imaging of Alteration Layers of Corroded International Standard Glass Particles using ToF-SIMS," in revision, *NIMB Proceedings*.

## CoDCon Demonstration

*G. J. Lumetta (PNNL), S. A. Bryan (PNNL), C. Pereira (ANL), and B. Cipiti (SNL)*

PNNL has been tasked to test a CoDCon flowsheet for separating a mixed uranium (U)/plutonium (Pu) product from dissolved used nuclear fuel. The CoDCon testing will be performed at a scale of 1 to 2 kg of uranium using simulated dissolved fuel solutions containing uranium and plutonium in concentrations that would be expected in actual irradiated fuel. The primary purpose of the project is to quantify, using laboratory-scale equipment, the accuracy and precision to which a specific uranium-to-plutonium (uranium/plutonium) ratio can be achieved in a) the mixed uranium/plutonium nitrate solution produced during the solvent extraction portion of the flowsheet and b) the solidified mixed uranium/plutonium oxide product resulting from the co-conversion section of the flowsheet. The uncertainty associated with achieving a specific target uranium/plutonium ratio will be established. For the purpose of this project, a target value of 7/3 is established for the uranium/plutonium mass ratio, in both the mixed uranium/plutonium nitrate stream from the solvent extraction and in the final mixed oxide product. Additional objectives of the project include the demonstration of optical spectroscopic techniques for real-time monitoring of key components (e.g., plutonium, uranium, and HNO<sub>3</sub> concentrations) in the process solutions, and developing and testing a method for conversion of the mixed uranium/plutonium nitrate solution to the mixed metal oxide product at a scale suitable for the uranium/plutonium stream obtained from the solvent extraction portion of the test.

Figure 69 conceptually illustrates the most important aspects of the CoDCon test, including the solvent extraction steps to produce the mixed uranium/plutonium nitrate stream and its subsequent conversion to the mixed oxide. Under the scope of the existing project, the key steps to be performed in the CoDCon tests are

- Preparing simulated dissolved fuel solutions to be used as feed for the tests
- Performing solvent extraction to separate the desired uranium/plutonium (uranium/plutonium) product
- Converting the uranium/plutonium nitrate solution to oxide
- Characterizing the uranium/plutonium product and the bulk uranium product.

The capability to perform the CoDCon tests will be established in PNNL's Radiochemical Processing Laboratory (RPL). On-line monitoring will be incorporated into the CoDCon testing equipment to provide real-time feedback to the researchers as to the concentrations of key components at strategic points in the test system. The testing apparatus will be constructed using a bank of sixteen 2-cm centrifugal contactors that is already installed in a shielded glovebox in the RPL.

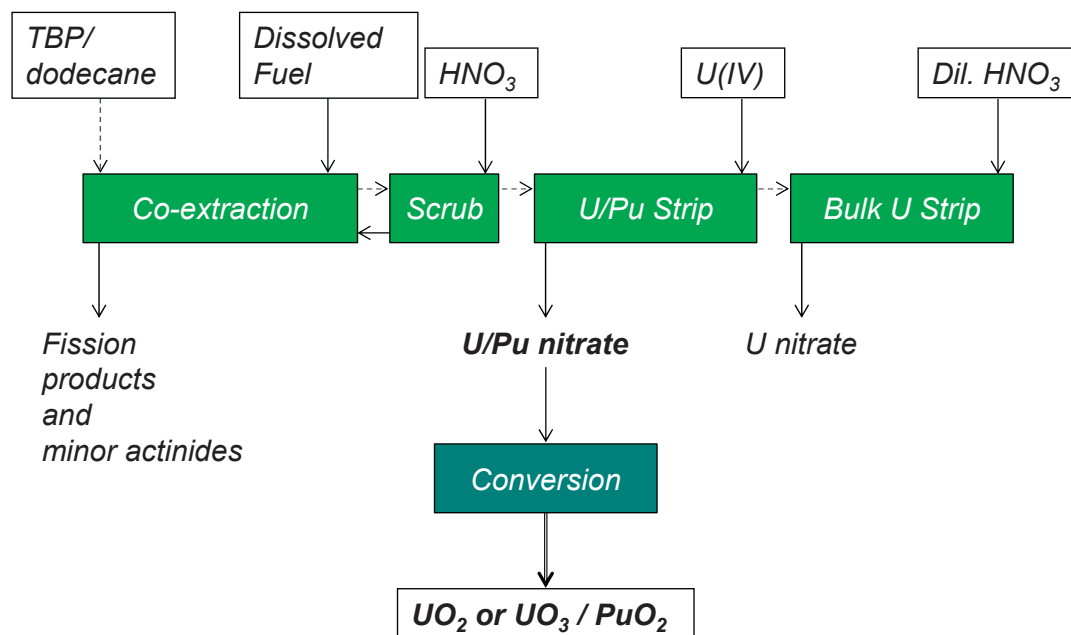


Figure 69. Conceptual schematic of the CoDCon flowsheet.

**CoDCon Flowsheet**

A CoDCon flowsheet was developed by C. Pereira (ANL), J.D. Law (INL), and C.J. Phillips (Atkins Global), using the AMUSE code. The flowsheet is designed so that each test run can be performed in three steps (as constrained by the 16 contactor stages installed in the glovebox). The first step involves uranium and plutonium co-extraction and nitric acid (HNO<sub>3</sub>) scrubbing of the loaded solvent, which consists of 30 vol% TBP in *n*-dodecane. In the second step, the loaded solvent collected from the first part of the test is stripped under reducing conditions to produce the desired uranium/plutonium nitrate stream; this step also includes a re-extraction section. In the third step, the bulk uranium is stripped from the solvent.

**Development of an Online Monitoring System**

Control of the process parameters will be essential to the success of the CoDCon testing effort. On-line monitoring systems will be employed to aid in maintaining the critical process parameters within the ranges required to meet the target uranium/plutonium ratio of 7/3. In FY 2016, a plan was developed for the on-line monitoring system (Bryan 2016). Six critical measurement locations were identified for instrumentation in the CoDCon testing system as shown in Figure 70. Progress to date includes preparing for and starting training-set measurements for chemometric analysis of process streams as well as initial instrument design, testing, and optimization. Additionally, subcontractors have been identified for building the software needed for implementing the chemometric models developed at PNNL for real-time monitoring during process runs.

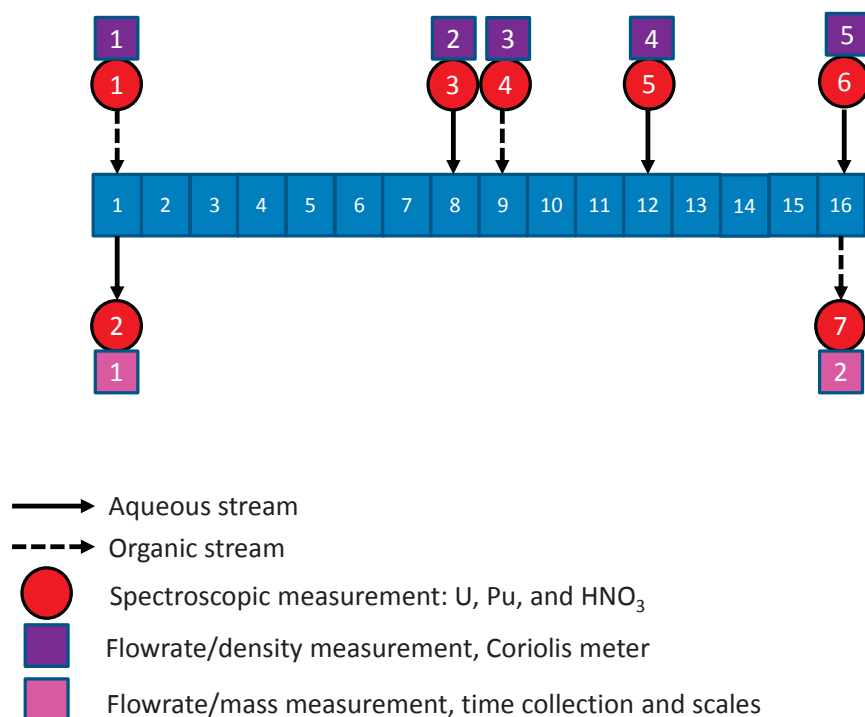


Figure 70. Schematic representation of the CoDCon testing system indicating the solution monitoring locations.

### Production of Uranium(IV)

Uranium(IV) will potentially be used in two parts of the CoDCon process. First, it will be used to reduce plutonium to the +3 oxidation state during stripping of the loaded TBP solvent to yield the uranium/plutonium nitrate product stream from the solvent extraction portion of the test. Second, if the uranium/plutonium nitrate solution is converted to the corresponding uranium/plutonium oxide product by oxalate precipitation/calcination, then reduction of the U(VI) to U(IV) will be needed to achieve efficient precipitation of the uranium. An electrochemical system has been developed to reduce U(VI) to U(IV) at the bench scale. The electrochemical cell is based on a design previously reported in the literature (Sini et al. 2013). Design of the cell was based on producing approximately 100 g of U(IV) at 100 g uranium/L (0.42 mol/L) and 3 mol/L HNO<sub>3</sub>.

Electrochemical reduction of U(VI) to U(IV) was demonstrated, with quantitative conversion of the UO<sub>2</sub><sup>2+</sup> to U<sup>4+</sup> within the uncertainty of the analytical methods used. To evaluate the stability of the U<sup>4+</sup> species over time, the electrolysis product was stored with a minimum headspace to prevent aerial oxidation, and sampled after a 21-day interval. Only 12% of the U<sup>4+</sup> was found to have decomposed, based on the absorbance at 647 nm (Figure 71).

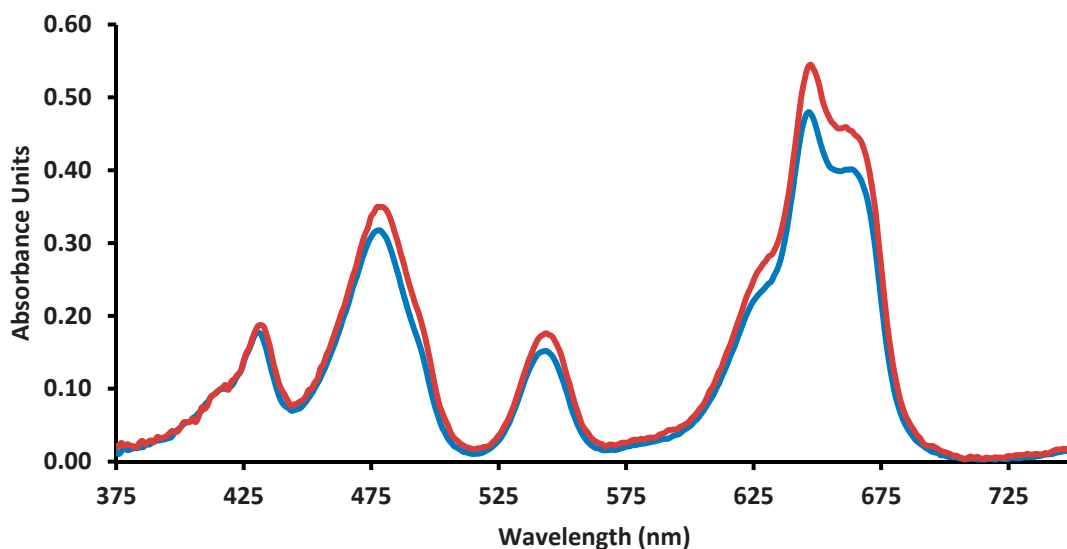


Figure 71. Visible spectrum of 100 g/L  $U^{4+}$  solution diluted 1:21 in 3 mol/L  $HNO_3$  taken immediately after electrolysis (red trace) and 21 days after electrolysis (blue trace).

#### Modified Direct Denitration

The uranium/plutonium nitrate solution generated during the solvent extraction portion of the CoDCon test must be converted to a solid oxide form to determine the uranium/plutonium ratio in the final product. Analyses of this solid product from multiple runs will be used to determine the uncertainty surrounding achievement of the 7/3 uranium/plutonium mass ratio. Modified direct denitration (MDD) is a leading candidate method for the conversion from nitrate solution to oxide (Collins 2015). Development of the MDD method at ORNL mostly utilized a rotary kiln method to heat the ammonium uranyl nitrate mixture to the proper temperature for thermal decomposition to  $UO_3$ . However, because of the relatively small amount of material requiring denitration in the CoDCon tests, and the complexity of implementing it in a radiological glovebox, work in FY 2016 focused on exploring a batch MDD protocol.

Three batch MDD experiments were successfully performed. The first used a uranyl nitrate solution in nitric acid. The second and third also used a nitric acid solution of uranyl nitrate, but cerium(III) nitrate was also added as a surrogate for plutonium. The uranium/cerium mass ratio in the latter two experiments was 7/3. Although successful conversion to the oxides was achieved in the first two tests, the apparatus used was plagued with a number of problems. Modifications were made to the apparatus before the third test and these problems were successfully mitigated.

Figure 72 shows the product obtained from the second batch MDD experiment. Scanning electron microscopy (SEM) examination of the mixed uranium/cerium oxide material indicated that it consisted of mostly irregularly shaped agglomerates. Some agglomerated particles were on the order of 50  $\mu m$  in size, but most of the primary particles appeared to be smaller than 10  $\mu m$ . Some thin plate-like particles were also observed. Elemental mapping of the SEM images using energy dispersive spectroscopy (EDS) revealed

## 2016 ACCOMPLISHMENTS

that the uranium and cerium were segregated from one another, suggesting the formation of their individual oxide phases, without co-crystallization (Figure 72). The uranium/cerium mass ratio was determined using EDS over two different areas of the SEM sample, yielding an average value of 71 wt% uranium, which is consistent with the targeted value of 70% in this experiment. X-ray diffraction analysis indicated the uranium/cerium oxide product to be mostly amorphous, but some gamma-phase  $UO_3$  and  $CeO_2$  were evident.

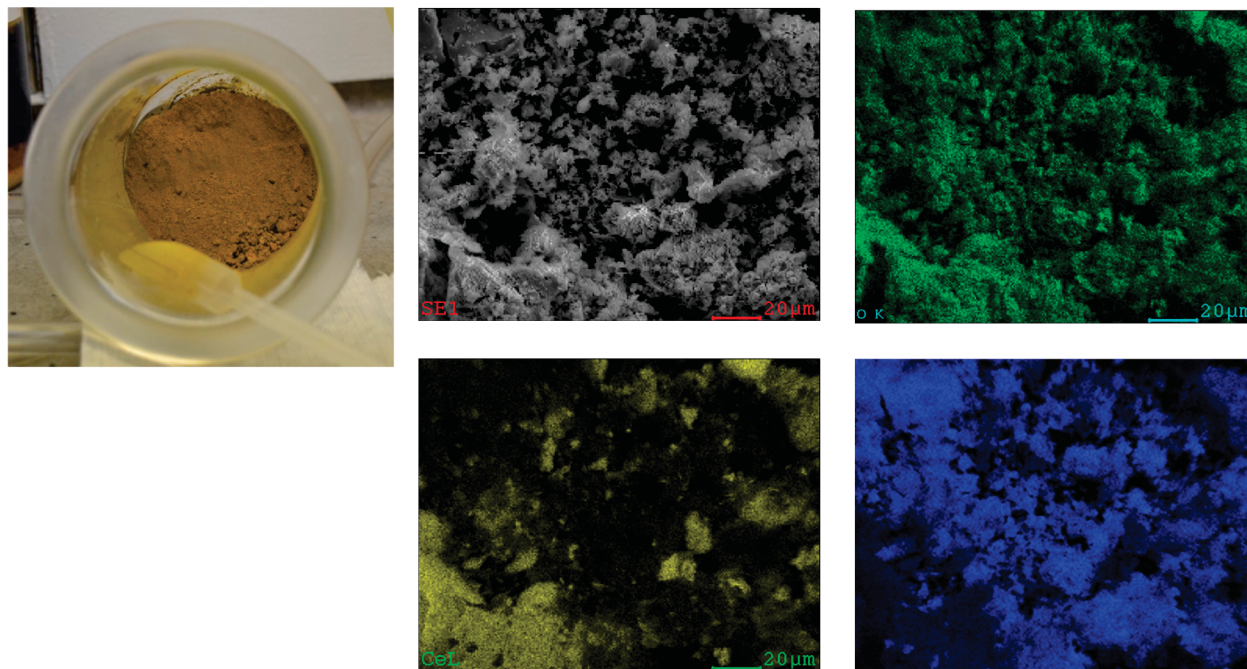


**Figure 72. Energy dispersive spectroscopy elemental mapping of the U/cerium oxide product from the second MDD experiment: upper left, primary SEM image; upper right, oxygen; lower left, cerium; lower right, uranium.**

### Modeling of On-Line Monitoring

A Matlab-Simulink model is being developed to guide and further investigate the use of on-line monitoring for real-time control of the process. While the majority of this effort will be in the next FY, initial planning meetings provided enough information to start building a model. The model will be calibrated using experimental data and then can be used to explore a variety of scenarios that may be too costly to perform experimentally. One of the key goals of the modeling effort is to determine uncertainties associated with controlling the process.

### Summary and Future Plans

A project to test the CoDCon flowsheet has been implemented. A proposed flowsheet for testing was developed by researchers at partnering laboratories. Experimental work was started to resolve critical technical uncertainties including the method to convert the mixed uranium/plutonium nitrate solution to a

mixed uranium/plutonium oxide, and reduction of U(VI) to U(IV). The spectroscopic instrumentation required to monitor the process streams during the CoDCon tests was identified. Collection of training-set data required to develop robust chemometric models was begun.

In FY 2017, work will focus on the following:

- Testing and verification of the U(VI) reduction system
- Testing of oxalate precipitation and calcination as a means to co-convert the uranium/plutonium nitrate solution to oxide, if the MDD method proves infeasible
- Deciding on the co-conversion method to be used
- Completing the collection of the training-set data
- Completing the chemometric model for determining solution compositions
- Procuring the needed spectroscopic equipment and installing it in a glovebox.

The first CoDCon flowsheet test is planned for the first quarter of FY 2018.

#### References

Bryan, S. A. and Lines, A. M., 2016, *CoDCon Project: Recommendation for on-line monitoring*; FCRD-MRWFD-2016-000014 (PNNL-25424; limited distribution); Pacific Northwest National Laboratory: Richland, Washington, 2016.

Sini, K., Mishra, S., Mallika, C., Pandey, N. K., Lawrence, F., Mudali, U. K., and Natarajan, R., 2013, "Reduction of uranyl nitrate ions in a continuous flow electrochemical reactor," *Journal of Radioanalytical and Nuclear Chemistry*, Vol. 295, pp. 1505–1510.

Collins, E. D., 2015, "Advanced thermal denitration conversion processes for aqueous-based reprocessing and recycling of spent nuclear fuels," *Reprocessing and Recycling of Spent Nuclear Fuel*, Taylor, R., Ed. Elsevier: Oxford, pp. 313–323.

## Fundamental Separation Data and Methods

### F-ELEMENT METRICS

*A. Gelis and C. Launieri (ANL)*

The microfluidic setup used for these experiments is described in a recent publication\*. In this work we have compared 2 new ligands-- HEDTTA (ORNL) and DTTA (INL) with HEDTA and DTPA for the americium stripping from the loaded solvent.

The solvent was loaded with lanthanide and fission products, and scrubbed with AHA to remove molybdenum. The experimental data points were fitted to a pseudo-first order reaction.

$$\ln(1 - C_{aq}/C_{eq}) = (k_{ao} + k_{oa}) * (A/V) * t$$

Where  $C_{aq}$  is the concentration of a nuclide in the aqueous phase;  $k_{ao}$  and  $k_{oa}$  are forward- and backward-extraction rate constants;  $(A/V)$  is the specific interfacial area. The data are summarized in

Table 14, where  $K_{obs} = (k_{ao} + k_{oa}) * (A/V)$ , and  $T_{1/2}$  is time of 50% mass transfer.

Based on these preliminary results, it appears that HEDTTA shows certain improvements over DTPA, but the kinetics somewhat slower than HEDTA. DTTA shows the fastest kinetics among the tested compounds likely due to the fact that it operates at pH 2.0. The experiments are underway to collect data points at different concentrations of the extractants and pH of the aqueous phase.

TABLE 14. 0.033M T2EHDGA/0.5M HEH[EHP]/N-DDN, LOADED WITH AMERICIUM, PROMETHIUM AND STABLE LANTHANIDE.

Aqueous phase*	Am $K_{obs}$ , 1/s,	Am $T_{1/2}$ , s,	Pm $K_{obs}$ , 1/s	Pm $T_{1/2}$ , s,	$SF_{eq}$ (Pm/Am)	D(Pm)
0.01M DTPA/0.6M malonate pH 2.8	0.038	18.4	0.018	53	35	5.7
0.125M HEDTA/ 0.2M Citrate, pH 2.8	0.11	5.4	0.081	9.9	23	2.11
0.125M HEDTTA/0.2M Citrate pH 3.0	0.093	7.4	0.10	7.1	33	6.23
0.02M DTTA/0.2M citrate pH 2.0	0.31	2.2	0.16	7.5	29	0.74

\*T=19 ±0.4° C for all experiments.

## Reference

Launiere, C. A., and A. V. Gelis, 2016, "Industrial and Engineering Chemistry Research," Vol. 55, No. 7, pp. 2272–2276.

## F-ELEMENT METRICS

P. R. Zalupski and J. D. Law (INL)

Two research directions continued harvesting data to support *f*-element solution chemistry efforts of MRWFD campaign. One focus area collects *f*-element optical absorbance data to construct a cross-actinide matrix of extinction coefficients to ease *f*-element monitoring in solution mixtures. Second effort is geared towards structural modification of aminopolycarboxylate aqueous holdback reagents to facilitate liquid-liquid systems capable of fast equilibration and efficient actinide/lanthanide separation.

Collection of extinction coefficient trends for Am<sup>3+</sup> in aqueous mixtures transitioning from perchloric acid to nitric acid: Optical absorption features for trivalent americium ion present in mixtures containing a wide range of acid concentrations were collected. Spectrophotometric characterization of 240 solutions of Am<sup>3+</sup> have been completed, collecting a total of 480 spectral signatures for peaks at  $\lambda_{\max} = 503$  nm and 813 nm. Measurements were carried out for five Am<sup>3+</sup> concentrations in 8 concentrations of total acid (0.1 M – 6.0 M), replacing perchloric acid with nitric acid in 20 % increments. Qualitative treatment of spectral information affords a convenient method for estimating concentration of trivalent americium in solution using the established linear acid dependencies for extinction coefficients as shown in Figure 73.

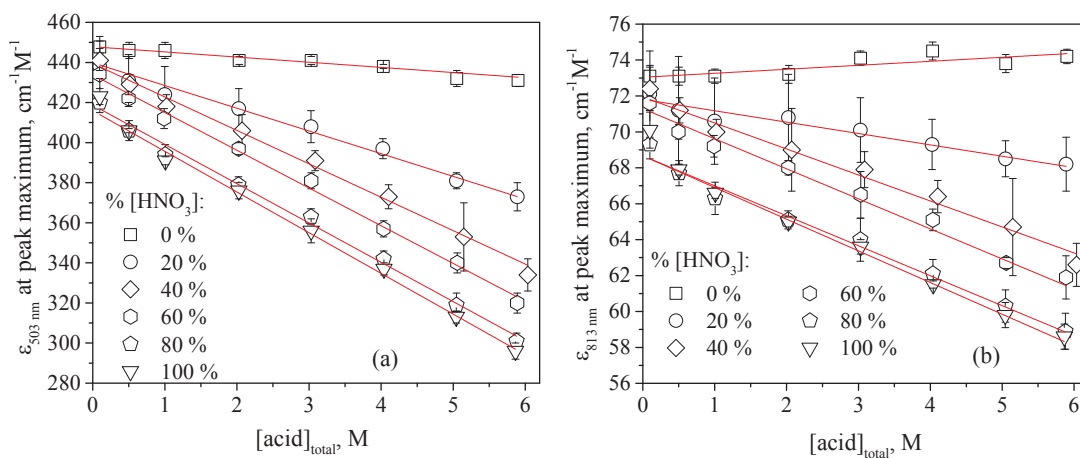


**Figure 73. Dependencies of molar extinction coefficients for optical absorption features of Am<sup>3+</sup> in 8 total acid concentrations, determined at six HClO<sub>4</sub>: HNO<sub>3</sub> proportions. (a)  $\lambda_{\max} = 503$  nm, (b)  $\lambda_{\max} = 813$  nm. Uncertainties are reported as  $\pm 3\sigma$ .**

Quantitative analyses of optical absorbance data yielded stability constants for complexation of trivalent americium by nitrate at a wide spectrum of acid concentrations.

*New and improved aqueous holdback complexant for ALSEP chemistry:* Efficient separation of  $\text{Am}^{3+}$  from all lanthanides was accomplished below  $\text{pH} = 2.0$  using a modified aminopolycarboxylate aqueous holdback complexant. The structural variation involved a replacement of two acetate pendant arms of diethylenetriaminepentaacetic acid, DTPA, by amide groups. Figure 74a demonstrates this capable separation, where liquid-liquid distribution of trivalent  $f$ -elements was facilitated by liquid cation exchanger 2-ethyl(hexyl)phosphonic acid mono-2-ethylhexyl ester, HEH[EHP]. The new complexant, diethylenetriamine- $N,N''$ -di(acetyl)glycine)- $N,N',N''$ -triacetic acid, DTTA-DAG, effectively holds  $\text{Am}^{3+}$  in the aqueous environment, while all trivalent lanthanides are extracted into organic phase. Efficient differentiation of trivalent americium from trivalent lanthanides, and flat pH dependence in  $1.5 < \text{pH} < 2.75$  range, afford an opportunity to enhance the kinetic features of this liquid-liquid system.

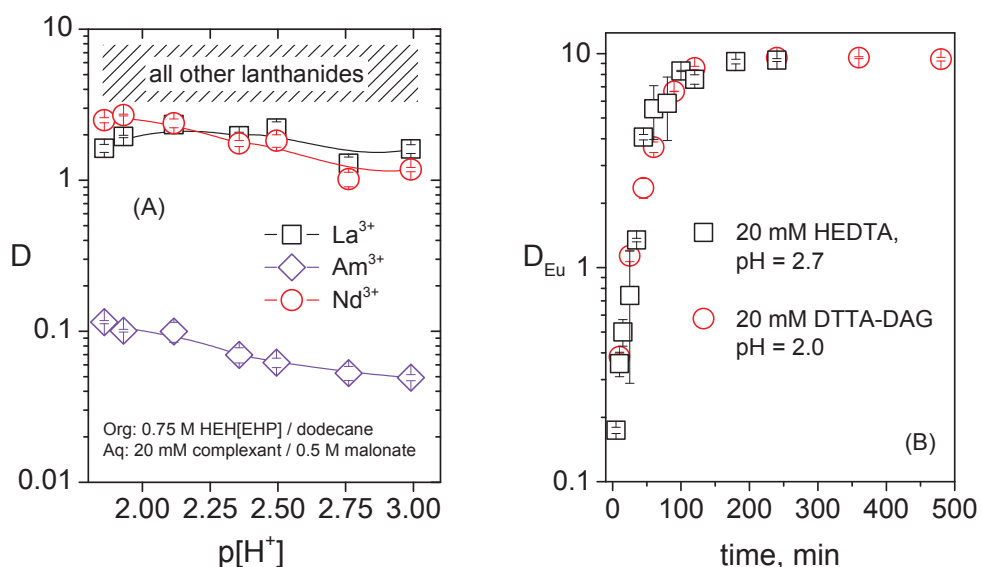


**Figure 74. (A) Liquid-liquid distribution of 0.1 mM  $\text{La}^{3+}$  -  $\text{Ho}^{3+}$  (each), and  $\text{Am}^{3+}$  (tracer) between organic mixture of 0.75 M HEH[EHP] in  $n$ -dodecane and an aqueous electrolyte phase containing 0.02 M DTTA-DAG, 0.5 M malonate,  $I = 1.0$  M adjusted with  $\text{NaNO}_3$ , at  $\text{p}[\text{H}^+] = 2.99, 2.76, 2.50, 2.36, 2.12, 1.93$  and  $1.86$ . (B) Comparison of time dependent partitioning of  $^{154}\text{Eu}^{3+}$  for liquid-liquid distribution systems containing HEDTA and DTTA-DAG. (○) 0.095 M HDEHP / 20.4 mM DTTA-DAG,  $\text{pH} = 2.3$ ; (□) 0.065 M HEH[EHP] / 20.0 mM HEDTA,  $\text{pH} = 2.7$ .**

The dominant kinetic barrier to fast attainment of equilibrium resides with high energetic cost of restructuring the metal – aminopolycarboxylate complex. One of the mechanisms of its dissociation begins with the complex protonation, and the kinetic rate of this reaction depends directly on the concentration of hydrogen ions in solution. Accordingly, DTTA-DAG complexant, while lowering the operational pH scale for efficient actinide/lanthanide separations, also yields a significant  $\text{H}^+$ -catalyzed kinetic enhancement. Figure 74b demonstrates this kinetic “boost” by comparing the time-dependent studies for the partitioning of  $\text{Eu}^{3+}$  in liquid-liquid systems containing either DTTA-DAG or HEDTA. The matching trends collected for the octadentate DTTA-DAG and pentadentate HEDTA predict that the new complexant will afford an efficient, fast-equilibrating liquid-liquid system below pH of 2.0

Preliminary measurements of promethium and americium back-extraction kinetics using droplet based microfluidic method (Art Gelis, ANL) show a two-fold rate enhancement for DTTA-DAG (pH = 2.0), relative to HEDTA (pH = 2.8). The liquid-liquid system based on DTTA-DAG yielded promethium/amerium separation factor of 29, reinforcing the results presented in Figure 74a.

## FUNDAMENTAL RADIATION CHEMISTRY

*B. Mincher (INL)*

Radiation chemistry efforts for FY 2016 focused on three tasks:

- *DGA Radiolysis:* Investigate the radiolysis and hydrolysis of the short-chain DGAs and the radiolysis of the non-symmetrical, dodecane-soluble DGA: D<sub>3</sub>DODGA in collaboration with SACSESS; both studies designed to better understand structure/activity effects in ligand radiolysis
- *Monoamide Radiolysis:* Study the radiation chemistry of the monoamides in collaboration with CEA Marcoule to better understand how these compounds and their degradation products will behave under process application
- *Acid protection:* Work to understand the mechanism of nitric acid radio-protection of some ligands, including continued radical cation rate constant measurements, and the examination of additional ligands under acidic conditions in an attempt to understand what structural features contribute to this effect

*DGA Radiolysis:* The non-symmetrical DGA: didodecyldioctyldiglycolamide (D<sub>3</sub>DODGA) was irradiated for comparison to previous radiation chemistry program work on symmetrical DGAs such as TODGA and T(EH)DGA, (Zarzana et al. 2015) and Me-TODGAs (Galan et al. 2015). The D<sub>3</sub>DODGA results were published in Roscioli-Johnson et al. (2016). There was little difference between the degradation rate of D<sub>3</sub>DODGA and those of TODGA and T(EH)DGA, and that rate was unaffected by contact with nitric acid or air sparging. There is also a striking similarity in the degradation pathways of all the organic-soluble DGAs, as revealed by their identified radiolysis products. This indicates that the diglycolamide center of these molecules and not the side-chains is most vulnerable to radiolytic degradation, apparently all by reaction with a common species produced by radiolysis of the diluent. For comparison, water-soluble DGAs were also irradiated in FY 2016. Their radiolysis mechanism and products may be different in the absence of the organic diluent radical cation. Since the water-soluble DGAs are subject to acid hydrolysis, hydrolytic studies were also conducted to provide baseline information prior to irradiation. The HNO<sub>3</sub> hydrolysis studies are complete, while HCl hydrolysis samples, and the initial irradiation samples are currently being analyzed. These studies were conducted in collaboration with co-authors in the SACSESS program, as witnessed by the author lists in Zarzana et al. (2015), Galan et al. (2015), and Roscioli-Johnson et al. (2016).

*Monoamide Radiolysis:* The monoamide: diethylhexylisobutyramide (DEHiBA) was irradiated under various conditions of acidity and aeration and the radiolysis rates and products were evaluated at both INL and CEA. Similarly to the DGAs, the aqueous phase and air sparging had little effect on degradation rates. However, the rate of monoamide radiolysis is about a factor of 10 slower than for the diamides. A loss of only about 30% of the monoamide concentration was found after delivery of an absorbed dose of 1,000 kGy. The main

products of radiolysis were the diethylhexylamine, and monoethylhexylisobutyramide. In agreement with these low degradation rates and the appearance of only these inoffensive products, there was little effect on uranium extraction distribution ratios with irradiation. Uranium distribution ratios measured at INL using irradiated DEHiBA samples are shown in Figure 75. These results support the reputation of the monoamides as being relatively radiation-stable with respect to effects on their solvent extraction performance. A manuscript that addresses these findings in detail is currently in collaborative preparation with co-authors at CEA Marcoule.

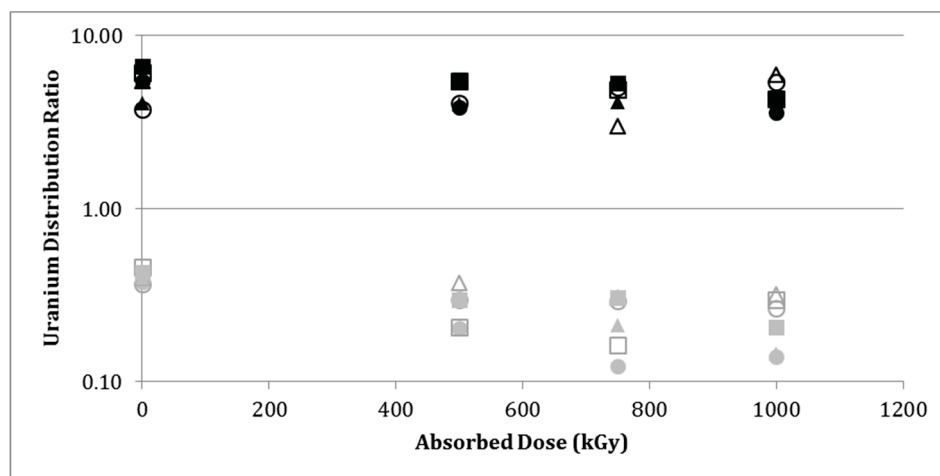


**Figure 75. Uranium solvent extraction ( $D_U$ ) from 6.5 M  $\text{HNO}_3$ , (black symbols) and stripping, (grey symbols) using irradiated, initially 1 M DEHiBA in dodecane. Irradiated organic phase only (open circles); sparged organic phase (filled circles); contact with 0.1 M  $\text{HNO}_3$  (open triangles); sparged contact with 0.1 M  $\text{HNO}_3$  (filled triangles); contact with 4 M  $\text{HNO}_3$  (open squares); and sparged contact with 4 M  $\text{HNO}_3$  (filled squares). Mean error bars of  $\pm 8\%$  omitted for clarity.**

*Acid protection:* The origin of the acid protection seen for some (for example, CMPO; Mincher et al. 2013), but not all (for example, DGAs; Zarzana et al. 2015, Galan et al. 2015, and Roscioli-Johnson et al. 2016), ligands remains elusive, although progress was made during FY 2016. It is believed that acid radioprotection and zero-order radiolytic degradation kinetics are related. For example, CMPO, C5-BPP, (Wilden et al. 2016) and CyMe4BTBP and CyMe4BTPhen, (Schmidt et al. 2016) are aromatic compounds that show both zero-order kinetic degradation and acid protection. The non-aromatic TODGA and T(EH)DGA (Zarzana et al. 2015), Me-TODGAs (Galan et al. 2015),  $\text{D}_3\text{DODGA}$  (Roscioli-Johnson et al. 2016), and DEHiBA (above) exhibit first-order kinetic degradation and no acid protection. It is hypothesized here that the phenyl ring may stabilize the charge transfer product of the ligand reaction with the diluent radical cation. This would allow for slow, zero-order kinetic degradation rates. However, the acid protection phenomenon is more difficult to explain. For CMPO, at least, it has been hypothesized that a strong CMPO acid complex reacts with the radical cation to regenerate free CMPO, thus providing the reported radioprotection (Mezyk et al. 2016). CMPO extracts about three times as much acid as does TODGA, and the acid complex is detectable by mass spectrometry. Recently, DFT calculations have suggested that the diluent radical cation reaction is actually a proton transfer, rather than the expected electron transfer. If this is the case, formation of the acid complex may prevent proton transfer to the aromatic ring. This idea is speculative at this time, and aromatic DGAs were recently irradiated in an attempt to address this question. These samples are currently being analyzed.

## References

- Galán, H., Zarzana, C. A., Wilden, A., Núñez, A., Schmidt, H., Egberink, R. J. M., Leoncini, A., Cobos, J., Verboom, W., Modolo, G., Groenewold, G.S., and Mincher, B. J., 2015, "Gamma-radiolytic stability of new methylated TODGA derivatives for minor actinide recycling," *Dalton Transactions*, Vol. 44, pp.18049–18056.
- Mezyk, S. P., Horne, G. P., Mincher, B. J., Zalupski, P. R., Cook, A. R., and Wishart, J. F., 2016, "The chemistry of separations ligand degradation by organic radical cations," *Procedia Chemistry*, in review.
- Mincher, B. J., Mezyk, S. P., Elias, G., Groenewold, G. S., and Olson, L. G., 2013, "The radiation chemistry of CMPO: Part 1. Gamma radiolysis," *Solvent Extraction and Ion Exchange*, Vol. 31, pp.715–730.
- Roscioli-Johnson, K.M.; Zarzana, C.A.; Groenewold, G.S.; Mincher, B.J.; Wilden, A.; Schmidt, H.; Modolo, G., 2016, "A study of the  $\gamma$ -radiolysis of N,N-di-doecyl-N',N'-di-octyl digycolamide using UHPLC-ESI-MS analysis," *Solvent Extraction and Ion Exchange*, Vol. 34, No. 5, pp. 439–453.
- Schmidt, H., Wilden, A., Modolo, G., Bosbach, D., Santiago-Schübel, B., Hupert, M., Švehla, J., Grüner, B., and Ekberg, C., 2016, "Gamma radiolysis of the highly selective ligands CyMe4BTBP and CyMe4BTPhen: Qualitative and quantitative investigation of radiolysis products," *Procedia Chemistry*, in review.
- Wilden, A., Modolo, G.; Hupert, M.; Santiago-Schübel, B.; Löfström-Engdahl, E.; Halleröd, J.; Ekberg, C.; Mincher, B.J.; and Mezyk, S.P., 2016, "Gamma-radiolytic stability of solvents containing C5-BPP (2,6-Bis(5-(2,2-dimethylpropyl)-1H-pyrazol-3-yl)pyridine) for actinide(III)/lanthanide(III) separation," *Solvent Extraction and Ion Exchange*, Vol. 34, pp. 1–12.
- Zarzana, C.A., Groenewold, G.S., Mincher, B.J., Mezyk, S.P., Wilden, A., Schmidt, H., Modolo, G., Wishart, J.F., and Cook, A.R., 2015, "A comparison of the  $\gamma$ -radiolysis of TODGA and T(EH)DGA using UHPLC-MS analysis," *Solvent Extraction and Ion Exchange*, Vol. 33, pp. 431–447.

## THERMODYNAMICS AND KINETICS

*A. Gelis (ANL), C. Launieri (ANL), and P. Bartl (ANL)*

In the frame of the US-Czech scientific collaboration program, a Ph.D. student from Czech Technical University in Prague, Faculty of Nuclear Sciences and Physical Engineering, Pavel Bartl spent over 5 months at ANL under supervision of Dr. Artem Gelis to study the kinetics of actinide solvent extraction. Experiments on Pu(IV), Am(III) and Pm(III) solvent extraction separation kinetics obtained with the Argonne microfluidic solvent extraction setup were completed (Figure 76). Americium, plutonium and promethium forward and backward extraction rates and mechanisms relevant to the EURATOM FP7 SACSESS program were studied. Selected rate dependencies on the extractant and acid power are reported. It has been found that partitioning of plutonium and americium in the TODGA-Dodecane-Nitric acid extraction system is extremely rapid, indicating great potential for a successful process application. However, a non-integral reaction order for plutonium and americium extraction by TODGA was observed, and more experimental studies are required to determine the mechanism of the reaction. In the case of BTBP-Cyclohexanone-Nitric acid system, the reaction follows pseudo-first order kinetics; however, the high miscibility of cyclohexanone diluent with nitric acid prevented direct measurements of the specific interfacial areas, thus no extraction

rate constants are reported for that system. The results were presented at the Ninth International Nuclear and Radiochemistry Conference at Helsinki, Finland in September 2016.

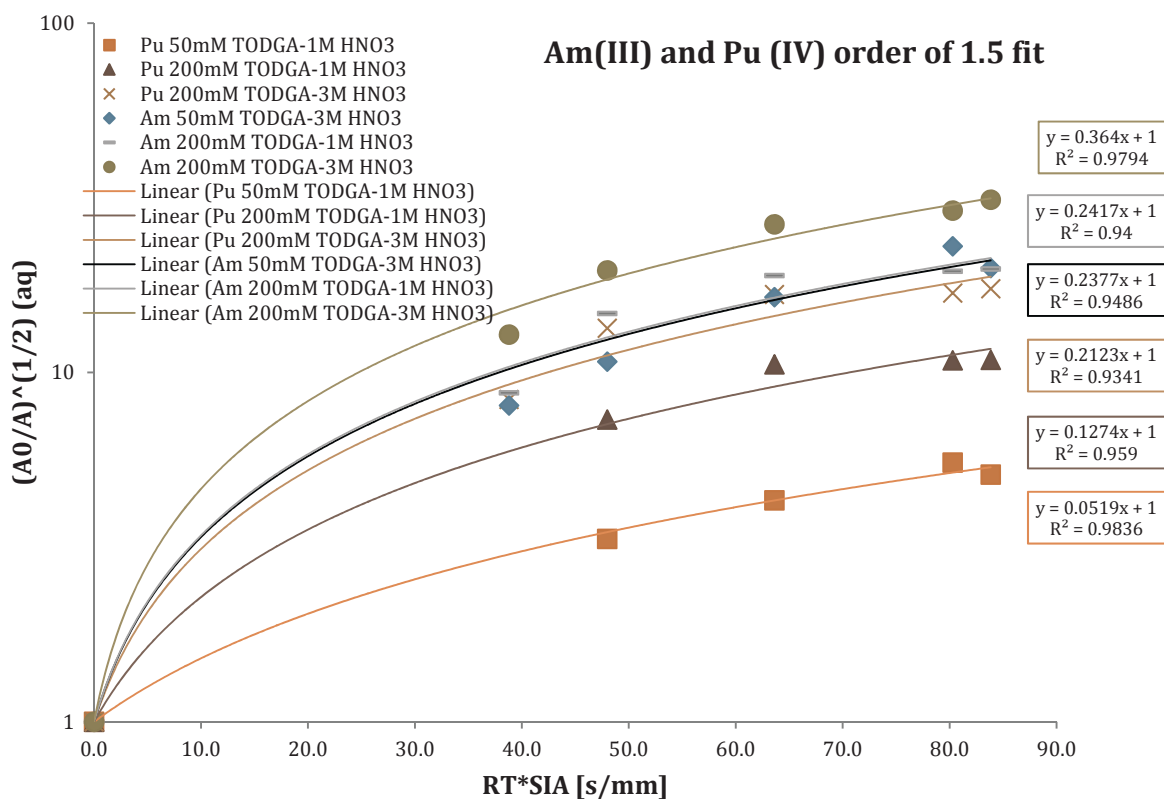


Figure 76. Kinetic curves of several Am(III) and Pu(IV) systems (see legend) fitted as a 1.5<sup>th</sup> order. T = 23.0 ± 1.0 °C.

## THERMODYNAMICS AND KINETICS

L. Rao (LBNL)

In FY 2016, thermodynamic data were collected for the complexation of Np(V) with HEDTA in a wide pH region, and the modelled by including a dimeric complex species,  $(\text{NpO}_2)_2(\text{OH})_2\text{L}_2^{6-}$  where  $\text{L}^{3-}$  stands for the fully deprotonated HEDTA ligand. The model provides better fits for the spectrophotometric titration data. The presence of the dimeric complex species in high pH region was verified for the first time by the EXAFS experiments at Stanford Synchrotron Radiation Laboratory (SSRL).

## Results

*Thermodynamic data (stability constants and enthalpy)*

Data from spectrophotometry and microcalorimetry are shown in Figure 77 and Figure 78. The best model to fit the spectrophotometric data include the species  $\text{NpO}_2\text{L}^{2-}$ ,  $\text{NpO}_2\text{HL}^-$ , and  $(\text{NpO}_2)_2(\text{OH})_2\text{L}_2^{6-}$ .

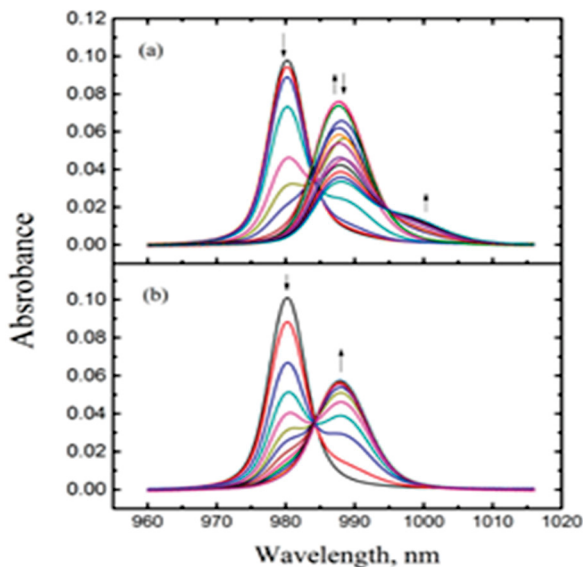


Figure 77. Spectrophotometric titrations of Np(V) with HEDTA at  $I = 1.0 \text{ mol}\cdot\text{L}^{-1} \text{ NaClO}_4$ ,  $t = 25^\circ\text{C}$ .

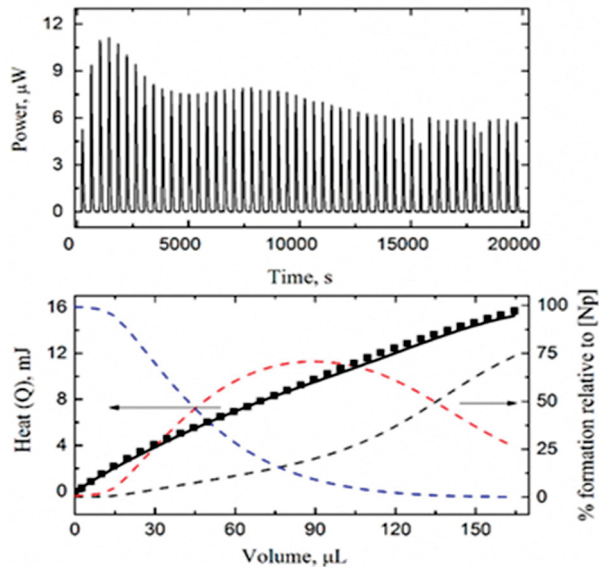


Figure 78. Calorimetric titration of  $\text{NpO}_2^+/\text{HEDTA}$  ( $t = 25^\circ\text{C}$ ,  $I = 1.0 \text{ mol}\cdot\text{L}^{-1} \text{ NaClO}_4$ ).

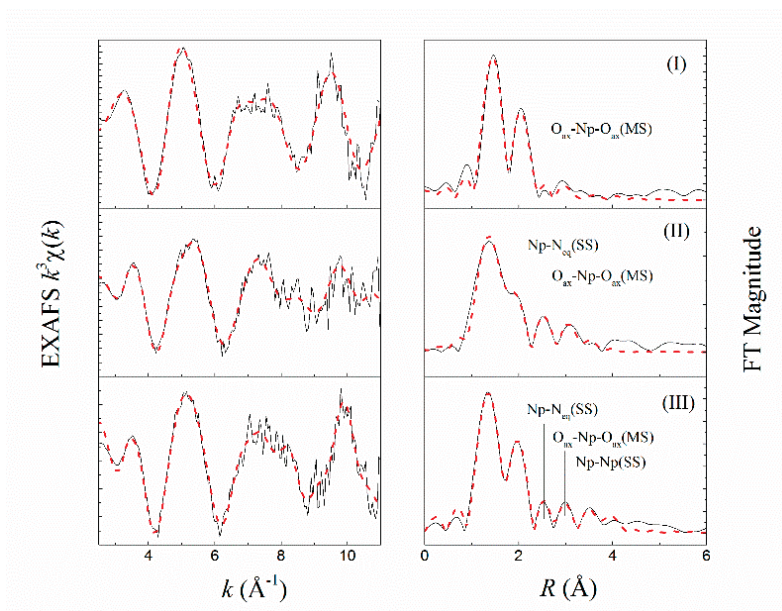
The equilibrium constants of for these species are summarized in Table 15. The equilibrium constants for the first two reactions from this work are in reasonable agreement with the values from previous studies, taking into consideration the difference in ionic strength. However, discrepancy exists in the model describing the data in the high  $pC_H$  region: the data in the present study are best represented by the formation of  $(\text{NpO}_2)_2(\text{OH})_2\text{L}_2^{6-}$ , while the data from the previous study suggest the formation of  $\text{NpO}_2(\text{OH})\text{L}^{3-}$ . The EXAFS data from this work support the presence of  $(\text{NpO}_2)_2(\text{OH})_2\text{L}_2^{6-}$ .

TABLE 15. THERMODYNAMIC PARAMETERS OF THE NP(V) COMPLEXATION WITH HEDTA AT  $25^\circ\text{C}$  IN  $1 \text{ M NaClO}_4$ .

Reaction	$\log\beta$	$\Delta H$ $\text{kJ}\cdot\text{mol}^{-1}$	$\Delta S$ $\text{J}\cdot\text{mol}^{-1}\cdot\text{K}^{-1}$
$\text{NpO}_2^+ + \text{L}^{3-} = \text{NpO}_2\text{L}^{2-}$	$6.91 \pm 0.06$	$-(8.0 \pm 2.0)$	$105 \pm 7$
$\text{NpO}_2^+ + \text{HL}^{2-} = \text{NpO}_2\text{HL}^-$	$4.28 \pm 0.03$	$-(2.2 \pm 2.0)$	$75 \pm 7$
$2\text{NpO}_2^+ + 2\text{L}^{3-} + 2\text{H}_2\text{O} = (\text{NpO}_2)_2(\text{OH})_2\text{L}_2^{6-} + 2\text{H}^+$	$-(4.93 \pm 0.03)$		

**EXAFS: Coordination structures in Np(V)/HEDTA complexes**

The  $k^3$ -weighted Np L<sub>III</sub> EXAFS spectra and the fourier transform (FT) of three Np(V) solutions are presented in Figure 79. An excellent fit was achieved with the proposed coordination structures for those Np(V) species (Table 16).



**Figure 79.** Np L<sub>III</sub> EXAFS of three Np(V) solutions. (I) [Np] = 3.0 mmol·L<sup>-1</sup>, p<sub>CH</sub> = 2.5; (II) [Np] = 1.0 mmol·L<sup>-1</sup>, [HEDTA] = 2.3 mmol·L<sup>-1</sup>, p<sub>CH</sub> = 9.4; (III) 2.0 mL, [Np] = 1.0 mmol·L<sup>-1</sup>, [HEDTA] = 23 mmol·L<sup>-1</sup>, p<sub>CH</sub> = 12. Black solid line – experimental, red dash line – fit.

**TABLE 16.** EXAFS FITTING RESULTS OF NP(V) SPECIES IN SOLUTIONS FROM THIS WORK.

Solution <sup>a</sup>	Shell	N	R (Å)	$\sigma^2$	Notice
I Speciation: 100% NpO <sub>2</sub> <sup>+</sup>	Np-O <sub>ax</sub>	2.0	1.82	0.0025	$S_0^2 = 0.85$ , $\Delta E^0 = 5.56$ eV $r = 0.005$ , $\chi^2_{red} = 13.0$
	Np-O <sub>eq</sub>	4.6	2.51	0.0096	
II Speciation: 100 % NpO <sub>2</sub> L <sup>2-</sup>	Np-O <sub>ax</sub>	2.0	1.82	0.0046	$S_0^2 = 0.75$ , $\Delta E^0 = 8.05$ eV $r = 0.004$ , $\chi^2_{red} = 14.5$
	Np-O <sub>eq</sub>	3.8	2.41	0.0114	
	Np-N <sub>eq</sub>	1.0	3.95	0.0047	
III Speciation: 11% NpO <sub>2</sub> L <sup>2-</sup> 87 % (NpO <sub>2</sub> ) <sub>2</sub> (OH) <sub>2</sub> L <sub>2</sub> <sup>6-</sup>	Np-O <sub>ax</sub>	2.0	1.82	0.0038	$S_0^2 = 0.77$ , $\Delta E^0 = 9.01$ eV $r = 0.005$ , $\chi^2_{red} = 15.1$
	Np-O <sub>eq</sub>	3.7	2.40	0.0089	
	Np-N <sub>eq</sub>	1.0	2.93	0.0039	
	Np-Np	1.0	3.95	0.0046	

a. The Np(V) speciation (relevant to total [Np]) was calculated with the simulation program HySS2009 using the complexation constants determined in this work.

### Summary

Three Np(V) complexes with HEDTA,  $\text{NpO}_2\text{L}^{2-}$ ,  $\text{NpO}_2\text{HL}^-$ , and  $(\text{NpO}_2)_2(\text{OH})_2\text{L}_2^{6-}$ , were included in the modelling of spectrophotometric titration data. The hydrolyzed dimeric species,  $(\text{NpO}_2)_2(\text{OH})_2\text{L}_2^{6-}$ , becomes significant in the high pH region. Data by EXAFS provide support for the presence of this species in aqueous solutions of high pH.

### PUBLICATIONS FOR FUNDAMENTAL SEPARATION DATA AND METHODS

Heathman, C. R., Grimes, T. S., and Zalupski, P. R., 2016, "Coordination Chemistry and *f*-element Complexation by Diethylenetriamine-*N,N'*-di(acetylglycine)-*N,N',N''*-triacetic Acid," *Inorganic Chemistry*, Vol. 55, No. 21, pp. 11600–11611.

Heathman, C. R., Grimes, T. S., and Zalupski, P. R., 2016, "Thermodynamic and Spectroscopic Studies of Trivalent *f*-element Complexation with Ethylenediamine-*N,N'*-di(acetylglycine)-*N,N'*-diacetic acid," *Inorganic Chemistry*, Vol. 55, pp. 2977–2985.

Xingliang Li, Zhicheng Zhang, Leigh R. Martin, Shunzhong Luo, and Linfeng Rao, 2016, "Complexation of  $\text{NpO}_2^+$  with (2-Hydroxyethyl) ethylenediaminetriacetic Acid (HEDTA) in Aqueous Solutions: Thermodynamic Studies and Structural Analysis," *RSC Advances*, in review.

## Domestic Echem

### URANIUM/TRU CO-DEPOSITION AND FLUORIDE SALT STUDIES

*J. Willit (ANL)*

The basic premise of U/TRU co-deposition, namely, that in a molten salt containing uranium and TRU if the current density exceeds the mass transfer limiting current density for uranium electrodeposition, the next most electropositive species in the system, the TRUs will co-deposit along with uranium. Results from small-scale electrochemical tests confirmed this premise.

Since completing those experiments, ANL has been conducting engineering-scale co-deposition tests using lanthanides (Ln) as simulants for TRUs to establish equipment design and scaling parameters. Technology development activities conducted over the last fiscal year included redesign of the cathode system to reduce iR losses when passing current, installing a mechanism for making controlled, measured changes in the electrode immersion depth, and upgrading to a new LabVIEW-based data acquisition system with greater flexibility and ability to control the electrodeposition process.



**Figure 80. U-Ln co-deposit on engineering-scale solid cathode. Inset shows section of co-deposit.**

With the equipment improvements, U-Ln co-deposition was successfully demonstrated with uranium concentrations below approximately 5wt% U in molten LiCl-KCl eutectic salt. One of these co-deposits is shown in Figure 80. As expected, plotting the cathode potential vs. a Ag/Ag<sup>+</sup> reference electrode during periodic open circuit current interrupts showed a voltage plateau at a potential corresponding to the lanthanide metals present in the electrolyte salt.

Tests also confirmed that the high current density U-Ln co-deposition cathode can be operated in parallel with uranium deposition at a second set of low current density cathodes. Simultaneous U and U-Ln electrodeposition are driven by two power supply circuits that share a common anode. The anode common to both circuits is the steel basket containing metallic fuel constituents.

With feasibility demonstrated at the engineering scale, the next phase of testing in FY 2017 will be to develop procedures for characterizing and optimizing the co-deposition cathode that take into account iR effects, and cell geometry parameters.

### Fluoride Salt Study

In the fluoride salt studies, AC voltammetry was used to measure the fundamental electrochemical kinetics of electron transfer during the deposition of uranium from a LiF-CaF<sub>2</sub> salt containing UF<sub>4</sub>. DC electrochemical measurements are not able to measure all the key electrochemical parameters independently because there are more variables than independent equations. Adding an AC component to the technique however introduces additional independent equations that allow for all the variables to be determined independently. AC voltammetry has been used to study electrochemical kinetics for the case when both reactant and product are dissolved in the electrolyte. Use of this technique in the case where the product is an insoluble solid deposited on the electrode required derivation of equations describing the process. After developing experimental techniques that generated highly reproducible data, the general behavior of the system predicted by the newly derived equations was validated experimentally in an extensive series of tests. Rate constants and diffusion coefficients calculated using the newly derived equations were consistent with reported values for uranium or analogue species in molten fluoride salts. This work demonstrated that our extensive experience in high precision electrochemical measurements in molten chloride salts can be utilized in similar studies in molten fluoride systems.

### URANIUM/TRU CO-DEPOSITION AND FLUORIDE SALT STUDIES

*G. Fredrickson (INL)*

Voltammetry measurements and codeposition tests were performed in five different molten salt compositions beginning with salt retrieved from the Mark-IV electrorefiner in the INL Fuel Conditioning Facility (FCF). A series of lithium metal additions were made to reduce the uranium trichloride from the salt, increasing the Pu:U ratio from 0.42 to 1.98. Codeposits of uranium and plutonium were collected on a solid cathode at each of these five salt compositions. Results show that, in general, the Pu:U ratio in the deposit increases along with the Pu:U ratio in the salt while lanthanide metals primarily remain in the salt phase. A computational model was developed to help understand the codeposition process. Using the model, separation factors for actinide and lanthanide elements with respect to plutonium were calculated. Both the model and experimental results show that codeposition of plutonium and uranium with lanthanide element rejection is possible using a solid cathode.

Cyclic voltammetry scans of the five different salt compositions are shown in Figure 81. As previously mentioned, the immersion depth, and therefore surface area, of the working electrode was changed following the first lithium addition. Because of this, direct quantitative comparison between these scans is difficult. In general, all scans show the same features. At approximately -1.42 V (beginning at -1.36 V), there is a cathodic peak representing the reduction of trivalent uranium to metallic uranium, followed by a peak at approximately -1.75 (beginning at -1.62 V) caused by the reduction of transuranics, and -2.4 V (beginning at -1.92 V), which represents the reduction of lanthanides:

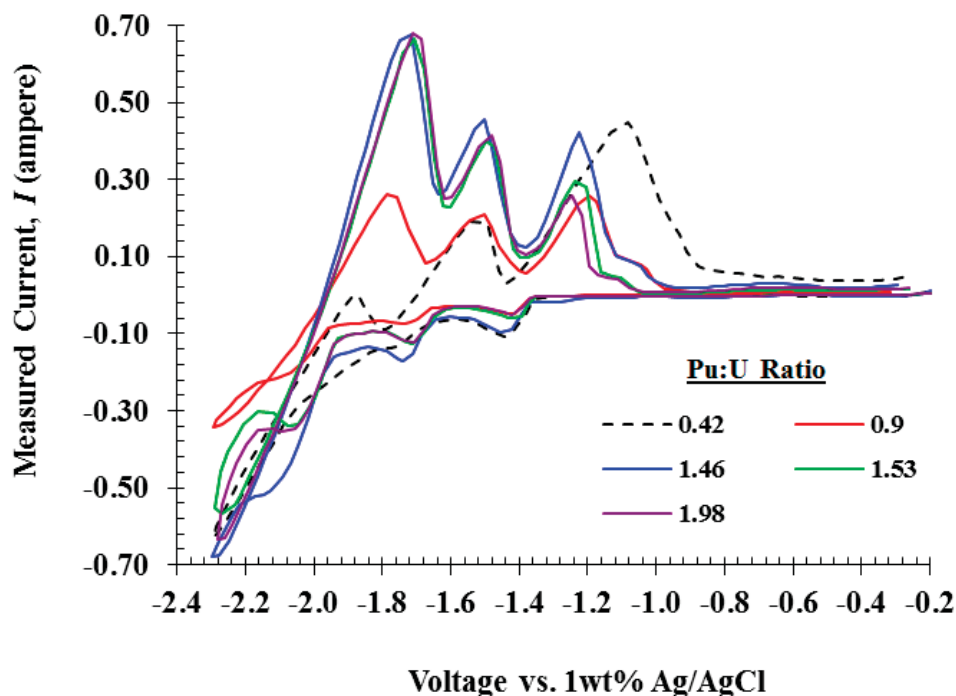


Figure 81. Cyclic voltammograms recorded at  $200 \text{ mV s}^{-1}$  in the range of -2.3 V to -0.2 V.

Constant deposition coulomb open circuit potential (CDCOCP) is a technique that involves passing a known amount of charge at a given potential to deposit species onto the working electrode. After this deposition step, no current or potential are applied and the resulting OCP of the deposit on the working electrode is measured over a period of time as the deposit either oxidizes or dissolves away from the working electrode. OCP measurements following 2 coulomb deposits are shown at various deposition potentials in Figure 82. These data show that at deposition potentials more positive than -1.7 V, the resulting OCP begins at approximately -1.35 V and eventually rises to -1.1 V. This is indicative of a uranium metal deposit on the working electrode, which dissolves away ending in the OCP of the clean tungsten wire. At a deposition of -1.7 V, the OCP begins at a much more negative potential of around -1.65 V, indicating a TRU deposit on the working electrode. As this TRU metal oxidizes off the electrode by reacting with the  $\text{UCl}_3$  in the salt, the OCP rises to the uranium potential, and eventually the OCP of the bare tungsten wire. There is another jump in beginning OCP when deposition is performed at -2 V. When this potential is applied, the resulting OCP starts at approximately -1.9V, indicating lanthanide metal deposition. As the lanthanides oxidize from the electrode, the potential rises to the TRU potential, followed by uranium and the clean tungsten wire OCP. Finally at a deposition potential of -2.5 V, the OCP begins at around -2.25 V, likely indicating lithium reduction. This OCP then rises to the lanthanide potential, followed by transuranics, uranium, and the tungsten wire OCP.

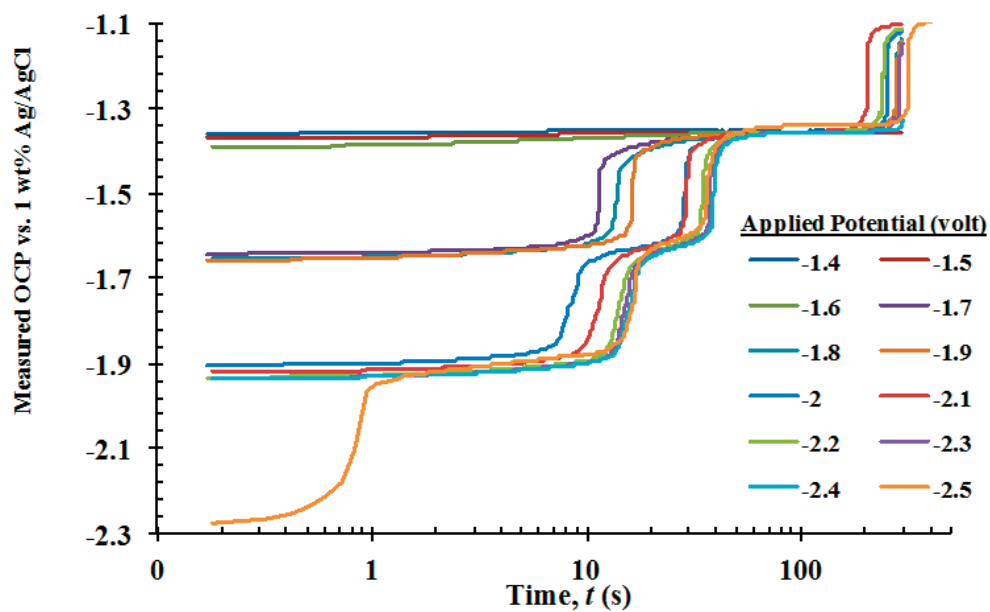


Figure 82. Open circuit potential measurement after a 2 C deposition at various potentials following the third lithium addition resulting in a Pu:U ratio of 1.53.

Photographs of the five codeposits are shown in Figure 83. These deposits were formed at Pu:U ratios of 0.42, 0.9, 1.46, 1.53, and 1.98, respectively.

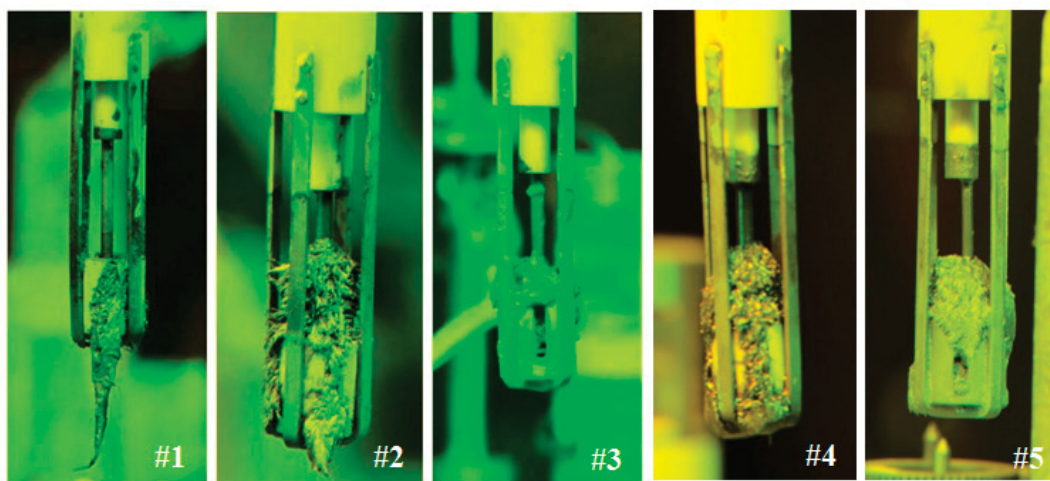


Figure 83. Photographs of the ASC deposits.

The compositions of the deposits are shown in Figure 84. From these data it is clearly seen that with increasing Pu:U ratio in the salt, more plutonium and less uranium is deposited. Additionally, these data show good separation between the transuranics (i.e., plutonium) and the lanthanides under all conditions. The data in Figure 84 do not follow a consistent trend. For example, the upward trend observed in the first three codeposits is discontinuous with the upward trend observed in the last two codeposits. The reason for this discontinuity is technical; in programming the control and operation of the potentiostat, a 200-mV IR compensation was applied to the first three codeposits and no IR compensation was applied to the last two codeposits. The consequence is that the true deposition potentials of the last two codeposits were less negative than anticipated; resulting in a decrease in the Pu:U ratio of the metallic deposits.

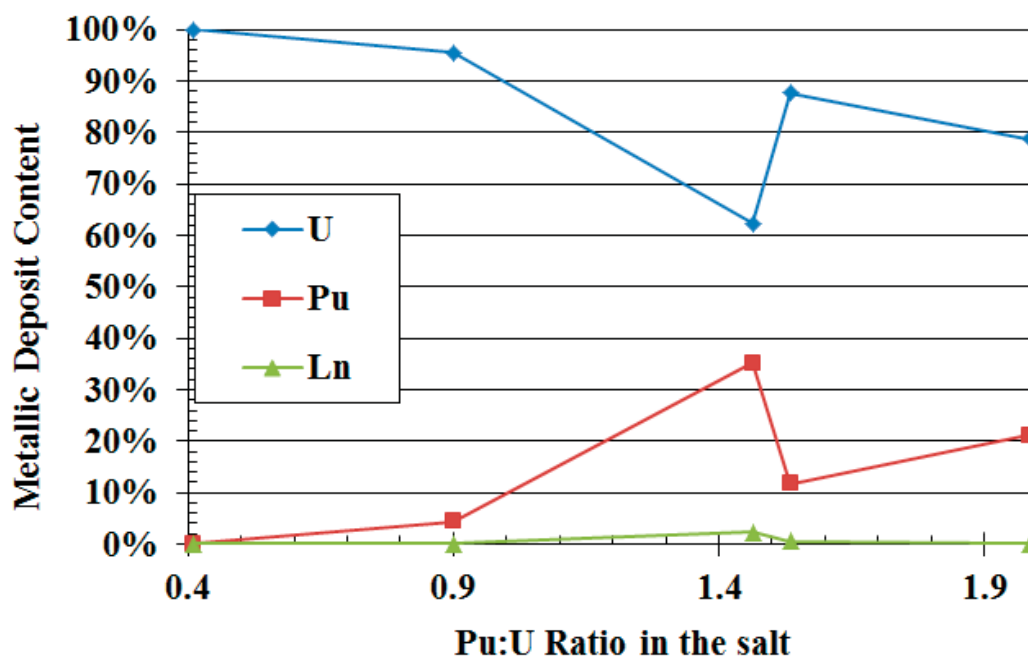


Figure 84. Mass percent of uranium, plutonium, and lanthanides deposited versus the Pu:U ratio in the salt.

#### PUBLICATION FOR DOMESTIC ECHEM

Shaltry, M., R. Hoover, T. S. Yoo, N. Gese, B. Serrano, G. Fredrickson, and S. Li, 2016, *FY-16 U/TRU Codeposition Technical Report (Applied Technology)*, FCRD-MRWFD-2016-000050.

## Fuel Resources

### SEAWATER URANIUM RECOVERY

*S. Kung (DOE)*

The Fuel Resources Program seeks to identify and implement actions the Department can take to assure the long-term availability of economical nuclear fuel. The program evaluates fuel resources and develops recovery technologies to increase resource accessibility to enable a sustainable fuel cycle. Priority attention in the near term is focused on developing the technology for extraction of uranium from seawater. The following activities are included in this effort: (1) Technical Support/Management provides technical coordination of R&D activities within the Fuel Resources area and coordinates participation in working group and review meetings, as well as international cooperative activities. (2) Advanced Grafting focuses on the development of advanced adsorbent materials prepared by irradiation (electron-beam and gamma-ray) induced and chemical grafting methods to increase the uranium adsorption capacity and selectivity; (3) Advanced Nanosynthesis incorporates nanotechnology and nano-manufacturing techniques into the development of advanced adsorbent materials to provide increased selectivity and capacity for uranium recovery; (4) Ligand Design and Thermodynamics uses computational screening tools to rationally design and evaluate ligands for enhanced selectivity and capacity, followed by rational synthesis of promising ligands for subsequent experimental validation. (5) Marine Testing and Modeling conducts sorption and uranium recovery experiments in several distinct marine environments, while the modeling component provides data and adsorption models for scale-up and evaluation of marine deployment. (6) Cost Analysis conducts cost and energy analyses and develops cost/energy models for newly developed adsorbents and technologies. The purpose of this subtask is to aid in focusing R&D efforts on achieving evidence-based cost minimization strategies. (7) Durability and Recycle conducts material durability evaluation and degradation studies during the reuse of adsorbent to reduce the technology cost and performance uncertainties. Contributions to the aforementioned activities are made by researchers at ORNL, LBNL, and PNNL, as well as by university collaborators under the Nuclear Energy University Program.

Overall, the main accomplishment of the Fuel Resources Program in the past 6 years is revealed in Figure 85, where it is shown that adsorbents developed in this program have tripled the uranium extraction from seawater compared to adsorbents developed over the previous 50 years. Specifically, in 2016, adsorbents developed by atom-transfer radical polymerization exceeded a capacity of 6 g uranium per Kg adsorbent, following contact with seawater for a period of 8 weeks. Two additional classes of materials also exceeded 5 g uranium per Kg adsorbent: adsorbents prepared by radiation-induced graft polymerization on high-surface area trunk polymers, and commercially-available polymers that were surface modified without radiation through application of a simple, scalable chemical treatment. These remarkable achievements are the result of increased adsorbent density on trunk polymer fibers accompanied by an optimized ratio of amidoxime ligand and co-polymer organic acid. In addition to increased adsorbent uranium capacity, enhanced understanding of the functional activity of the amidoxime ligand has been demonstrated through advanced spectroscopy, computational chemistry, and adsorption modeling. Major accomplishments in all the activities of the Fuel Resources Program are described in this section.

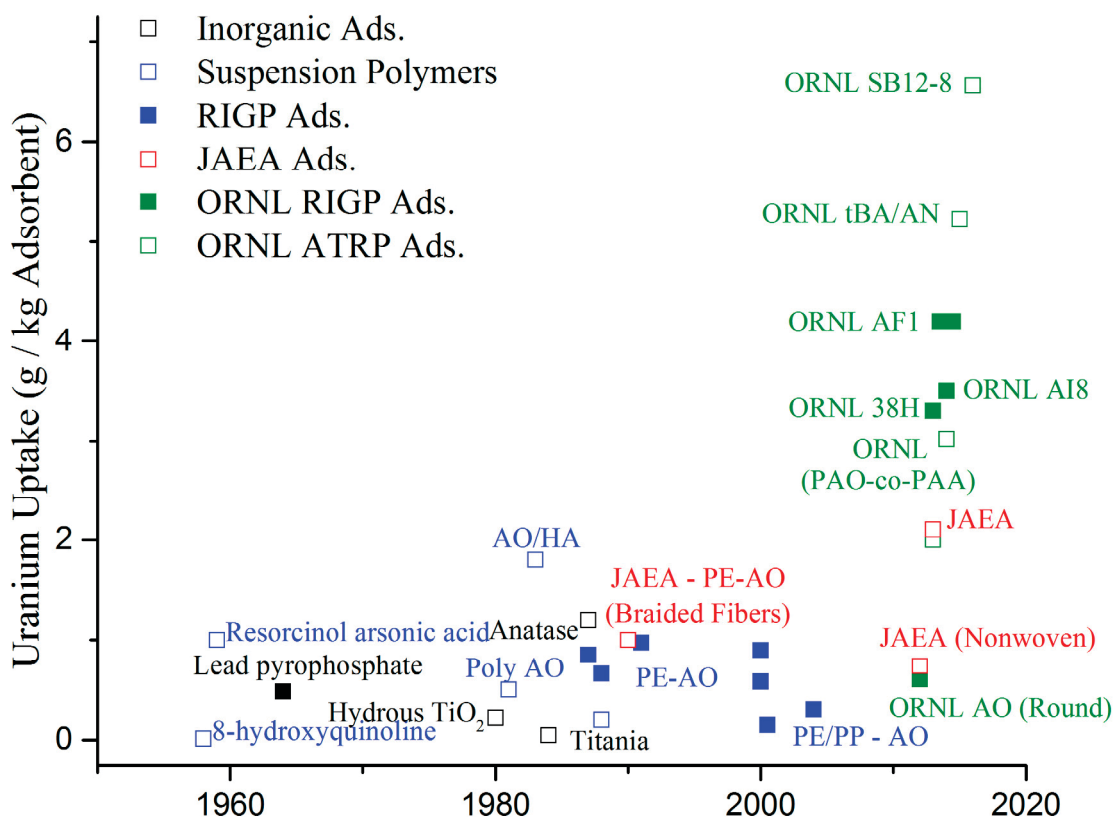


Figure 85. Review of uranium adsorbent capacity reported in the literature for adsorbents developed in the past six decades. Adsorbents developed by the Fuel Resources Program in the past 6 years demonstrated a 3-fold increase in uranium capacity from seawater, as compared to adsorbents developed in the previous 50 years. Data are not normalized for deployment time.

#### Development of Novel Amidoxime-Based Polymeric Adsorbents

Various novel fiber adsorbents were synthesized in FY 2016 using radiation-induced graft polymerization (RIGP), atom-transfer radical polymerization (ATRP), and through surface modification of commercially available acrylic fibers. The goal was to develop new materials of high uranium adsorption capacity and selectivity.

For the RIGP sub-task, the focus has been on improving uranium adsorption capacity, kinetics, and selectivity by the incorporation of new hydrophilic co-monomers onto the high-surface-area polyethylene trunk fibers and optimization of a large number of synthesis and process conditions. Several new adsorbents were developed in FY 2016 that demonstrated uranium adsorption capacities ranging from 5.0 to 5.4 g-uranium/kg-adsorbent after 56 days of seawater exposure at 20°C in flow-through column experiments at PNNL (Figure 86). A key step in achieving these capacity improvements was the discovery of using dimethyl sulfoxide as the solvent in the amidoximation reaction, as opposed to using the conventional water-methanol solution. In addition, new co-monomers were grafted onto the high-surface-area

polyethylene fibers that enhanced the adsorption capacities including methacrylonitrile, hydroxyethyl acrylate, and methyl acrylate. The adsorbent grafted with methyl acrylate and acrylonitrile, AN/MA-42kGy-AO-DMSO, yielded particularly high uptake kinetics and attained a uranium adsorption capacity of 4.0 g-uranium/kg-adsorbent after only 21 days of seawater exposure at 20°C in flow-through columns.

This result translated to a greater than 50% increase in adsorption capacity as compared to the AF1 adsorbent. Promising results were also realized by several adsorbents that were tested at Broad Key Island, FL, in flumes containing ambient flowing seawater, and included 56-day capacities of 6.4 and 6.8 g-uranium/kg adsorbent for the AF1 and AF1-AO-DMSO adsorbents, respectively. Adsorbents having high uranium selectivity were also developed that contained hydroxyethyl acrylate and acrylonitrile. These adsorbents achieved relatively low V/U ratios of less than 1.85.

ATRP-synthesized fiber adsorbents, including P(AN-co-HEA) on PVC-co-CPVC fibers, showed the highest performance so far, achieving 6.56 g uranium/kg adsorbent after 56 days of exposure in natural seawater (Figure 87).

PNNL staff collaborating with LCW Technologies and the University of Idaho have developed an amidoxime-based polymeric adsorbent (Figure 88) using commercially available and inexpensive

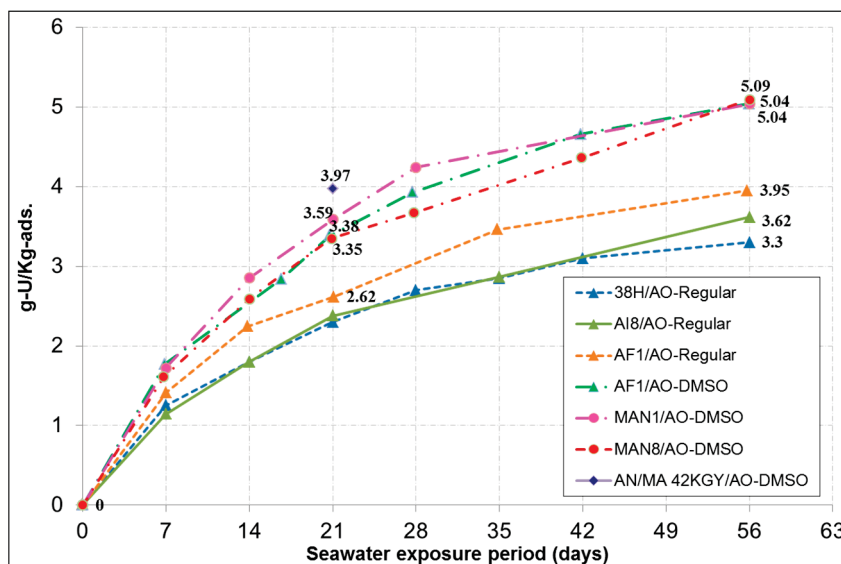


Figure 86. Comparison of uranium adsorption capacities for ORNL's new (2016) and old adsorbents (regular).

These adsorbents achieved relatively low V/U ratios of less than 1.85.

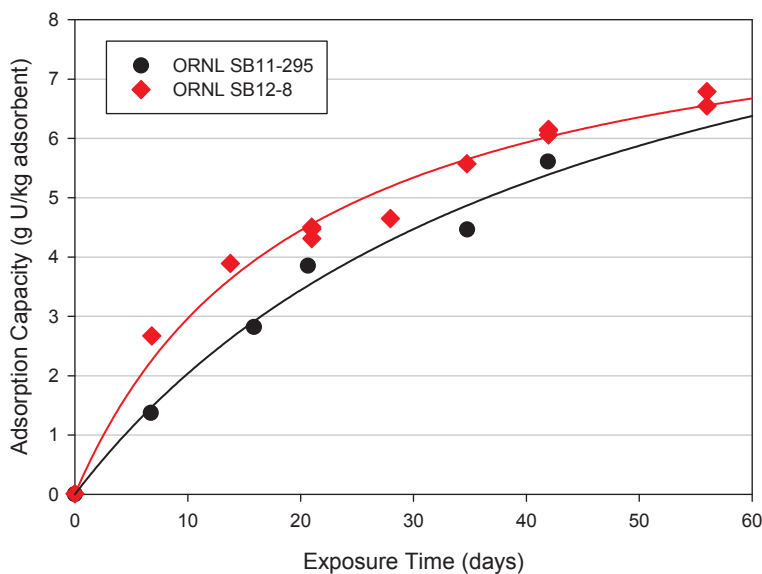


Figure 87. Kinetic data of uranium adsorption by ATRP synthesized adsorbent at ORNL.

## 2016 ACCOMPLISHMENTS

acrylic fibers. An adsorption capacity of  $5.28 \pm 0.16$  g uranium/kg adsorbent (LCW-10 adsorbent, Table 1) was achieved after 56 days of seawater contact. The LCW adsorbent has a half-saturation time ( $11.2 \pm 1.3$  days) that is about half of the AF1 adsorbent ( $22.9 \pm 1.7$  days) and displays greater uranium selectivity; the LCW-10 adsorbent has a V/U mass ratio of nearly 1, compared to ORNL adsorbents which typically have V/U mass ratios between 1.2 and 4. Because of the inexpensive starting material and simple production chemistry (no radiation exposure or surface polymerization is necessary) this adsorbent is predicted to have a production cost around \$330/kg, which would make it competitive with current uranium mining technologies. PNNL and LCW Technologies jointly submitted an invention disclosure to the U.S. Patent and Trademark Office on this new technology entitled: Converting acrylic fibers to amidoxime-carboxylate containing polymer adsorbents for sequestering uranium and other elements from seawater. Application number 15/179,766.



**Figure 88. Example of an LCW adsorbent material prepared using the polyacrylonitrile fiber K1 provided by ORNL. The fiber was shaped into a form factor for exposure in the PNNL flume for time series capacity testing.**

### Summary of Adsorption Capacity Studies Using Flow-Through Columns

Significant advances in uranium adsorption capacity have been achieved in FY 2016 by adsorbents synthesized under the Fuel Resources Program. The new adsorbents are compared in Table 17 to earlier adsorbents developed in this program. The adsorbents tested in prior years include the 38H, AI8 and AF1 adsorbents that were developed at ORNL. All the others listed in Table 17 were developed and tested in FY 2016. There is nearly a doubling in adsorption capacity over the approximately 4 years of testing that this table covers (2012–2016), from the 38H adsorbent with a 56-day capacity of 3.30 g uranium/kg adsorbent to the more recent SB12-8 adsorbent with a capacity of 6.56 g uranium/kg adsorbent.

TABLE 17. SUMMARY OF FLOW-THROUGH COLUMN TESTING OF AMIDOXIME-BASED POLYMERIC ADSORBENTS DEVELOPED BY THE FUEL RESOURCES PROGRAM USING FILTERED SEQUIM BAY SEAWATER AT PNNL.

Adsorbent	N	Saturation Capacity <sup>a,b</sup> (g U/kg adsorbent)	56-day Adsorption Capacity <sup>a,b</sup> (g U/kg adsorbent)	Half-saturation Time <sup>a,b</sup> (days)
38H	4	4.29 ± 0.24	3.30 ± 0.18	16.9 ± 2.8
AI8	1	5.17 ± 0.18	3.54 ± 0.12	25.8 ± 2.1
AF1	5	5.56 ± 0.15	3.91 ± 0.11	24.0 ± 1.5
AF1FR2	1	7.05 ± 0.21	5.00 ± 0.15	22.9 ± 1.7
MAN1-AO/DMSO	1	6.70 ± 0.22	5.04 ± 0.16	18.5 ± 1.6
MAN8-AO/DMSO	1	7.75 ± 0.37	5.09 ± 0.24	29.2 ± 3.0
AN/MA/42kGY-a1	1	8.43 ± 0.72	5.13 ± 0.44	36.0 ± 6.1
LCW-MSL-10	1	6.34 ± 0.19	5.28 ± 0.16	11.2 ± 1.3
SB12-8	1	8.90 ± 0.45	6.56 ± 0.33	20.0 ± 2.6

a. Determined at a temperature of 20°C using one-site ligand saturation modeling.  
 b. Normalized to a salinity of 35.

**Effect of Current Velocity of Adsorption Capacity**

A collaborative study into the effect of current velocity on amidoxime-based polymeric uranium adsorbent performance was conducted by PNNL in collaboration with ORNL and Georgia Tech. Markedly different results were obtained depending on whether the exposure was conducted using a flow-through column or a recirculating flume (Figure 89). There was a minor difference in uranium adsorption capacity as a function of the linear velocity for the seawater exposure using flow-through columns, but a very significant increase in adsorption capacity was observed with increasing linear velocity in the recirculating flume studies. The 56-day uranium adsorption capacity at a linear velocity of 0.48 cm/s was 2.02 ± 1.08 g uranium/kg adsorbent, while the 56-day uranium adsorption capacity at a linear velocity of 8.24 cm/s was 4.71 ± 0.20 cm/s, more than a two-fold difference.

Modeling results showed that the mass-transfer coefficient increased mostly linearly with seawater velocity in the flume studies, while remaining flat for the column studies. The difference in adsorbent performance between the columns and the flume can be attributed to two features: (1) flow resistance provided by the adsorbent braid in the flume, which significantly reduces the seawater velocity through the braid and (2) enhancement in braid movement (i.e., fluttering) as linear velocity increases. Based on the flume studies, we suggest that when ocean currents are greater than approximately 6 cm/s, adsorption capacities will be maximized for a given adsorbent braid of a certain fiber density and form-factor.

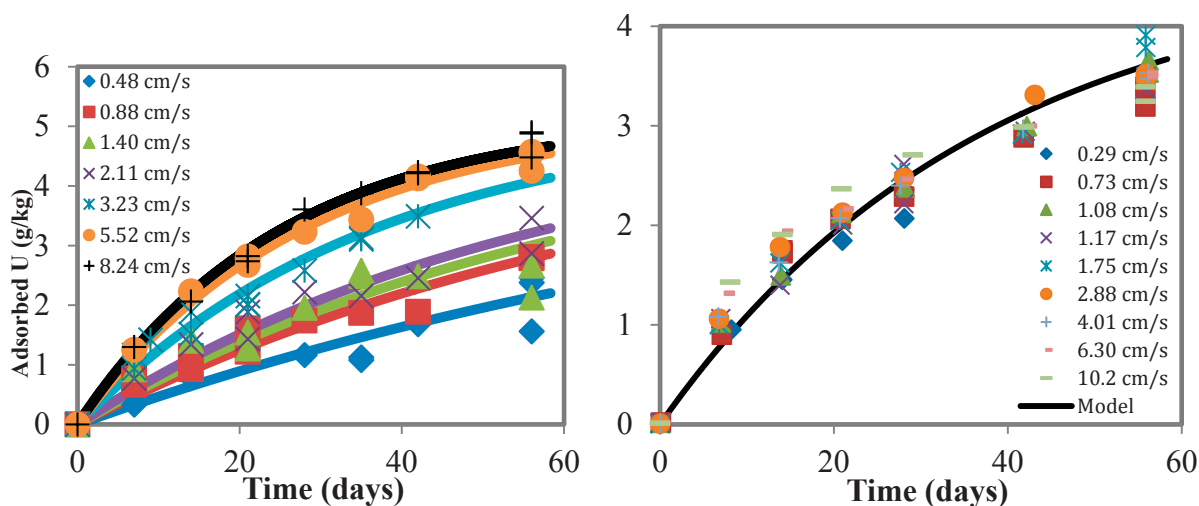


Figure 89. Time series measurements of uranium adsorption capacity as a function of the linear velocity of the ambient seawater exposure. Left panel: Exposure in a recirculating flume. Right panel: exposure in a flow-through column.

#### Marine Testing at the University of Miami's Broad Key Island Research Station

Marine testing at Broad Key Island (BKI), FL, was conducted to validate adsorption capacity and adsorption kinetics results obtained in Sequim Bay, WA, and to assess the effect of different oceanographic and water quality conditions (e.g., temperature, dissolved organic carbon, salinity and trace element content) on uranium uptake. Several formulations of the ORNL amidoxime-based polymeric adsorbents were investigated. Marine testing at BKI offers the opportunity to test adsorbent performance under warmer ambient and more saline conditions than those exist at the marine test site on Sequim Bay off the Washington coast. This is particularly important since the uranium capacity of amidoxime-based adsorbents responds strongly to temperature; the higher the temperature the higher the uranium adsorption capacity.

Flow-through column and recirculating flume experiments were conducted on five different amidoxime-based adsorbent materials, four produced by ORNL (AF1, AI8, AF8, and AF1-DMSO) and one by LCW technologies (LCW-10), using ambient filtered seawater and identical exposure systems. All exposures were conducted at ambient seawater temperatures in order to provide results consistent with a natural seawater deployment in Florida coastal waters. The ORNL adsorbents AF1, AI8, and AF1-AO-DMSO all had fairly similar adsorption capacities (6.0 to 6.6 g uranium/ kg adsorbent) after 56 days of exposure at ambient temperature (26 to 31°C) and salinity (35.7 to 37.4), while the AF8 adsorbent was considerably lower at 4.4 g uranium/kg adsorbent (Table 18). All adsorbents tested at BKI had higher capacities than those observed at PNNL, with the higher temperatures likely a major factor contributing to this difference.

TABLE 18. COMPARISON OF 56-DAY URANIUM ADSORPTION CAPACITIES AND HALF-SATURATION TIMES WITH ORNL ADSORBENTS FOR FLUME EXPERIMENTS CONDUCTED AT BROAD KEY ISLAND AND AT PNNL.

PNNL			Broad Key Island			
Adsorbent	56-day Adsorption Capacity <sup>a</sup> (g U/kg adsorbent)	Half Saturation Time (days)	Average Temperature (°C)	Average Salinity	56-day Adsorption Capacity <sup>b</sup> (g U/kg adsorbent)	Half Saturation Time (days)
ORNL AF1	3.86 ± 0.18	23 ± 1	30.1 ± 0.7	35.7 ± 0.9	6.35 ± 0.10	25 ± 1
ORNL AI8	3.54 ± 0.17	26 ± 2	26.6 ± 1.4	35.9 ± 0.7	5.96 ± 0.24	21 ± 2
ORNL AF8 <sup>c</sup>			26.6 ± 1.4	35.9 ± 0.7	4.43 ± 0.81	51 ± 2
ORNL AF1-AO-DMSO	5.04 ± 0.16	18 ± 2	30.6 ± 1.1	36.4 ± 0.7	6.77 ± 0.56	21 ± 2

a. Determined from one-site ligand saturation modeling of time series data obtained at a temperature of 20°C and normalized to a salinity of 35.  
 b. Determined from one-site ligand saturation modeling of time series data obtained at the ambient temperature and ambient salinity given in the table.  
 c. Characterization of AF8 at PNNL is ongoing.

In general, the elemental distribution (expressed as a relative percentage) on all the adsorbents agreed well, including good agreement with the elemental distribution pattern for AF1 adsorbent exposed at PNNL (Figure 90). The most notable exception to a uniform elemental distributional pattern occurs with vanadium. The relative mass percentage for vanadium retained by the adsorbents ranged from a minimum of 13% for the AF8 formulation to a maximum of 29% for the AI8 formulation; expressed in terms of a V/U mass ratio, it varies from a low of 1.2 to a high of 2.7 for AF8 and AI8 adsorbents, respectively. All V/U mass ratios at BKI are lower than those observed for the AF1 adsorbent at PNNL, with temperature likely playing a significant role. As uranium has a higher adsorption capacity at higher temperatures, one would expect that warmer exposures would favor a lower V/U mass ratio, which could explain why the V/U mass ratio for the PNNL exposures are higher than observed for the BKI exposures.

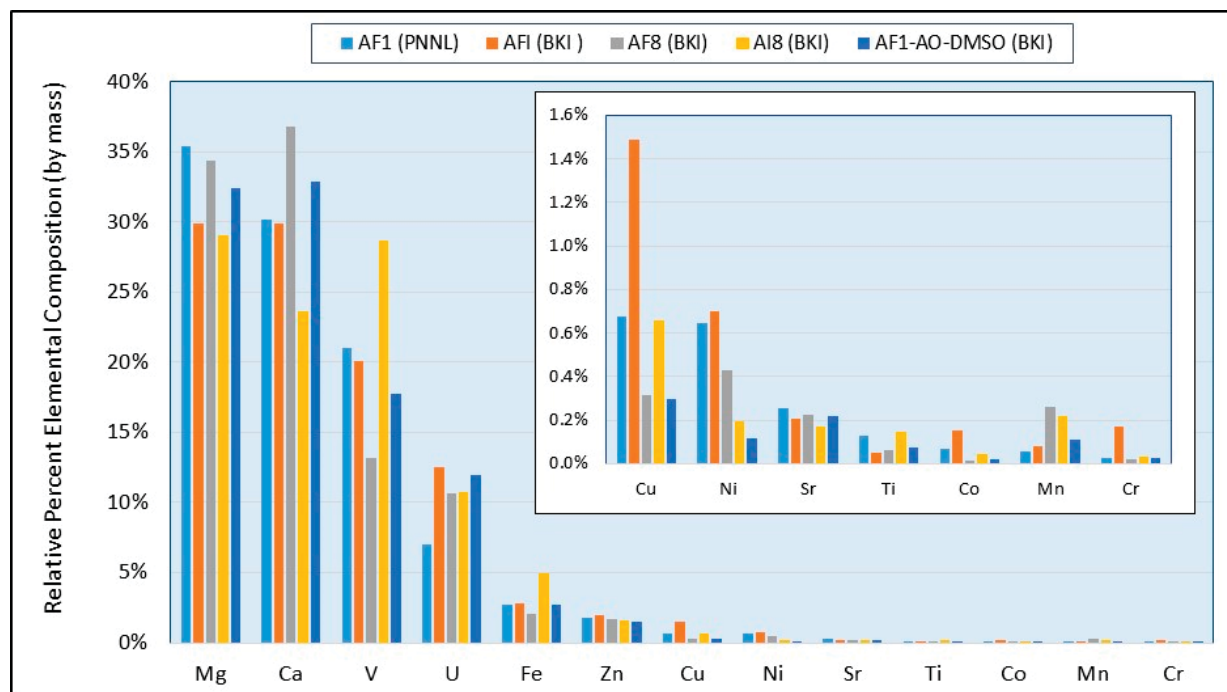


Figure 90. Relative percentage of the major elements adsorbed onto four different ORNL formulations of amidoxime-based adsorbents from 56-day exposures at Broad Key Island, FL. Also included for comparison is the AF1 adsorbent elemental distribution determined at PNNL in Sequim Bay seawater.

## Ligand Design, Characterization, and Thermodynamic Studies

### Ligand Design Modeling

A key step in predicting ligand selectivity and efficiency at sequestering uranium is the ability to accurately predict the stability constants (i.e.,  $K_1$  values, commonly reported in logarithmic form) for the uranyl and major competing  $\text{VO}_2^+$  and  $\text{VO}^{2+}$  ions. A computational protocol has been developed based on density functional theory calculations to accurately predict the  $\log K_1$  for  $\text{UO}_2^{2+}$ ,  $\text{VO}_2^+$  and  $\text{VO}^{2+}$  complexes (Figure 91). This protocol was used to elucidate the main factors influencing the selectivity of the current generation of amidoxime-derived sorbents. As follows from our results, the cyclic imide dioxime ( $\text{H}_2\text{IDO}$ ) affords a more

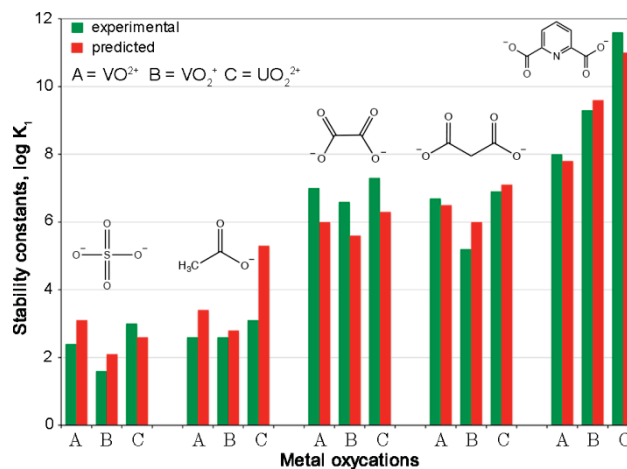


Figure 91. Comparison of experimental (green) and predicted (red)  $\log K_1$  values for A)  $\text{VO}_2^+$ , B)  $\text{VO}^{2+}$ , and C)  $\text{UO}_2^{2+}$  complexes with identical ligands.

preferable configuration for sequestration of uranium from seawater than the acyclic amidoxime (HAO). At the same time, however, IDO<sup>2-</sup> shows stronger binding affinity and higher selectivity for VO<sub>2</sub><sup>+</sup> over UO<sub>2</sub><sup>2+</sup> and is likely responsible for the higher sorption of vanadium ions in marine tests, while AO<sup>-</sup> does not appear to bind the VO<sub>2</sub><sup>+</sup> ions at all under seawater conditions. Thus, selectivity of poly(acrylamidoxime) adsorbents toward UO<sub>2</sub><sup>2+</sup> versus VO<sub>2</sub><sup>+</sup> could be improved by minimizing the formation of the cyclic imide dioxime. It was also found that simple dicarboxylic functional groups possess low binding affinity and selectivity for uranyl because they are poorly organized for the UO<sub>2</sub><sup>2+</sup> complexation, which is consistent with experiments. Moreover, the obtained data enabled us to propose the utilization of the ligand design principles based on structural preorganization to achieve a dramatic enhancement of carboxylates in UO<sub>2</sub><sup>2+</sup> ion binding affinity and selectivity. This concept was exemplified through the investigation of the complexes of the UO<sub>2</sub><sup>2+</sup>, VO<sub>2</sub><sup>+</sup>, and VO<sup>2+</sup> ions with the highly preorganized ligand PDA (1,10-phenanthroline-2,9-dicarboxylic acid), which was found to be very selective for uranyl.

### **Characterization**

Efforts in the characterization activity involved the continued application of X-ray Absorption Fine Structure (XAFS) spectroscopy to determine how the adsorbent polymers actually bind uranium. Due to possessing high sensitivity and atomic specificity, XAFS is the only technique capable of directly investigating the coordination environment of metals extracted from environmental seawater by amidoxime-functionalized polymers. Work completed during the previous year revealed small molecule surrogates do not adequately represent how the more structurally and chemically complex adsorbents bind uranium, which was published in the journal *Energy and Environmental Science* (Impact Factor 25.4). This article was also highlighted on the rear cover of the journal, as well as in *DOE Pulse*, the webpage of the Advanced Photon Source, and [energy.doe.gov](http://energy.doe.gov). XAFS investigation of an adsorbent copolymer composed of amidoxime and phosphonic acid groups revealed similar behavior. This constitutes an instance of emergent phenomena, macroscopic behavior arising from the interaction of molecules that individually do not display such properties, and is expected to be critical for rational development of adsorbents possessing the desired uranium uptake and selectivity. XAFS data regarding the vanadium binding environment have also been collected, but in contrast to the aforementioned uranium binding mode, preliminary analysis indicates vanadium is bound in a consistent fashion between the adsorbent polymer, the small molecule standards, and the computationally-predicted binding model. These results are in the process of being published. Ongoing efforts involve more detailed interrogation of emergent phenomena through investigation of uranium binding as a function of polymer chain length and morphology by application of XAFS and small angle neutron scattering.

### **Thermodynamic and Structural Studies**

A rare, non-oxido V(V) complex with glutaroimide-dioxime (H<sub>3</sub>L), Na[V(L)<sub>2</sub>] · 2H<sub>2</sub>O(cr), was crystallized from aqueous solution and characterized via x-ray diffraction. The complex was found to contain two fully deprotonated L<sup>3-</sup> ligands bound to the bare V<sup>5+</sup> cation via two oxime oxygens and the imide nitrogen. An intermediate complex, Na[VO<sub>2</sub>(HL)](cr), was also isolated and found to contain the typical VO<sub>2</sub><sup>+</sup> moiety present in many V(V) complexes. Further characterizations using <sup>51</sup>V, <sup>17</sup>O, <sup>1</sup>H, and <sup>13</sup>C NMR spectroscopy demonstrated the unprecedented stepwise displacement of the oxido oxygens to form the bare V(V)-glutaroimide-dioxime complex. ESI-MS studies of V(V)-glutaroimide-dioxime solutions allowed the identification the intermediate 1:1 M:L complex as well as the bare V(L)<sub>2</sub> complex at m/z = 330.8.

## 2016 ACCOMPLISHMENTS

Structural insights into the much higher sorption of V(V) to amidoxime-based sorbents relative to U(VI) and Fe(III) were gained by comparing the structural parameters of the V(V)-glutaroimide-dioxime complex with the analogous U(VI)- and Fe(III)-glutaroimide-dioxime complexes. For these complexes, the degree of protonation of the ligand was found to decrease from U(VI) to V(V). In conjunction with the substantially shorter bond lengths observed for the V(V) complex relative to the other complexes, this implies stronger bonding in the V(V) complex and higher thermodynamic stability. In fact, the trend in binding strengths parallels the observed trend in sorption of these cations to poly(amidoxime) sorbents in marine tests.

### PUBLICATIONS FOR FUEL RESOURCES

Abney, C. W., Das, S., Mayes, R. T., Kuo, L.-J., Wood, J., Gill, G., Piechowicz, M., Lin, Z., Lin, W., and Dai, S., 2016, "A Report of Emergent Uranyl Binding Phenomena by an Amidoxime Phosphonic Acid Co-Polymer," *Physical Chemistry Chemical Physics*, Vol. 18, pp. 23462–23468.

Abney, C. W., Mayes, R. T., Piechowicz, M., Lin, Z., Bryantsev, V. S., Veith, G. M., Dai, S., and Lin, W., 2016, "XAFS Determination of the Uranyl Coordination Environment as Bound by an Amidoxime-Functionalized Polymer," *Energy and Environmental Science*, Vol. 9, pp. 448–453. (Highlighted on journal cover).

Alexandratos, S. D., Kung, S., 2016, "Preface to the Special Issue: Uranium in Seawater," *Industrial and Engineering Chemistry Research*, Vol. 55, pp. 4101–4102.

Alexandratos, S. D., and Zhu, X. P., 2016, "Polymer-Supported Aminomethylphosphinate as a Ligand with a High Affinity for U(VI) from Phosphoric Acid Solutions: Combining Variables to Optimize Ligand-Ion Communication," *Solvent Extraction and Ion Exchange*, Vol. 34, 290–295.

Alexandratos, S. D., Zhu, X. P., Florent, M., and Sellin, R., 2016, "Polymer-Supported Bifunctional Amidoximes for the Sorption of Uranium from Seawater," *Industrial and Engineering Chemistry Research*, Vol. 55, pp. 4208–4216.

Ansari, S., Yang, Y., Zhang, Z., Gagnon, K., Teat, S. J., Luo, S., and Rao, L., 2016, "Complexation of Lanthanides with Glutaroimide-dioxime: Binding Strength and Coordination Modes," *Inorganic Chemistry*, Vol. 55, pp. 1315–1323.

Berton, P., Kelley, S. P., and Rogers, R. D., 2015, "Stripping uranium from seawater-loaded sorbents with the ionic liquid hydroxylammonium acetate in acetic acid for efficient reuse," *Industrial and Engineering Chemistry Research*, Vol. 55, pp. 4321–4327.

Brown, S., Chatterjee, S., Li, M., Yue, Y., Tsouris, C., Janke, C.J., Saito, T., and Dai, S., 2016, "Uranium Adsorbent Fibers Prepared by Atom-Transfer Radical Polymerization from Chlorinated Polypropylene and Polyethylene Trunk Fibers," *Industrial and Engineering Chemistry Research*, Vol. 55, pp. 4130–4138.

Chatterjee, S., Bryantsev, V. S., Brown, S., Johnson, J. C., Grant, C. D., Mayes, R. T., Hay, B. P., Dai, S., and Saito, T., 2016, "Naphthalimidedioxime Ligand-Containing Fiber Adsorbent for Uranium Recovery from Seawater," *Industrial and Engineering Chemistry Research*, Vol. 55, pp. 4161–4169.

Chouyyok, W., Pittman, J. W., Warner, M. G., Nell, K. M., Clubb, D. C., Gill, G. A., and Addleman, R. S., 2016, "Surface Functionalized Nanostructured Ceramic Sorbents for the Effective Collection and Recovery of Uranium from Seawater," *Dalton Transactions*, Vol. 45, pp. 11312–11325.

Chouyyok, W., Warner, C. L., Mackie, K. E., Warner, M. G., Gill G., and Addleman, R. S., 2016, "Evaluation of Nanostructured Metal Oxide Sorbents for the Collection and Recovery of Uranium from Seawater," *Industrial and Engineering Chemistry Research*, Vol. 55, No. 15, pp. 4195–4207.

Das, S., Brown, S., Mayes, R.T., Janke, C.J., Tsouris, C., Kuo, L.-J., Gill, G. A., and Dai, S., 2016, "Novel Poly(imidedioxime) Sorbent: Development and Testing for Enhanced Extraction of Uranium from Natural Seawater," *Chemistry: A European Journal*, Vol. 298, pp. 125–135.

Das, S., Liao, W.-P., Byers, M. F., Tsouris, C., Janke, C.J., Mayes, R.T., Schneider E., Kuo, L.-J., Wood, J.R., Gill, G.A., and Dai, S., 2016, "Alternative Alkaline Conditioning of Amidoxime based Adsorbent for Uranium Extraction from Seawater," *Industrial and Engineering Chemistry Research*, Vol. 55, pp. 4303–4312.

Das, S., Oyola, Y., Mayes, R.T., Janke, C.J., Kuo, L.-J., Wood, J.R., Gill, G.A., and Dai, S., 2016, "Extraction of Uranium from Seawater: Promising AF Series Adsorbent," *Industrial and Engineering Chemistry Research*, Vol. 55, pp. 4110–4117.

Das, S., Oyola, Y., Mayes, R.T., Janke, C.J., Kuo, L.-J., Wood, J.R., Gill, G.A., and Dai, S., 2016, "Extraction of Uranium from Seawater: Promising AI Series Adsorbent," *Industrial and Engineering Chemistry Research*, Vol. 55, pp. 4103–4109.

Das, S., Tsouris, C., Zhang, C., Kim, J., Brown, S., Oyola, Y., Janke, C.J., Mayes, R.T., Kuo, L.-J., Wood, J.R., Gill, G.A., and Dai, S., 2016, "Enhancing Uranium Uptake by Amidoxime Adsorbent in Seawater: An Investigation for Optimum Alkaline Conditioning Parameter," *Industrial and Engineering Chemistry Research*, Vol. 55, pp. 4294–4302.

Dietz, T. C., Tomaszewski, C. E., Tsinas, Z., Poster, D., Barkatt, A., Adel-Hadadi, M., Bateman, F., Cumberland, L.T., Schneider, E., Gaskel, K., LeVerne, J., Al-Sheikhly, M., 2016, "Uranium Removal from Seawater by Means of Polyamide Fibers Directly Grafted with Diallyl Oxalate through a Single-Step Solvent-Free Irradiation Process," *Industrial and Engineering Chemistry Research*, Vol. 55, pp. 4179–4186.

Endrizzi, F., Leggett, C. J., and Rao, L., 2016, "Scientific Basis for Efficient Extraction of Uranium from Seawater. I: Understanding the Chemical Speciation of Uranium under Seawater Conditions," *Industrial and Engineering Chemistry Research*, Vol. 55, pp. 4249–4256.

Endrizzi, F., Melchior, A., Tolazzi, M., and Rao, L. 2015, "Complexation of Uranium(VI) with Glutarimidoxime: Thermodynamic and Computational Studies," *Dalton Transactions*, Vol. 44, pp. 13763–14180.

Gill, G. A., Kuo, L.-J., Janke, C. J., Wood, J. R., Mayes, R. T., Tsouris, C., Oyola, Y., Strivens, J. E., Cobb, M., Bonheyo, G., Jeters, R., Park, J., Khangaonkar, T., Addleman, R. S., Chouyyok, W., Warner, M., Peterson, Sonja, Abrecht, D. G., Das, S., Buesseler, K., Breier, C., D'Alessandro, E., Pan, H.-B., and Wai, C., 2016, "The Uranium from Seawater Program at PNNL: Overview of Marine Testing, Adsorbent Characterization, Adsorbent Durability,

## 2016 ACCOMPLISHMENTS

Adsorbent Toxicity, and Deployment Studies," *Industrial and Engineering Chemistry Research*, Vol. 55, pp. 4264–4277.

Ivanov, A.S., and Bryantsev, V. S., 2016, "Assessing Ligand Selectivity for Uranium over Vanadium Ions to Aid in the Discovery of Superior Adsorbents for Extraction of UO<sub>2</sub><sup>2+</sup> from Seawater," *Dalton Transactions*, Vol. 45, No. 26, pp. 10744–10751.

Kelley, S. P., Nuss, J. S., and Rogers, R. D., 2015, "Nonstoichiometric, Protic Azolium Azolate Ionic Liquids Provide Unique Environments for N-Donor Coordination Chemistry," *Chemistry: A European Journal*, Vol. 21, pp. 17196–17199.

Kelley, S. P., and Rogers, R. D., 2015, "Isolation of Uranyl Dicyanamide Complexes from N-Donor Ionic Liquids," *Inorganic Chemistry*, Vol. 54, pp. 10323–10334.

Kennedy, Z. C., Cardenas, A. J. P., Corbey J. F., and Warner, M. G., 2016, "2,6-diiminopiperidin-1-ol: an overlooked motif relevant to uranyl and transition metal binding on poly(amidoxime) adsorbents," *Chemical Communications*, Vol. 52, pp. 8802–8805.

Kuo, L.-J., Janke, C., Wood, J. R., Strivens, J. E., and Gill, G. A., 2016, "Characterization and Testing of Amidoxime-Based Adsorbent Materials to Extract Uranium from Natural Seawater," *Industrial and Engineering Chemistry Research*, Vol. 55, pp. 4285–4293.

Ladshaw, A.P., Das, S., Liao, W.-P., Yiaccoumi, S., Janke, C.J., Mayes, R.T., Dai, S., and Tsouris, C., 2016, "Experiments and Modeling of Uranium Adsorption in the Presence of Other Ions in Simulated Seawater," *Industrial and Engineering Chemistry Research*, Vol. 55, pp. 4241–4248.

Lashley, M. A., Mehio, N., Nugent, J. W., Holguin, E., Do-Thanh, C.-L., Bryantsev, V. S., Dai, S., and Hancock, R. D., 2016, "Amidoximes as Ligand Functionalities for Braided Polymeric Materials for the Recovery of Uranium from Seawater," *Polyhedron*, Vol. 109, pp. 81–91.

Leggett, C. J., Endrizzi, F., and Rao, L., 2016, "Scientific Basis for Efficient Extraction of Uranium from Seawater. II, Fundamental Thermodynamic and Structural Studies," *Industrial and Engineering Chemistry Research*, Vol. 55, pp. 4257–4263.

Leggett, C. J., Parker, B. F., Teat, S. J., Zhang, Z., Dau, P. D., Lukens, W., Peterson, S. M., Cardenas, A. J. P., Warner, M. G., Gibson, J. K., Arnold, J., and Rao, L., 2016, "Structural and spectroscopic studies of a rare non-oxido V(V) complex crystallized from aqueous solution," *Chemical Science*, 2016, Vol. 7, pp. 2775–2786.

Leggett, C. J., and Rao, L., 2015, "Complexation of Calcium and Magnesium with Glutarimidedioxime: Implications for the Extraction of Uranium from Seawater," *Polyhedron*, Vol. 95, pp. 54–59.

Mayes, R. T., Gorka, J., Dai, S., 2016, "Impact of Pore Size on the Sorption of Uranyl under Seawater Conditions," *Industrial and Engineering Chemistry Research*, Vol. 55, pp. 4339–4343.

Mehio, N. Johnson, J. C., Dai, S., and Bryantsev, V. S., 2015, "Theoretical Study of the Coordination Behavior of Formate and Formamidoximate with Dioxovanadium(V) Cation: Implications for Selectivity towards Uranyl," *Physical Chemistry Chemical Physics*, Vol. 17, pp. 31715–31726.

- Mehio, N., Ivanov, A. S., Ladshaw, A. P., Dai, S., Bryantsev, V. S., 2016, Theoretical Study of Oxovanadium(IV) Complexation with Formamidoxime: Implications for the Design of Uranyl-Selective Adsorbents *Industrial and Engineering Chemistry Research*, Vol. 55, pp. 4231–4240.
- Mehio, N., Ivanov, S. A., Williams, N. J., Mayes, R. T., Bryantsev, V. S., Hancock, R. D., and Dai, S., 2016, “Quantifying the Binding Strength of Salicylaldoxime-Uranyl Complexes Relative to Competing Salicylaldoxime-Transition Metal Ion Complexes in Aqueous Solution: A Combined Experimental and Computational Study,” *Dalton Transactions*, Vol. 45, pp. 9051–9064. (Showcasing research on the cover, Issue 22)
- Mehio, N., Lashely, M. A., Nugent, J. W., Tucker, L., Correia, B., Do-Thanh, C.-L., Dai, S., Hancock, R.D., and Bryantsev, V. S., 2015, “Acidity of the Amidoxime Functional Group in Aqueous Solution: A Combined Experimental and Computational Study,” *Journal of Physical Chemistry B*, Vol. 119, pp. 3567–3576.
- Oyola, Y., and Dai, S., 2016, “High Surface-Area Amidoxime-based Polymer Fibers co-Grafted with Various Acid Monomers Yielding Increased Adsorption Capacity for the Extraction of Uranium from Seawater,” *Dalton Transactions*, Vol. 45, pp. 8824–8834.
- Oyola, Y., Janke, C.J., and Dai, S., 2016, “Synthesis Development and Testing of High Surface Area Polymer-based Adsorbents for the Selective Recovery of Uranium from Seawater,” *Industrial and Engineering Chemistry Research*, Vol. 55, pp. 4149–4160.
- Pan, H.-B., Kuo, L.-J., Miyamoto, N., Wood, J. R., Strivens, J. E., Gill, G. A., Janke, C. J., and Wai, C. M., 2016, “Elution of Uranium and Transition Metals from Amidoxime-Based Polymer Adsorbents for Sequestering Uranium from Seawater,” *Industrial and Engineering Chemistry Research*, Vol. 55, pp. 4313–4320.
- Pan, H.-B., Kuo, L.-J., Wai, C. M., Miyamoto, N., Joshi, R., Wood, J. R., Strivens, J. E., Janke, C. J., Oyola, Y., Das, S., Mayes, R. T., and Gill, G. A., 2016, “Elution of Uranium and Transition Metals from Amidoxime-Based Polymer Adsorbents for Sequestering Uranium from Seawater,” *Industrial and Engineering Chemistry Research*, Vol. 55, pp. 4313–4320.
- Pan, H.-B., Kuo, L.-J., Wood, J. R., Strivens, J. E., Gill, G. A., Janke, C. J., and Wai, C. M., 2015, “Towards Understanding KOH Conditioning of Amidoxime-based Polymer Adsorbents for Sequestering Uranium from Seawater,” *RSC Advances*, Vol. 5, pp. 100715–100721.
- Park, J., Gill, G. A., Strivens, J. E., Kuo, L.-J., Jeters, R. T., Avila, A., Wood, J. R., Schlafer, N. J., Janke, C. J., Miller, E. A., Thomas, M., Addleman R. S., and Bonheyo, G. T., 2016, “Effect of Biofouling on the Performance of Amidoxime-based Polymeric Uranium Adsorbents,” *Industrial and Engineering Chemistry Research*, Vol. 55, pp. 4328–4338.
- Park, J., Jeters, R. T., Kuo, L.-J., Strivens, J. E., Gill, G. A., Schlafer, N. J., and Bonheyo G. T., 2016, “Potential Impact of Seawater Uranium Extraction on Marine Life,” *Industrial and Engineering Chemistry Research*, Vol. 55, pp. 4278–4284.
- Parker, B. F., Knight, A. S., Vukovic, S., Arnold, J., Francis, M. B., 2016, “A Peptoid-Based Combinatorial and Computational Approach to Developing Ligands for Uranyl Sequestration from Seawater,” *Industrial and Engineering Chemistry Research*, Vol. 55, pp. 4187–4194.

## 2016 ACCOMPLISHMENTS

Piechowicz, M., Abney, C. W., Zhou, X., Thacker, N. C., Li, Z., Lin, W., 2016, "Design, Synthesis, and Characterization of a Bifunctional Chelator with Ultrahigh Capacity for Uranium Uptake from Seawater Simulant," *Industrial and Engineering Chemistry Research*, Vol. 55, pp. 4170–4178.

Priest, C., Tian, Z. Q., Jiang, D. E., 2016, "First-principles Molecular Dynamics Simulation of the  $\text{Ca}_2\text{UO}_2(\text{CO}_3)_3$  Complex in Water," *Dalton Transactions*, Vol. 45, pp. 9812–9819.

Sun, X., Zanonato, P., Di Bernardo, P., Zhang, Z., Rao, L., 2015, "Sorption of Uranium and Other Metal Ions on Amine-Functionalized Silica Materials," *Separation Science Technology*, Vol. 50, pp. 2769–2775.

Vukovic, S., Hay, B. P., and Bryantsev, V. S., 2015, "Predicting Stability Constants for Uranyl Complexes Using Density Functional Theory," *Inorganic Chemistry*, Vol. 54, pp. 3995–4001.

Wood, J. R., Gill, G. A., Kuo, L.-J., Strivens, J. E., and Choe K.-Y., 2016, "Comparison of Analytical Methods for the Determination of Uranium in Seawater using Inductively Coupled Plasma Mass Spectrometry," *Industrial and Engineering Chemistry Research*, Vol. 55, pp. 4344–4350.

Yue, Y., Mayes, R. T., Gill, G., Kuo, L.-J., Wood, J., Binder, A., Brown, S., and Dai, S., 2015, "Macroporous Monoliths for Trace Metal Extraction from Seawater," *RSC Advances*, Vol. 5, pp. 50005–50010.

Yue, Y., Zhang, C., Tang, Q., Mayes, R. T., Liao, W.-P., Liao, C., Tsouris, C., Stankovich, J., Chen, J., Hensley, D., Abney, C., Jiang, D. E., Brown, S., and Dai, S. A., 2016, "Poly(acrylonitrile)-Functionalized Porous Aromatic Framework Synthesized by Atom-Transfer Radical Polymerization for Extraction of Uranium from Seawater," *Industrial and Engineering Chemistry Research*, Vol. 55, pp. 4125–4129.

### **Patents Granted and Pending**

Janke, C. J., S. Dai, and Y. Oyola, 2016, "Fiber-Based Adsorbents Having High Adsorption Capacities for Recovering Dissolved Metals and Methods Thereof," U.S. Patent No. 9,433,920 B2, September 6, 2016.

Janke, C. J., S. Dai, and Y. Oyola, 2016, "Powder-Based Adsorbents Having High Adsorption Capacities for Recovering Dissolved Metals and Methods Thereof," U.S. Patent No. 9,327,267 B2, May 3, 2016.

Janke, C. J., R. T. Mayes, and S. Dai, 2016, "Advanced Adsorbents and Methods for Extraction of Metals from Aqueous Sources," U.S. Patent Application No. 62350778, June 16, 2016.

Dai, S., S. Brown, and T. Saito, "Surface-Functionalized Polyolefin Fibers and their Use in Methods for Extracting Metal Ions from Liquid Solutions," U.S. Patent Application No.: 15/154,437.

Gill, G. A., L.-J., Kuo, H.-B. Pan, and C. Wai, 2016, "Converting acrylic fibers to amidoxime-carboxylate containing polymer adsorbents for sequestering uranium and other elements from water," U.S. Patent Application No. 15/179,766, June 10, 2016.

## Acronyms and Abbreviations

3-D	three-dimensional
ACSEPT	Actinide Recycling by Separation
ACWF	advanced ceramic waste form
AgZ	silver-exchanged mordenite
AHA	acetohydroxamic acid
ALSEP	actinide lanthanide separation
AMUSE	Argonne Model for Universal Solvent Extraction
ANL	Argonne National Laboratory
ANSTO	Australian Nuclear Science and Technology Organization
APC	aminopolycarboxylate
ATALANTE	ATelier Alpha et Laboratoires pour ANalyses, Transuraniens et Etudes de retraitement
BTP	bis(triazinyl)pyridine
CEA	Commissariat à l'Énergie Atomique
CECE	combined electrolysis and catalyst exchange
CNWG	Civil Nuclear Working Group
CodCon	Co-decontamination Process
COG	cell off-gas
CRADA	cooperative research and development agreement
CRIEPI	Central Research Institute of the Electric Power Industry
CWF	ceramic waste form
DAAP	diamylamyl phosphonate
DEHBA	<i>N,N</i> -di-2-ethylhexylbutyramide
DEHiBA	diethylhexylisobutyramide
DF	decontamination factor
DFT	density functional theory
DOE	U.S. Department of Energy
DOE-NE	Department of Energy Office of Nuclear Energy

## 2016 ACCOMPLISHMENTS

DOG	dissolver off-gas
dpa	displacements per hour
DTPA	diethylenetriaminepentaacetic acid
EDS	energy dispersive spectroscopy
EDX	energy-dispersive x-ray spectroscopy
EIS	electrochemical impedance spectroscopy
EM	DOE Office of Environmental Management
EU	European Union
FCR&D	Fuel Cycle Research and Development
FCT	Fuel Cycle Technologies
FY	fiscal year
FZ-J	Forschungszentrum Jülich
GCMT	Glass Corrosion Modeling Tool
GEM	Gel End Member
GPU	gas permeation unit
GWF	glass waste form
HDO	deuterated water
HEDTA	N-(2-hydroxyethyl)ethylenediamine-N,N',N'-triacetic acid
HEDTTA	N-hydroxyethyl-diethylenetriaminetetraacetic acid
HEH[EHP]	2-ethylhexylphosphonic acid mono-2-ethylhexyl ester
HIP	hot isostatic pressing
HLW	high-level waste
HTO	tritiated water
IAEA	International Atomic Energy Agency
ICP-MS	inductively coupled plasma mass spectrometry
INL	Idaho National Laboratory
JAEA	Japan Atomic Energy Agency
LANL	Los Alamos National Laboratory
LAMM	Laboratory of Analysis and Material Metrology

Ln	Lanthanide
LSA	Liquid Scintillation Analyzer
MA	minor actinide
MC	Monte Carlo
MCFT	Micro-channel flow-through
MOF	metal organic framework
MOG	melter off-gas
MOU	Memorandum of Understanding
MPACT	Material Protection, Accounting, and Control Technologies
MRWFD	Material Recovery and Waste Form Development
NE	Nuclear Energy
NEUP	Nuclear Energy University Program
NNL	National Nuclear Laboratory
NORM'16	Northwest Regional Meeting of the American Chemical Society
NTD	national technical director
ORNL	Oak Ridge National Laboratory
PA	performance assessment
PAN	polyacrylonitrile
PD	potentiodynamic
PNNL	Pacific Northwest National Laboratory
PRC	People's Republic of China
PS	potentiostatic
q/S	solution-flow-rate-to-glass-surface-area ratio
R&D	research and development
RAW	representative alloy waste form
RPL	Radiochemical Processing Laboratory
RT	room temperature
SAC	steam-assisted conversion
SACSESS	Safety of Actinide Separation Processes

## 2016 ACCOMPLISHMENTS

SAED	selected-area electron diffraction
SANEX	selective actinide extraction
SEM	scanning electron microscopy
SIMS	secondary ion mass spectrometry
SPS	spark plasma sintering
SRNL	Savannah River National Laboratory
STAAR	Sigma Team for Advanced Actinide Recycle
SYNROC	synthetic rock
TALSPEAK	Trivalent Actinide-Lanthanide Separations by Phosphorus-reagent Extraction from Aqueous Komplexes
TBP	tributyl phosphate
TEM	transmission electron microscopy
TRU	transuranic
UK	United Kingdom
UNC-CH	University of North Carolina at Chapel Hill
UNF	used nuclear fuel
VOG	vessel off-gas
XRD	x-ray diffraction

## Publications (5-year cumulative)

### ADVANCED WASTE FORMS AND PROCESSES

1. Alaniz, A. J., L. Delgado, B. Werbick, and T. Hartmann, 2012, "Remote operated hot uniaxial press to fabricate Tc-99 bearing waste forms," *Procedia Chemistry*, Vol. 7, pp. 534–539.
2. Amoroso, J., J. C. Marra, M. Tang, Y. Lin, F. Chen, D. Su, and K. S. Brinkman, 2014, "Melt Processed Multiphase Ceramic Waste Forms for Nuclear Waste Immobilization," *Journal of Nuclear Material*, Vol. 454, No. 1–3, pp. 12–21.
3. Amoroso, J., J. Marra, S. Conradson, M. Tang, and K. Brinkman, 2013, "Melt Processed Single Phase Hollandite Waste Forms for Nuclear Waste Immobilization: Ba<sub>1.0</sub>Cs<sub>0.3</sub>A<sub>2.3</sub>Ti<sub>5.7</sub>O<sub>16</sub>, A = Cr, Fe, Al," *Journal of Alloys and Compounds*, Vol. 584, pp. 590–599.
4. Amoroso, J., J. Marra, S. D. Conradson, M. Tang, and K. Brinkman, 2014, "Melt Processed Single Phase Hollandite Waste Forms for Nuclear Waste Immobilization: Ba<sub>1.0</sub>Cs<sub>0.3</sub>A<sub>2.3</sub>Ti<sub>5.7</sub>O<sub>16</sub>, A = Cr, Fe, Al," *Journal of Alloys and Compounds*, Vol. 584, pp. 590–599.
5. Asmussen, R. M., J. J. Neeway, T. Kaspar, J. V. Crum, 2016, "Corrosion Behavior and Impact of Microstructure of Glass-Ceramic Waste Forms," submitted to *Journal of the American Chemical Society*.
6. Bourg, I. C. and C. I. Steefel, 2012, "Molecular Dynamics Simulations of Water Structure and Diffusion in Silica Nanopores," *Journal of Physical Chemistry C*, Vol. 116: pp. 11556–11564.
7. Brinkman, K. S., K. M. Fox, J. C. Marra, J. Reppert, J. Crum, and M. Tang, 2012, "Single Phase Melt Processed Powellite (Ba,Ca)MoO<sub>4</sub> for the Immobilization of Mo-Rich Nuclear Waste," *Journal of Alloys and Compounds*, Vol. 551, pp. 136–142.
8. Collins, E. D., G. D. DelCul, B. B. Spencer, R. R. Brunson, and J. A. Johnson, 2013, "Establishment of the Roadmap for Chlorination Process Development for Zirconium Recovery and Recycle," *Proceedings from GLOBAL 2013*, Salt Lake City, Utah, September 29–October 4, 2013.
9. Collins, E. D., G. D. Delcul, B. B. Spencer, R. R. Brunson, J. A. Johnson, D. S. Terekhov, and N. V. Emmanuel, 2012, "Process Development Studies for Zirconium Recovery/Recycle from Used Nuclear Fuel Cladding," *Procedia Chemistry*, Vol. 7, pp. 72–76.
10. Collins, E. D., G. D. Delcul, K. A. Williams, and J. E. Rushton, 2012, "A Practical Approach to a Closed Nuclear Fuel Cycle and Sustained Nuclear Energy," *Waste Management 2012 Conference*, February 26–March 1, 2012, Phoenix, Arizona.
11. Crawford, C. L., and J. C. Marra, 2012, *Characterization of Glass Solids from Long-Term Corrosion Testing*, FCRD-SWF-2012-000250, Savannah River National Laboratory, Aiken, SC.
12. Crum, J. V., D. Strachan, A. Rohatgi, and M. Zumhoff, 2013, "Epsilon Metal Waste Form for Immobilization of Noble Metals from Used Nuclear Fuel," *Journal of Nuclear Materials*, Vol. 441, No. 1–3, pp. 103–12.

## 2016 ACCOMPLISHMENTS

13. Crum, J. V., L. A. Turo, B. J. Riley, M. Tang, and A. Kossoy, 2012, "Multi-Phase Glass-Ceramics as a Waste Form for Comined Fission Products: Alkalis, Alkaline Earths, Lanthanides, and Transisition Metals," *Journal of the American Ceramics Society*, Vol. 95, No. 4, pp. 1297–1303.
14. Crum, J., V. Maio, J. McCloy, C. Scott, B. Riley, B. Benefiel, J. Vienna, K. Archibald, C. Rodriguez, V. Rutledge, Z. Zhu, J. Ryan, and M. Olszta, 2014, "Cold Crucible Induction Melter Studies for Making Glass Ceramic Waste Forms: A Feasibility Assessment," *Journal of Nuclear Materials*, Vol. 444, No. 1–3, pp. 481–492.
15. Crum, J.V., J.J. Neeway, B.J. Riley, Z. Zhu, M.J. Olszta, and M. Tang, 2016, "Dilute condition corrosion behavior of glass-ceramic waste form," *Journal of Nuclear Materials*, Vol. 482, pp. 1–11.
16. Fernandez, C. A., J. Liu, P. K. Thallapally, and D. M. Strachan, 2012, "Switching Kr/Xe Selectivity with Temperature in a Metal–Organic Framework," *Journal of the American Chemical Society*, Vol. 134, No. 22, pp. 9046–9049.
17. Fortner, J. A., A. J. Kropf, and W. L. Ebert, 2013, "Characteristics of Metal Waste Forms Containing Technetium and Uranium," *Proceedings from GLOBAL 2013*, Salt Lake City, Utah, September 29–October 4, 2013.
18. Gin, S., A. Abdelouas, L. J. Criscenti, W. L. Ebert, K. Ferrand, T. Geisler, M. T. Harrison, Y. Inagaki, S. Mitsui, K. T. Mueller, J. C. Marra, C. G. Pantano, E. M. Pierce, J. V. Ryan, J. M. Schofield, C. I. Steefel, and J. D. Vienna, 2013, "An International Initiative on Long-Term Behavior of High-Level Nuclear Waste Glass," *Materials Today*, Vol. 16, pp. 243–248.
19. Gin, S., J. V. Ryan, D. K. Schreiber, J. Neeway, and M. Cabié, 2013, "Contribution of Atom-Probe Tomography to a Better Understanding of Glass Alteration Mechanisms: Application to a Nuclear Glass Specimen Altered 25 Years in a Granitic Environment," *Chemical Geology*, Vol. 349–350, pp. 99–109.
20. Gin, S., P. Jollivet, M. Fournie, Z. Wang, Z. Zhu, A. V. Mitroshkov, and J. V. Ryan, 2015, "The Fate Of Silicon During Glass Corrosion Under Alkaline Conditions: A Mechanistic And Kinetic Study With The International Simple Glass," *Geochimica et Cosmochimica Acta*, Vol 151, pp. 68–85.
21. Greenhalgh, M., T. G. Garn, and J. D. Law, 2013, "Development of a hydrogen mordenite sorbent for the capture of krypton from used nuclear fuel reprocessing off-gas streams," *Journal of Nuclear Science and Technology*, Vol. 51, No. 4, pp. 476–481.
22. Hartmann, T., A. J. Alaniz, and D. J. Antonio, 2012, "Fabrication and Properties of Technetium-Bearing Pyrochlores and Perovskites as Potential Waste Forms," *ATALANTE 2012: Nuclear Fuel Cycle for a Sustainable Fuel Cycles*. 2-7 September, Proceedings, A210 (2012), to be published in *Procedia Chemistry*.
23. Hartmann, T., A. J. Alaniz, and D. J. Antonio, 2012, "Fabrication and properties of Tc-bearing pyrochlores, perovskites and spinel derivates," *243<sup>rd</sup> ACS National Meeting: Chemistry for Life, session: Waste Forms for Environmental Remediation*, San Diego, 25–29 March, Pub 253.

24. Icenhower, J. P. and C. Steefel, 2012, "Experimentally Determined Dissolution Kinetics of SON68 Glass at 90°C over a Silica Saturation Interval: Evidence against a Linear Rate Law," *Journal of Nuclear Materials*, Vol. 439, No. 1–3, pp. 137–147.
25. Jaffe, J. E., R. M. V. Ginhoven, and W. Jiang, 2012, "Interstitial and Substitutional Zirconium in SrTiO<sub>3</sub>," *Computational Materials Science*, Vol. 53, No. 1, pp.153–157. DOI: 10. 1016/j. commatsci. 2011. 08. 023.
26. Jantzen C., C. Crawford, J. Pareizs, J. Pickett, 2016, "Accelerated Leach Testing of GLASS: II. Leachate-Hydrogel Interactions, Glass Structure, and Accelerated Dissolution," submitted to *International Journal of Applied Glass Science*.
27. Jiang, W., M. E. Bowden, Z. Zhu, P. A. Jozwik, J. Jagielski, and A. Stonert, 2012, "Defects and Minor Phases in O<sup>+</sup> and Zr<sup>+</sup> Ion Co-Implanted SrTiO<sub>3</sub>," *Industrial and Engineering Chemistry Research*, Vol. 51, No. 2, pp. 621–628.
28. Jiang, W., R. M. Van Ginhoven, L. Kovarik, J. E. Jaffe, and B. W. Arey, 2012, "Superlattice Structure and Precipitates in O<sup>+</sup> and Zr<sup>+</sup> Ion Co-implanted SrTiO<sub>3</sub>: a Model Waste Form for <sup>90</sup>Sr," *Journal of Physical Chemistry C*, Vol. 116, pp. 16709–16715.
29. Jubin, R. T., 2012, "Impact of Pretreatment and Aging on the Iodine Capture Performance of Silver Exchanged Mordenite," *Waste Management 2012 Conference*, February 26–March 1, 2012, Phoenix, AZ.
30. Kerisit, S. N., E. M. Pierce, and J. V. Ryan, 2015, "Monte Carlo Simulations of Coupled Diffusion and Surface Reactions during the Aqueous Corrosion of Borosilicate Glasses," *Journal of Non-Crystalline Solids*, Vol. 408, pp. 142–149.
31. Kerisit, S., J. V. Ryan, and E. M. Pierce, 2013, "Monte Carlo Simulations of the Corrosion of Aluminoborosilicate Glasses," *Journal of Non-Crystalline Solids*, Vol. 378, pp. 273–281.
32. Kossoy, A., R. Schulze, M. Tang, D. J. Safarik, and R. J. McCabe, 2013, "Nd–Mo–Borosilicate Glass–Ceramic: Synthesis, Characterization and Response to Ionizing Radiation," *Journal of Nuclear Materials*, Vol. 437, pp. 216–221.
33. Liu, J., D. Strachan, and P. Thallapally, 2014, "Enhanced Noble Gas Adsorption in Ag@MOF-74Ni Article," *Chemical Communications*, Vol. 50, No. 4, pp. 466–468.
34. Liu, J., P. K. Thallapally, and D. M. Strachan, 2012, "Metal–Organic Frameworks for Removal of Xe and Kr from Nuclear Fuel Reprocessing Plant," *Langmuir*, Vol. 28, pp. 11584–11589.
35. Matyáš, J. and R. K. Engler, 2013, *Assessment of Methods to Consolidate Iodine-Loaded Silver-Functionalized Silica Aerogel*, PNNL-22874, Pacific Northwest National Laboratory.
36. Matyáš, J., G. E. Fryxell, and M. J. Robinson, 2012, *Silver-Functionalized Silica Aerogel for Capture and Immobilization of Gaseous Radioiodine from Reprocessing Off-Gas*, PNNL-21792, Pacific Northwest National Laboratory, Richland, WA.

## 2016 ACCOMPLISHMENTS

37. Matyáš, J., M. J. Robinson, and G. E. Fryxell, 2012, "The Effect of Temperature and Uniaxial Pressure on the Densification Behavior of Silica Aerogel Granules," *Ceramic Engineering and Science*, Vol. 33, No. 9, pp. 121–125.
38. Murphy, K.A., N. M. Washton, J. V. Ryan, C. G. Pantano, and K. T. Mueller, 2013, "Solid-State NMR Examination of Alteration Layers on Nuclear Waste Glasses," *Journal of Non-Crystalline Solids* Vol. 369, pp. 44–54.
39. Nenoff, T. M. and J. L. Krumhansl, 2012, "Cs+ Removal from Seawater by Commercially Available Molecular Sieves," *Solvent Extraction and Ion Exchange*, Vol. 30, pp. 33–40.
40. Nenoff, T. M., 2012, "Alternative Energy Systems: Nuclear Energy, Introduction to the Special Section on Nuclear Energy," *Industrial and Engineering Chemistry Research*, Vol. 51 No. 2, pp. 605–606.
41. Pierce, E. M., P. Frugier, L. J. Criscenti, K. D. Kwon, and S. Kerisit, "Modeling the Glass-Water Reaction from Interface to Pore Scale: Recent Advances and Current Limitations," *International Journal of Applied Glass Science*, accepted for publication.
42. Reiser, J., L. M. Neill, J. Weaver, C. Musa, J. J. Neeway, J. V. Ryan, N. Qafoku, S. Gin, N. A. Wall, 2014, "Glass corrosion in the presence of iron-bearing materials and potential corrosion suppressors," *MRS Proceedings 2014*.
43. Riley, B. J., B. T. Rieck, J. S. McCloy, J. V. Crum, S. K. Sundaram, and J. D. Vienna, 2012, "Tellurite Glass as a Waste Form for Mixed Alkali-Chloride Waste Streams: Candidate Materials Selection and Initial Testing," *Journal of Nuclear Materials*, Vol. 424, No. 1–3, pp. 29–37.
44. Riley, B. J., J. V. Crum, J. Matyas, J. S. McCloy, and W. C. Lepry, 2012, "Solution-Derived, Chloride-Containing Minerals as a Waste Form for Alkali Chlorides," *Journal of the American Ceramic Society*, Vol. 95, No.10, pp. 3115–3123.
45. Roy, L. E., N. J. Bridges, and L. R. Martin, 2013, "Theoretical insights into covalency driven f element separations," *Dalton Transactions*, Vol. 42, pp. 2636–2642.
46. Rutledge, V. J., 2013, "Off-gas Adsorption Model and Simulation," *Proceedings from GLOBAL 2013*, Salt Lake City, Utah, September 29–October 4, 2013.
47. Rutledge, V. J., 2013, *Osprey Model*, INL/EXT-13-28150, Idaho National Laboratory, January.
48. Ryan, J. V., D. M. Strachan, J. McCloy, J. V. Crum, D. Jansik, D. Dixon, D. K. Schreiber, and C. Chamberlain, 2012, *Ancient Roman Glass Characterization for Use in Glass Corrosion Modeling*, PNNL-21847, Pacific Northwest National Laboratory, Richland, WA.
49. Ryan, J. V., W. L. Ebert, J. P. Icenhower, D. K. Schreiber, D. M. Strachan, and J. D. Vienna, 2012, "Joint EM-NE-International Study of Glass Behavior over Geologic Time Scales," *Proceedings of Waste Management 2012*, Phoenix, AZ.

50. Sava, D. F., T. J. Garino, and T. M. Nenoff, 2012, "Iodine Confinement into Metal-Organic Frameworks (MOFs): Low Temperature Sintering Glasses to Form Novel Glass Composite Material (GCM) Alternative Waste Forms," *Industrial and Engineering Chemistry Research*, Vol. 51 No. 2, pp. 612–618.
51. Schreiber, D. K. and J. V. Ryan, 2015, "Atom Probe Tomography," *Modern Glass Characterization*, Edited by M. Affatigato. Wiley.
52. Soelberg, N. R., T. G. Garn, M. R. Greenhalgh, J. D. Law, R. Jubin, D. M. Strachan, and P. K. Thallapally, 2013, "Radioactive Iodine and Krypton Control for Nuclear Fuel Reprocessing Facilities," *Hindawi Publishing Corporation, Science and Technology of Nuclear Installations*, Article ID 702496, 12 pages.
53. Strachan, D. M., J. V. Crum, J. V. Ryan, and A. Silvestri, 2014, "Characterization and Modeling of the Cemented Sediment Surrounding the Iulia Felix Glass," *Applied Geochemistry*, Vol. 41, pp. 107–114.
54. Strachan, D., and J. Neeway, 2014, "Effects of Alteration Product Precipitation on Glass Dissolution," *Applied Geochemistry*, Vol. 45, pp. 144–157.
55. Tang M., A. Kossoy, G. D. Jarvinen, J. V. Crum, L. A. Turo, B. J. Riley, K. Brinkman, K. M. Fox, J. Amoroso, and J. C. Marra, 2014, "Radiation Stability Test on Multiphase Glass Ceramic and Crystalline Ceramic Waste Forms," *Nuclear Instruments and Methods in Physics Research Section B: Beam Interactions with Materials and Atoms*, Vol. 326, pp. 293–297.
56. Tang, M., A. Kossoy, G. Jarvinen, J. Crum, L. Turo, B. Riley, K. Brinkman, K. Fox, J. Amoroso, and J. Marra, 2014, "Radiation Stability Test on Multiphase Glass Ceramic and Crystalline Ceramic Waste Forms," *Nuclear Instruments and Methods in Physics Research Section B: Beam Interactions with Materials and Atoms*, Vol. 326, pp. 293–297.
57. Tang, M., A. T. Nelson, E. S. Wood, S. A. Maloy, and Y-B. Jiang, 2016, "Grazing incidence X-ray diffraction and transmission electron microscopy studies on the oxide formation of molybdenum in a water vapor environment," *Scripta Mater.*, Vol. 120, pp. 49–53.
58. Tang, M., J. A. Valdez, Y. Wang, J. Zhang, B. P. Uberuaga, and K. E. Sickafus, 2016, "Ion irradiation-induced crystal structure changes in inverse spinel MgIn<sub>2</sub>O<sub>4</sub>," *Scripta Mater.*, Vol. 125, pp. 10–14.
59. Tang, M., P. Fuierer, P. Dickens, and E. Fu, 2013, "Irradiation Study on Sr<sub>n+1</sub>Ti<sub>n</sub>O<sub>3n+1</sub> Ruddlesden-Popper Phases Synthesized by Hot-Forging," *Physica Status Solidi (c)*, Vol. 10, No. 2, pp. 216–220.
60. Tang, M., P. Tumurugoti, B. M. Clark, S. K. Sundaram, J. Amoroso, J. Marra, C. Sun, P. Lu, Y. Wang, and Y-B. Jiang, 2016, "Heavy ion irradiations on synthetic hollandite-type materials: Ba<sub>1.0</sub>Cs<sub>0.3</sub>A<sub>2.3</sub>Ti<sub>5.7</sub>O<sub>16</sub> (A = Cr, Fe, Al)," *Journal of Solid State Chemistry*, Vol. 239, pp. 58–63.
61. Thallapally, P. K. and D. M. Strachan, 2013, *Initial Proof of Principle for near Room Temperature Xe and Kr Separation from Air with Mofs*, PNNL-21452, Pacific Northwest National Laboratory, Richland, WA.
62. Thallapally, P. K., J. W. Grate, and R. K. Motkuri, 2012, "Facile Xenon Capture and Release at Room Temperature Using a Metal–Organic Framework: A Comparison with Activated Charcoal," *Chemical Communication*, Vol. 48: pp. 347–349.

## 2016 ACCOMPLISHMENTS

63. Thallapally, P., J. Liu, and D. M. Strachan, 2013, *Demonstrate the Removal Efficiency and Capacity of MOF Materials for Krypton Recovery*, PNNL-22693, Pacific Northwest National Laboratory.
64. Trivelpiece, C. L., J. J. Petrunis, R. G. Downing, and C. G. Pantano, 2012, "Glass Surface Gel-Layer Density by Neutron Depth Profiling," *International Journal of Applied Glass Science*, Vol. 3, No. 2, pp. 137–143.
65. Tumurugoti, P., S. K. Sundaram, S. T. Misture, J. C. Marra, and J. W. Amoroso, 2016, "Crystallization behavior during melt-processing of ceramic waste forms," *Journal of Nuclear Materials*, Vol. 473, pp. 178–188
66. Uberuaga, B. P., M. Tang, C. Jiang, J. A. Valdez, R. Smith, Y. Wang, and K. E. Sickafus, 2015, "Opposite correlations between cation disordering and amorphization resistance in spinels versus pyrochlores," *Nature Communications*, Vol. 6., Article No. 8750.
67. Van Ginhoven, R., J. Jaffe, and W. Jiang, 2012, "Combined Theoretical/Experimental Study of Zr-implanted SrTiO<sub>3</sub> as a Model Wasteform for the Decay of Sr to Zr," *Spring MRS*, San Francisco, CA, April 2012.
68. Vienna, J. D., S. Gin, J. V. Ryan, and Y. Inagaki, 2013, "Current Understanding and Remaining Challenges in Modeling Long-Term Degradation of Borosilicate Nuclear Waste Glasses," *International Journal of Applied Glass Science*, Vol. 4, No. 4, pp. 283–294.
69. Wang, S., M. Tang, K. S. Brinkman, and F. Chen, 2014, "Ion-irradiation Induced Reduction in Sr<sub>2</sub>Fe<sub>1.5</sub>Mo<sub>0.5</sub>O<sub>6δ</sub> Perovskite," *Nuclear Instruments and Methods in Physics Research Section B: Beam Interactions with Materials and Atoms*, Vol. 326, pp. 298–302.
70. Wang, S., M. Tang, L. Zhang, G. Xiao, K. S. Brinkman, and F. Chen, 2013, "Irradiation Effect on the Structure Change for Sr<sub>2</sub>Fe<sub>1.5</sub>Mo<sub>0.5</sub>O<sub>6-δ</sub> Perovskite Ceramic," *Journal of Alloys and Compounds*, Vol. 578, pp. 170–175.
71. Wang, Y. C., D. K. Schreiber, J. J. Neeway, S. Thevuthasan, J. E. Evans, J. V. Ryan, Z. Zhu, and W. Wei, 2014, "NanoSIMS Imaging Alternation Layers of a Leached SON68 Glass Via A FIB-made Wedged Crater," *Surface and Interface Analysis*, Vol. 46, pp. 233–237.
72. Wang, Z., J. V. Ryan, Z. Zhu, et al., 2015, "High Sputter Rate and Accurate Interfacial Chemical Information: Using Argon Cluster Sputtering Source in ToF-SIMS Depth Profiling of Leached Nuclear Waste Glass and Functional Metal Oxide Films," *Journal of the American Society for Mass Spectrometry*, Vol. 26, No. 8.
73. Wang, Z., Liu, J., Zhou, Y., Neeway, J. J., Schreiber, D. K., Crum, J. V., Ryan, J. V., Wang, X. -L., Wang, F., and Zhu, Z., 2016, "Nanoscale imaging of Li and B in nuclear waste glass, a comparison of ToF-SIMS, NanoSIMS, and APT," *Surface and Interface Analysis*, Vol. 49, No. 1, pp. 1–74.
74. Wen, J., C. Sun, P. P. Dholabhai, Y. Xia, M. Tang, D. Chen, D.Y. Yang, Y. H. Li, B. P. Uberuaga, Y. Q. Wang, 2016, "Temperature dependence of the radiation tolerance of nanocrystalline pyrochlores A<sub>2</sub>Ti<sub>2</sub>O<sub>7</sub> (A: Gd, Ho and Lu)," *Acta Materialia*, Vol. 110, pp. 175–184.

## AQUEOUS REPROCESSING

1. Braley, J. C., J. C. Carter, S. I. Sinkov, K. L. Nash, and G. J. Lumetta, 2012, "The Role of Carboxylic Acids in TALSQUEAK Separations," *Journal of Coordination Chemistry*, Vol. 65, pp. 2862–2876.
2. Brown, M. A., A. Paulenova, and A. V. Gelis, 2012, "Aqueous Complexation of Thorium(IV), Uranium(IV), Neptunium(IV), Plutonium(III/IV), and Cerium(III/IV) with DTPA," *Inorganic Chemistry*, Vol. 51, No. 14, pp. 7741–7748.
3. Bryan, S. A., T. G. Levitskaia, J. M. Schwantes, C. R. Orton, J. M. Peterson, and A. J. Casella, 2012, "Monitoring, Controlling and Safeguarding Radiochemical Streams at Spent Fuel Reprocessing Facilities, Part 1: Optical Spectroscopic Methods," *International Journal on Nuclear Energy Management and Safety*, December 2012.
4. Burns, J. D., A. Clearfield, T. C. Shehee, and D. T. Hobbs, 2012, "Separation of Americium from Curium by Oxidation and Ion Exchange," *Analytical Chemistry*, Vol. 84, No. 16, pp. 6930–6932.
5. Burns, J. D., M. Borkowski, A. Clearfield, and D. T. Reed, 2012, "Separation of Oxidized Americium from Lanthanides by Use of Pillared Metal(IV) Phosphate-Phosphonate Hybrid Materials," *Radiochimica Acta*, Vol. 100, pp. 901–906.
6. Burns, J., A. Clearfield, M. Borkowski, and D. Reed, 2012, "Pillared Metal(IV) Phosphate-Phosphonate Extraction of Actinides," *Radiochimica Acta*, Vol. 100, pp. 381–387.
7. Casella, A. J., T. G. Levitskaia, J. M. Peterson, and S. A. Bryan, 2013, "Water O–H Stretching Raman Signature for Strong Acid Monitoring via Multivariate Analysis," *Analytical Chemistry*, Vol. 85, pp. 4120–4128.
8. Cullen, T. D., S. P. Mezyk, L. R. Martin, and B. J. Mincher, 2013, "Elucidating the Radical Kinetics Involved in the Radiolytic Destruction of Lanthanide-Complexed Dtpa," *Journal of Radioanalytical and Nuclear Chemistry*, Vol. 296, No. 2, pp. 717–720.
9. Daly, S. R., J. M. Keith, E. R. Batista, K. S. Boland, D. L. Clark, S. A. Kozimor, and R. L. Martin, 2012, "Sulfur K-Edge X-Ray Absorption Spectroscopy and Time-Dependent Density Functional Theory of Dithiophosphate Extractants: Minor Actinide Selectivity and Electronic Structure Correlations," *Journal of the American Chemical Society*, Vol. 134, No. 35, pp. 14408–14422.
10. Daly, S. R., J. M. Keith, E. R. Batista, K. S. Boland, S. A. Kozimor, R. L. Martin, and B. L. Scott, 2012, "Probing Ni[S2pr2]2 Electronic Structure to Generate Insight Relevant to Minor Actinide Extraction Chemistry," *Inorganic Chemistry*, Vol. 51, No. 14, pp. 7551–7560.
11. Daly, S. R., J. R. Klaehn, K. S. Boland, S. A. Kozimor, M. M. Macinnes, D. R. Peterman, and B. L. Scott, 2012, "NMR Spectroscopy and Structural Characterization of Dithiophosphate Ligands Relevant to Minor Actinide Extraction Processes," *Dalton Transactions*, Vol. 41, No. 7, pp. 2163–2175.
12. Devore, M. A., and A. E. V. Gorden, 2012, "Copper and Uranyl Extraction from Aqueous Solutions Using Bis-Dithiophosphate Ligands Have Been Characterized," *Polyhedron*, Vol. 42, No. 1, pp. 271–275.

## 2016 ACCOMPLISHMENTS

13. Elias G., G. S. Groenewold, B. J. Mincher, and S. P. Mezyk, 2012, "Determination of CMPO using HPLC-UV," *Journal of Chromatography A*, Vol. 1243, pp. 47–52.
14. Elvington, M. C., T. C. Shehee, T. S. Rudisill, and D. T. Hobbs, 2012, "Separation of Americium and Lanthanides Using Titanium-Based Materials," *Solvent Extraction and Ion Exchange*, Vol. 30, No. 7, pp. 669–682.
15. Fondeur, F. F., and T. S. Rudisill, 2012, "Thermal Stability of Formohydroxamic Acid," *Separation Science and Technology*, Vol. 47, No. 14–15, pp. 2038–2043.
16. Francois, M. M., and N. N. Carlson, 2013, "The Global Embedded Interface Formulation for Interfacial Mass Transfer within a Volume Tracking Framework," *Computers and Fluids*, Vol. 87, pp. 102–114.
17. Gandhir, A. and K. E. Wardle, 2012, "CFD Analysis of Fluid Flow above the Upper Weir of an Annular Centrifugal Contactor 4," *Separation Science and Technology*, Vol. 47, pp. 1–10.
18. Gray, M. F., P. R. Zalupski, and M. Nilsson, 2013, "Determination of Activity Coefficients of Di-(2-Ethylhexyl)Phosphoric Acid Dimer in Select Organic Solvents Using Vapor Phase Osmometry," *Solvent Extraction and Ion Exchange*, Vol. 31, No. 5, pp. 550–563.
19. Grimes, T. S., G. Tian, L. Rao, and K. L. Nash, 2012, "Optical Spectroscopy Study of Lanthanide Organic Phase Complexes in the TALSPEAK Separations Process," *Inorganic Chemistry*, Vol. 51, No. 11, pp. 6299–6307.
20. Grimes, T. S., M. P. Jensen, L. Debeer-Schmidt, K. Littrell, and K. L. Nash, 2012, "Small Angle Neutron Scattering (SANS) Study of Organic Phase Aggregation in the TALSPEAK Process," *Journal of Physical Chemistry B*, Vol. 116, No. 46, November 26, 2012, pp. 13722–13730.
21. Groenewold, G. S., D. R. Peterman, J. R. Klaehn, L. H. Delmau, P. Marc, and R. Custelcean, 2012, "Oxidative Degradation of Bis(2,4,4-trimethylpentyl)dithiophosphinic Acid in Nitric Acid Studied by Electrospray Ionization Mass Spectrometry," *Rapid Communications in Mass Spectrometry*, 2012, Vol. 26, No. 19, pp. 2195–2203.
22. Groenewold, G. S., G. Elias, B. J. Mincher, S. P. Mezyk, and J. A. Laverene, 2012, "Characterization of CMPO and Its Radiolysis Products by Direct Infusion ESI-MS," *Talanta*, Vol. 99, pp. 909–917.
23. Heathman, C. R., and K. L. Nash, 2012, "Characterization of Europium and Americium Dipicolinate Complexes," *Separation Science and Technology*, Vol. 47, No. 14–15, pp. 2029–2037.
24. Kang, S. O., S. Vukovic, R. Custelcean, and B. P. Hay, 2012, "Cyclic Imide Dioximes: Formation and Hydrolytic Stability," *Industrial and Engineering Chemistry Research*, Vol. 51, No. 19, pp. 6619–6624.
25. Kang, S. O., S. Vukovic, R. Custelcean, and B. P. Hay, 2012, "Cyclic Imide Dioximes: Formation and Hydrolytic Stability," *243rd National Meeting of the American Chemical Society*, San Diego, California, March 25–29, 2012.

26. Keith, J. M., and E. R. Batista, 2012, "Theoretical Examination of the Thermodynamic Factors in the Selective Extraction of Am<sup>3+</sup> from Eu<sup>3+</sup> by Dithiophosphinic Acids," *Inorganic Chemistry*, Vol. 51, No. 1, pp. 13–15.
27. Law, J. D., J. L. Tripp, T. E. Smith, J. M. Svoboda, V. J. Rutledge, T. G. Garn, and L. Macalusso, 2014, "Development and Testing of A Microfluidic Based Robotic Sampling System for Remote Sampling and Analysis of radioactive solutions," *Nuclear Technology*, Vol. 185, No. 2, February 2014, pp. 216–225.
28. Leggett, C. J., Ph. D., 2012, "Thermodynamic Investigations of Aqueous Ternary Complexes for Am/Cm Separation," University of California, Berkeley, California.
29. Levitskaia, T. G., J. M. Peterson, E. L. Campbell, A. J. Casella, D. R. Peterman, and S. A. Bryan, 2013, "Fourier Transform Infrared Spectroscopy and Multivariate Analysis for Online Monitoring of Dibutyl Phosphate Degradation Product in Tributyl Phosphate/n-Dodecane/Nitric Acid Solvent," *Industrial and Engineering Chemistry Research*, Vol. 52, No. 49, pp. 17607–17617.
30. Lumetta, G. J., A. V. Gelis, J. C. Braley, J. C. Carter, J. W. Pittman, M. G. Warner, and G. F. Vandegrift, 2012, "The TRUSPEAK Concept: Combining Cmpo and HDEHP for Separating Trivalent Lanthanides from the Transuranic Elements," *Solvent Extraction and Ion Exchange*, Vol. 31, No. 3, pp. 223–236.
31. Lumetta, G. J., T. G. Levitskaia, S. L. Latesky, R. V. Henderson, E. A. Edwards, J. C. Braley, and S. I. Sinkov, 2012, "Lipophilic Ternary Complexes in Liquid-Liquid Extraction of Trivalent Lanthanides," *Journal of Coordination Chemistry*, Vol. 65, No. 5, pp. 741–753.
32. Marc, P., R. Custelcean, G. S. Groenewold, J. R. Klaehn, D. R. Peterman, and L. H. Delmau, 2012, "Degradation of CYANEX® 301 in Contact with Nitric Acid Media," *Industrial and Engineering Chemistry Research*, 2012, Vol. 51, No. 40, pp. 13238–13244.
33. Marie, C., B. Hiscox, and K. L. Nash, 2012, "Characterization of HDEHP-Lanthanide Complexes Formed in a Non-Polar Organic Phase Using 31p NMR and ESI-MS," *Dalton Transactions*, Vol. 41, No. 3, pp. 1054.
34. Mezyk, S. P., B. J. Mincher, C. Ekberg, and G. Skarnemark, 2013, "Alpha and Gamma Radiolysis of Nuclear Solvent Extraction Ligands Used for An(III) and Ln(III) Separations," *Journal of Radioanalytical and Nuclear Chemistry*, Vol. 296, No. 2, May 2013, pp. 711–715.
35. Mezyk, S. P., B. J. Mincher, W. J. Cooper, S. K. Cole, R. V. Fox, and P. R. Gardinali, 2012, "Kinetic Model for the Radical Degradation of Trihalonitromethane Disinfection Byproducts in Water," *Radiation Physics and Chemistry*, Vol. 81, pp. 1646–1652.
36. Minasian, S. G., K. S. Boland, R. K. Feller, A. J. Gaunt, S. A. Kozimor, I. May, S. D. Reilly, B. L. Scott, and D. K. Shuh, 2012, "Synthesis and Structure of (Pph<sub>4</sub>)<sub>2</sub>mcl<sub>6</sub> (M = Ti, Zr, Hf, Th, U, Np, Pu)," *Inorganic Chemistry*, Vol. 51, No. 10, pp. 5728–5736.
37. Mincher, B. J., 2012, "Degradation issues in aqueous reprocessing systems," Ch. 104 in *Comprehensive Nuclear Materials*, Allen, T., ed. Elsevier, July 13, 2012.

## 2016 ACCOMPLISHMENTS

38. Mincher, B. J., L. R. Martin, and N. C. Schmitt, 2012, "Diamylamylphosphonate Solvent Extraction of Am(VI) from Nuclear Fuel Raffinate Simulant Solution," *Solvent Extraction and Ion Exchange*, Vol. 30, pp. 445–456.
39. Mincher, M. E., D. L. Quach, Y. J. Liao, B. J. Mincher, and C. M. Wai, 2012, "The Partitioning of Americium and the Lanthanides Using Tetrabutyl diglycolamide (TBDGA) in Octanol and in Ionic Liquid Solution," *Solvent Extraction and Ion Exchange*, Vol. 30, No. 7, pp. 735–747.
40. Nichols, K. P., R. R. Pompano, L. Li, A. V. Gelis, and R. F. Ismagilov, 2012, "Toward Mechanistic Understanding of Nuclear Reprocessing Chemistries by Quantifying Lanthanide Solvent Extraction Kinetics via Microfluidics with Constant Interfacial Area and Rapid Mixing," *Journal of the American Chemical Society*, Vol. 133, No. 39, pp. 15721–15729.
41. Ogden, M. D., S. I. Sinkov, G. J. Lumetta, and K. L. Nash, 2012, "Affinity of an(VI) for N4-Tetradentate Donor Ligands: Complexation of the Actinyl(VI) Ions with N4-Tetradentate Ligands," *Journal of Solution Chemistry*, Vol. 41, No. 4, pp. 616–629.
42. Rao, L., and G. Tian, 2011, "Effect of Temperature on the Complexation of Cm(III) with Nitrate in Aqueous Solutions," *Dalton Transactions*, Vol. 40, No. 4, pp. 914–918.
43. Rodriguez, M. A., D. F. Sava, and T. M. Nenoff, 2012, "Catena-Poly[Zinc-Tris(M-Dimethyl-Carbamato-K2O:O')-Zinc-M-(2-Phenyl-Benzimidazolido-K2n:N')]," *Acta Crystallographica Section*, Vol. 68, pp. M59.
44. Roy, L. E., N. J. Bridges, and L. R. Martin, 2012, "Theoretical Insights into Covalency Driven F Element Separations," *Dalton Transactions*, Vol. 42, No. 7, pp. 2636–2642.
45. Schroll, C. A., S. Chatterjee, W. R. Heineman, and S. A. Bryan, 2012, "Thin-Layer Spectroelectrochemistry on an Aqueous Microdrop," *Electroanalysis*, Vol. 24, No. 5, pp. 1065–1070.
46. Schwantes, J. M., S. A. Bryan, C. R. Orton, T. G. Levitskaia, and C. G. Fraga, 2011, "Monitoring, Controlling and Safeguarding Radiochemical Streams at Spent Fuel Reprocessing Facilities, Part 2: Gamma-Ray Spectroscopic Methods," *International Journal on Nuclear Energy Management and Safety*, No. 1, pp. 39–58.
47. Shehee, T. C., K. M. L. Taylor-Pashow, and D. T. Hobbs, 2012, "Advances in Inorganic and Hybrid Ion-Exchangers," *Solvent Extraction and Ion Exchange*, Vol. 31, No. 2, pp. 122–170.
48. Sinkov, S. I., G. J. Lumetta, M. G. Warner, and J. W. Pittman, 2012, "Binding of Stereognostically Designed Ligands to Trivalent, Pentavalent, and Hexavalent F-Block Elements," *Radiochimica Acta*, Vol. 100, pp. 349–357.
49. Sulakova, J., R. T. Paine, M. Chakravarty, and K. L. Nash, 2012, "Extraction of Lanthanide and Actinide Nitrate and Thiocyanate Salts by 2,6-Bis[(Bis(2-N-Octyl)Phosphino)Methyl]Pyridine N,P,P'-Trioxide N Toluene," *Separation Science and Technology*, Vol. 47, No. 14–15, pp. 2015–2023.
50. Tian, G., P. Zhang, Y. Shen, J. Wang, and L. Rao, 2012, "Bench-Scale Test for Separation of Sr<sup>2+</sup> and Nd<sup>3+</sup> from Hllw Using Tiboga," *Separation Science and Technology*, Vol. 47, No. 14–15, pp. 2160–2165.

51. Tkac, P., G. F. Vandegrift, G. J. Lumetta, and A. V. Gelis, 2012, "Study of the Interaction between HDEHP and CMPO and Its Effect on the Extraction of Selected Lanthanides," *Industrial and Engineering Chemistry Research*, Vol. 51, No. 31, pp. 10433–10444.
52. Tripp, J. L., J. D. Law, and T. Smith, 2013, "Recent Results of the Investigation of a Microfluidic Sampling Chip and Sampling System for Hot Cell Aqueous Processing Streams," *Proceedings from GLOBAL 2013*, Salt Lake City, Utah, September 29–October 4, 2013.
53. Tripp, J. L., J. D. Law, T. E. Smith, V. J. Rutledge, W. Bauer, D. Ball, and P. Hahn, 2015, "Microfluidic-based Sample Chips for Radioactive Solutions," *Nuclear Technology*, Vol. 189, No. 3, March 2015, pp. 301–311.
54. Vedantam, S., K. E. Wardle, T. V. Tamhane, V. V. Ranade, and J. B. Joshi, 2012, "CFD Simulation of Annular Centrifugal Extractors," *International Journal of Chemical Engineering*, Vol. 2012, Article No. 759397.
55. Wardle, K. E., and T. Lee, 2012, "Finite Element Lattice Boltzmann Simulations of Free Surface Flow in a Concentric Cylinder" *Computers and Mathematics with Applications*, Vol. 65, No. 2, pp. 230–238.

#### ELECTROCHEMICAL REPROCESSING

1. Rodriguez, M. A., J. Griego, H. J. Brown-Shaklee, M. A. Blea-Kirby, J. F. Ihlefeld, and E. D. Spoerke, 2015, "X-ray Powder Diffraction Study of  $\text{La}_2\text{LiTaO}_6$ ," *Powder Diffraction*, Vol. 30, No. 1, pp. 57–62.
2. Schroll, C. A., S. Chatterjee, T. G. Levitskaia, W. R. Heineman, and S. A. Bryan, 2013, "Electrochemistry and Spectroelectrochemistry of Europium(III) chloride in  $3 \text{ LiCl} - 2 \text{ KCl}$  from 643 K to 1123 K," *Analytical Chemistry*, Vol. 85, No. 20, pp. 9924–9931.

#### FUEL RESOURCES

1. Abney, C. W., Das, S., Mayes, R. T., Kuo, L.-J., Wood, J., Gill, G., Piechowicz, M., Lin, Z., Lin, W., Dai, S., 2016, "A Report of Emergent Uranyl Binding Phenomena by an Amidoxime Phosphonic Acid Co-Polymer," *Physical Chemistry Chemical Physics*, Vol. 18, pp. 23462–23468.
2. Abney, C. W., Mayes, R. T., Piechowicz, M., Lin, Z., Bryantsev, V. S., Veith, G. M., Dai, S., Lin, W., 2016, "XAFS Determination of the Uranyl Coordination Environment as Bound by an Amidoxime-Functionalized Polymer," *Energy and Environmental Science*, Vol. 9, pp. 448–453. (Highlighted on journal cover).
3. Alexandratos, S. D., and Kung, S., 2016, "Preface to the Special Issue: Uranium in Seawater," *Industrial and Engineering Chemistry Research*, Vol. 55, pp. 4101–4102.
4. Alexandratos, S. D., and Zhu, X. P., 2016, "Polymer-Supported Aminomethylphosphinate as a Ligand with a High Affinity for U(VI) from Phosphoric Acid Solutions: Combining Variables to Optimize Ligand-Ion Communication," *Solvent Extraction and Ion Exchange*, Vol. 34, pp. 290–295.

## 2016 ACCOMPLISHMENTS

- Alexandratos, S. D., Zhu, X.P., Florent, M., and Sellin, R., 2016, "Polymer-Supported Bifunctional Amidoximes for the Sorption of Uranium from Seawater," *Industrial and Engineering Chemistry Research*, Vol. 55, pp. 4208–4216.
- Ansari, S., Yang, Y., Zhang, Z., Gagnon, K., Teat, S. J., Luo, S., and Rao, L., 2016, "Complexation of Lanthanides with Glutarimide-dioxime: Binding Strength and Coordination Modes," *Inorganic Chemistry*, Vol. 55, pp. 1315–1323.
- Berton, P., Kelley, S. P., and Rogers, R. D., 2015, "Stripping uranium from seawater-loaded sorbents with the ionic liquid hydroxylammonium acetate in acetic acid for efficient reuse," *Industrial and Engineering Chemistry Research*, Vol. 55, pp. 4321–4327.
- Brown, S., Chatterjee, S., Li, M., Yue, Y., Tsouris, C., Janke, C.J., Saito, T., and Dai, S., 2016, "Uranium Adsorbent Fibers Prepared by Atom-Transfer Radical Polymerization from Chlorinated Polypropylene and Polyethylene Trunk Fibers," *Industrial and Engineering Chemistry Research*, Vol. 55, pp. 4130–4138.
- Brown, S., Yue, Y., Kuo, L.-J., Mehio, N., Li, M., Gill, G.A., Tsouris, C., Mayes, R.T., Saito, T., and Dai, S., 2016, "Uranium Adsorbent Fibers Prepared by Atom-Transfer Radical Polymerization (ATRP) from Poly(vinyl chloride)-co-chlorinated poly(vinyl chloride) (PVC-co-CPVC) Fiber," *Industrial and Engineering Chemistry Research*, Vol. 55, pp. 4139–4148.
- Chatterjee, S., Bryantsev, V. S., Brown, S., Johnson, J. C., Grant, C. D., Mayes, R. T., Hay, B. P., Dai, S., and Saito, T., 2016, "Naphthalimidedioxime Ligand-Containing Fiber Adsorbent for Uranium Recovery from Seawater," *Industrial and Engineering Chemistry Research*, Vol. 55, pp. 4161–4169.
- Chouyyok, W., Pittman, J. W., Warner, M. G., Nell, K. M., Clubb, D. C., Gill, G. A., and Addleman, R. S., 2016, "Surface Functionalized Nanostructured Ceramic Sorbents for the Effective Collection and Recovery of Uranium from Seawater," *Dalton Transactions*, Vol. 45, pp. 11312–11325.
- Chouyyok, W., Warner, C. L., Mackie, K. E., Warner, M. G., Gill, G., Addleman, R. S., 2016, Evaluation of Nanostructured Metal Oxide Sorbents for the Collection and Recovery of Uranium from Seawater," *Industrial and Engineering Chemistry Research*, Vol. 55, No. 15, pp. 4195–4207.
- Das, S., Brown, S., Mayes, R.T., Janke, C.J., Tsouris, C., Kuo, L.-J., Gill, G. A., and Dai, S., 2016, "Novel Poly(imidedioxime) Sorbent: Development and Testing for Enhanced Extraction of Uranium from Natural Seawater," *Chemical Engineering Journal*, Vol. 298, pp. 125–135.
- Das, S., Liao, W.-P., Byers, M. F., Tsouris, C., Janke, C.J., Mayes, R.T., Schneider E., Kuo, L.-J., Wood, J.R., Gill, and G.A., Dai, S., 2016, "Alternative Alkaline Conditioning of Amidoxime based Adsorbent for Uranium Extraction from Seawater," *Industrial and Engineering Chemistry Research*, Vol. 55, pp. 4303–4312.

15. Das, S., Oyola, Y., Mayes, R.T., Janke, C.J., Kuo, L.-J., Wood, J.R., Gill, G.A., and Dai, S., 2016, "Extraction of Uranium from Seawater: Promising AF Series Adsorbent," *Industrial and Engineering Chemistry Research*, Vol. 55, pp. 4110–4117.
16. Das, S., Oyola, Y., Mayes, R.T., Janke, C.J., Kuo, L.-J., Wood, J.R., Gill, G.A., and Dai, S., 2016, "Extraction of Uranium from Seawater: Promising AI Series Adsorbent," *Industrial and Engineering Chemistry Research*, Vol. 55, pp. 4103–4109.
17. Das, S., Tsouris, C., Zhang, C., Kim, J., Brown, S., Oyola, Y., Janke, C.J., Mayes, R.T., Kuo, L.-J., Wood, J.R., Gill, G.A., and Dai, S., 2016, "Enhancing Uranium Uptake by Amidoxime Adsorbent in Seawater: An Investigation for Optimum Alkaline Conditioning Parameter," *Industrial and Engineering Chemistry Research*, Vol. 55, pp. 4294–4302.
18. Dietz, T. C., Tomaszewki, C. E., Tsinas, Z., Poster, D., Barkatt, A., Adel-Hadadi, M., Bateman, F., Cumberland, L.T., Schneider, E., Gaskel, K., LeVerne, J., Al-Sheikhly, M., 2016, "Uranium Removal from Seawater by Means of Polyamide Fibers Directly Grafted with Diallyl Oxalate through a Single-Step Solvent-Free Irradiation Process," *Industrial and Engineering Chemistry Research*, Vol. 55, pp. 4179–4186.
19. Endrizzi, F., Leggett, C. J., and Rao, L., 2016, Scientific Basis for Efficient Extraction of Uranium from Seawater. I: Understanding the Chemical Speciation of Uranium under Seawater Conditions. *Industrial and Engineering Chemistry Research*, 2016, Vol. 55, pp. 4249–4256.
20. Endrizzi, F., Melchoir, A., Tolazzi, M., and Rao, L., 2015, Complexation of Uranium(VI) with Glutarimidoxime: Thermodynamic and Computational Studies, *Dalton Transactions*, 2015, Vol. 44, pp. 13763–14180.
21. Gill, G. A., Kuo, L.-J., Janke, C. J., Wood, J. R., Mayes, R. T., Tsouris, C., Oyola, Y., Strivens, J. E., Cobb, M., Bonheyo, G., Jeters, R., Park, J., Khangaonkar, T., Addleman, R. S., Chouyyok, W., Warner, M., Peterson, Sonja, Abrecht, D. G., Das, S., Buessler, K., Breier, C., D'Alessandro, E., Pan, H.-B., and Wai, C., 2016, "The Uranium from Seawater Program at PNNL: Overview of Marine Testing, Adsorbent Characterization, Adsorbent Durability, Adsorbent Toxicity, and Deployment Studies," *Industrial and Engineering Chemistry Research*, 2016, Vol. 55, pp. 4264–4277.
22. Grant, C. D., S. O. Kang, and B. P. Hay, 2013, "Synthesis of a Hydrophilic Naphthalimidodioxime," *Journal of Organic Chemistry*, Vol. 78, pp. 7735–7740.
23. Górka, J., R. T. Mayes, L. Baggetto, G. M. Veith, and S. Da, 2013, "Sonochemical Functionalization of Mesoporous Carbon for Uranium Extraction from Seawater," *Journal of Materials Chemistry A*, Vol. 1, pp. 3016.

## 2016 ACCOMPLISHMENTS

24. Ivanov, A.S., and Bryantsev, V. S., 2015, "Assessing Ligand Selectivity for Uranium over Vanadium Ions to Aid in the Discovery of Superior Adsorbents for Extraction of UO<sub>2</sub><sup>2+</sup> from Seawater," *Dalton Transactions*, Vol. 45, No. 26, pp. 10744–10751.
25. Jacoby, M., 2012, "Extracting Uranium from Seawater," *Chemical and Engineering News*, Vol. 90, No. 36, pp. 60–63.
26. Kelley, S. P., Nuss, J. S., Rogers, R. D., 2015, "Nonstoichiometric, Protic Azolium Azolate Ionic Liquids Provide Unique Environments for N-Donor Coordination Chemistry," *Chemistry: A European Journal*, Vol. 21, pp. 17196–17199.
27. Kelley, S. P., and Rogers, R. D., 2015, "Isolation of Uranyl Dicyanamide Complexes from N-Donor Ionic Liquids," *Inorganic Chemistry*, Vol. 54, pp. 10323–10334.
28. Kennedy, Z. C., Cardenas, A. J. P., Corbey J. F., and Warner, M. G., 2016, "2,6-diiminopiperidin-1-ol: an overlooked motif relevant to uranyl and transition metal binding on poly(amidoxime) adsorbents," *Chemical Communications*, Vol. 52, pp. 8802–8805.
29. Kim, J., C. Tsouris, R. T. Mayes, Y. Oyola, T. Saito, C. J. Janke, S. Dai, E. Schneider, and D. Sachde, 2013, "Recover of Uranium from Seawater: A Review of Current Status and Future Research Needs," *Separation Science and Technology*, Vol. 48, pp. 367–387.
30. Kim, J., Oyola, Y., Tsouris, C., Cole, C.R., Mayes, R.T., Janke, J.C., and Dai, S., 2013, "Characterization of uranium uptake kinetics from seawater in batch and flow-through experiments," *Industrial and Engineering Chemistry Research*, Vol. 52, pp. 9433–9440.
31. Kim, J., Tsouris, C., Oyola, Y., Janke, C.J., Mayes, R.T., Dai, S., Gill, G., Kuo, L.-J., Wood, J., Choe, K.-Y., Schneider, E., and Lindner, H., 2014, "Uptake of uranium from seawater by amidoxime-based polymeric adsorbent: Field experiments, modeling, and economic assessment," *Industrial and Engineering Chemistry Research*, Vol. 53, pp. 6076–6083.
32. Kim, J., Y. Oyola, C. Tsouris, C. R. Hexel, R. T. Mayes, C. J. Janke, and S. Dai, 2013, "Characterization of Uranium Uptake Kinetics from Seawater in Batch and Flow-Through Experiments," *Industrial and Engineering Chemistry Research*, Vol. 52, pp. 9433–9440.
33. Kuo, L.-J., Janke, C., Wood, J. R., Strivens, J. E., Gill, G. A., 2016, "Characterization and Testing of Amidoxime-Based Adsorbent Materials to Extract Uranium from Natural Seawater," *Industrial and Engineering Chemistry Research*, 2016, Vol. 55, pp. 4285–4293.

34. Ladshaw, A.P., Das, S., Liao, W.-P., Yiaccoumi, S., Janke, C.J., Mayes, R.T., Dai, S., Tsouris, C., 2016, "Experiments and Modeling of Uranium Adsorption in the Presence of Other Ions in Simulated Seawater," *Industrial and Engineering Chemistry Research*, Vol. 55, pp. 4241–4248.
35. Lashley, M. A., Mehio, N., Nugent, J. W., Holguin, E., Do-Thanh, C.-L., Bryantsev, V. S., Dai, S., and Hancock, R. D., 2016, "Amidoximes as Ligand Functionalities for Braided Polymeric Materials for the Recovery of Uranium from Seawater," *Polyhedron*, Vol. 109, pp. 81–91.
36. Leggett, C. J., and Rao, L., 2015, "Complexation of Calcium and Magnesium with Glutarimidedioxime: Implications for the Extraction of Uranium from Seawater," *Polyhedron*, Vol. 95, pp. 54–59.
37. Leggett, C. J., Endrizzi, F., and Rao, L., 2016, "Scientific Basis for Efficient Extraction of Uranium from Seawater. II, Fundamental Thermodynamic and Structural Studies," *Industrial and Engineering Chemistry Research*, Vol. 55, pp. 4257–4263.
38. Leggett, C. J., Parker, B. F., Teat, S. J., Zhang, Z., Dau, P. D., Lukens, W., Peterson, S. M., Cardenas, A. J. P., Warner, M. G., Gibson, J. K., Arnold, J., and Rao, L., 2016, "Structural and spectroscopic studies of a rare non-oxido V(V) complex crystallized from aqueous solution," *Chemical Science*, Vol. 7, pp. 2775–2786.
39. Mayes, R. T., Gorka, J., and Dai, S., 2016, "Impact of Pore Size on the Sorption of Uranyl under Seawater Conditions," *Industrial and Engineering Chemistry Research*, Vol. 55, pp. 4339–4343.
40. Mehio, N., Johnson, J. C., Dai, S., Bryantsev, V. S., 2015, "Theoretical Study of the Coordination Behavior of Formate and Formamidoximate with Dioxovanadium(V) Cation: Implications for Selectivity towards Uranyl," *Physical Chemistry Chemical Physics*, Vol. 17, pp. 31715–31726.
41. Mehio, N., Ivanov, A. S., Ladshaw, A. P., Dai, S., Bryantsev, V. S., 2016, "Theoretical Study of Oxovanadium(IV) Complexation with Formamidoxime: Implications for the Design of Uranyl-Selective Adsorbents," *Industrial and Engineering Chemistry Research*, 2016, Vol. 55, pp. 4231–4240.
42. Mehio, N., Ivanov, S. A., Williams, N. J., Mayes, R. T., Bryantsev, V. S., Hancock, R. D., and Dai, S., 2016, "Quantifying the Binding Strength of Salicylaldoxime-Uranyl Complexes Relative to Competing Salicylaldoxime-Transition Metal Ion Complexes in Aqueous Solution: A Combined Experimental and Computational Study," *Dalton Transactions*, Vol. 45, pp. 9051–9064. (Showcasing research on the cover, Issue 22, <http://pubs.rsc.org/en/Content/ArticleLanding/2016/DT/C6DT00116E>)
43. Mehio, N., M. A. Lashley, J. W. Nugent, L. Tucker, B. Correia, C.-L. Do-Thanh, S. Dai, R. D. Hancock, and V. S. Bryantsev, 2015, "Acidity of the Amidoxime Functional Group in Aqueous Solution: A Combined Experimental and Computational Study," *Journal of Physical Chemistry B*, Vol. 119, No. 8, pp. 3567–3576.

## 2016 ACCOMPLISHMENTS

44. Oyola, Y., and Dai, S., 2016, "High Surface-Area Amidoxime-based Polymer Fibers co-Grafted with Various Acid Monomers Yielding Increased Adsorption Capacity for the Extraction of Uranium from Seawater," *Dalton Transactions*, Vol. 45, pp. 8824–8834.
45. Oyola, Y., Janke, C.J., and Dai, S., 2016, "Synthesis, Development and Testing of High Surface Area Polymer-based Adsorbents for the Selective Recovery of Uranium from Seawater," *Industrial and Engineering Chemistry Research*, Vol. 55, pp. 4149–4160.
46. Pan, H.-B., Kuo, L.-J., Miyamoto, N., Wood, J. R., Strivens, J. E., Gill, G. A., Janke, C. J., and Wai, C. M., 2016, "Elution of Uranium and Transition Metals from Amidoxime-Based Polymer Adsorbents for Sequestering Uranium from Seawater," *Industrial and Engineering Chemistry Research*, Vol. 55, pp. 4313–4320.
47. Pan, H.-B., Kuo, L.-J., Wai, C. M., Miyamoto, N., Joshi, R., Wood, J. R., Strivens, J. E., Janke, C. J., Oyola, Y., Das, S., Mayes, R. T., and Gill, G. A., 2016, "Elution of Uranium and Transition Metals from Amidoxime-Based Polymer Adsorbents for Sequestering Uranium from Seawater," *Industrial and Engineering Chemistry Research*, Vol. 55, pp. 4313–4320.
48. Pan, H.-B., Kuo, L.-J., Wood, J. R., Strivens, J. E., Gill, G. A., Janke, C. J., and Wai, C. M., 2015, "Towards Understanding KOH Conditioning of Amidoxime-based Polymer Adsorbents for Sequestering Uranium from Seawater," *RSC Advances*, Vol. 5, pp. 100715–100721.
49. Pan, H.-B., Kuo, L.-J., Wood, J., Strivens, J., Gill, G. A., Janke, C. J., and Wai, C. M., 2015, "Towards Understanding KOH Conditioning of Amidoxime-based Polymer Adsorbents for Sequestering Uranium from Seawater," *RSC Advances*, Vol. 5, pp. 100715–100721.
50. Pan, H.B., Liao, W.S., Wai, C.M., Oyola, Y., Janke, C.J., Tian, G.X., and Rao, L.F., 2014, "Carbonate-H<sub>2</sub>O<sub>2</sub> leaching for sequestering uranium from seawater," *Dalton Transactions*, Vol. 43, No. 28, pp. 10713–10718.
51. Pan, H.-B., Liao, W., Wai, C. M., Oyola, Y., Janke, C., Tian, G., and Rao, L., 2014, "Carbonate-H<sub>2</sub>O<sub>2</sub> leaching for sequestering uranium from seawater," *Dalton Transactions*, Vol. 43, No. 28, pp. 10653–11078.
52. Park, J., Gill, G. A., Strivens, J. E., Kuo, L.-J., Jeters, R. T., Avila, A., Wood, J. R., Schlafer, N. J., Janke, C. J., Miller, E. A., Thomas, M., Addleman R. S., and Bonheyo, G. T., 2016, "Effect of Biofouling on the Performance of Amidoxime-based Polymeric Uranium Adsorbents," *Industrial and Engineering Chemistry Research*, Vol. 55, pp. 4328–4338.

53. Park, J., Jeters, R. T., Kuo, L.-J., Strivens, J. E., Gill, G. A., Schlafer, N. J., and Bonheyo, G. T., 2016, "Potential Impact of Seawater Uranium Extraction on Marine Life," *Industrial and Engineering Chemistry Research*, Vol. 55, pp. 4278–4284.
54. Parker, B. F., Knight, A. S., Vukovic, S., Arnold, J., and Francis, M. B., 2016, "A Peptoid-Based Combinatorial and Computational Approach to Developing Ligands for Uranyl Sequestration from Seawater," *Industrial and Engineering Chemistry Research*, Vol. 55, pp. 4187–4194.
55. Piechowicz, M., Abney, C. W., Zhou, X., Thacker, N. C., Li, Z., and Lin, W., 2016, "Design, Synthesis, and Characterization of a Bifunctional Chelator with Ultrahigh Capacity for Uranium Uptake from Seawater Simulant," *Industrial and Engineering Chemistry Research*, Vol. 55, pp. 4170–4178.
56. Priest, C., Tian, Z. Q., and Jiang, D. E., 2016, "First-principles Molecular Dynamics Simulation of the  $\text{Ca}_2\text{UO}_2(\text{CO}_3)_3$  Complex in Water," *Dalton Transactions*, Vol. 45, pp. 9812–9819.
57. Rao, L., 2012, "Application of Radiation Grafting: Progress and Status of the Extraction of Uranium from Seawater in Japan," *Journal of Isotopes*, Vol. 25, No. 3, pp. 129–139.
58. Saito, T., Brown, S., Chatterjee, S., Kim, J., Tsouris, C., Mayes, R., Kuo, L.-J., Gill, G., Oyola, Y., Janke, C.J., and Dai, S., 2014, "Uranium Recovery from Seawater: Development of Fiber Adsorbents Prepared via Atom-Transfer Radical Polymerization," *Journal of Materials Chemistry A*, Vol. 2, pp. 14674–14681.
59. Sun, X., Tian, G., Xu, C., Rao, L., Vukovic, S., Kang, S. O., and Hay, B. P., 2014, "Quantifying the binding strength for U(VI) with phthalimidedioxime in comparison with glutarimidedioxime," *Dalton Transactions*, Vol. 43, No. 2, pp. 551–557.
60. Sun, X., Xu, C., Tian, G., and Rao, L., 2013, "Complexation of glutarimidedioxime with Fe(III), Cu(II), Pb(II), and Ni(II), the competing ions for the sequestration of U(VI) from seawater," *Dalton Transactions*, Vol. 42, pp. 14621–14627.
61. Sun, X., Zanonato, P., Di Bernardo, P., Zhang, Z., and Rao, L., 2015, "Sorption of Uranium and Other Metal Ions on Amine-Functionalized Silica Materials," *Separation Science and Technology*, Vol. 50, pp. 2769–2775.
62. Tian, G., S. J. Teat, and L. Rao, 2013, "Thermodynamic Studies of U(VI) Complexation with Glutardiamidoxime for Sequestration of Uranium from Seawater," *Dalton Transactions*, Vol. 42, pp. 5690–5696.

## 2016 ACCOMPLISHMENTS

63. Tian, G., S. J. Teat, Z. Zhang, and L. Rao, 2012, "Sequestering Uranium from Seawater: Binding Strength and Modes of Uranyl Complexes with Glutarimidedioxime," *Dalton Transactions*, Vol. 41, No. 38, pp. 11579–11586 (Journal Cover October 2012).
64. Vukovic, S., and B. P. Hay, 2013, "De Novo Structure-Based Design of Bis-Amidoxime Uranophiles," *Inorganic Chemistry*, Vol. 52, pp. 7805–7801.
65. Vukovic, S., B. P. Hay, and V. S. Bryantsev, 2015, "Predicting Stability Constants for Uranyl Complexes Using Density Functional Theory," *Inorganic Chemistry*, Vol. 54, No. 8, April 2, 2015, pp. 3995–4001.
66. Vukovic, S., L. A. Watson, R. Custelcean, S. O. Kang, and B. P. Hay, 2012, "How Amidoxime Binds Uranyl Cation," *Inorganic Chemistry*, Vol. 51: pp. 5502–5512.
67. Wood, J. R., Gill, G. A., Kuo, L.-J., Strivens, J. E., and Choe K.-Y., 2016, "Comparison of Analytical Methods for the Determination of Uranium in Seawater using Inductively Coupled Plasma Mass Spectrometry," *Industrial and Engineering Chemistry Research*, Vol. 55, pp. 4344–4350.
68. Yue, Y. F., Xun, X. G., Mayes, R. T., Kim, J., Fulvio, P. F., Ziao, Z. A., Brown, S., Tsouris, C., Oyola, Y., and Dai, S., 2013, "Polymer-coated nanoporous carbons for trace seawater uranium adsorption," *Science China Chemistry*, Vol. 56, No. 11, pp. 1510–1515.
69. Yue, Y., Mayes, R. T., Gill, G., Kuo, L.-J., Wood, J., Binder, A., Brown, S., and Dai, S., 2015, "Macroporous Monoliths for Trace Metal Extraction from Seawater," *RSC Advances*, Vol. 5, pp. 50005–50010.
70. Yue, Y., Zhang, C., Tang, Q., Mayes, R. T., Liao, W.-P., Liao, C., Tsouris, C., Stankovich, J. Chen, J., Hensley, D., Abney, C., Jiang, D. E., Brown, S., and Dai, S., 2016, "A Poly(acrylonitrile)-Functionalized Porous Aromatic Framework Synthesized by Atom-Transfer Radical Polymerization for Extraction of Uranium from Seawater," *Industrial and Engineering Chemistry Research*, Vol. 55, pp. 4125–4129.
71. Yue, Y. F., Mayes, R. T., Kim, J., Fulvio, P.F., Sun, X. G., Tsouris, C., Chen, J., Brown, S., and Dai, S., 2013, "Seawater uranium sorbents: Preparation from a mesoporous copolymer initiator by Atom-Transfer Radical Polymerization," *Angewandte Chemie International Edition*, Vol. 52, No. 50, pp. 13458–13462.

## FUNDAMENTAL SEPARATION DATA AND METHODS

1. Boland, K. S., D. E. Hobart, S. A. Kozimor, M. M. MacInnes, and B. L. Scott, 2013, "The Coordination Chemistry of Trivalent Lanthanides with Diphenyldithiophosphate Anions," *Polyhedron*, Vol. 67, pp. 540–548.
2. Bridges, N. J., and L. Roy, 2013, *Computational and Spectroscopic Investigation of the DTPA Complexes*, SRNL-TR-2011-00185, Rev. 0, Savannah River National Laboratory, August 30.

3. Bryan S. A., A. J. Casella, A. M. Lines, G. L. Nelson, and J. M. Bello, 2015, "Advances in On-Line Monitoring for Measurement within Nuclear Fuel Reprocessing Streams" *Proceedings of GLOBAL 2015: 21st International Conference and Exhibition*, Paris, France, September 21–24, 2015.
4. Bryan, S. A., A. J. Casella, and T. G. Levitskaia, 2014, "On-Line Monitoring for Process Control and Safeguarding of Radiochemical Streams at Spent Fuel Reprocessing Plants," *Proceedings of the IAEA International Safeguards Symposium: Linking Strategy, Implementation and People*, Vienna, Austria, October 20–24, 2014.
5. Casella A. J., L. R. Hylden, E. L. Campbell, T. G. Levitskaia, J. M. Peterson, F. N. Smith, and S. A. Bryan, 2015, "Development of On-Line Spectroscopic pH Monitoring for Nuclear Fuel Reprocessing Plants: Weak Acid Schemes," *Analytical Chemistry*, Vol. 87, No. 10, pp. 5139–5147.
6. Casella A. J., Lines, A. M., Nelson G. L., Bello J. M., and Bryan, S. A., 2016, "MicroRaman Measurements for Nuclear Fuel Reprocessing Applications" *Procedia Chemistry*, Vol. 21, No. 99, pp. 466–472.
7. Collins, E. D., G. D. DelCul, B. B. Spencer, R. R. Brunson, J. A. Johnson, D. S. Terekhov, and N. V. Emmanuel, 2012, "Process Development Studies for Zirconium Recovery/Recycle, from Used Nuclear Fuel Cladding," *Procedia Chemistry*, Vol. 7, pp. 72–76.
8. Cynthia A. Schroll, Amanda M. Lines, William R. Heineman, and Samuel A. Bryan, 2016, "Absorption Spectroscopy for Quantitative Prediction of Lanthanide Concentrations in 3 LiCl – 2 CsCl Eutectic at 723 K," *Analytical Methods*, Vol. 8, pp. 7731–7738.
9. DelCul, G. D., J. A. Johnson, B. B. Spencer, and E. D. Collins, 2013, "Roadmap for Development of an Advanced Head-End Process," *Proceedings from GLOBAL 2013*, Salt Lake City, Utah, September 29–October 4, 2013.
10. Frost, A., and W. Bratton, 2015, *Design Analysis of Tritium Graphene Oxide Membrane System*, KUR-BATT04-001-RPT-001, Rev. A, Kurion, Richland, WA.
11. Gandhir, A., Wardle, K. E., 2012, "CFD analysis of fluid flow above the upper weir of an annular centrifugal contactor," *Separation Science and Technology*, Vol. 47, pp. 1–10.
12. Gray, M. F., P. R. Zalupski, and M. Nilsson, 2013, "Determination of Activity Coefficients Of Di-(2-Ethylhexyl)phosphoric Acid Dimer in Select Organic Solvents Using Vapor Phase Osmometry," *Solvent Extraction and Ion Exchange*, Vol. 31, pp. 5.
13. Griffiths, T. L., L. R. Martin, P. R. Zalupski, J. Rawcliffe, M. J. Sarsfield, N. D. M. Evans and C. A. Sharrad, 2013, "Understanding the Solution Behaviour of Minor Actinides in the Presence of EDTA, Carbonate and Hydroxide Ligands," *Inorganic Chemistry*, Vol. 52, pp. 3728–3737.
14. Grimes, T. S., P. R. Zalupski, and L. R. Martin, 2014, "Features of the Thermodynamics of Trivalent Lanthanide/Actinide Distribution Reactions by Tri-n-Octylphosphine Oxide and Bis(2-EthylHexyl) Phosphoric Acid," *Journal of Physical Chemistry B*, Vol. 118, No. 44, pp. 12725–12733.

## 2016 ACCOMPLISHMENTS

15. Grimes, T. S., R. D. Tillotson, and L. R. Martin, 2014, "Trivalent Lanthanide/Actinide Separation Using Aqueous-Modified TALSPEAK Chemistry," *Solvent Extraction and Ion Exchange*, Vol. 32, No. 4, pp. 378–390.
16. Guoxin Tian, Z. Zhang, L. R. Martin, and L. Rao, 2015, "Complexation of Curium(III) with DTPA at 10–70°C: Comparison with Eu(III)/DTPA in Thermodynamics, Luminescence and Coordination Modes," *Inorganic Chemistry*, Vol. 54, No. 4, pp. 1232–1239.
17. Heathman, C.R., Grimes, T.S., and Zalupski, P.R., 2016, "Thermodynamic and Spectroscopic Studies of Trivalent *f*-element Complexation with Ethylenediamine-*N,N'*-di(acetylglycine)-*N,N'*-diacetic acid," *Inorganic Chemistry*, Vol. 55, pp. 2977–2985.
18. Jaffe, J. E., R. M. Van Ginhoven, and W. Jiang, 2012, "Interstitial and Substitutional Zirconium in SrTiO<sub>3</sub>," *Computational Materials Science*, Vol. 53, pp. 153–157.
19. Jiang, W., and R. M. Van Ginhoven, 2012, *Chemical and Charge Imbalance Induced by Radionuclide Decay: Effects on Waste Form Structure*, PNNL-20312-3, Pacific Northwest National Laboratory.
20. Jiang, W., M. E. Bowden, Z. Zhu, P. A. Jozwik, J. Jagielski, and A. Stonert (2012). "Defects and Minor Phases in O<sup>+</sup> and Zr<sup>+</sup> Ion Co-implanted SrTiO<sub>3</sub>," *Industrial and Engineering Chemistry Research*, Vol. 51, pp. 621–628.
21. Jiang, W., R. M. Van Ginhoven, and D. M. Strachen, 2010, *Chemical and Charge Imbalance Induced by Radionuclide Decay: Effects on Waste Form Structure*, PNNL-20049, Pacific Northwest National Laboratory.
22. Jiang, W., R. M. Van Ginhoven, L. Kovarik, J. E. Jaffe, and B. W. Arey, 2012, "Superlattice Structure and Precipitates in O<sup>+</sup> and Zr<sup>+</sup> Ion Co-implanted SrTiO<sub>3</sub>: a Model Waste Form for <sup>90</sup>Sr," *Journal of Physical Chemistry C*, Vol. 116, pp. 16709–16715.
23. Law, J. D., N. R. Soelberg, T. A. Todd, J. Tripp, C. Pereira, M. A. Williamson, W. L. Ebert, R. T. Jubin, B. A. Moyer, J. D. Vienna, G. J. Lumetta, J. V. Crum, T. S. Rudisill, J. Bresee, C. Phillips, B. Willis, P. Murray, and S. Bader, 2014, *Separation and Waste Form Campaign Full Recycle Case Study*, FCRD-SWF-2013-000380, Rev. 1, Idaho National Laboratory.
24. Li, X., Z. Zhang, L. R. Martin, S. Luo, and L. Rao, 2015, "Effect of Temperature on the Protonation of *N*-(2-hydroxyethyl)ethylenediamine-*N,N'*-triacetic Acid in Aqueous Solutions: Potentiometric and Calorimetric Studies," *Journal of Chemical Thermodynamics*, Vol. 85, pp. 35–41.
25. Mezyk, S. P., B. J. Mincher, C. Ekberg, and G. Skarnemark, 2013, "Alpha and Gamma Radiolysis of Nuclear Solvent Extraction Ligands Used for An(III) and Ln(III) Separations," *Journal of Radioanalytical and Nuclear Chemistry*, Vol. 296, pp. 711–715.
26. Mincher, B. J., and S. P. Mezyk, 2013, "Development of a Method to Measure the Rate Constant for the Reaction of •NO<sub>3</sub> with Metal-Complexed CMPO in the Organic Phase," FCRD-SWF-2013-000231, July 25.

27. Mincher, B. J., S. P. Mezyk, G. Elias, G. S. Groenewold, and L. G. Olson, 2013, "The Radiation Chemistry of CMPO: Part 1. Gamma Radiolysis," *Solvent Extraction and Ion Exchange*, Vol. 31, pp. 715–730.
28. Mincher, B. J., S. P. Mezyk, G. Elias, G. S. Groenewold, J. A. Laverene, M. Nilsson, and J. Pearson, 2014, "The Radiation Chemistry of CMPO: Part 2. Alpha Radiolysis," *Solvent Extraction and Ion Exchange*, Vol. 32, No. 2, pp.167–178.
29. Nee, K., S. Bryan, T. Levitskaia, J. Wei-Ju Kuo, and M. Nilsson, 2015, "Combinations of NIR and Raman spectroscopy for Improved Monitoring of Material in Used Nuclear Fuel Separation Processes," submitted to *Chemical Engineering Science*.
30. Nishihama, S., R. P. Witty, L. R. Martin, and K. L. Nash, 2013, "Thermodynamic Features of Benzene-1,2-Diphosphonic Acid Complexes with Several Metal Ions," *Solvent Extraction and Ion Exchange*, Vol. 31, pp. 370–383.
31. Peterman, D., Geist, A., Mincher, B., Modolo, G., Galan M., Olson, L., and McDowell, R., 2016, "Performance of an i-SANEX system based on a water-soluble BTP under continuous irradiation in a  $\gamma$ -radiolysis test loop," *Industrial and Engineering Chemistry Research*, Vol. 55, No. 39, pp. 10427–10435.

#### REFERENCE TECHNOLOGIES AND ALTERNATIVES

1. Li, X., Z. Zhang, L. R. Martin, S. Luo, and L. Rao, 2016, "Complexation of  $\text{NpO}_2^+$  with (2-Hydroxyethyl) ethylenediaminetriacetic Acid (HEDTA) in Aqueous Solutions: Thermodynamic Studies and Structural Analysis," *RSC Advances*, Vol. 6, pp. 114916–114926.
2. Roy, L. E., and Martin, and L. R., 2016, "Theoretical Prediction of Coordination Environments and Stability Constants of Lanthanum Lactate Complexes in Solution," *Dalton Transactions*, Vol. 45, No. 39, pp. 15517–15522.
3. Schroll, C.A., A. M. Lines, W. R. Heineman, and S. A. Bryan, 2016, "Absorption Spectroscopy for Quantitative Prediction of Lanthanide Concentrations in 3 LiCl – 2 CsCl Eutectic at 723 K," *Analytical Methods*, Vol. 8, pp. 7731–7738.
4. Taylor, C. D., and X. Y. Liu, 2013, "Investigation of Structure and Composition Control Over Active Dissolution of Fe-Tc Binary Metallic Waste Forms by Off-Lattice Kinetic Monte-Carlo Simulation," *Journal of Nuclear Materials*, Vol. 434, pp. 382–388.
5. Van Ginhoven, R. M., W. Jiang, and C. Stanek, 2013, *DRAFT Roadmap for Understanding  $\beta$  Decay Effects of Fission Products in Waste Forms*, PNNL-22363, Pacific Northwest National Laboratory.
6. Vedantam, S., K. E. Wardle, T. V. Tamhane, V. V. Ranade, and J. B. Joshi, 2012, "CFD Simulation of Annular Centrifugal Extractors," (invited review article) *International Journal of Chemical Engineering*, Article No. 759397.
7. Wardle, K. E., 2013, "Hybrid Multiphase CFD Simulation for Liquid-Liquid Interfacial Area Prediction in Annular Centrifugal Contactors," *Proceedings from GLOBAL 2013*, Salt Lake City, Utah, September 29–October 4, 2013.

## 2016 ACCOMPLISHMENTS

8. Wardle, K. E., and H. Weller, 2013, "Hybrid Multiphase CFD Solver for Coupled Dispersed/Segregated Flows in Liquid-Liquid Extraction," *International Journal of Chemical Engineering*, Article No. 128936.
9. Wardle, K. E., and Lee, T., 2013, "Finite element lattice boltzmann simulations of free surface flow in a concentric cylinder," *Computers and Mathematics with Applications*, Vol. 65, pp. 230–238.
10. Zapol, P., H. He, K. D. Kwon, and L. J. Criscenti, 2013, "First-Principles Study of Hydrolysis Reaction Barriers in a Sodium Borosilicate Glass," *International Journal of Applied Glass Science*, Vol. 4, pp. 395–407.
11. Zarzana, C. A., D. R. Peterman, G. S. Groenewold, L. G. Olson, R. G. McDowell, W. F. Bauer, and S. J. Morgan, 2015, "Investigation of the Impacts of Gamma Radiolysis on an Advanced TALSPEAK Separation," *Separations Science and Technology*, Vol. 50, No. 18, pp. 2836–2843.

### SIGMA TEAM FOR ADVANCED ACTINIDE RECYCLE

1. Braley, J. C., D. McAlister, E. P. Horwitz, and K. L. Nash, 2013, "Explorations of TALSPEAK Chemistry in Extraction Chromatography: Comparisons of TTHA with DTPA and HDEHP with HEH[EHP]," *Solvent Extraction and Ion Exchange*, Vol. 31, No. 2, pp. 107–121.
2. Braley, J. C., G. J. Lumetta, and J. C. Carter, 2013, "Combining CMPO and HEH[EHP] for Separating Trivalent Lanthanides from the Transuranic Elements," *Solvent Extraction and Ion Exchange*, Vol. 31, No. 6, pp. 567–577.
3. Brigham, D., 2013, "Lanthanide-Polyaminopolycarboxylate Complexation Kinetics in High Lactate Media: Investigating the Aqueous Phase of TALSPEAK," Ph.D. Dissertation, Washington State University, May.
4. Brown, M. A., Kropf, A. J., Paulenova, A., and Gelis. A. V., 2014, "Aqueous Complexation of Citrate with Neodymium(III) and Americium(III): A Study by Potentiometry, Absorption Spectrophotometry, Microcalorimetry, and XAFS," *Dalton Transactions*, Vol. 43, pp. 6446–6454.
5. Brown, M. A., Wardle, K. E., Lumetta, G. J., and Gelis. A. V., 2016, "Accomplishing Equilibrium in ALSEP: Demonstrations of Modified Process Chemistry on 3-D Printed Enhanced Annular Centrifugal Contactors," *Procedia Chemistry*, Vol. 21, pp. 167–173.
6. Bruffey, S. H., R. T. Jubin, J. A. Jordan, 2016, "Capture of Elemental and Organic Iodine from Dilute Gas Streams by Silver-exchanged Mordenite," *Procedia Chemistry*, Vol. 21, pp. 293–299.
7. Bryantsev, V. S. and B. P. Hay, 2015, "Theoretical prediction of Am(III)/Eu(III) Selectivity to Aid the Design of Actinide-Lanthanide Separation Agents," *Dalton Transactions*, Vol. 44, pp. 7935–7942.
8. Burns, J. D., and Moyer, B. A., 2016, "Group Hexavalent Actinide Separations: A New Approach to Used Nuclear Fuel Recycling," *Inorganic Chemistry*, Vol. 55, No. 17, pp. 8913–8919.

9. Carrick, J. D., Tai, S., and Williams, N. J., 2014, "Synthesis of Bis-1,2,4-triazines via Telescoped Condensation of [1,10]-Phenanthroline-2,9-dicarbonitrile with Aromatic 1,2-Dicarbonyls," *Journal of Heterocyclic Chemistry*, Vol. 5, No. 1, pp. 307–312.
10. Dares, C. J., A. M. Lapides, B. J. Mincher, and T. J. Meyer, 2015, "Electrochemical Oxidation of  $^{243}\text{Am}(\text{III})$  in Nitric acid by a Terpyridyl-Derivatized Electrode," *Science*, Vol. 350, No. 6261, pp. 652–655.
11. De Sahb, C., L. A. Watson, J. Nadas, and B. P. Hay, 2013, "Design Criteria for Polyazine Extractants to Separate An(III) from Ln(III)," *Inorganic Chemistry*, Vol. 52, No. 18, pp. 10632–10642.
12. Delmau, L. H., K. N. Tevepaugh, and M. E. Freiderich, 2013, *Trivalent Actinide-Lanthanide Separation Using Bis-Dithio Phosphinic Acids and Bis Triazinyl Pyridine Derivatives*, FCRD-SWF-2013-000274, Oak Ridge National Laboratory, August 30.
13. Freiderich, M. E., D. R. Peterman, J. R. Klaehn, P. Marc, and L. H. Delmau, 2014, "Chemical Degradation Studies on a Series of Dithiophosphinic Acids (DPAHs)," *Industrial and Engineering Chemistry Research*, Vol. 53, No. 9, pp. 3606–3611.
14. Gelis, A. V., and Lumetta, G. J., 2014, "Actinide Lanthanide Separation Process—ALSEP," *Industrial and Engineering Chemistry Research*, Vol. 53, pp. 1624–1631.
15. Grimes, T. S., and K. L. Nash, 2014, "Acid Dissociation Constants and Rare Earth Stability Constants for DTPA," *Journal of Solution Chemistry*, Vol. 43, No.2, pp. 298–313.
16. Gullekson, B. J., A. Breshears, M. A. Brown, J. B. Essner, G. A. Baker, J. R. Walensky, A. Paulenova, and A. V. Gelis, 2016, "Extraction of Water and Speciation of Trivalent Lanthanides and Americium in Organophosphorous Extractants," *Inorganic Chemistry*, Vol. 55, No. 24, pp. 12675–12685.
17. Hay, B. P., A. M. Panagopoulos, L. H. Delmau, R. Custelcean, B. A. Moyer, L. A. Watson, 2015, "Ligand Preorganization Leads to 108-fold Increase in Extraction Efficiency of Trivalent f-block Metal Ions by Lipophilic Picolinamides," submitted to *Inorganic Chemistry*.
18. Heathman, C., 2013, "Functionalization Characterization and Evaluation of Dipycolinate Derivatives with f- Element Complexes," Ph.D. Dissertation, Washington State University, September.
19. Ivanov, A. S., and Bryantsev, V. S., 2016, "A Computational Approach to Predicting Ligand Selectivity for the Size-Based Separation of Trivalent Lanthanides," *European Journal of Inorganic Chemistry*, pp. 3474–3479.
20. Jensen, M. P., Chiarizia, R., Shkrob, I. A., Ulicki, J. S., Spindler, B. D., Murphy, D. J., Hossain, M., Roca-Sabio, A., Platas-Iglesias, C., de Blas, A., and Rodríguez-Blas, T., 2014, "Aqueous Complexes for Efficient Size-based Separation of Americium from Curium," *Inorganic Chemistry*, Vol. 53, pp. 6003–6012.
21. Jensen, M. P., Chiarizia, R., Ulicki, J. S., Spindler, B. D., Murphy, D. J., Hossain, M. M., Roca-Sabio, A., de Blas, A., and Rodríguez-Blas, T., 2015, "Solvent Extraction Separation of Trivalent Americium from Curium and the Lanthanides," *Solvent Extraction and Ion Exchange*, Vol. 33, No. 4, pp. 329–345.

## 2016 ACCOMPLISHMENTS

22. Johnson, A. T. and K. L. Nash, 2015, "Mixed Monofunctional Extractants for Trivalent Actinide/Lanthanide Separations: TALSPEAK MME," *Solvent Extraction and Ion Exchange*, Vol. 33, No. 7, pp. 642–655.
23. Johnson, J., and K. L. Nash, 2013, "A Combined Cyanex-923/HEH[EHP]/Dodecane Solvent for Recovery of Transuranic Elements from Used Nuclear Fuel," *Proceedings of GLOBAL 2013*, Salt Lake City, Utah, September 29–October 4, 2013, Paper 8247.
24. Krahn, E. O. and K. L. Nash, 2015, "Insights in Lanthanide-HEH[EHP] Exchange Dynamics in Advanced TALSPEAK Systems," *Proceedings of GLOBAL 2015*, Paris, France, September 20–24, 2015, Paper 5360.
25. Lapka, J. L. and K. L. Nash, 2015, "Advanced TALSPEAK Separations Using a Malonate Buffer System," *Solvent Extraction and Ion Exchange*, Vol. 33, No., 4, pp. 346–361.
26. Launiere, C. A., and Gelis, A. V., 2016, "High Precision Droplet-Based Microfluidic Determination of Americium(III) and Lanthanide(III) Solvent Extraction Separation Kinetics," *Industrial and Engineering Chemistry Research*, Vol. 55, No. 7, pp. 2272–2276.
27. Law, J., Mincher, B., Garn, T., Greenhalgh, M., Schmitt, N., and Rutledge, V., 2014, "Development and Testing of an Americium/Lanthanide Separation Flowsheet Using Sodium Bismuthate," *Proceedings of ICAPP*, Charlotte, NC, Apr. 4–6, 2014, American Nuclear Society, La Grange Park, IL, Paper 14040.
28. Leggett, C. J., and M. P. Jensen, 2013, "Studies of Size-Based Selectivity in Aqueous Ternary Complexes of Americium(III) or Lanthanide(III) Cations," *Journal of Solution Chemistry*, in press.
29. Lumetta, G. J., D. Neiner, S. I. Sinkov, J. C. Carter, J. C. Braley, S. L. Latesky, A. V. Gelis, P. Tkac, G. F. Vandegrift, 2011, "Combining Neutral and Acidic Extractants for Recovering Transuranic Elements from Nuclear Fuel," *Proceedings of the 19<sup>th</sup> International Solvent Extraction Conference*, L. F. Valenzuela, B. A. Moyer, Eds., Gecamin Ltd: Santiago, Chile, Paper No. 68.
30. Lumetta, G. J., A. J. Casella, B. M. Rapko, T. G. Levitskaia, N. K. Pence, J. C. Carter, C. M. Niver, and M. R. Smoot, 2015, "An Advanced TALSPEAK Concept Using 2-Ethylhexylphosphonic Acid Mono-2-ethylhexyl Ester as the Extractant," *Solvent Extraction and Ion Exchange*, Vol. 33, pp. 211–223.
31. Lumetta, G. J., A. V. Gelis, J. C. Braley, J. C. Carter, J. W. Pittman, M. G. Warner, and G. F. Vandegrift, 2013, "The TRUSPEAK Concept: Combining CMPO and HDEHP for Separating Trivalent Lanthanides from the Transuranic Elements," *Solvent Extraction and Ion Exchange*, Vol. 31, No.3, pp. 223–236.
32. Lumetta, G. J., A. V. Gelis, J. C. Carter, C. M. Niver, and M. R. Smoot, 2014, "The Actinide-Lanthanide Separation Process," *Solvent Extraction and Ion Exchange*, Vol. 32, No. 4, pp. 333–347.
33. Lumetta, G. J., Casella, A. J., and Gelis, A. V., 2015, "Kinetics Challenges Associated with Minor Actinide Separations using 2-Ethylhexylphosphonic Acid Mono-2-ethylhexyl Ester," *Proceedings of GLOBAL 2015*, Paris, France, September 21–24, 2015, Société Française d'Énergie Nucléaire, Paris, France.
34. Lumetta, G. J., Levitskia, T. G., Rapko, B. M., Carter, J. C., Niver, C. M., and Gelis, A. V., 2014, "Development of the Actinide-Lanthanide Separation (ALSEP) Process," *Proceedings of the 20th International Solvent*

- Extraction Conference*, Würzburg, Germany, Sept. 7–11, 2014, DECHEMA, Gesellschaft für Chemische Technik und Biotechnologie e.V., Frankfurt am Main, Germany, 2014, Paper No. 8709, pp. 557–562.
35. Marie, C., E. O. Krahn, and K. L. Nash, 2014, “Probing Ligand Exchange Kinetics in Actinide/Lanthanide Solvent Extraction Systems using NMR Spectrometry,” *Proceedings of the 20th International Solvent Extraction Conference*, Würzburg, Germany, Sept. 7–11, 2014, DECHEMA, Gesellschaft für Chemische Technik und Biotechnologie e.V., Frankfurt am Main, Germany, 2014, Paper No. 4850.
  36. Mincher, B. J., N. C. Schmitt, and T. S. Grimes, 2016, “The Persistence of Am(VI) in Nitric Acid Solution,” submitted to *Solvent Extraction and Ion Exchange*.
  37. Mincher, B. J., N. C. Schmitt, B. K. Schuetz, T. C. Shehee, D. T. Hobbs, 2015, “Recent Advances in *f*-Element Separations Based on a New Method for the Production of Pentavalent Americium in Acidic Solution,” *RSC Advances*, Vol. 5, pp. 27205–27210.
  38. Mincher, B. J., N. C. Schmitt, R. D. Tillotson, G. Elias, B. M. White, and J. D. Law, 2013, “Characterizing Diamylmethylphosphonate (DAAP) as an Americium Ligand for Nuclear Fuel Cycle Applications,” *Solvent Extraction and Ion Exchange*, in press.
  39. Mincher, B. J., R. D. Tillotson, J. D. Law, T. Garn, V. Rutledge, and N. C. Schmitt, 2015, “The Solvent Extraction of Am(VI) Using Centrifugal Contactors,” submitted to *Journal of Radioanalytical Nuclear Chemistry*, June 2015.
  40. Mincher, B. J., Schmitt, N. C., Tillotson, R. D., Elias, G., White, B. M., and Law, J. D., 2014, “Characterizing Diamylmethylphosphonate (DAAP) as an Americium Ligand for Nuclear Fuel Cycle Applications,” *Solvent Extraction and Ion Exchange*, Vol. 32, pp. 153–166.
  41. Mincher, B. J., Tillotson, R. D., Law, J. D., Garn, T., Rutledge, V., and Schmitt, N. C., 2016, “The Solvent Extraction of Am(VI) Using Centrifugal Contactors,” *Journal of Radioanalytical Nuclear Chemistry*, Vol. 307, pp. 1833–1836.
  42. Moyer, B. A., Lumetta, G. L., and Mincher, B. J., 2015, “Minor actinide separation in the reprocessing of spent nuclear fuels: recent advances in the United States,” Chapter 11, *Reprocessing and Recycling of Spent Nuclear Fuels*, Oxford: Woodhead Publishing, ISBN: 978-1-78242-212-9, pp. 289–312.
  43. Nash, K. L., 2013, “Advancing the Scientific Basis of Trivalent Actinide-Lanthanide Separations,” Paper 8246, *Proceedings from GLOBAL 2013*, Salt Lake City, Utah, September 29–October 4, 2013.
  44. Nash, K. L., 2015, “The Chemistry of TALSPEAK: A Review of the Science,” *Solvent Extraction and Ion Exchange*, Vol. 33, No. 1, pp. 1–57.
  45. Nash, K. L., and Heathman, C., 2014, “New Dicolinic Acid Derivatives for Actinide-Lanthanide Separations,” *Proceedings of the 20th International Solvent Extraction Conference*, Würzburg, Germany, Sept. 7–11, 2014, DECHEMA, Gesellschaft für Chemische Technik und Biotechnologie e.V., Frankfurt am Main, Germany, 2014, Paper No. 8947.

## 2016 ACCOMPLISHMENTS

46. Nash, K. L., G. J. Lumetta, and J. D. Vienna, 2013, "Irradiated Nuclear Fuel Management: Resource Versus Waste," Chapter 5, *Radioactive Waste Management and Contaminated Site Clean-Up*. W. E. Lee, M. I. Ojovan, and C. M. Jantzen, Eds. Oxford: Woodhead Publishing Ltd, Vol. 48, ed. WE Lee, MI Ojovan and CM Jantzen, pp. 145–170.
47. Nash, K. L., J. L. Lapka, S. Wahu, G. Ferru, C. R. Heathman, and A. T. Johnson, 2015, "Improving TALSPEAK Separations: New Knowledge Leading to Alternate Extractants, Holdback Reagents, and Buffers," *Proceedings of GLOBAL 2015*, September 20–24, 2015, Paris, France, Paper 5128.
48. Pillon, S., Somers, J., Grandjean, S., and Lacquement, J., 2003, "Aspects of fabrication of curium-based fuels and targets," *Journal of Nuclear Materials*, Vol. 320, pp. 36–43.
49. Sinkov, S. I., Lumetta, G. J. "Americium(III) oxidation by copper(iii) periodate in nitric acid solution as compared with the action of bi(v) compounds of sodium, lithium, and potassium," *Radiochimica Acta*, 2015, Vol. 103, No. 8, pp. 541–552.
50. Tai, S., Marchi, S. V., Carrick, J. D., 2014, "Efficient preparation of pyridinyl-1,2,4-triazines via telescoped condensation with diversely functionalized 1,2-dicarbonyls," *Journal of Heterocyclic Chemistry*, Vol. 53, No. 4, pp. 1138–1146.
51. Tai, S., N. J. Williams, J. D. Carrick, 2015, "Synthesis of *bis*-1,2,4-triazines via Telescoped Condensation of [1,10]-Phenanthroline-2,9-dicarbonitrile with Aromatic 1,2-Dicarbonyls" *Journal of Heterocyclic Chemistry*, Vol. 53, No. 1, pp. 307–312.
52. Tai, S., S. V. Marchi, and J. D. Carrick, 2015, "Efficient Preparation of Pyridinyl-1,2,4-triazines via Telescoped Condensation with Diversely Functionalized 1,2-Dicarbonyls," *Journal of Heterocyclic Chemistry*, Vol. 53, No. 4, pp. 997–1332.
53. Tai, S., S. V. Marchi, E. J. Dover, and J. D. Carrick, 2015, "Pd-Catalyzed Diamination of Dibromo-1,2,4-triazinyl Complexant Scaffolds," *Journal of Organic Chemistry*, Vol. 80, No. 12, pp. 6275–6282.
54. Tevepough, K. N., Carrick, J. D., Tai, S., Coonce, J. G., Delmau, L. H., and Ensor, D. D., 2016, "Separation of Americium from Europium using Camphor-BisTriazinyl Pyridine, A Fundamental Study," *Solvent Extraction and Ion Exchange* Vol. 34, pp. 13–25.
55. Tkac, P., G. F. Vandegrift, G. J. Lumetta, and A. V. Gelis, 2012, "Study of the Interaction between HDEHP and CMPO and its Effect on the Extraction of Selected Lanthanides," *Industrial and Engineering Chemistry Research*, Vol. 51, No.31, pp. 10433–10444.
56. Zalupski, P. R., D. E. Ensor, C. L. Riddle, and D. R. Peterman, 2013, "Complete Recovery of Actinides from UREX-like Raffinates using a Combination of Hard and Soft Donor Ligands," *Solvent Extraction and Ion Exchange*, Vol. 31, pp. 430–441.
57. Zalupski, P. R., J. R. Klaehn, and D. R. Peterman, 2015, "Complete Recovery of Actinides from UREX-like Raffinates using a Combination of Hard and Soft Donor Ligands. II. Soft Donor Structure Variation," *Solvent Extraction and Ion Exchange*, Vol. 33, No. 6, pp. 523–539.

## SIGMA TEAM OFF-GAS

1. Banerjee, D. et al., 2016, "Metal-organic framework with optimally selective xenon adsorption and separation," *Nature Communications*, Vol. 7, Article No. 11831.
2. Chen, E. A., Riess, P. S., Chong, S. Y., Holden, D., Jelfs, K. E., Hasell, T., Little, M. A., Kewley, A., Briggs, M. E., Stephenson, A., Thomas, M., Armstrong, J. A., Bell, J., Busto, J., Noel, R., Liu, J., Strachan, D. M., Thallapally, P. K., and Cooper, A. I., 2014, "Separation of rare gases and chiral molecules by selective binding in porous organic cages," *Nature Materials*, pp. 1–7.
3. Elsaidi, S. K., T. Pham, K. A. Forrest, H. T. Schaefer, A. Hogan, L. Wojtas, W. Xu, B. Space, M. J. Zaworotko, and P. K. Thallapally, 2016, "Hybrid Ultra-Microporous Materials for Selective Xenon Adsorption and Separation," *Angewandte Chemie International Edition*, Vol. 55, No. 29, pp. 8285–8289.
4. Feng, X. H., Z. W. Zong, S. K. Elsaidi, J. B. Jasinski, R. Krishna, P. K. Thallapally, and M. A. Carreon, 2016, "Kr/Xe Separation over a Chabazite Zeolite Membrane," *Journal of the American Chemical Society*, Vol. 138, pp. 9791–9794.
5. Fernandez, C. A., J. Liu, P. K. Thallapally, and D. M. Strachan, 2012, "Switching Kr/Xe Selectivity with Temperature in a Metal-Organic Framework," *Journal of the American Chemical Society*, Vol. 134, No. 22, pp. 9046–9049.
6. Garn, T. G., M. R. Greenhalgh, and J. D. Law, 2016, "Development and evaluation of a silver mordenite composite sorbent for the partitioning of xenon from krypton in gas compositions," *Journal of Nuclear Science and Technology*, Vol. 53, No. 10, pp. 1484–1488.
7. Gullekson, B. J., A. Breshears, M. A. Brown, J. B. Essner, G. A. Baker, J. R. Walensky, A. Paulenova, and A. V. Gelis, 2016, "Extraction of Water and Speciation of Trivalent Lanthanides and Americium in Organophosphorous Extractants," *Inorganic Chemistry*, Vol. 55, No. 24, pp. 12675–12685.
8. Leggett, C. J., and M. P. Jensen, 2013, "Studies of Size-Based Selectivity in Aqueous Ternary Complexes of Americium(III) or Lanthanide(III) Cations," *Journal of Solution Chemistry*, in press.
9. Liu, J., C. A. Fernandez, P. F. Martin, P. K. Thallapally, and D. M. Strachan, 2014, "A Two-Column Method for the Separation of Kr and Xe from Process Off-Gases," *Industrial and Engineering Chemistry Research*, Vol. 53, No. 32, pp. 12893–12899.
10. Liu, J., D. M. Strachan, and P. K. Thallapally, 2014, "Enhanced noble gas adsorption in Ag@MOF-74Ni," *Chemical Communications*, Vol. 50, No. 4, pp. 466–468.
11. Liu, J., P. K. Thallapally, and D. M. Strachan, 2012, "Metal-Organic Frameworks for Removal of Xe and Kr from Nuclear Fuel Reprocessing Plants," *Langmuir*, Vol. 28, No. 31, pp. 11584–11589.
12. Matyáš, J., N. Canfield, S. Sulaiman, and M. Zumhoff, 2016, "Silica-based waste form for immobilization of iodine from reprocessing plant off-gas streams," *Journal of Nuclear Materials*, Vol. 476, pp. 255–261.

## 2016 ACCOMPLISHMENTS

13. Nenoff, T. M., M. A. Rodriguez, N. Soelberg, and K. W. Chapman, 2014, "Silver-mordenite for radiologic gas capture from complex streams: Dual catalytic CH<sub>3</sub>I decomposition and I confinement," *Microporous and Mesoporous Materials*, Vol. 200, pp. 297–303.
14. Patil, R. S., D. Banerjee, J. L. Atwood, and P. K. Thallapally, 2016, "Gas Sorption and Storage Properties of Calixarenes," *Calixarene Functionalization and Applications*, edited by Prof. Placido Neri, Jonathan L. Sessler and Mei-Xiang Wang, Springer.
15. Patil, R. S., D. Banerjee, S. Cory, J. L. Atwood, P. K. Thallapally, and A. Noria, 2016, "A highly Xe-Selective Nanoporous Organic Solid," *Chemistry: A European Journal*, Vol. 22, pp. 1–7.
16. Soelberg, N. R., T. G. Garn, M. R. Greenhalgh, J. D. Law, R. Jubin, D. M. Strachan and P. K. Thallapally, 2013, "Radioactive Iodine and Krypton Control for Nuclear Fuel Reprocessing Facilities," *Science and Technology of Nuclear Installations*, Vol. 2013, Article No. 702496.
17. Thallapally, P. K., J. W. Grate, and R. K. Motkuri, 2012, "Facile xenon capture and release at room temperature using a metal-organic framework: A comparison with activated charcoal," *Chemical Communications*, Vol. 48, No. 3, pp. 347–349.

### GENERAL SEPARATIONS AND WASTE FORMS AND OTHER

1. DelCul, G. D., R. T. Jubin, and B. B. Spencer, 2012, *1-Kg Scale Nitration Test Equipment – Initial Test*, ORNL/LTR-2012/251, Oak Ridge National Laboratory, Oak Ridge, TN.
2. Farawila, A. F., M. J. O'Hara, H. Z. Taylor, C. M. Wai, and Y.-J. Liao, 2012, *Selective Extraction of Uranium from Liquid or Supercritical Carbon Dioxide*, PNNL-21590, Pacific Northwest National Laboratory, Richland, WA.
3. Nenoff, T. M., 2012, "Alternative Energy Systems: Nuclear Energy, Introduction to the Special Section on Nuclear Energy," *Industrial and Engineering Chemistry Research*, Vol. 51, No. 2, pp. 605–606.
4. Scheele, R. D., B. K. Mcnamara, A. M. Casella, and A. Kozelisky, 2012, "On the Use of Thermal NF<sub>3</sub> as the Fluorination and Oxidation Agent in Treatment of Used Nuclear Fuels," *Journal of Nuclear Materials*, Vol. 424: pp. 224–236.
5. Schwantes, J. M., S. A. Bryan, C. R. Orton, T. G. Levitskaia, and C. G. Fraga, 2012, "Monitoring, Controlling and Safeguarding Radiochemical Streams at Spent Fuel Reprocessing Facilities, Part 2: Gamma-Ray Spectroscopic Methods," *International Journal on Nuclear Energy Management and Safety*.
6. Wanigasekara, E., X. G. Sun, R. A. Meisner, H. M. Meyer, H. Luo, L. H. Delmau, S. Dai, and B. A. Moyer, 2014, "Direct Electrodeposition of UO<sub>2</sub> from Uranyl Bis(Trifluoromethanesulfonyl)Imide Dissolved in 1-Ethyl-3-Methylimidazolium Bis(Trifluoromethanesulfonyl)Imide Room Temperature Ionic Liquid (Rtil) System," *Electrochimica Acta*, Vol. 115, pp. 630–638.



## Material Recovery and Waste Form Development Program Contact Information

**TERRY TODD**  
**DIRECTOR**

**Tel** 208-526-3365  
Terry.Todd@inl.gov

**JOHN VIENNA**  
**DEPUTY DIRECTOR**

**Tel** 509-372-6201  
John.Vienna@pnnl.gov

**PATRICIA PAVIET**  
**DOE OFFICE DIRECTOR**

**Tel** 301-903-1542  
Patricia.Paviet@nuclear.energy.gov

**Released through:**

